IRE Transactions

on Microwave Theory and Techniques

Volume MTT-8 **JANUARY, 1960** Number 1

In This Issue

PUBLISHED BY THE

Professional Group on Microwave Theory and Techniques

IRE TRANSACTIONS®
on Microwave Theory and Techniques

Published by the Institute of Radio Engineers, Inc., for the Professional Group on Microwave Theory and Techniques, at 1 East 79th Street, New York 21, New York. Responsibility for the contents rests upon the authors, and not upon the IRE, the Group, or its members. Price per copy: IRE PGMTT members, $2.10; IRE members, $3.15, nonmembers, $6.30. Annual subscription price: IRE members, $8.50; colleges and public libraries, $12.75; nonmembers, $17.00.

Address all manuscripts to Donald D. King, PGMTT Editor, Electronic Communications, Inc., 1830 York Road, Timonium, Md. Submission of three copies of manuscripts, including figures, will expedite the review.

IRE Transactions on Microwave Theory and Techniques

Volume MTT-8 JANUARY, 1960 Number 1

TABLE OF CONTENTS

Message from the Editor

Publication Schedules

With this issue of the IRE Transactions on Microwave Theory and Techniques, we begin a new publication schedule of six issues per year appearing on alternate months. The principal reason for adopting this more frequent schedule is to reduce the interval between the receipt and publication of a paper. The rate of progress in microwaves is now so rapid that publication delays are a significant factor to both authors and readers. Thanks to our competent and conscientious editorial board, papers are reviewed promptly. However, with our previous quarterly publication cycle, papers received in the wrong phase were inevitably held up for several extra months. This factor will now be much reduced.

Letters ordinarily do not require review procedures, and the new publication schedule should particularly benefit the correspondence section. We therefore take this opportunity to invite communications from those who read the Transactions. Letters afford a simple means for communicating pertinent results and comments in a minimum time. To achieve this result, they should be concisely written with only a few simple illustrations.

Symposium Papers

The January issue of these Transactions is traditionally devoted to the PGMTT National Symposium. We have departed somewhat from this policy in the present issue. While several pages are devoted to symposium events, the technical papers have been assembled without taking note of whether they were presented at the symposium or not. Although a unified symposium issue appears attractive, there are several advantages in an independent treatment of papers. These include freedom from added delays for non-Symposium papers, and the absence of an absolute deadline for symposium authors. More important than the time element is our ability to review each published paper in the normal manner. The constructive criticism and occasional rejection of manuscripts by the editorial board greatly improve the technical level of the published papers. Both authors and readers benefit from the consistent use of this editorial review. All published papers, whether presented at the symposium or not, are now subject to the same review.

—Donald D. King

Microwave Prize

The Professional Group on Microwave Theory and Techniques has established the Microwave Prize to recognize annually a significant paper which appeared in the IRE TRANSACTIONS ON MICROWAVE THEORY AND TECHNIQUES. In selecting the paper, consideration is given primarily to the subject of the contribution and secondarily to its presentation. All members and affiliates of PGMTT are eligible. The award consists of a certificate, a monetary sum of $100, and a feature publication in these TRANSACTIONS. If the paper has more than one author, the monetary sum is divided equally among the authors.—The Editor

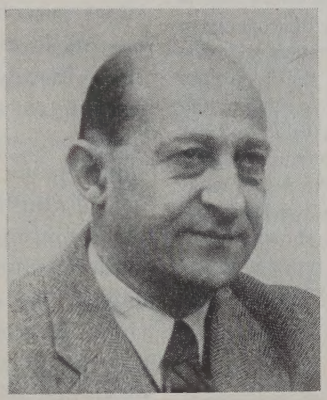

LADISLAS GOLDSTEIN
"Nonreciprocal Electromagnetic Wave Propagation in Ionized Gaseous Media"
IRE TRANSACTIONS ON MICROWAVE THEORY AND TECHNIQUES
Vol. MTT-6, No. 1, pp. 19–29; January, 1958

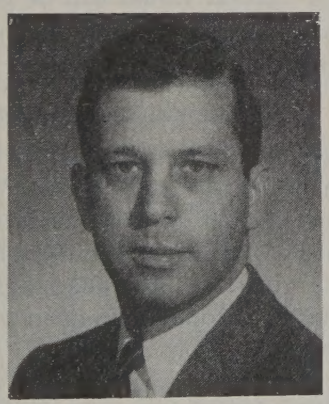

SEYMOUR COHN
Honorable Mention
"Parallel-Coupled Transmission-Line-Resonator Filters"
IRE TRANSACTIONS ON MICROWAVE THEORY AND TECHNIQUES
Vol. MTT-6, No. 2, pp. 223–231; April, 1958

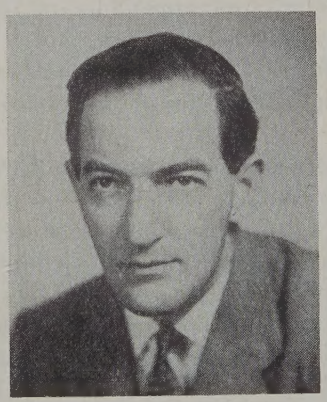

H. E. D. SCOVIL
Honorable Mention
"The Three-Level Solid-State Maser"
IRE TRANSACTIONS ON MICROWAVE THEORY AND TECHNIQUES
Vol. MTT-6, No. 1, pp. 29–38; January, 1958

We announce with pleasure the award of the Microwave Prize for 1958 to Dr. Ladislas Goldstein. It was the opinion of the Awards Committee and of the Administrative Committee that two other papers were deserving of special mention. In recognition of their achievement, we give Honorable Mention to the authors of these two papers.

THEODORE S. SAAD, *Chairman*, 1958
PGMTT Administrative Committee

Theoretical Limitations to Ferromagnetic Parametric Amplifier Performance*

R. W. DAMON† AND J. R. ESHBACH†

Summary—**It has been commonly expected that improved operation of the ferrite parametric amplifier could be obtained by use of materials of narrower resonance linewidth, ΔH. This parameter is critical in determining the pumping power (P_p) required for operation of the device. Also of importance, however, is the limitation of device properties determined by the dependence on ΔH of the instability threshold of the spin-wave system. Considering this limitation, the maximum voltage gain-fractional bandwidth product ($g_v\Delta\omega/\omega_1$) has been determined as a function of other device parameters, and typical values calculated for several modes of operation. In the electromagnetic mode, for example, there is an optimum ΔH which yields maximum $g_v\Delta\omega/\omega_1$ at a given pumping power. It is also shown that a minimum filling factor, also a function of ΔH for some types of operation, is required to reach the oscillation threshold even in the unloaded device.**

Introduction

THE parametric amplifier is based on a regenerative feedback process which results from coupling together two tuned circuits with a time-varying reactance. For particular conditions of tuning, and for a sufficiently large modulation amplitude of the variable reactance, the input impedance of the tuned circuits exhibits a negative resistance, which can be used to obtain amplification of applied signals or to produce oscillations at the natural frequencies of the tuned circuits.

One of the earliest proposals for a parametric amplifier at microwave frequencies utilized the ferromagnetic resonance effect, the uniform precession of the magnetization serving as a means of coupling between the tuned circuits.[1] This proposal was based on earlier work[2] which led to an interpretation of some anomalous results obtained in resonance experiments at high microwave power levels.[3,4] These anomalous results were shown to arise from inherent instabilities in the uniform motion of the magnetization. At sufficiently high power levels, these instabilities prevent further increase in the amplitude of the uniform mode and couple energy from the uniform precession into short wavelength (spin-wave) modes of motion of the sample magnetization. The effect is similar to the processes used in parametric amplification, but the modes into which the energy is dissipated are unsuitable for device use because the short wavelength of these modes makes it impossible to couple out useful energy. Instead the existence of these instabilities can interfere with the operation of a parametric amplifier if energy from the precessing uniform magnetization is dissipated in these modes at a pump power-level less than that required for operation of the amplifier.

The pump frequency magnetic field strength required for a specified amplifier performance can be calculated, as can the critical RF field strength for the onset of these instabilities. The purpose of this note is to point out the limitations imposed on amplifier design by the existence of the potentially unstable behavior of the magnetization. The results will be expressed as the maximum gain-bandwidth product attainable for the device. Since the results depend on the properties of both the sample and of the circuits to which it is coupled, only typical values can be given, but similar calculations can be performed for any specific device following the method outlined here.

General Procedure

The principles of the analysis can be illustrated by the diagram shown as Fig. 1. The uniform mode of precession is represented by the magnetization vector M precessing about the steady magnetic field H, driven by the circularly polarized pumping magnetic field of amplitude h. At the resonance frequency, the angle θ between M and H is approximately $\theta = h/\Delta H$, where ΔH is the width of the resonance line. The coupling between signal and idler circuits increases with increasing θ, so a large precession angle is desired to obtain good amplifier performance.

The angle θ_{th} represents the threshold angle for operation of a parametric device. At θ_{th}, the transverse magnetization couples sufficient energy to the two pertinent cavity modes to overcome the losses of the cavities. As an amplifier, the gain becomes unity for $\theta = \theta_{th}$. The coupling is proportional to the total transverse magnetization, so θ_{th} depends on the size of the sample, or the filling factor, as well as on the losses of the resonant systems.

While θ_{th} is the minimum angle for operation of a parametric amplifier, an increased gain-bandwidth product is obtained by coupling an external load and increasing the precession angle. The maximum gain-bandwidth product increases roughly as $(\theta/\theta_{th})^2$, and

* Manuscript received by the PGMTT, June 10, 1959; revised manuscript received, July 27, 1959. This paper was presented at the PGMTT National Symposium, June 1–3, 1959, Cambridge, Mass.

† G.E. Res. Lab., Schenectady, N. Y.

[1] H. Suhl, "The theory of the ferromagnetic microwave amplifier," *J. Appl. Phys.*, vol. 28, pp. 1225–1236; November, 1957.

[2] H. Suhl, "The theory of ferromagnetic resonance at high signal powers," *J. Phys. Chem., Solids*, vol. 1, pp. 209–227; 1957.

[3] R. W. Damon, "Relaxation effects in the ferromagnetic resonance," *Rev. Mod. Phys.*, vol. 25, pp. 239–245; January, 1953.

[4] N. Bloembergen and S. Wang, "Relaxation effects in para- and ferromagnetic resonance," *Phys. Rev.*, vol. 93, pp. 72–83; January, 1954.

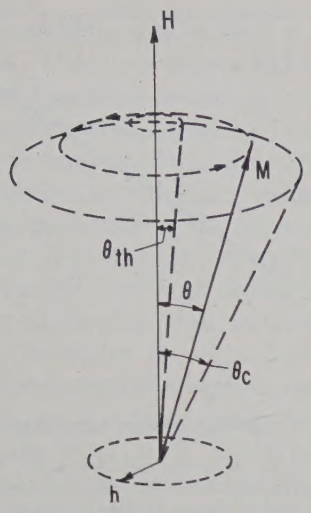

Fig. 1—Vector diagram representing uniform precession of magnetization M about the uniform magnetic field H, driven by the circularly polarized pumping field h. At resonance, M and h rotate about H at the Larmor frequency, with M at an angle $\theta = h/\Delta H$ with H. In parametric amplifier use, θ_{th} is the threshold angle for net gain. The critical angle θ_c is the limit determined by spin-wave instability.

since θ varies inversely with ΔH, a narrow linewidth material is desirable to obtain large θ at a given pump power. The variation of θ with linewidth is shown in Fig. 2 for several values of pump magnetic field strength.

The angle θ_c represents the critical angle for spin-wave instability. The value of θ_c depends only on properties of the magnetic material, and represents the angle at which the transverse magnetization is large enough to couple energy catastrophically from the uniform precession into certain spin-wave modes. For angles $\theta < \theta_c$, the coupling to the spin-waves acts as a damping mechanism on the motion of M, but at $\theta = \theta_c$ the spin-wave system absorbs all additional energy fed into the uniform mode and any attempt to increase θ only increases the oscillation amplitude of the spin-wave mode while leaving $\theta = \theta_c$. The critical angle, θ_c, is determined by the losses of the pertinent spin-wave mode, and is independent of sample size.

It should be noted that the steady-state precession angle for the uniform mode has been calculated only for the case of degeneracy of the uniform mode and the subsidiary absorption which arises from spin-waves of half the pump frequency.[2] In assuming that the precession angle cannot exceed θ_c in the nondegenerate case, we are utilizing experimental results obtained on Ni ferrite which show a power dependence in agreement with this assumption.[3] Such a well-defined critical angle may not be found in all materials. In fact, Schlömann[5] has recently extended Suhl's calculations to the nondegenerate case considered here, and shows that in magnetically inhomogeneous materials, the power coupled to the spin-waves increases smoothly with θ and that no well-defined critical angle exists. Recent experiments by Green verify this result in some materials.[6] For these materials, the results obtained in our analysis would be modified. Since no well-defined critical angle exists, there is no absolute limit to amplifier properties, but only a practical limit arising from increased loss, and decreased pump efficiency, as the precession angle is increased.

A combination of the homogeneous and inhomogeneous mechanisms is likely, exhibiting a decline in pump efficiency at the critical angle, but with the possibility of a slow increase in precession angle beyond θ, with further increase in pump power. The present results then would correspond to the practical limit of device properties.

In one important case,[7] the relation between critical angle and loss is given by $\theta_c = \sqrt{2\Delta H_k/4\pi M}$, where ΔH_k represents the losses in the spin-wave modes of interest. The maximum precession angle, and thus the maximum amplifier performance, is limited by the inherent instability of the spin-wave system. Since it has been found that ΔH_k may be considerably less than ΔH in some materials,[8] we will retain the distinction in most of our mathematical results. In other materials, however, it appears approximately correct to use $\Delta H_k = \Delta H$, and this will be assumed in numerical examples. The observed linewidth, ΔH, represents the sum of all loss mechanisms, so ΔH_k cannot exceed ΔH. Thus this latter assumption leads to the largest value of θ_c for a given linewidth. The limiting precession angle is shown in Fig. 2 for this case.

This figure shows that if a given pumping power is available, there is an optimum linewidth material giving maximum θ. If the linewidth is too large, the pump cannot supply enough power to reach a large precession angle. If too narrow a linewidth is used, the precession angle is limited by instability effects. When the pump field available is $h = 1$ oe, for example, $\Delta H = 9.5$ oe provides the maximum value of θ for sample magnetization of $4\pi M = 1700$ gauss. If $\Delta H < 9.5$ oe, θ is limited to a θ_c which is less than the optimum and the pump power is not utilized. If $\Delta H > 9.5$ oe, θ is limited by the material losses and a larger pump power is needed to achieve the same amplifier characteristisc.

The optimum linewidth is that for which $\theta = \theta_c$ at the available pumping field. If $\Delta H_k = \Delta H$, this condition re-

[5] E. Schlömann, "Ferromagnetic resonance at high signal powers," *Bull. Am. Phys. Soc.*, Ser. II, vol. 4, p. 53; January, 1959.

[6] J. J. Green and E. Schlömann, "High Power Ferromagnetic Resonance at X-Band in Polycrystalline Garnets," PGMTT National Symposium, Cambridge, Mass.; June 1–3, 1959.

[7] We assume that the subsidiary mode, arising from spin-waves of half the pump frequency, is not degenerate with the uniform mode, since this degeneracy would lead to an exceptionally small value of θ_c. Thus we assume $f_p > 2N_T(\gamma/2\pi)\cdot 4\pi M$, where f_p is pump frequency. N_T is the transverse demagnetizing factor of the sample and $\gamma/2\pi = 2.8$ mc/gauss. For spherical samples, $N_T = \frac{1}{3}$, and this condition requires $f_p > 3400$ mc for yttrium iron garnet and $f_p > 8000$ mc for manganese ferrite. With disks magnetized normally, $N_T \to 0$, and nondegenerate behavior is obtained at any operating frequency.

[8] R. C. LeCraw and E. G. Spencer, "Surface-independent spin-wave relaxation in ferromagnetic resonance of yttrium iron garnet," *J. Appl. Phys.*, vol. 30, pp. 185S–186S; April, 1959.

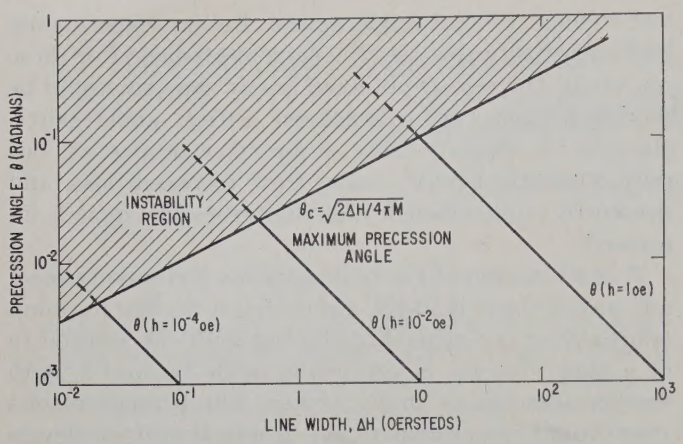

Fig. 2—For a given pump field strength h, material of narrower line width ΔH permits attainment of a larger precession angle θ. The critical angle for spin-wave instability, θ_c, is also a function of linewidth and sets an upper limit to θ for a given pump field strength.

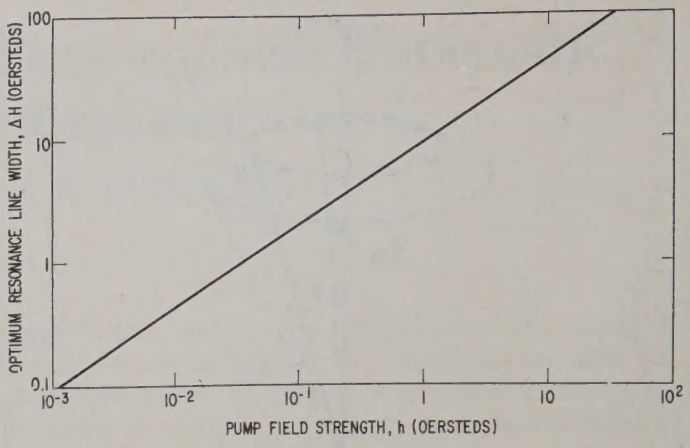

Fig. 3—At a given value of pump field strength, the optimum linewidth for parametric amplifier use is determined by the spin-wave instability limit, and is shown in this graph of $(\Delta H)_{opt}$ vs h.

sults in the optimum linewidth

$$\Delta H_{opt} = (\tfrac{1}{2}h^2 \cdot 4\pi M)^{1/3} \qquad (1)$$

This is plotted in Fig. 3 for $4\pi M = 1700$ gauss. This expression for ΔH enables us to calculate the maximum gain-bandwidth product in terms of available pump power for typical values of θ_{th} in each of several modes of amplifier operation.

Application to Specific Amplifiers

Electromagnetic Operation

Suhl has calculated the gain-bandwidth product for this mode of operation,[1] obtaining, for large gains

$$g_v \Delta\omega/\omega_1 = \frac{1}{\beta Q_1}\left[(\theta/\theta\text{th})^2 - 1\right]. \qquad (2)$$

Here g_v is the voltage gain at the signal frequency ω_1, $\Delta\omega/\omega_1$ is the fractional bandwidth, Q_1 is the unloaded Q of the signal cavity and β is a factor of order unity. For optimum performance, the operating conditions are chosen so $\theta = \theta_c = \sqrt{2\Delta H_k/4\pi M}$.

In determining θ_{th}, we restrict the analysis to spherical samples to avoid complicating demagnetizing effects. The results for other shapes would differ by only small factors. In a cavity having only the fields h_{z_1} and h_{x_2} at the signal and idler frequencies respectively,

$$\theta_{th} = \frac{2\omega_1/\gamma}{4\pi M}\,\frac{1}{F\sqrt{Q_1 Q_2}},$$

where the filling factor is defined as

$$F = \int_{\text{sample}} h_{z_1} h_{x_2} dv \Big/ \left[\int_{\text{cavity}} h_{z_1}^2 dv \int_{\text{cavity}} h_{x_2}^2 dv\right]^{1/2}.$$

In this mode of operation, the threshold angle is independent of sample linewidth, and can be represented as shown in Fig. 4 for typical cavity and sample parameters and for several values of F. Clearly if θ_{th} exceeds θ_c, operation of the amplifier is impossible, and the ratio of

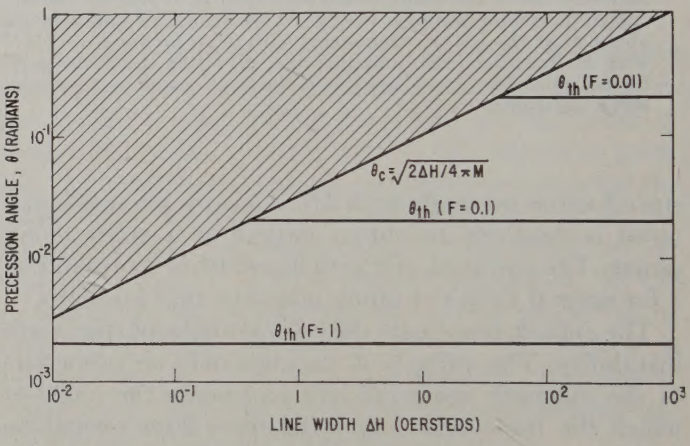

Fig. 4—In electromagnetic operation, the threshold precession angle for net gain is a function of frequency, circuit losses, sample magnetization and filling factor. It is independent of linewidth. For three values of filling factor F, threshold angles are shown with the other parameters: $4\pi M = 1700$, $\omega_1^2 = 10^{21}$, and $Q_1 = Q_2 = 10^3$. Since the maximum precession angle θ_c is a function of linewidth, ΔH, the amplifier properties will also be a function of ΔH.

θ_c to θ_{th} at the linewidth appropriate to the sample used determines the maximum gain-bandwidth product of the device. The important point is that the threshold angle is determined by the cavity configuration, while the spin-wave instability limit decreases for narrow linewidth, leading to a reduction in the maximum gain-bandwidth product when narrow linewidth materials are used in this mode of operation.

A quantitative statement of this relation is obtained by substituting in (2) the expression for θ_{th} and using $\theta = \theta_c$, giving

$$(g_v \Delta\omega/\omega_1)_{max} = \frac{1}{\beta Q_1}\left[\frac{F^2 Q_1 Q_2 \cdot 4\pi M}{2\omega_1^2/\gamma^2}\Delta H_k - 1\right]. \qquad (3)$$

From (3) it is clear that materials are desired for which the spin-wave linewidth is large. But since $\Delta H_k \leq \Delta H$, and ΔH should be small to permit large θ at the given pump level, it is desirable to obtain $\Delta H_k = \Delta H$. This gives the maximum value of $g_v \Delta\omega/\omega_1$ for a given pump power level. The desirability of a large filling

factor is also evident, and in fact, no operation is obtained unless $F^2 > (2\omega_1^2/\gamma^2)/4\pi M Q_1 Q_2 \Delta H$. Thus, although narrow linewidth materials reduce pump power requirements, an increased filling factor is required to achieve a given gain-bandwidth product.

It is instructive to calculate values of $g_v \Delta\omega/\omega_1$ for typical device parameters. We have chosen the signal frequency to be $f_1 \approx 5000$ mc ($\omega^2_1 = 10^{21}$ sec^{-2}), and have taken the unloaded Q of both signal and idle circuit as 10^3. Since a pump level of a few watts or less is desirable, the optimum linewidth is under 20 oe. Only yttrium iron garnet has linewidths in this range, so the value $4\pi M = 1700$ gauss has been used. Substituting in (3) we find $(g_v \Delta\omega/\omega_1)_{max} = 10^{-3}[340F^2\Delta H - 1]$. This is plotted in Fig. 5 for several values of F. A linewidth of 3 oe, for example, would be a desirable value since this requires a pump field strength of only 0.2 oe. With some care a filling factor of 0.1 should be possible. The maximum performance attainable under these conditions corresponds to 20-db gain and 5 mc/sec bandwidth at the signal frequency of 5000 mc/sec.

Only one device has been reported using the electromagnetic mode of operation,[9] and in this case a manganese ferrite sample was employed. Assuming the sample had a linewidth of 50 oe, the optimum pump field-strength is $h = \Delta H\sqrt{2\Delta H/4\pi M} \sim 8$ oe. For the conditions under which the device was operated, this was probably achieved. The theoretical gain-bandwidth product for the frequency, Q, and sample magnetization used is $g_v \Delta\omega/\omega_1 = 2\times10^{-3}$ $(10^4F^2 - 1)$. The observed value of 4×10^{-3} implies $F = 1.7\times10^{-2}$. Calculations of F using a reasonable field configuration and the known sample size lead to values in agreement with this. Note that a value of at least $F = 1\times10^{-2}$ is required for even marginal operation.

Semistatic Operation

For a given sample size, improved filling factor and increased gain-bandwidth product can be obtained by using a magnetostatic mode of the sample[10] as one of the resonant systems required in the parametric amplifier. The theoretical gain-bandwidth product has not been reported for this case, but can be readily calculated in direct analogy to the electromagnetic mode. Eq. (2) is obtained with an appropriate redefinition of θ_{th}.

If the signal circuit is a cavity mode with unloaded loss characterized by Q_1, and the idle mesh is a magnetostatic mode of linewidth ΔH_2, then the threshold angle is

$$\theta_{th} = \frac{1}{F}\sqrt{\frac{\Delta H_2}{4\pi M}}\,\frac{1}{\sqrt{Q_1}}.$$

[9] M. T. Weiss, "Solid-state microwave amplifier and oscillator using ferrite," *J. Appl. Phys.*, vol. 29, p. 421; March, 1958.

[10] R. L. White and I. H. Solt, Jr., "Multiple ferromagnetic resonance in ferrite spheres," *Phys. Rev.*, vol. 104, pp. 56–62; October 1, 1956. Also L. R. Walker, "Magnetostatic modes in ferromagnetic resonance," *Phys. Rev.*, vol. 105, pp. 390–399; January 15, 1957.

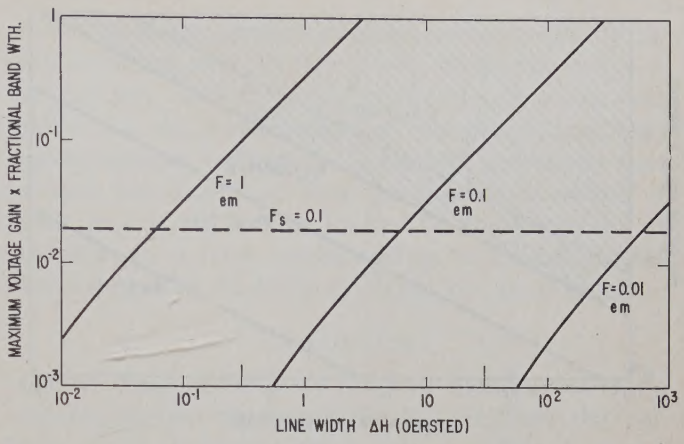

Fig. 5—For the parameters used in Fig. 4 the maximum voltage-gain bandwidth product is calculated as a function of linewidth. The solid lines are for electromagnetic operation, and the dashed line corresponds to semistatic operation.

The filling factor is

$$F = \frac{1}{2\sqrt{2}}\,\frac{\left|\int_s V_{z1}(M_{x2} + iM_{y2})dv\right|}{\left[\mathrm{Im}\int_s M_{x2}M_{y2}^{*}dv\right]^{1/2}\left[\int_c V_1^2 dv\right]^{1/2}},$$

where the M's are magnetization components of the magnetostatic mode and the V's are the vector potential functions of the cavity mode.[1] In contrast to the electromagnetic case, θ_{th} decreases with linewidth in the same way as θ_c, since one resonant mode of the amplifier is a magnetostatic mode. Typical values of θ_{th} are shown in Fig. 6. If $\Delta H_2 \sim \Delta H_k$, the required filling factor for semistatic operation and the maximum gain-bandwidth product are independent of linewidth. Material of narrow linewidth is thus desired to minimize the pump power required, being limited only by the necessity of having the resonance sufficiently wide to meet bandwidth specifications.

The maximum gain-bandwidth product can be calculated from the expression

$$g_v \Delta\omega/\omega_1 = \frac{1}{\beta Q_1}\left[2F^2 Q_1 \Delta H_k/\Delta H_2 - 1\right].$$

If $\Delta H_2 = \Delta H_k$, it is seen that $F > 1/\sqrt{2Q_1}$ is required for operation, and

$$g_v \Delta\omega/\omega_1 = \frac{1}{\beta Q_1}(2F^2 Q_1 - 1).$$

This expression is plotted in Fig. 5 for typical values of Q and F.

The semistatic type of operation offers the advantage of large filling factor, even for samples of moderate size. While in electromagnetic operation, the filling factor $F_{em} \approx$ (sample volume per cavity volume), it is found for simple field configurations that semistatic operation leads to $F_{ss} \approx$ (sample volume per cavity volume)$^{1/2}$. Thus with limited size samples, substantially improved performance should be obtained in the latter case. If

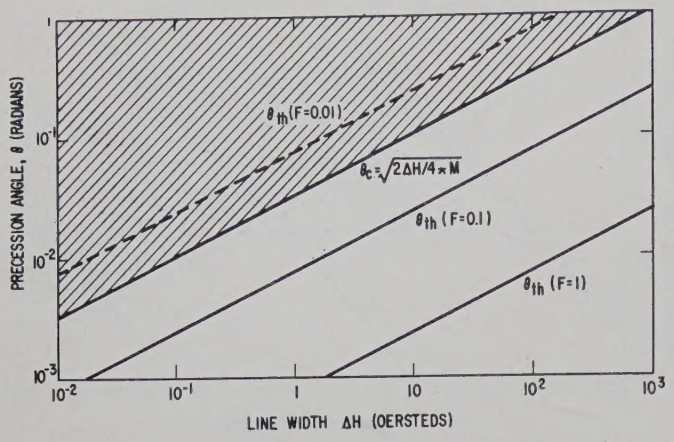

Fig. 6—In semistatic operation, the threshold precession angle for net gain is a function of losses in the signal circuit and in the magnetostatic mode used as idler, and of sample magnetization and filling factor. The dependence on magnetostatic mode losses, or linewidth, leads to amplifier gain-bandwidth independent of ΔH. For several values of filling factor F, θ_{th} is shown with other parameters $\Delta H_2=\Delta H$, $4\pi M=1700$, $Q_1=10^3$. The dashed line for $F=0.01$ indicates that net gain cannot be observed, since θ cannot achieve the threshold value.

sample dimensions are taken similar to those used in achieving $F_{em}=0.1$ in the electromagnetic case, a value $F_{ss}=0.3$ will be obtained in semistatic operation. This would permit substantial improvement in gain bandwidth product, to a value of 10^3 mc at a signal frequency of 5000 mc/sec, corresponding to about 100 mc bandwidth at 20-db gain if ΔH_2 does not limit the bandwidth.

Operation of this type of amplifier has also been reported by Weiss.[9] He gives only incomplete data, but it is interesting to compare these results with the present limitations. The pump power of 40 watts corresponds to a microwave field strength of about $\frac{1}{2}$ oe in his structure. In turn, this is the critical field for a YIG sample ($4\pi M=1700$ gauss) having the reasonable linewidth $\Delta H=6$ oe. To obtain device operation, we require $\theta_{th}<h_p/\Delta H$. For the assumed parameters, this can be achieved if $F>3.1\times10^{-2}$. This value is in approximate agreement with the filling factor estimated for Weiss's device. That such a large filling factor can be obtained with a sample volume one-sixteenth that which Weiss used in electromagnetic operation is indeed a tribute to the semistatic device.

Magnetostatic Operation

In magnetostatic operation, no microwave cavity resonance is necessary; two magnetostatic modes of the sample are used as the two parametric amplifier meshes. Still further improvement in filling factor is achieved for a given sample volume. Suhl has pointed out the limitations imposed by the fact that the magnetostatic mode spectrum could provide alternative pairs of magnetostatic modes which might break into oscillation and preclude operation of this type of device; we consider the limitations set by spin-wave instabilities even if these alternative modes can be avoided.

The lowest frequency for magnetostatic modes is $\omega_{\min}=\gamma(H-N_z\cdot4\pi M)$, while in cylindrically symmetric samples the resonant frequency at which it is desired to pump is

$$\omega_p=\gamma\left[H+\frac{1-3N_z}{2}4\pi M\right].$$

To obtain magnetostatic operation it is necessary to have $\omega_{\min}\leq\frac{1}{2}\omega_p$. This condition imposes the restriction on pump frequency $\omega_p\leq\gamma(1-N_z)4\pi M$. But this is also the condition for the occurrence of a particularly low instability threshold. This decreased instability threshold arises from a coincidence of the main resonance and a subsidiary absorption by a set of spinwaves driven at twice their natural frequency. From the above result, the conditions for coincidence will be satisfied whenever magnetostatic operation is possible. In this case the critical angle for spin-wave instability is $\theta_c=\alpha\Delta H_k/4\pi M$, where α is a factor of order unity which depends on sample magnetization, frequency and geometry.

The threshold angle for operation in the magnetostatic mode has been previously derived[1] as

$$\theta_{th}=\frac{1}{F_{ms}}\sqrt{\frac{\Delta H_1}{4\pi M}}\sqrt{\frac{\Delta H_2}{4\pi M}}.$$

The filling factor, F_{ms}, has been calculated by Suhl[1] and will not be repeated here. It is a measure of the overlap of the two magnetostatic modes relative to the magnetic energy of these modes. Combining θ_{th} with the maximum precession angle, θ_c, the maximum gain-bandwidth product is found,

$$(g_v\Delta\omega/\omega_1)_{\max}=\frac{\gamma\Delta H_1}{\beta Q_1}\left[\frac{(\alpha\Delta H_k)^2}{\Delta H_1\Delta H_2}F^2-1\right].$$

Since F is necessarily less than unity, no operation is obtained unless $\Delta H_1\ \Delta H_2/(\alpha\Delta H_k)^2\leq1$. Thus in addition to the potential instabilities arising from unwanted pairs of magnetostatic modes, the excitation of spin-wave modes restricts the performance of the magnetostatic type of amplifier. Since the linewidth of the signal mode, ΔH_1, must include the coupled load, the performance of this class of amplifier is seriously impaired.

Modified Semistatic Operation

A fourth mode of operation has been proposed by Berk, Kleinman and Nelson,[11] and experimentally studied by Whirry and Wang.[12] As in the semistatic type, a sample mode is used as idler. This device differs from the earlier proposal, however, since it utilizes the uniform mode for this function rather than a higher

[11] A. D. Berk, L. Kleinman and C. E. Nelson, "Modified semistatic ferrite amplifier," 1958 WESCON Convention Record, pt. 3, pp. 9–12.

[12] W. L. Whirry and F. B. Wang, "Experimental Study of the Modified Semistatic Ferrite Amplifier," presented at Conference on Magnetism and Magnetic Materials, Philadelphia, Pa.; November 17–20, 1958.

order magnetostatic mode. The pump is necessarily at a higher frequency and does not have the advantage of driving the sample at resonance. The resultant decrease in pump effectiveness is partially compensated by the possibility of obtaining higher cavity Q at the pump frequency.

The threshold pump field strength has been calculated by Berk, *et al.* To utilize our expression for gain-bandwidth product, it is desirable to convert this to a threshold precession angle. Since the pump is not at the resonance frequency, the angle is obtained by dividing h_{th} by the difference between pump frequency and resonance frequency, $\theta_{th}=\gamma h_{th}/(\omega_p-\omega_r)=\gamma h_{th}/\omega_1$. The result obtained is

$$\theta_{th}=\frac{1}{F}\left[\frac{\Delta H}{4\pi M}\frac{1}{Q_1}\right]^{1/2},$$

where

$$F=\left[\int_s h_1^2 dv \Big/ \int_c h_1^2 dv\right]^{1/2}$$

is the filling factor for the signal mode.[13] θ_{th}, as shown in Fig. 6 for semistatic operation, is also applicable to this type of operation.

Since the coupling from the precessing magnetization driven at the pump frequency to spin-waves of the same frequency depends only on the precession angle, the critical angle for spin-wave instability is unchanged from our previous value, $\theta_c=\sqrt{2\Delta H_k/4\pi M}$. Coupling this with the threshold angles we find the maximum gain-bandwidth product

$$(g_v\Delta\omega/\omega_1)_{\max}=\frac{1}{Q_1\beta}\left[F^2Q_1\frac{2\Delta H_k}{\Delta H}-1\right].$$

If $\Delta H_k=\Delta H$, this expression is independent of linewidth as in the conventional semistatic case, since the decreased loss in the uniform mode used as idler reduces the threshold angle at the same rate that the critical angle is decreased. This device thus should achieve a gain-bandwidth product comparable to that in semistatic operation.

Other Devices

The preceding analysis has been limited to the regenerative type of amplifier, utilizing cavity or sample modes as resonant circuits. Distributed amplifiers probably offer advantages of larger bandwidth or increased stability, but it should be noted that similar limitations on the maximum precession angle are imposed by the instabilities considered here.[14] The nonlinear nature of the uniform mode of the magnetization has also been applied in the construction of microwave frequency converters and multipliers. It has not previously been pointed out, however, that the maximum output of these devices will also be limited by the spin-wave instabilities to a level corresponding to the critical RF field-strength of the local oscillator, or pump source.

Conclusion

It has been shown that inherent instabilities in the uniform motion of the magnetization limit the performance of the ferrite parametric amplifier. A general expression for the voltage gain-bandwidth product has been utilized and applied to four different types of amplifiers. From the threshold precision angle for device operation and the critical angle for spin-wave instability, it is found that a minimum filling factor is required for a given ΔH, regardless of pump power, to obtain even marginal operation of any of these devices. It is also noted that a material linewidth should be chosen which permits the precession angle to be opened out to the critical angle at the available pump power level. For filling factors exceeding the minimum requirements, the maximum gain-bandwidth product possible has been calculated. The results are summarized in Table I.

TABLE I

Mode of Operation	Maximum Voltage Gain Fractional Bandwidth
Electromagnetic	$1/\beta Q_1\left[\frac{F^2Q_1Q_2 4\pi M}{2\omega_1^2/\gamma^2}\Delta H_k-1\right]$
Semistatic	$1/\beta Q_1\left[2F^2Q_1\frac{\Delta H_k}{\Delta H_2}-1\right]$
Magnetostatic	$1/\beta Q_1\left[2F\frac{(\alpha\Delta H_k)^2}{\Delta H_1\Delta H_2}-1\right]$
Modified Semistatic	$1/\beta Q_1\left[2F^2Q_1\frac{\Delta H_k}{\Delta H}-1\right]$

The gain-bandwidth product possible in practical devices is substantial, in spite of this limitation, provided that fairly large filling factors can be obtained. The limits set by this analysis, however, together with previous expressions for pumping power requirements, serve as a useful basis for comparing the ferrite amplifier with other types of amplifiers.

[13] The usage of the symbol F is slightly different from Berk, *et al.*,[11] in order to conform to comparable terminology used in the remainder of this paper.

[14] P. K. Tien and H. Suhl, "A traveling-wave ferromagnetic amplifier," Proc. IRE, vol. 46, pp. 700–706; April, 1958.

An Extension of the Mode Theory to Periodically Distributed Parametric Amplifiers with Losses*

K. KUROKAWA† AND J. HAMASAKI†

Summary—**For the extension of the mode theory of the lossless periodically distributed parametric amplifier to the lossy case, a "conjugate circuit" is introduced in this paper. The conjugate circuit is an imaginary circuit which is obtained in the pass band by replacing each resistance in the original circuit with the negative resistance of the same magnitude. The orthogonality properties between the modes of the original circuit and those of the conjugate circuit are derived. The power gain and the noise figure of the amplifier are calculated, showing the usefulness of this mode theory in accounting for the spreading resistance of the semiconductor diode.**

Introduction

In a previous paper,[1] an operator T_θ was introduced for the analysis of the lossless periodically distributed parametric amplifiers. The operator T_θ is the product of a diagonal matrix expressing the pumping phase relation and the T matrix of the basic section of the amplifier. The eigenvectors of T_θ are called the modes of the amplifier. The orthogonality properties among the modes were proved, using one of the Manley-Rowe relations. However, the proof required that the circuit be lossless. In practical amplifiers the spreading resistance of the semiconductor diode cannot be neglected. Therefore, it is desired to obtain some substitutes for the orthogonal properties among the modes. For this purpose, a "conjugate circuit" is introduced in this paper. The orthogonality properties which exist between the modes of the original circuit and those of the conjugate circuit are proved, thereby showing that the mode theory remains useful even when the spreading resistance and the other losses of the circuit are taken into account.

* Manuscript received by the PGMTT, June 30, 1959; revised manuscript received, August 28, 1959.

† Inst. of Industrial Science, University of Tokyo, Chiba City, Japan.

[1] K. Kurokawa and J. Hamasaki, "Mode theory of lossless periodically distributed parametric amplifiers," IRE TRANS. ON MICROWAVE THEORY AND TECHNIQUES, vol. MTT-7, pp. 360–365; July, 1959.

The Operator T_θ

The equivalent circuit of the semiconductor diode is shown in Fig. 1. In this figure, r represents the spreading resistance, which is assumed to be independent of the frequency.

The relation between the current i flowing into the diode and the applied voltage v is

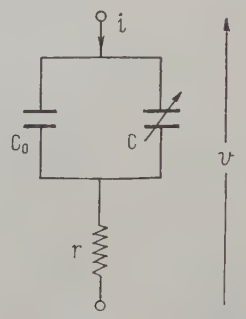

Fig. 1—Equivalent circuit of semiconductor diode.

$$\begin{bmatrix} i_1 \\ i_2^* \end{bmatrix} = \begin{bmatrix} j\omega_1 c_0, & j\omega_1 \frac{c}{2} \\ -j\omega_2 \frac{c^*}{2}, & -j\omega_2 c_0 \end{bmatrix} \begin{bmatrix} v_1 - ri_1 \\ v_2^* - ri_2^* \end{bmatrix} \tag{1}$$

where the subscripts 1 and 2 refer to the angular frequencies ω_1 and ω_2, respectively, and the pumping angular frequency ω_p is assumed to be $\omega_1+\omega_2$. Rewriting (1) in the form

$$\left\{ I + r \begin{bmatrix} j\omega_1 c_0, & j\omega_1 \frac{c}{2} \\ -j\omega_2 \frac{c^*}{2}, & j\omega_2 c_0 \end{bmatrix} \right\} \begin{bmatrix} i_1 \\ i_1^* \end{bmatrix} = \begin{bmatrix} j\omega_1 c_0, & j\omega_1 \frac{c}{2} \\ -j\omega_2 \frac{c^*}{2}, & -j\omega_2 c_0 \end{bmatrix} \begin{bmatrix} v_1 \\ v_2^* \end{bmatrix} \tag{2}$$

where I is a unit matrix, and then multiplying by

$$\left\{ I + r \begin{bmatrix} j\omega_1 c_0, & j\omega_1 \frac{c}{2} \\ -j\omega_2 \frac{c^*}{2}, & -j\omega_2 c_0 \end{bmatrix} \right\}^{-1}$$

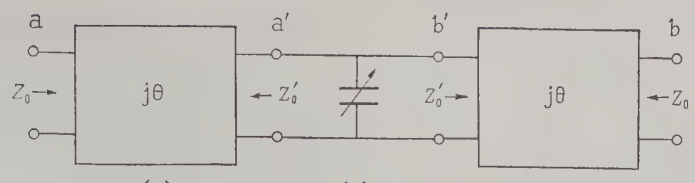

Fig. 2—Basic section of the amplifier.

from the left, we have

$$\begin{bmatrix} i_1 \\ i_2^* \end{bmatrix} \doteqdot \left\{ I - r \begin{bmatrix} j\omega_1 c_0, & j\omega_1 \frac{c}{2} \\ -j\omega_2 \frac{c^*}{2}, & -j\omega_2 c_0 \end{bmatrix} \right\} \begin{bmatrix} j\omega_1 c_0, & j\omega_1 \frac{c}{2} \\ -j\omega_2 \frac{c^*}{2}, & -j\omega_2 c_0 \end{bmatrix} \begin{bmatrix} v_1 \\ v_2^* \end{bmatrix}$$

$$= \left\{ \begin{bmatrix} j\omega_1 c_0, & j\omega_1 \frac{c}{2} \\ -j\omega_2 \frac{c^*}{2}, & -j\omega_2 c_0 \end{bmatrix} - r \begin{bmatrix} -\omega_1^2 c_0^2 + \omega_1\omega_2 \frac{|c|^2}{4}, & -\omega_1^2 \frac{c_0 c}{2} + \omega_1\omega_2 \frac{c c_0}{2} \\ \omega_1\omega_2 \frac{c^* c_0}{2} - \omega_2^2 \frac{c_0 c^*}{4}, & \omega_1\omega_2 \frac{|c|^2}{4} - \omega_2^2 c_0^2 \end{bmatrix} \right\} \begin{bmatrix} v_1 \\ v_2^* \end{bmatrix}. \quad (3)$$

In (3) we neglect the higher order terms of r which are assumed to be small. The c_0 in the first matrix on the right hand side of (3) is divided into two parts, each of which is included in the two terminal pair networks (a) and (b) of the basic section of the amplifier, which is shown in Fig. 2. The relation between the current I_c flowing into the remaining circuit (c) and the applied voltage V_c is

$$I_c = \begin{bmatrix} I_1 \\ I_2^* \end{bmatrix} = \begin{bmatrix} r\left(\omega_1^2 c_0^2 - \omega_1\omega_2 \frac{|c|^2}{4}\right), & j\omega_1 \frac{c}{2}\{1 + j(\omega_2 - \omega_1)c_0 r\} \\ -j\omega_2 \frac{c^*}{2}\{1 + j(\omega_2 - \omega_1)c_0 r\}, & r\left(\omega_2^2 c_0^2 - \omega_1\omega_2 \frac{|c|^2}{4}\right) \end{bmatrix} \begin{bmatrix} V_1 \\ V_2^* \end{bmatrix}. \quad (4)$$

The voltage and current at each terminal in Fig. 2 are, in terms of the incident waves (subscript i) and the reflected waves (subscript r),

$$\begin{aligned} V_a &= \sqrt{Z_0}(a_i + a_r), & V_a' &= \sqrt{Z_0'}(a_i e^{-j\theta} + a_r e^{j\theta}) \\ I_a &= \frac{1}{\sqrt{Z_0}}(a_i - a_r), & I_a' &= \frac{1}{\sqrt{Z_0'}}(a_i e^{-j\theta} - a_r e^{j\theta}) \\ V_b &= \sqrt{Z_0}(b_i + b_r), & V_b' &= \sqrt{Z_0'}(b_i e^{j\theta} + b_r e^{-j\theta}) \\ I_b &= \frac{1}{\sqrt{Z_0}}(b_i - b_r), & I_b' &= \frac{1}{\sqrt{Z_0'}}(b_i e^{j\theta} - b_r e^{-j\theta}) \end{aligned} \quad (5)$$

where the prime notation indicates the values of the (c) side terminals. Since the voltages at the (c) terminals must be equal,

$$V_a' = V_b' = V_c. \quad (6)$$

The equation of continuity is

$$I_a' = I_b' + I_c. \quad (7)$$

Using (4)–(7), we obtain the relation

$$B = TA \quad (8)$$

between the input vector A and the output vector B of the basic section, where

$$A = \begin{bmatrix} a_{i1} \\ a_{r1} \\ a_{i2}^* \\ a_{r2}^* \end{bmatrix}, \qquad B = \begin{bmatrix} b_{i1} \\ b_{r1} \\ b_{i2}^* \\ b_{r2}^* \end{bmatrix}, \quad (9)$$

$$T = \begin{bmatrix} (1-\sigma_1)e^{-2j\theta_1}, & -\sigma_1, & -j\omega_1 c Z e^{j(\theta_2^* - \theta_1)}, & -j\omega_1 c Z e^{-j(\theta_1 + \theta_2^*)} \\ \sigma_1, & (1+\sigma_1)e^{2j\theta_1}, & j\omega_1 c Z e^{j(\theta_1 + \theta_2^*)}, & j\omega_1 c Z e^{j(\theta_1 - \theta_2^*)} \\ j\omega_2 c^* Z e^{j(\theta_2^* - \theta_1)}, & j\omega_2 c^* Z e^{j(\theta_1 + \theta_2^*)}, & (1-\sigma_2)e^{2j\theta_2^*}, & -\sigma_2 \\ -j\omega_2 c^* Z e^{-j(\theta_1 + \theta_2^*)}, & -j\omega_2 c^* Z e^{j(\theta_1 - \theta_2^*)}, & \sigma_2, & (1+\sigma_2)e^{-2j\theta_2^*} \end{bmatrix}, \quad (10)$$

and

$$\sigma_1 = \frac{Z_{01}'}{2} r\left(\omega_1^2 c_0^2 - \omega_1\omega_2 \frac{|c|^2}{4}\right)$$

$$\sigma_2 = \frac{Z_{02}'^*}{2} r\left(\omega_2^2 c_0^2 - \omega_1\omega_2 \frac{|c|^2}{4}\right)$$

$$Z = \frac{\sqrt{Z'_{01}Z_{02}'^*}}{4}\{1 + j(\omega_2 - \omega_1)c_0 r\}. \tag{11}$$

Next, we shall consider the n similar circuits connected in cascade. The variable capacitor of each circuit has the pumping phase lagged by $2\theta_p$ (θ_p: real) from that of the preceding one. These circuits are represented by matrices similar to T except they have $ce^{-2j\theta_p}$, $ce^{-4j\theta_p}$ $\cdots$ in place of c. The pumping phase does not appear in σ_1, σ_2 and Z. Thus we can write the T matrix of the kth section in the form

$$I_\theta^{k-1} T I_\theta^{-(k-1)}$$

$$\tilde{T} = \begin{bmatrix} (1+\sigma_1)e^{2j\theta_1}, & -\sigma_1, & -j\omega_2 cZe^{j(\theta_1-\theta_2^*)}, & j\omega_2 cZe^{j(\theta_1+\theta_2^*)} \\ \sigma_1 & (1-\sigma_1)e^{-2j\theta_1}, & -j\omega_2 cZe^{-j(\theta_1+\theta_2^*)}, & j\omega_2 cZe^{j(\theta_2^*-\theta_1)} \\ j\omega_1 c^* Ze^{j(\theta_1-\theta_2^*)}, & -j\omega_1 c^* Ze^{-j(\theta_1+\theta_2^*)}, & (1+\sigma_2)e^{-2j\theta_2^*}, & -\sigma_2 \\ j\omega_1 c^* Ze^{j(\theta_1+\theta_2^*)}, & -j\omega_1 c^* Ze^{j(\theta_2^*-\theta_1)}, & \sigma_2, & (1-\sigma_2)e^{2j\theta_2^*} \end{bmatrix}. \tag{15}$$

---

where

$$I_\theta = \begin{bmatrix} e^{-j\theta_p} & 0 & 0 & 0 \\ 0 & e^{-j\theta_p} & 0 & 0 \\ 0 & 0 & e^{j\theta_p} & 0 \\ 0 & 0 & 0 & e^{j\theta_p} \end{bmatrix}. \tag{12}$$

The output vector of the amplifier is, therefore,

$$B = (I_\theta^{n-1} T I_\theta^{-n+1})(I_\theta^{n-2} T I_\theta^{-n+2}) \cdots (I_\theta T I_\theta^{-1}) TA$$
$$= I_\theta^n T_\theta^n A \tag{13}$$

where A is the input vector and

$$T_\theta = I_\theta^{-1} T \tag{14}$$

as in the previous paper.

Conjugate Circuit and Orthogonality Properties

From (13), we see that each eigenvector A_k of T_θ is independently transformed by the amplifier into $\lambda_k^n I_\theta^n A_k$, where λ_k is the eigenvalue of A_k. This is the result which we first obtained in the lossless case. In the lossless case, we had another useful result: there are orthogonality properties between the modes. Naturally, we wish to prove them. The proof requires, however, that the circuit be lossless, and this condition is not satisfied in the present case. Without the orthogonality properties, the mode theory loses most of its power. To get the substitutes, we shall introduce a conjugate circuit.[2]

The conjugate circuit is an imaginary circuit with θ_1^*, θ_2^*, $Z_{01}'^*$, $Z_{02}'^*$ and $-r$ in place of θ_1, θ_2, Z_{01}', Z_{02}' and r, respectively, of the original circuit. Assuming that the losses are small, we can obtain the conjugate circuit in the pass band of ω_1 and ω_2 by replacing each resistance in the original circuit by the negative resistance of the same magnitude. We shall use the symbol $\sim$ to indicate the complex conjugate transpose of the corresponding matrix for the conjugate circuit.

The T matrix of the basic section of the conjugate circuit is the matrix with θ_1^*, θ_2, $-\sigma_1^*$, $-\sigma_2^*$ and Z^* in place of θ_1, θ_2^*, σ_1, σ_2 and Z, respectively, of the T matrix given by (10). Its complex conjugate transposed matrix is

A little manipulation shows that

$$\tilde{T}\Omega^{-1}T = \Omega^{-1} \tag{16}$$

where

$$\Omega^{-1} = \begin{bmatrix} \frac{1}{\omega_1} & 0 & 0 & 0 \\ 0 & -\frac{1}{\omega_1} & 0 & 0 \\ 0 & 0 & -\frac{1}{\omega_2} & 0 \\ 0 & 0 & 0 & \frac{1}{\omega_2} \end{bmatrix}. \tag{17}$$

Since $T_\theta = I_\theta^{-1} T$,

$$\tilde{T}_\theta = \widetilde{I_\theta^{-1}T} = \tilde{T}\tilde{I}_\theta^{-1} = \tilde{T}I_\theta. \tag{18}$$

[2] The T-matrix of the conjugate circuit is closely related to the notion of the inverse of the conjugate operator in functional analysis. For the conjugate operator, the reader is referred to A. E. Taylor, "Introduction to Funcational Analysis," John Wiley and Sons, Inc., New York, N. Y., ch. 4, 1958. The waveguide directly related to the conjugate operator has been discussed in A. D. Bresler, G. H. Joshi, and N. Marcuvitz, "Orthogonality properties for modes in passive and active uniform wave guides," *J. Appl. Phys.*, vol. 29, pp. 794–799; May, 1958.

From (16) and (18), we obtain

$$\tilde{T}_\theta \Omega^{-1} T_\theta = \tilde{T} I_\theta \Omega^{-1} I_\theta^{-1} T = \tilde{T} \Omega^{-1} T = \Omega^{-1};$$

that is,

$$\tilde{T}_\theta \Omega^{-1} T_\theta = \Omega^{-1}. \tag{19}$$

This is the relation which corresponds to (27) in the previous paper.[1]

If A_l is an eigenvector of the operator T_θ,

$$(T_\theta - \lambda_l I) A_l = 0. \tag{20}$$

Taking the complex conjugate transpose of the corresponding relation for the conjugate circuit, we have

$$\tilde{A}_k (\tilde{T}_\theta - \tilde{\lambda}_k I) = 0 \tag{21}$$

where $\tilde{A}_k$ is the complex conjugate transpose of the eigenvector of the conjugate circuit, and $\tilde{\lambda}_k$ is the complex conjugate of the eigenvalue.

From (19)–(21), the following theorems can be derived in a similar way as for the lossless case (see Appendix).

Theorem 1: There is always an eigenvalue λ_k of T_θ, corresponding to an eigenvalue $\tilde{\lambda}_k$ of $\tilde{T}_\theta$, such that $\lambda_k = 1/\tilde{\lambda}_k$.

Theorem 2: If $l \neq k$, then A_l and $\tilde{A}_k$ are orthogonal in the sense that

$$\tilde{A}_k \Omega^{-1} A_l = 0. \tag{22}$$

Theorem 3: The corresponding modes $\tilde{A}_k$ and A_k are not orthogonal in the above sense; *i.e.*,

$$\tilde{A}_k \Omega^{-1} A_k \neq 0. \tag{23}$$

In the case of lossless amplifiers, the conjugate and original circuits are identical in the pass band of ω_1 and ω_2. Thus, $\tilde{A}_k$ is the complex conjugate transpose of the eigenvector of T_θ with the eigenvalue $1/\lambda_k^*$, leading to the same result obtained in the previous paper.

For the sake of convenience, we normalize the mode amplitudes so that we can rewrite (22) and (23) in the form

$$\tilde{A}_k \Omega^{-1} A_l = \delta_{kl} \tag{24}$$

where δ_{kl} is the Kronecker delta.

An arbitrary vector can be expressed as a sum of eigenvectors:

$$A = \sum \alpha_k A_k.$$

Multiplying by $\tilde{A}_k \Omega^{-1}$ from the left and using (24), we have

$$\alpha_k = \tilde{A}_k \Omega^{-1} A.$$

Therefore, for an arbitrary vector A, we obtain

$$A = \sum A_k (\tilde{A}_k \Omega^{-1} A). \tag{25}$$

Multiplying by T_θ^n from the left, we have

$$T_\theta^n A = \sum \lambda_k^n A_k (\tilde{A}_k \Omega^{-1} A). \tag{26}$$

Since A is an arbitrary vector, then

$$T_\theta^n = \sum \lambda_k^n A_k \cdot \tilde{A}_k \Omega^{-1}. \tag{27}$$

If $n = 1$,

$$T_\theta = \sum \lambda_k A_k \cdot \tilde{A}_k \Omega^{-1}. \tag{28}$$

This is the spectral representation of the operator T_θ.

Power Gain of the Amplifier

To obtain the expressions for the power gain of the amplifier, we need the solutions of the eigenvalue problem of the operator T_θ. We assume that

$$\theta_p = \theta_1 + \theta_2^* + \Delta\theta. \tag{29}$$

All the eigenvalues and the corresponding eigenvectors can be obtained by the method of perturbation. To the first order of approximation, they are

$$\lambda_1 = \left(1 - \frac{\sigma_1 + \sigma_2}{2} + \delta\right) e^{j(\theta_2^* - \theta_1)}, \quad \lambda_2 = (1 + \sigma_1 + j\Delta\theta) e^{j(3\theta_1 + \theta_2^*)}$$

$$A_1 = \begin{bmatrix} \sqrt{\frac{\omega_1}{2}} \\ \frac{-j}{2\sin 2\theta_1}(\delta + \epsilon - \sigma_1)\sqrt{\frac{\omega_1}{2}} \\ j\frac{\delta + \epsilon}{\delta_0}\sqrt{\frac{\omega_2}{2}}\frac{c^*}{|c|}e^{-j\theta_p} \\ \frac{-1}{2\sin 2\theta_2^*}(\delta - \epsilon - \sigma_2)\frac{\delta + \epsilon}{\delta_0}\sqrt{\frac{\omega_2}{2}}\frac{c^*}{|c|}e^{-j\theta_p} \end{bmatrix}, \quad A_2 = \begin{bmatrix} \frac{j\sigma_1}{2\sin 2\theta_1}\sqrt{\omega_1} \\ \sqrt{\omega_1} \\ \frac{\delta_0}{2\sin 2\theta_1}\sqrt{\omega_2}\frac{c^*}{|c|}e^{-j\theta_p} \\ \frac{-\delta_0}{2\sin 2(\theta_1 + \theta_2^*)}\sqrt{\omega_2}\frac{c^*}{|c|}e^{-j\theta_p} \end{bmatrix},$$

$$\lambda_3 = \left(1 - \frac{\sigma_1 + \sigma_2}{2} - \delta\right) e^{j(\theta_2^* - \theta_1)}, \qquad \lambda_4 = (1 + \sigma_2 - j\Delta\theta) e^{-j(\theta_1 + \theta_2^*)},$$

$$A_3 = \begin{bmatrix} \sqrt{\frac{\omega_1}{2}} \\ \frac{j}{2 \sin 2\theta_1} (\delta - \epsilon + \sigma_1) \sqrt{\frac{\omega_1}{2}} \\ -j \frac{\delta - \epsilon}{\delta_0} \sqrt{\frac{\omega_2}{2}} \frac{c^*}{|c|} e^{-j\theta_p} \\ \frac{-1}{2 \sin 2\theta_2^*} (\delta + \epsilon + \sigma_2) \frac{\delta - \epsilon}{\delta_0} \sqrt{\frac{\omega_2}{2}} \frac{c^*}{|c|} e^{-j\theta_p} \end{bmatrix}, \qquad A_4 = \begin{bmatrix} \frac{\delta_0}{2 \sin 2\theta_2^*} \sqrt{\omega_1} \frac{c}{|c|} e^{j\theta_p} \\ \frac{-\delta_0}{2 \sin 2(\theta_1 + \theta_2^*)} \sqrt{\omega_1} \frac{c}{|c|} e^{j\theta_p} \\ \frac{-j\sigma_2}{2 \sin 2\theta_2^*} \sqrt{\omega_2} \\ \sqrt{\omega_2} \end{bmatrix} \tag{30}$$

where

$$\delta_0 = \sqrt{\omega_1 \omega_2}\, |c|\, Z$$

$$\epsilon = \left(\frac{\sigma_1 - \sigma_2}{2} - j\Delta\theta\right)$$

$$\delta = \sqrt{\delta_0^2 + \epsilon^2}. \tag{31}$$

The first and third modes are the forward waves traveling from the input to the output. $-(\sigma_1+\sigma_2)/2$ in the eigenvalues roughly represents the attenuation due to the spreading resistance. On the other hand, δ roughly represents the amplification due to the variable capacitor. If the real part of $(\sigma_1+\sigma_2)/2$ is larger than the real part of δ, no net amplification takes place. It is worth noting that the components of the first and third modes are considerably influenced by the spreading resistance if $\sigma_1 \neq \sigma_2$.

The second and fourth modes are the backward waves, which remain almost unaffected. The magnitude of the eigenvalues are greater than unity, which means that these backward waves attenuate with propagation.

Replacing θ_1, θ_2^*, $\Delta\theta$, σ_1, σ_2 and Z in (30) by θ_1^*, θ_2, $\Delta\theta^*$, $-\sigma_1^*$, $-\sigma_2^*$ and Z^*, respectively, and interchanging the subscripts $k=1$ and 3, we have the eigenvectors of the conjugate circuit. The complex conjugate transposes of the eigenvectors multiplied by appropriate normalization constants give $\tilde{A}_k$'s:

$$\tilde{A}_1 = \left[\frac{\delta_0^2}{\delta(\delta + \epsilon)} \sqrt{\frac{\omega_1}{2}}, \frac{-j}{2 \sin 2\theta_1} \frac{\delta_0^2}{\delta(\delta + \epsilon)} (\delta + \epsilon - \sigma_1) \sqrt{\frac{\omega_1}{2}}, j \frac{\delta_0}{\delta} \sqrt{\frac{\omega_2}{2}} \frac{c}{|c|} e^{j\theta_p}, \right.$$

$$\left. \frac{-1}{2 \sin 2\theta_2^*} \frac{\delta_0}{\delta} (\delta - \epsilon - \sigma_2) \sqrt{\frac{\omega_2}{2}} \frac{c}{|c|} e^{j\theta_p}\right],$$

$$\tilde{A}_2 = \left[\frac{-j\sigma_1}{2 \sin 2\theta_1} \sqrt{\omega_1}, -\sqrt{\omega_1}, \frac{-\delta_0}{2 \sin 2\theta_1} \sqrt{\omega_2} \frac{c}{|c|} e^{j\theta_p}, \frac{\delta_0}{2 \sin 2(\theta_1 + \theta_2^*)} \sqrt{\omega_2} \frac{c}{|c|} e^{j\theta_p}\right],$$

$$\tilde{A}_3 = \left[\frac{\delta_0^2}{\delta(\delta - \epsilon)} \sqrt{\frac{\omega_1}{2}}, \frac{j}{2 \sin 2\theta_1} \frac{\delta_0^2}{\delta(\delta - \epsilon)} (\delta - \epsilon + \sigma_1) \sqrt{\frac{\omega_1}{2}}, -j \frac{\delta_0}{\delta} \sqrt{\frac{\omega_2}{2}} \frac{c}{|c|} e^{j\theta_p}, \right.$$

$$\left. \frac{-1}{2 \sin 2\theta_2^*} \frac{\delta_0}{\delta} (\delta + \epsilon + \sigma_2) \sqrt{\frac{\omega_2}{2}} \frac{c}{|c|} e^{j\theta_p}\right],$$

$$\tilde{A}_4 = \left[\frac{\delta_0}{2 \sin 2\theta_2^*} \sqrt{\omega_1} \frac{c^*}{|c|} e^{-j\theta_p}, \frac{-\delta_0}{2 \sin 2(\theta_1 + \theta_2^*)} \sqrt{\omega_1} \frac{c^*}{|c|} e^{-j\theta_p}, \frac{-j\sigma_2}{2 \sin 2\theta_2^*} \sqrt{\omega_2}, \sqrt{\omega_2}\right]. \tag{32}$$

Eqs. (30) and (32) satisfy the orthogonality theorems (24) to the first order of approximation.

Substituting (30) and (32) in (26) and then using (13), we obtain four equations.

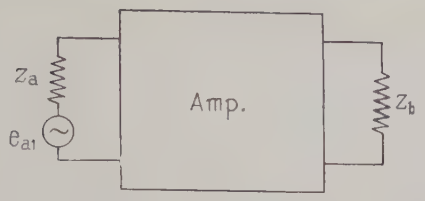

Fig. 3—Input and output conditions of the amplifier.

$$b_{i1} = e^{-jn\theta_p}\left\{\left(\frac{\lambda_1^n}{2}\frac{\delta-\epsilon}{\delta}+\frac{\lambda_3^n}{2}\frac{\delta+\epsilon}{\delta}\right)a_{i1} + \left(\frac{\lambda_1^n}{2}-\frac{\lambda_3^n}{2}\right)(-j)\frac{\delta_0}{\delta}\sqrt{\frac{\omega_1}{\omega_2}}\frac{c}{|c|}e^{j\theta_p}a_{i2}^* + \cdots\right\},$$

$$b_{r1} = e^{-jn\theta_p}\{\lambda_2^n a_{r1} + \cdots\},$$

$$b_{i2}^* = e^{jn\theta_p}\left\{\left(\frac{\lambda_1^n}{2}-\frac{\lambda_3^n}{2}\right)j\frac{\delta_0}{\delta}\sqrt{\frac{\omega_2}{\omega_1}}\frac{c^*}{|c|}e^{-j\theta_p}a_{i1} + \left(\frac{\lambda_1^n}{2}\frac{\delta+\epsilon}{\delta}+\frac{\lambda_3^n}{2}\frac{\delta-\epsilon}{\delta}\right)a_{i2}^* + \cdots\right\},$$

$$b_{r2}^* = e^{jn\theta_p}\{\lambda_4^n a_{r2}^* + \cdots\}. \tag{33}$$

From the input and output conditions shown in Fig. 3, we have

$$a_{i1} = \frac{\sqrt{Z_{01}}}{Z_{01}+Z_{a1}}e_{a1} + \Gamma_{a1}a_{r1}, \qquad a_{i2}^* = \Gamma_{a2}^* a_{r2}^*$$

$$b_{r1} = \Gamma_{b1}b_{i1}, \qquad b_{r2}^* = \Gamma_{b2}^* b_{i2}^* \tag{34}$$

where the Γ's are the reflection coefficients:

$$\Gamma_a = \frac{Z_a - Z_0}{Z_a + Z_0}, \qquad \Gamma_b = \frac{Z_b - Z_0}{Z_b + Z_0}. \tag{35}$$

There are altogether eight equations with eight unknown quantities a_{i1}, a_{i2}^*, $\cdots$, b_{r1}, b_{r2}^*. The simultaneous equations can be solved by the standard method of algebra. Neglecting the higher-order terms of δ and of the reflection coefficients, we have, for example,

$$b_{i1} \doteq \frac{\left(\frac{\lambda_1^n+\lambda_3^n}{2}-\frac{\epsilon}{\delta}\frac{\lambda_1^n-\lambda_3^n}{2}\right)e^{-jn\theta_p}\frac{\sqrt{Z_{01}}}{Z_{01}+Z_{a1}}e_{a1}}{1-\left(\frac{\lambda_1^n+\lambda_3^n}{2}-\frac{\epsilon}{\delta}\frac{\lambda_1^n-\lambda_3^n}{2}\right)\frac{\Gamma_{a1}\Gamma_{b1}}{\lambda_2^n}-\left(\frac{\lambda_1^n+\lambda_3^n}{2}+\frac{\epsilon}{\delta}\frac{\lambda_1^n-\lambda_3^n}{2}\right)\frac{\Gamma_{a2}^*\Gamma_{b2}^*}{\lambda_4^n}}. \tag{36}$$

We define the power gain G of the amplifier to be the ratio of the power dissipated in the load at ω_1 to the available power from the generator:

$$G = |b_i|^2 \operatorname{Re}\left\{\frac{Z_{01}}{|Z_{01}|}(1-|\Gamma_{b1}|^2 + \Gamma_{b1}-\Gamma_{b1}^*)\right\} \Big/ \frac{|e_{a1}|^2}{4\operatorname{Re}Z_{a1}}. \tag{37}$$

Substituting (36) in (37), we can obtain the power gain in its explicit form. For simplicity, we neglect the imaginary part of θ_1, θ_2, δ and Z_{01}, as well as the difference between σ_1 and σ_2 ($\sigma=\sigma_1=\sigma_2$). Furthermore, if the Γ's are all zero, (37) becomes

$$G_0 = \left\{\cosh^2 n\delta + \left(\frac{\Delta\theta}{\delta}\right)^2 \sinh^2 n\delta\right\} e^{-2n\sigma}. \tag{38}$$

If $\Gamma_{a1}\Gamma_{b1}$ and $\Gamma_{a2}^*\Gamma_{b2}^*$ are small but not zero,

$$G = \frac{G_0\frac{4\operatorname{Re}Z_{a1}}{|Z_{01}+Z_{a1}|^2}\operatorname{Re}\{Z_{01}(1-|\Gamma_{b1}|^2+\Gamma_{b1}-\Gamma_{b1}^*)\}}{(1-\sqrt{G_0}\operatorname{Re}R)^2+(\sqrt{G_0}\operatorname{Im}R)^2} \tag{39}$$

where

$$R = e^{-n\sigma}\{e^{-jn(4\theta_1+\Delta\theta)}\Gamma_{a1}\Gamma_{b1}e^{j\phi} + e^{jn(4\theta_2^*+\Delta\theta)}\Gamma_{a2}^*\Gamma_{b2}^*e^{-j\phi}\} \tag{40}$$

$$\tan\phi = \frac{\Delta\theta}{\delta}\tanh n\delta. \tag{41}$$

For a numerical example, let

$$Z_{01}' = Z_{02}' = 30\Omega, \quad |c| = 3.5\mu\mu F, \quad c_0 = 5\ \mu\mu F$$

$$\omega_1 \doteq \omega_2 \doteq 670\text{ mc}, \quad r = 1\Omega, \quad n = 16.$$

Then, from (11) and (31), we obtain

$$\delta_0 = 0.11 \qquad \sigma = 0.006.$$

Inserting these values in (38), we get

$$G_0 = 8.7\text{ db} \quad \text{for } \Delta\theta = 0$$

$$G_0 = 5.7\text{ db} \quad \text{for } \Delta\theta = 6°$$

which can be compared with the second experimental result by Engelbrecht.[3] If $|R| = 0.1$, because of the de-

[3] R. S. Engelbrecht, "Nonlinear-Reactance (Parametric) Traveling-Wave Amplifiers for UHF," Presented at the 1959 Solid-State Circuits Conf., Philadelphia, Pa., February, 1959.

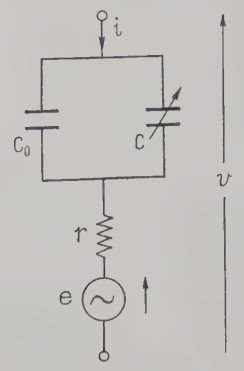

Fig. 4—Equivalent circuit of semiconductor diode with noise voltages.

nominator of (39), G varies from 6.6 db to 11.5 db, when $\Delta\theta = 0$, depending on the phase of R.

It should be recognized that (38) and (39) are the results of a three-frequency analysis. If the other sidebands are capable of propagating, the gain may be reduced.

Noise Figure Calculation

For the calculation of the noise figure, we must consider the noise voltages e_1 and e_2 due to the spreading resistance of the semiconductor diode. On the other hand, for simplicity, we neglect the losses, hence the noise generated in the two terminal pair networks (a) and (b) in Fig. 2.

The equivalent circuit of the diode is shown in Fig. 4. Replacing v_1 and v_2^* in (2) by $v_1 - e_1$ and $v_2^* - e_2^*$ respectively, we have the matrix representation of this equivalent circuit. Using this representation in a similar way as for (8), we get the relation

$$B = TA + KN \tag{42}$$

between the input vector A and the output vector B of the basic section of the amplifier, where T is given by (10) and

$$N = \begin{bmatrix} e_1 \\ e_2^* \end{bmatrix}.$$

$$K = \begin{bmatrix} \frac{1}{2}\sqrt{Z_{01}'}e^{-j\theta_1}\left\{j\omega_1 c_0 + r\left(\omega_1^2 c_0^2 - \omega_1\omega_2\frac{|c|^2}{4}\right)\right\}, & \frac{1}{2}\sqrt{Z_{01}'}e^{-j\theta_1}j\omega_1\frac{c}{2}\{1 + j(\omega_2 - \omega_1)c_0 r\} \\ -\frac{1}{2}\sqrt{Z_{01}'}e^{j\theta_1}\left\{j\omega_1 c_0 + r\left(\omega_1^2 c_0^2 - \omega_1\omega_2\frac{|c|^2}{4}\right)\right\}, & -\frac{1}{2}\sqrt{Z_{01}'}e^{j\theta_1}j\omega_1\frac{c}{2}\{1 + j(\omega_2 - \omega_1)c_0 r\} \\ -\frac{1}{2}\sqrt{Z_{02}'^*}e^{j\theta_2^*}j\omega_2\frac{c^*}{2}\{1 + j(\omega_2 - \omega_1)c_0 r\}, & -\frac{1}{2}\sqrt{Z_{02}'^*}e^{j\theta_2^*}\left\{j\omega_2 c_0 - r\left(\omega_2^2 c_0^2 - \omega_1\omega_2\frac{|c|^2}{4}\right)\right\} \\ \frac{1}{2}\sqrt{Z_{02}'^*}e^{-j\theta_2^*}j\omega_2\frac{c^*}{2}\{1 + j(\omega_2 - \omega_1)c_0 r\}, & \frac{1}{2}\sqrt{Z_{02}'^*}e^{-j\theta_2^*}\left\{j\omega_2 c_0 - r\left(\omega_2^2 c_0^2 - \omega_1\omega_2\frac{|c|^2}{4}\right)\right\} \end{bmatrix}. \tag{43}$$

Next, we shall consider the amplifier with n sections. For the mth section, c is replaced by $ce^{-2(m-1)j\theta_p}$ and K becomes

$$I_\theta^{m-1} K J_\theta^{-m+1}$$

where

$$J_\theta = \begin{bmatrix} e^{-j\theta_p} & 0 \\ 0 & e^{j\theta_p} \end{bmatrix}. \tag{44}$$

Therefore, the output vector of the amplifier is

$$\begin{aligned} B &= (I_\theta^{n-1} T I_\theta^{-n+1})(I_\theta^{n-2} T I_\theta^{-n+2}) \cdots (I_\theta T I_\theta^{-1}) TA \\ &\quad + \sum_{m=1}^{n} (I_\theta^{n-1} T I_\theta^{-n+1})(I_\theta^{n-2} T I_\theta^{-n+2}) \cdots \\ &\qquad \cdot (I_\theta^{m} T I_\theta^{-m}) I_\theta^{m-1} K J_\theta^{-m+1} N_m \\ &= I_\theta^{n} T_\theta^{n} A + \sum_{m=1}^{n} I_\theta^{n} T_\theta^{n-m} I_\theta^{-1} K J_\theta^{-m+1} N_m, \end{aligned} \tag{45}$$

where A is the input vector of the amplifier and N_m represents the matrix N with the noise voltages e_{m1} and e_{m2}^* of the mth diode. Using (27), we rewrite (45) in the form

$$\begin{aligned} B = I_\theta^{n} \Big\{ &\sum_k \lambda_k^{n} A_k (\tilde{A}_k \Omega^{-1} A) \\ &+ \sum_{m=1}^{n} \sum_k \lambda_k^{n-m} A_k (\tilde{A}_k \Omega^{-1} I_\theta^{-1} K J_\theta^{-m+1} N_m) \Big\}. \end{aligned} \tag{46}$$

Substituting (30) and (32) in (46), we obtain

$$b_{i1} \doteqdot e^{-jn\theta_p}\left[\left(\frac{\lambda_1^n+\lambda_3^n}{2}-\frac{\epsilon}{\delta}\frac{\lambda_1^n-\lambda_3^n}{2}\right)a_{i1}\right.$$
$$-\frac{\lambda_1^n-\lambda_3^n}{2}j\frac{\delta_0}{\delta}\sqrt{\frac{\omega_1}{\omega_2}}\frac{c}{|c|}e^{j\theta_p}a_{i2}^*+\cdots$$
$$+\sum_{m=1}^{n}\left\{\left(\frac{\lambda_1^{n-m}+\lambda_3^{n-m}}{2}-\frac{\epsilon}{\delta}\frac{\lambda_1^{n-m}-\lambda_3^{n-m}}{2}\right)m_{i1}\right.$$
$$\left.\left.-\frac{\lambda_1^{n-m}-\lambda_3^{n-m}}{2}j\frac{\delta_0}{\delta}\sqrt{\frac{\omega_1}{\omega_2}}\frac{c}{|c|}e^{j\theta_p}m_{i2}^*\right\}\right.$$
$$\left.+\cdots\right] \quad (47)$$

with similar equations for the other components, where

$$I_\theta^{-1}KJ_\theta^{-m+1}N_m=\begin{bmatrix}m_{i1}\\ m_{r1}\\ m_{i2}^*\\ m_{r2}^*\end{bmatrix}\doteqdot\begin{bmatrix}\frac{1}{2}j\omega_1\sqrt{Z_{01}'}e^{-j\theta_1}\left\{c_0e^{jm\theta_p}e_{m_1}+\frac{c}{2}e^{(2-m)j\theta_p}e_{m_2}^*\right\}\\ -\frac{1}{2}j\omega_1\sqrt{Z_{01}'}e^{j\theta_1}\left\{c_0e^{jm\theta_p}e_{m_1}+\frac{c}{2}e^{(2-m)j\theta_p}e_{m_2}^*\right\}\\ -\frac{1}{2}j\omega_2\sqrt{Z_{02}'^*}e^{j\theta_2}\left\{\frac{c^*}{2}e^{(m-2)j\theta_p}e_{m_1}+c_0e^{-jm\theta_p}e_{m_2}^*\right\}\\ \frac{1}{2}j\omega_2\sqrt{Z_{02}'^*}e^{-j\theta_2}\left\{\frac{c^*}{2}e^{(m-2)j\theta_p}e_{m_1}+c_0e^{-jm\theta_p}e_{m_2}^*\right\}\end{bmatrix}. \quad (48)$$

For simplicity, hereafter we shall confine ourselves to the case in which we obtained (38): $\sigma=\sigma_1=\sigma_2$ and the reflection coefficients are all zero. Then, from (47), the noise output power becomes

$$N_0=\overline{b_{c1}b_{c1}}^*\doteqdot G_0kT\Delta f$$
$$+\left(\frac{|\lambda_1|^n-|\lambda_3|^n}{2}\right)^2\frac{\delta_0^2}{\delta^2}\frac{\omega_1}{\omega_2}kT\Delta f$$
$$+kT_r\Delta fr\left[\frac{1}{4}\left(\frac{|-|\lambda_1|^{2n}}{|-|\lambda_1|^2}+\frac{|-|\lambda_3|^{2n}}{|-|\lambda_3|^2}\right)\right.$$
$$\cdot\left\{\frac{\delta_0^2}{\delta^2}\left(c_0^2+\frac{|c|^2}{4}\right)(\omega_1^2Z_{01}'+\omega_1\omega_2Z_{02}')\right.$$
$$\left.+\frac{2\Delta\theta\delta_0}{\delta^2}c_0|c|\omega_1\omega_2\sqrt{\frac{\omega_1}{\omega_2}}\sqrt{Z_{01}'Z_{02}'}\right\}$$
$$+\frac{1}{2}\frac{|-|\lambda_1\lambda_3|^n}{|-|\lambda_1\lambda_3|}\left\{\left(c_0^2+\frac{|c|^2}{4}\right)\right.$$
$$\cdot\left(\omega_1^2Z_{01}'-\frac{\Delta\theta^2}{\delta^2}\omega_1^2Z_{01}'-\frac{\delta_0^2}{\delta^2}\omega_1\omega_2Z_{02}'\right)$$
$$\left.\left.-\frac{2\Delta\theta\delta_0}{\delta^2}c_0|c|\omega_1\omega_2\sqrt{\frac{\omega_1}{\omega_2}}\sqrt{Z_{01}'Z_{02}'}\right\}\right] \quad (49)$$

where

k = Boltzmann's constant,
Δf = the noise band width of the amplifier,
T = standard noise temperature, and
T_r = the equivalent noise temperature of the spreading resistance.

If $|\lambda_1|^{2n}\gg|\lambda_3|^{2n}$, as is usually the case, (49) becomes

$$N_0=G_0kT\Delta f+\frac{|\lambda_1|^{2n}}{\lambda}\frac{\delta_0^2}{\delta^2}\frac{\omega_1}{\omega_2}kT\Delta f+kT_r\Delta fr\frac{|\lambda_1|^{2n}}{4}$$
$$\cdot\frac{1}{2(\delta-\sigma)}\left\{\frac{\delta_0^2}{\delta^2}\left(c_0^2+\frac{|c|^2}{4}\right)(\omega_1^2Z_{01}'\times\omega_1\omega_2Z_{02}')\right.$$
$$\left.+\frac{2\Delta\theta\delta_0}{\delta^2}c_0|c|\omega_1\omega_2\sqrt{\frac{\omega_1}{\omega_2}}\sqrt{Z_{01}'Z_{02}'}\right\}. \quad (50)$$

In this case,

$$G_0\doteqdot\frac{1}{4}|\lambda_1|^{2n}\frac{\delta_0^2}{\delta^2}.$$

Dividing N_0 by $G_0kT\Delta f$, we obtain the noise figure F_0.

$$F_0=1+\frac{\omega_1}{\omega_2}+\frac{T_r}{T}\frac{rZ_{01}'\omega_1^2c_0^2}{2(\delta-\sigma)}\left\{\left(1+\frac{\omega_2}{\omega_1}\frac{Z_{02}'}{Z_{01}'}\right)\right.$$
$$\left.\cdot\left(1+\frac{|c|^2}{4c_0^2}\right)+\frac{2\Delta\theta}{\delta_0}\frac{|c|}{c_0}\sqrt{\frac{\omega_2}{\omega_1}}\sqrt{\frac{Z_{02}'}{Z_{01}'}}\right\}. \quad (51)$$

For a numerical example, we use the same values described in the previous section, and assume that $T_r=T$. Then (54) gives

$F_0=3.3$ db for $\Delta\theta=0$
$F_0=4.5$ db for $\Delta\theta=6°$.

Appendix

Theorems 1, 2, and 3 will be proved.
From (21), the determinant of $(\bar{T}_\theta-\bar{\lambda}_kI)$ vanishes:

$$\det(\bar{T}_\theta-\lambda_kI)=0. \quad (52)$$

Since det $T_\theta \neq 0$, $\tilde{\lambda}_k \neq 0$. From these relations, we have

$$\begin{aligned}\det (\tilde{T}_\theta - \tilde{\lambda}_k I) \det (\Omega^{-1} T_\theta) &= \det (\tilde{T}_\theta \Omega^{-1} T_\theta - \tilde{\lambda}_k \Omega^{-1} T_\theta) \\ &= \det (\Omega^{-1} - \tilde{\lambda}_k \Omega^{-1} T_\theta) \\ &= \det (\Omega^{-1} \tilde{\lambda}_k) \det \left(\frac{1}{\tilde{\lambda}_k} I - T_\theta \right) = 0.\end{aligned}$$

The final result is

$$\det \left(T_\theta - \frac{1}{\tilde{\lambda}_k} I \right) = 0. \tag{53}$$

From (53), it follows that there is always an eigenvalue $1/\tilde{\lambda}_k$ of T_θ, corresponding to an eigenvalue $\tilde{\lambda}_k$ to $\tilde{T}_\theta$, (Theorem 1).

We shall use the same subscript for the corresponding solutions of the eigenvalue problems of the two circuits:

$$\lambda_k = \frac{1}{\tilde{\lambda}_k}. \tag{54}$$

Multiplying (21) by $\Omega^{-1} T_\theta A_l$ from the right and using (19) and (20), we obtain

$$\left(\lambda_l - \frac{1}{\tilde{\lambda}_k} \right) \tilde{A}_k \Omega^{-1} A_l = 0. \tag{55}$$

If $\lambda_l \neq 1/\tilde{\lambda}_k$, (55) shows that $\tilde{A}_k \Omega^{-1} A_l = 0$. In the non-degenerate case, $\lambda_l \neq 1/\tilde{\lambda}_k$ for $k \neq l$. Thus, we obtain the desired orthogonality relation (Theorem 2):

$$\tilde{A}_k \Omega^{-1} A_l = 0, \qquad k \neq l. \tag{56}$$

In the degenerate case, $k \neq l$ does not necessarily mean that $\lambda_l \neq 1/\tilde{\lambda}_k$. However, we are justified in assuming (56), for it is always possible to introduce the degenerate eigenvectors in such a way as to secure the orthogonality.

Next, we expand $\Omega \tilde{A}_k^+$ by the eigenvectors A_l, where the symbol $^+$ indicates the complex conjugate transpose:

$$\Omega \tilde{A}_k^+ = \sum \alpha_l A_l.$$

Multiplying by $\tilde{A}_k \Omega^{-1}$ from the left and using (56), we have

$$\tilde{A}_k \tilde{A}_k^+ = \alpha_k \tilde{A}_k \Omega^{-1} A_k.$$

Since $\tilde{A}_k \neq 0$, the left hand side of the above equation is not zero. Thus we conclude that (Theorem 3):

$$\tilde{A}_k \Omega^{-1} A_k \neq 0. \tag{57}$$

Acknowledgment

The authors wish to thank M. Uenohara and R. S. Engelbrecht of Bell Telephone Labs., Inc., for valuable suggestions and J. D. Tebo, publication supervisor of the Whippany Laboratory for sending a reprint of the summary of R. S. Engelbrecht's paper. The continued support and encouragement of Prof. M. Hoshiai, Prof. N. Takagi and Prof. S. Saito have been greatly appreciated.

Action of a Progressive Disturbance on a Guided Electromagnetic Wave*

J. C. SIMON†

I. Introduction

A.

A PROBLEM often encountered in wave physics concerns the interaction of various types of waves, and the energy transfer from one wave to another.

In the particular case of waves of the same nature, "modes" can be distinguished in such a way that a wave can be represented as a sum of these modes. Their essential character is that the energy associated with each does not vary with time. It is also said that these modes are not "coupled." This, for instance, is the case of waves guided in an electric waveguide, of mechanical vibration in a bar, and of energy levels in quantum physics.

Although this possibility of decomposition in "normal modes" corresponds to particular physical conditions, it has made it possible to deduce general notions of a fundamental character essential to the physicist. In the most general case, the normal modes are said to be coupled that is the energy passes from one to the other, so much that this decomposition into normal modes appears to be indispensable in deducing physical concepts.

* Original manuscript received by the PGMTT, May, 1959; revised manuscript received, September 25, 1959.

† Département de Physique Applique, C.S.F., Orsay, S.O., France.

Such problems are treated by using a method of approximation known as the "theory of perturbations." Much could no doubt be said about the validity of the application of this method and the convergence of solutions. Nevertheless, it is frequently employed in many fields of physics, in particular, in quantum physics such as solid-state physics or atomic physics. It has enabled physicists to obtain results which have been confirmed by experiment. We shall therefore apply it to the particular problem of the action of a progressive disturbance on an electromagnetic wave.

B.

One of the principal applications of the study of the action of a progressive disturbance will, as we shall see, concern parametric amplification.

What are the essentials of parametric amplification? They consist of a signal to be amplified, of frequency $\omega/2\pi$, "pumping" energy at frequency $\omega_1/2\pi$, and a medium whose characteristics vary in function with the applied pumping energy. Usually, "pumping" energy and signal energy are of the same kind, electromagnetic for instance. It is always implied that it is the "pumping" energy alone which acts on the medium, to the exclusion of the signal or of the resulting beats.

Therefore, it appears legitimate to say that *it is the medium modified by the pumping which acts on the signal.* Pumping can therefore be ignored in formulating the problem which in any case becomes much clearer physically.

A modification of the medium may be produced by something other than an electromagnetic wave—by a mechanical wave, for instance, as in the case of heat photons and X-rays.

Thus, the following scheme may be adopted. Because of its energy, the pumping modifies the medium (ϵ or μ variable as a function of the pumping field). Knowing the modification of the medium, an action on the signal can be deduced. *This point of view is, of course, legitimate only because the Maxwell equations are linear for the signal, which is assumed not to act on the medium* (for small signals approximation, see Section V, B).

Modification of a medium can be obtained in various ways. In the case of electromagnetic pumping energy, it is naturally necessary that the characteristics ϵ or μ vary with the level of the field. *The medium is said to be nonlinear.* This is obtained in general only for rather high pumping energy, or, in any case, energy much greater than that of the incident signal.

Action on a nonlinear medium of an electromagnetic field in order to modify appreciably the characteristics of the medium is a difficult problem. It must be dealt with if the problems of parametric amplification are to be fully solved.

However, in the case of a progressive pumping wave, it appears physically plausible that the modification of the medium is akin to a sinusoidal disturbance accompanying the pumping wave, at least as a first approximation. For this reason the disturbance of the medium will be described by the relations (1) or (1′). It should be noted that such a disturbance can arise only if the medium "follows" the electromagnetic field at the frequency of the pumping wave. This condition limits parametric amplification at the higher frequencies.

Section II

A. Establishing the General Propagation Equation

Consider a three dimensional medium, such that $\mu=\mu_0=c^{te}$, $\epsilon_0=c^{te}$:

$$\epsilon = \epsilon_0 + \epsilon_1 \cos(\omega_1 t - \bar{k}_1 \cdot \bar{r}). \tag{1}$$

The components of $\bar{r}$ are the direction cosines of direction $\bar{k}_1(0, 0, k_1)$.

The Maxwell equations are written:

$$\nabla \times \overline{E} = -\frac{\partial \overline{B}}{\partial t} \tag{2}$$

$$\nabla \times \overline{H} = \frac{\partial \overline{D}}{\partial t} \tag{4}$$

$$\nabla \cdot \overline{B} = 0 \tag{3}$$

$$\nabla \cdot \overline{D} = 0. \tag{5}$$

Eliminating $\overline{H}$ and $\overline{B}=\mu_0\overline{H}$ from (2) and (4), we have

$$\nabla \times \nabla \times \overline{E} = -\mu_0 \frac{\partial^2 \overline{D}}{\partial t^2} = \nabla(\nabla \cdot \overline{E}) - \nabla^2 \overline{E}. \tag{6}$$

Assume $E_z=0$. As ϵ does not vary following directions x and y, (5) becomes $\nabla \cdot \overline{E}=0$; under these conditions (6) takes the form

$$\nabla^2 \overline{E} = \mu_0 \frac{\partial^2 \overline{D}}{\partial t^2} \cdot \tag{7}$$

It should be noted that formulas corresponding to a variable permeability are written in similar fashion if similar hypotheses can be made on μ. Let

$$\epsilon = \epsilon_0 = \text{constant and } \mu = \mu_0 + \mu_1 \cos(\omega_1 t - \bar{k}_1 \bar{r}). \tag{1′}$$

Taking $H_z=0$ we have

$$\nabla^2 \overline{H} = \epsilon_0 \frac{\partial^2 \overline{B}}{\partial t^2} \cdot \tag{7′}$$

B. Introduction of Boundary Conditions

The conditions in cases where one of the two parameters ϵ or μ is variable are satisfied by TEM modes guided in the direction O_z. This, in particular, is the case if the guiding structure consists of two plane walls of zero impedance, and of two perpendicular walls of infinite impedance. A portion of a plane wave can be propagated in such a guided structure. In the case of the usual waveguide with zero impedance walls, it is the variable ϵ case, magnetic mode, which satisfies simply the boundary conditions. Let us deal with this case, from which the preceding case is easily deduced.

Take a metallic waveguide with sides a and b. The magnetic modes satisfy $E_z=0$ and $\nabla\cdot\overline{E}=0$ (see Fig. 1). Let H_{01} be the fundamental mode

$$\begin{cases} E_x = E_0 \sin\dfrac{\pi y}{b} P \\ E_y = 0 \\ E_z = 0 \end{cases} \quad (8) \qquad \begin{cases} H_x = 0 \\ \mu_0 \dfrac{\partial H_y}{\partial t} = -\dfrac{\partial E_x}{\partial z} \\ \mu_0 \dfrac{\partial H_z}{\partial t} = -\dfrac{\partial E_x}{\partial y} \end{cases} \quad (9)$$

with $P=\exp -j(\omega t-kz)$.

Eqs. (8) and (9) are valid when the waveguide is filled with a homogeneous material. In order to make it valid in the case where ϵ satisfies (1), we write:

$$E_x = E_0 \sin\frac{\pi y}{b} P \cdot \sum_{-\infty}^{+\infty} a_n \exp - jn(\omega_1 t - k_1 z). \quad (8')$$

Eqs. (2) and (4) are satisfied if (6) is satisfied.

Since (5) is satisfied because of the choice of $\overline{E}$, (6) takes the form of (7). If (7) is satisfied, $\overline{H}$ is deduced from $\overline{E}$ by group (9), which is deduced from (2). It is easy to verify that the boundary conditions are also satisfied.

The term under the exponential is written:

$$(\omega + n\omega_1)t - (k + nk_1)z.$$

If ω_1 is of the order of ω, rigorously speaking, it would be necessary to introduce modes of higher order, H_{0p}, since the latter could be propagated.

Let us restrict ourselves to the case of a sum of modes H_{01}. Transfer (8′) into (7), which is written:

$$\frac{\partial^2 E_x}{\partial y^2} + \frac{\partial^2 E_x}{\partial z^2} = \mu_0 \frac{\partial t^2}{\partial t^2} \left\{ [\epsilon_0 + \epsilon_1 \cos(\omega_1 t - k_1 z)] E_x \right\}, \quad (7)$$

and transform the cosine into an exponential sum, ordinating in n. The resulting equation will be satisfied if the coefficients of the variable terms are all zero.

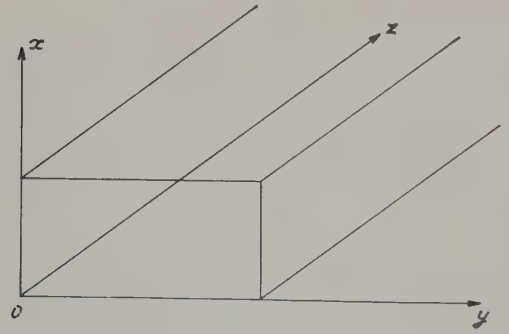

Fig. 1

For this we must have

$$\left[\epsilon_0 - \frac{(k+nk_1)^2 + \dfrac{\pi^2}{b^2}}{\mu_0(\omega + n\omega_1)^2}\right] a_n + \frac{\epsilon_1}{2}(a_{n-1} + a_{n+1}) = 0. \quad (10)$$

Verification: make $\epsilon_1=0$. We have only one coefficient $a_n\neq 0$, *i.e.*, a_0, if

$$\omega^2\epsilon_0\mu_0 - \frac{\pi^2}{b^2} - k^2 = 0, \quad (11)$$

but

$$\omega^2\epsilon_0\mu_0 = k_0^2 \quad \left(k_0 = \frac{2\pi}{\lambda_0};\ \lambda_0 = \text{wavelength in vacuum}\right)$$

and (11) becomes

$$k_0^2 - k^2 = \frac{\pi^2}{b^2}. \quad (11')$$

C. The Perturbation Method

The solution of (7) has become the solution of a system of an infinity of homogeneous equations with an infinite number of unknowns. Such a process is often employed in mathematical physics. It is the one used, for instance, in solid-state physics,[1] or in quantum physics when a solution is sought for the perturbed Schrödinger equation.[2] Historically, astronomers Mathieu and Hill were the first to use such a mathematical technique.[3]

The system whose general equation is given by (10) has a solution only if the determinant is zero. We then have to find the values of ω and k which make an infinite determinant zero. The general problem is very complex, so we shall only introduce approximations which will give the result simply.

Examination of (10) shows that the a_n coefficient bracket is large compared to $\epsilon_1/2$ coefficient of the term $a_{n-1}+a_{n+1}$. It is desirable to obtain an expression for a_n in which ϵ_1 may be considered as being infinitely small. This is the "perturbation method."

For instance, let us try to solve the system step by step, taking two a_n, a_0 and a_1. We establish that a_n tends to infinity. It is possible that a_n tends to zero for n infinite positive or infinite negative, but not for both. This, of course, is due to the fact that the system determinant is not zero.

Assume a_n infinitely small compared to a_0 in $\epsilon_1^{|n|}$ and ignore infinitely small terms of an order greater than 2.

[1] See section 40 of [2].
[2] See section 2 of [1].
[3] See Chapter 19 of [3].

We shall then say that we are using the perturbation method of order 2. From the physics point of view, this means ignoring beats of order greater than $+1$ and -1.

Only three equations of the type of (10) are involved; those corresponding to $n=-1$, 0, and $+1$. That is to say

$$[n=-1]a_{-1}+\frac{\epsilon_1}{2}a_0=0 \tag{12}$$

$$[n=0]a_0+\frac{\epsilon_1}{2}(a_{-1}+a_{+1})=0 \tag{13}$$

$$[n=+1]a_1+\frac{\epsilon_1}{2}a_0=0. \tag{14}$$

Making these three equations compatible, we have

$$[n=0]-\frac{\epsilon_1^2}{4}\left[\frac{1}{[n=+1]}+\frac{1}{[n=-1]}\right]=0. \tag{15}$$

Eq. (15) connects ω and k as a function of parameters ω_1, k_1 and ϵ_1/ϵ_0.

In order to simplify the discussion without changing the physical conclusions, let us restrict ourselves to the case of the ideal TEM mode, already mentioned—that of a waveguide which has two walls of zero impedance and two of infinite impedance. All that is needed is to write in (10) $1/b=0$. Eq. (15) is written, remembering that $k_0^2=\epsilon_0\mu_0\omega^2$,

$$\left(1-\frac{k^2}{k_0^2}\right)-\frac{\epsilon_1^2}{4\epsilon_0^2}\cdot\left[\frac{1}{1-\dfrac{(k+k_1)^2}{k_0^2\left(1+\dfrac{\omega_1}{\omega}\right)^2}}+\frac{1}{1-\dfrac{(k-k_1)^2}{k_0^2\left(1-\dfrac{\omega_1}{\omega}\right)^2}}\right]=0.$$

Let

$$\frac{k}{k_0}=X;\qquad \frac{k_1}{k_0}=X_1;\qquad \frac{\epsilon_1^2}{4\epsilon_0^2}=Z;\qquad \frac{\omega_1}{\omega}=\Omega.$$

We have

$$\frac{1}{Z}=\frac{1}{1-X^2}\left[\frac{1}{1-\left(\dfrac{X+X_1}{1+\Omega}\right)^2}+\frac{1}{1-\left(\dfrac{X-X_1}{1-\Omega}\right)^2}\right]. \tag{16}$$

D. The Various Solutions

Because of the approximations of the perturbation theory, (16) may give correct results only for small and obviously positive values of Z, and for $|X|\sim 1$. It should be noted that (16), $Z=f(X)$, does not change if X and X_1 change to $-X$ and $-X_1$. This only means changing the sense of the axis Oz, thus changing nothing in the physical conditions. From this, it is possible to restrict the study of the approximation $Z=f(X)$ near the point $X=+1$, $Z=0$.

Eq. $f_x=0$ is satisfied for six values of X:

$$\pm 1; \qquad -X_1\pm(1+\Omega); \qquad +X_1\pm(1-\Omega).$$

In general, around $X=1$ there is a real solution, and one only, to $Z_0=f(X)$. This solution is real and little different from unity; the value of k is real and little different from k_0. This is no longer the case if one of the preceding roots is close to unity. Complex solutions of $Z_0=f(X)$ in X can appear. This will naturally happen only in the presence of double or triple roots. Let us examine the various possible cases:

1) $1=-X_1+1+\Omega$ $\quad X_1=\Omega$ triple root (see 3)
2) $1=-X_1-1-\Omega$ $\quad X_1=-2-\Omega$ double root
3) $1=X_1+1-\Omega$ $\quad X_1=\Omega$ triple root (see 1)
4) $1=X_1-1+\Omega$ $\quad X_1=2-\Omega$ double root.

It is easy to prove that the solutions corresponding to point $(-1, 0)$ are deduced from the latter by changing X_1 to $-X_1$; that is, by a simple change of the orientation of the axis Oz (see Fig. 2).

We shall therefore examine the case of triple roots 1) and 3), and the cases of double roots 2) and 4).

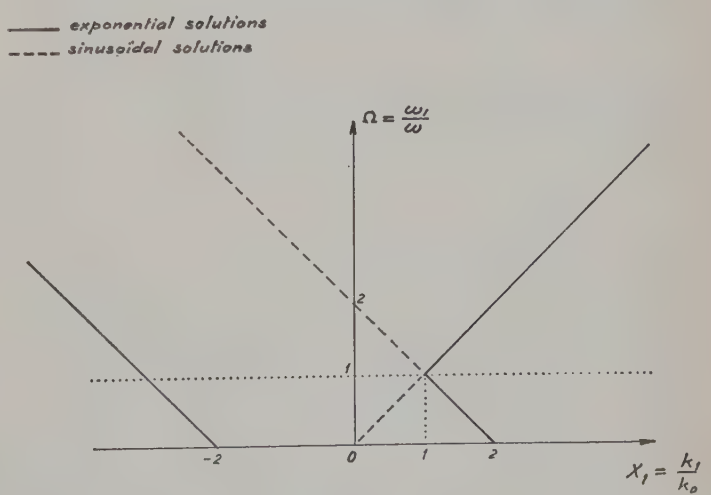

Fig. 2

E. Remarks

The relation 1) or 3) can be written

$$\frac{k_1}{\omega_1} = \frac{k_0}{\omega} = \frac{k_1 + k_0}{\omega_1 + \omega} = \frac{k_0 - k_1}{\omega - \omega_1}.$$

The field formula (8′) shows that it is written, in general, in the form of the sum of three waves corresponding to $n=-1$, $n=0$, $n=+1$.

If ϵ_1 is very small compared to ϵ_0, k is very little different from k_0, to within the perturbation term of k, the three waves in question have phases respectively equal to

$$(\omega - \omega_1)t - (k_0 - k_1)z;\ \omega t - k_0 z;\ (\omega + \omega_1)t - (k_0 + k_1)z.$$

Relation 1) therefore means that *these three waves have equal phase velocities.*

Similarly, the relations 2) and 4) are written:

$$\frac{k_1 + k_0}{\omega_1 + \omega} = -\frac{k_0}{\omega} \tag{2a}$$

$$\frac{k_1 - k_0}{\omega_1 - \omega} = -\frac{k_0}{\omega}. \tag{4a}$$

In these cases, waves $n=0$ and $n=+1$ or $n=-1$ have phase velocities which have *equal×absolute value but of opposite signs.* Physicists say that this concerns the Bragg phenomenon, and, in the cases considered previously, the *Bragg interference of the first order.*

Thus, the general formula for the Bragg phenomenon corresponds to the formula

$$\left(\frac{k_0 + nk_1}{\omega + n\omega_1}\right)^2 = \left(\frac{k_0}{\omega}\right)^2;$$

n is the order of the interference. Physically, this means that the wave with the phase factor $(\omega+n\omega_1)t - (k_0+nk_1)z$ and the wave $\omega t - k_0 z$ which correspond respectively to the terms n and 0 in the development of (8′), have phase velocities which have equal×absolute value. From the calculation point of view, the consequence of the above relation is that among (12), (13) and (14), equations corresponding to ranks n and 0 have equal coefficients. *The system is degenerate.*

Section III

A. Double Root Cases

In this case, one of the brackets of (12) or (14) is cancelled. It is no longer possible to say that the corresponding value of a_{+1} or a_{-1} is small compared to the value of a_0. If, for instance, it is the bracket corresponding to $n=+1$ which becomes zero when X is equal to unity, a_{+1} is of the order of a_0, but then a_{-1} is of the order of ϵ_1, and is therefore negligible compared to a_0 and a_1. Eqs. (12), (13) and (14) are reduced to (13) and (14) in which a_{-1} has been made zero. In quantum physics this solution is termed degenerate. We have seen that it corresponds to the Bragg interference case.

B. Case $X_1 = -2-\Omega$

It is the bracket corresponding to $n=+1$ which becomes zero if X tends towards unity. We shall assume that a_{+1} is of the order of a_0 and that a_{-1} is negligible. Eqs. (13) and (14) alone are to be considered and are written:

$$[n=0]a_0 + \frac{\epsilon_1}{2}a_1 = 0 \tag{13′}$$

$$[n=+1]a_1 + \frac{\epsilon_1}{2}a_0 = 0. \tag{14′}$$

In order that they shall be compatible, we must have

$$[n=1][n=0] - \frac{\epsilon_1^2}{4} = 0. \tag{15′}$$

Using the notation previously adopted,

$$\frac{k}{k_0} = X; \qquad \frac{k_1}{k_0} = X_1; \qquad \frac{\epsilon_1^2}{4\epsilon_0^2} = Z; \qquad \frac{\omega_1}{\omega} = \Omega;$$

we have

$$Z = (1 - X^2)\left[1 - \left(\frac{X + X_1}{1 + \Omega}\right)^2\right].$$

Replacing X_1 by its value and neglecting infinitely small terms of order 2 and beyond, we have with $\alpha = \pm 1$; $j^2 = -1$,

$$\frac{k}{k_0} = 1 + \alpha j \frac{\epsilon_1}{4\epsilon_0}\sqrt{1 + \frac{\omega_1}{\omega}}. \tag{17}$$

Let us calculate the corresponding values of the field. Inserting the value of X in either (13′) or (14′), ϵ_1 disappears. This justifies the hypothesis that a_0 and a_1 are of the same order, and we have

$$\frac{a_1}{a_0} = +\alpha j\sqrt{1 + \frac{\omega_1}{\omega}}. \tag{18}$$

Finally, the value of the electric field can be written in the form:

$$E_x = a \exp -\alpha k_0 z \frac{\epsilon_1}{4\epsilon_0}\sqrt{1 + \frac{\omega_1}{\omega}}\left[\exp -j(\omega t - k_0 z) + \alpha j\sqrt{1 + \frac{\omega_1}{\omega}} \exp -j[(\omega + \omega_1)t - (k_1 + k_0)z]\right]. \tag{19}$$

It can be easily verified that the result is not fundamentally changed by a change of phase on the wave of phase $\omega t - k_0 z$ and therefore equally on $(\omega_1 t - k_1 z)$. Terms in ω and $\omega+\omega_1$ are still in quadrature and are given by (18), the ratio k/k_0 being given by (17). Let us write

$$\sqrt{1 + \frac{\omega_1}{\omega}} = b; \qquad \frac{\epsilon_1}{4\epsilon_0}\sqrt{1 + \frac{\omega_1}{\omega}} = \mu.$$

We have:

$$E_x = a \exp - \alpha\mu z k_0[\cos(\omega t - k_0 z) + \alpha b \sin[(\omega + \omega_1)t - (k_0 + k_1)z]]. \quad (20)$$

$$Hy = \frac{ak_0}{\mu_0\omega} \exp - \alpha\mu z k_0[\cos(\omega t - k_0 z) + \alpha b \sin[(\omega + \omega_1)t - (k_0 + k_1)z]]. \quad (21)$$

Eq. (21) is obtained by inserting (20) in the second part of (9), taking into account the relation (2a), which can be written

$$\frac{k_1 + k_0}{\omega_1 + \omega} = -\frac{k_0}{\omega},$$

and neglecting the term in ϵ_1/ϵ_0. The general expression for the field is written in the form of the sum of two terms corresponding to the values $\alpha = +1$ and $\alpha = -1$, each having a coefficient which, as we shall see, depends on the boundary conditions. For instance:

$$E_x = a_1\phi_{+1}(z) \exp - \mu k_0 z + a_2\phi_{-1}(z) \exp \mu k_0 z. \quad (20')$$

$\phi(z)$, equal to the bracket in (20), in which α has been made equal to $+1$ or to -1, is a periodic function of z_0. We find a general expression in accordance with Floquet's theorem [3].

Let us now try to adapt these solutions to a non-perturbed medium. First, it should be noted that (20) and (21) show that the solution comprises two waves circulating in opposite directions, one of frequency ω in the positive sense, the other of frequency $\omega+\omega_1$ in the negative sense.

Let $\epsilon = \epsilon_0$ everywhere except in the segment $OA = z_0$, where it satisfies (1). The incident wave is the wave P_ω, such that $E_x = a \cos(\omega t - k_0 z)$. In segment OA only two groups of waves can exist. Each one of these groups consists of two waves, circulating in opposite directions, of frequencies $\omega/2\pi$ and $\omega+\omega_1/2\pi$. One decreases, and the other increases exponentially with z. They must come into accord in planes O and A. Because of the direction of propagation, it is possible to add only a wave $P_{\omega+\omega 1}$ of frequency $\omega+\omega_1/2\pi$ for $z<0$ and a wave P_ω'' of frequency $\omega/2\pi$ for $z>z_0$. In order to satisfy the boundary conditions the wave $P_{\omega+\omega 1}$ must become zero for $z=z_0$.

Neglecting terms in ϵ_1/ϵ_0, the boundary conditions are easily satisfied in the general case and make it possible to adopt the scheme of Fig. 3. One case of particular interest occurs when z is sufficiently large so that $\mu k_0 z_0$ is large. In this case P_ω'' is negligible, and it is only necessary to consider the group of waves with a negative exponential in order to satisfy the boundary conditions. By equating the electric and magnetic fields at the right and left of plane $z=0$, we have $a=a_1$. And if P_ω and $P_{\omega+\omega 1}$ represent the powers of the incident and reflected waves, we have

$$\frac{P_\omega}{\omega} = \frac{P_{\omega+\omega_1}}{\omega+\omega_1}. \quad (22)$$

The reflected wave is of frequency $\omega+\omega_1/2\pi$ and (22) shows that the ratio of the reflected to the incident waves is in the ratio of the frequencies.

The physical interpretation is simple. Let $\omega_1 = 0$, and we have $k_1 = 2k_0$. The medium is modulated sinusoidally at the spatial period of $\lambda_0/2$. It is well known that in this case the incident wave is reflected if the disturbance is large enough, and that in the disturbed medium the field is represented by two equal waves propagated in opposite directions and damped exponentially. Physicists designate this a case of *Bragg interference of the first order*, while for filter specialists it is a case of *a stopped band.*

When ω_1 differs from zero, things happen as if the medium moved toward negative values of z (in Fig. 3 wave P_1). The reflected wave is now at the upper frequency $\omega+\omega_1/2\pi$. The incident wave appears to be reflected by a moving mirror. This is a *Doppler effect.*

Finally, (22) is familiar to quantum physicists. It shows that to an incident photon of power $(h/2\pi)\omega$ there corresponds a reflected photon of power $h/2\pi(\omega+\omega_1)$. The number of photons is preserved.

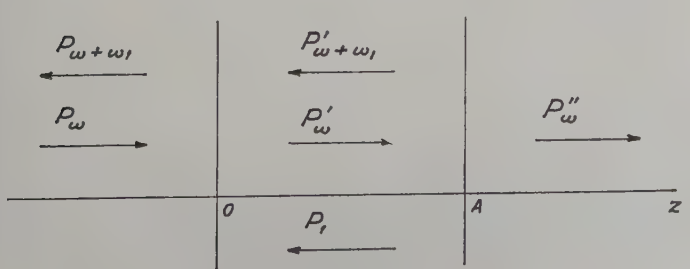

Fig. 3

C. Balance of Power

The reflected power is greater than the incident power. Energy has been transferred, obviously from the wave P_1 of the medium. Let us examine the balance of power in a slice dz with an abscissa less than z_0.

We can write:

$$\nabla\cdot(\overline{E}\times\overline{H}) = \overline{H}\cdot\nabla\times\overline{E} - \overline{E}\cdot\nabla\times\overline{H},$$

from which, using (2) and (4):

$$\nabla\cdot(\overline{E}\times\overline{H}) = -\overline{E}\cdot\frac{\partial\overline{D}}{\partial t} - \overline{H}\cdot\frac{\partial\overline{B}}{\partial t}. \quad (23)$$

Rigorously speaking, in order to establish (23) it would be necessary to consider the electric current density J[4].

[4] See section 2.19 of [4].

Term $\overline{E}\cdot\overline{J}$ would then appear in the first member of (23). But, in the case under consideration $\overline{J}$ is zero in the dielectric medium, and on the conducting walls the product $\overline{E}\cdot\overline{J}$ is obviously zero. Integrating over the volume V, we have

$$\int_S (\overline{E}\times\overline{H})_n\, dS = -\int_V \left(\overline{E}\frac{\partial\overline{D}}{\partial t}+\overline{H}\frac{\partial\overline{B}}{\partial t}\right)dV. \quad (24)$$

Let τ_1 represent the first member of (24), and τ_2 the second member. τ_2 is written

$$-\tau_2 = \frac{1}{2}\int_V \frac{\partial}{\partial t}(\epsilon E^2+\mu H^2)dV + \frac{1}{2}\int_V E^2\frac{\partial\epsilon}{\partial t}dV. \quad (25)$$

Eq. (25) differs from the usual formula with ϵ constant because of the second integral. If the fields expressed by (20) and (21) are inserted in (25), and if the average value of τ_2 is calculated over a sufficiently long interval of time, we have

$$\bar{\tau}_2 = +\frac{\alpha}{4}b\omega_1\epsilon_1 E_0^2 dz,$$

which arises exclusively from the second integral of (25). Further,

$$\tau_1 = \int_S E_0^2\frac{k}{\mu_0\omega}\exp -2\alpha\mu z k_0 \cdot[\cos^2(\omega t-kz)-\alpha^2 b^2\sin^2[(\omega+\omega_1)t-(k+k_1)z]].$$

Taking the average value of τ_1 we have

$$\bar{\tau}_1 = dzE_0^2\cdot 2\alpha\mu k_0\cdot\frac{k}{\mu_0\omega}\frac{1}{2}[b^2-1], \quad (26)$$

but

$$b=\sqrt{1+\frac{\omega_1}{\omega}};\quad k^2=\epsilon_0\mu_0\omega^2;$$

$$\mu=\frac{\epsilon_1}{4\epsilon_0}\times\sqrt{1+\frac{\omega_1}{\omega}},$$

and naturally, $\bar{\tau}_1=\bar{\tau}_2$. This verification shows that the fields actually satisfy the equations and also that τ, given by

$$\tau = \frac{1}{2}\int_V E^2\frac{\partial\epsilon}{\partial t}dV, \quad (27)$$

represents the work done by the medium, τ_1 being equal to the flux of the Poynting vector, or to the energy carried away by the electromagnetic wave. Eq. (26) shows that *this energy is proportional to* ϵ_1/ϵ_0, ω_1 *and to the incident energy.*

We have implicitly assumed that the medium was capable of supplying energy without becoming modified. Naturally this is only an approximation, all the closer to reality as the quantity of energy is small. This is the case of weak incident energy—*a case of "approximation for small signals."*

D. Case $X_1=2-\Omega$

The calculations are similar to those for the previous case. But now it is the bracket corresponding to $n=-1$ which becomes zero if X tends towards unity. Eqs. (12) and (13) alone are to be considered, a_{+1} being negligible. The equation which gives k in terms of the other parameters is written

$$Z=(1-X^2)\left[1-\left(\frac{X-X_1}{1-\Omega}\right)^2\right]. \quad (28)$$

Replacing X_1 by its value, we have for $\alpha=\pm 1$:

$$\frac{k}{k_0}=1+\alpha j\frac{\epsilon_1}{4\epsilon_0}\sqrt{1-\frac{\omega_1}{\omega}} \quad \text{if } \omega_1<\omega \quad (29)$$

$$\frac{k}{k_0}=1+\alpha\frac{\epsilon_1}{4\epsilon_0}\sqrt{\frac{\omega_1}{\omega}-1} \quad \text{if } \omega_1>\omega. \quad (30)$$

The solutions corresponding to $\omega_1<\omega_0$ or $\omega_1>\omega_0$ are now of a different kind; one is exponential, the other purely sinusoidal. The ratio a_{-1}/a_0 is written:

$$\frac{a_{-1}}{a_0}=\alpha j\sqrt{1-\frac{\omega_1}{\omega}} \quad \text{if } \omega_1<\omega \quad (31)$$

$$\frac{a_{-1}}{a_0}=\alpha\sqrt{\frac{\omega_1}{\omega}-1} \quad \text{if } \omega_1>\omega. \quad (32)$$

E. $\omega_1<\omega$

The electric and magnetic fields, for

$$\sqrt{1-\frac{\omega_1}{\omega}}=b;\quad \frac{\epsilon_1}{4\epsilon_0}\sqrt{1-\frac{\omega_1}{\omega}}=\mu,$$

where

$$\frac{k_1-k_0}{\omega_1-\omega}=-\frac{k_0}{\omega},$$

are written

$$E_x = a\exp-\alpha\mu z k_0[\cos(\omega t-k_0 z)+\alpha b\sin[(\omega-\omega_1)t-(k_0-k_1)z]], \quad (33)$$

$$Hy=\frac{ak_0}{\mu_0\omega}\exp-\alpha\mu z k_0[\cos(\omega t-k_0 z)-\alpha b\sin[(\omega-\omega_1)t-(k_0-k_1)z]]. \quad (34)$$

These expressions are very close to (20) and (21). Continuing with the reasoning in the previous paragraph, it is easily seen that the solution described by (33) and (34) consists of two waves P_ω and $P_{\omega-\omega_1}$ of frequency $\omega/2\pi$ and $\omega-\omega_1/2\pi$ circulating in opposite directions.

In the case of Fig. 4, if z_0 is sufficiently large, only wave $P_{\omega-\omega_1}$ at frequency $\omega-\omega_1/2\pi$, is reflected and the relation of the conservation of the number of photons is again satisfied:

$$\frac{P_\omega}{\omega} = \frac{P_{\omega-\omega_1}}{\omega-\omega_1}.$$

The perturbation wave P_1 of the medium moves in the positive direction. We are again dealing with Doppler reflection on a medium moving away instead of approaching, as in the previous case. The frequency as well as the energy decrease. Energy is imparted to the medium.

F. $\omega_1 > \omega$

The conditions of Fig. 4 are still valid. In the perturbed medium two groups of two waves of pulsation ω and $\omega_1-\omega$ can be propagated. A value of α corresponds to each one of these groups. For instance, the electric field is written

$$E_x = [a_1 \exp jk_0\mu z + a_2 \exp -jk_0\mu z] \exp -j(\omega t - k_0 z) + b[a_1 \exp + jk_0\mu z - a_2 \exp - jk_0\mu z] \cdot \exp + j[(\omega_1 - \omega)t + (k_0 - k_1)z], \quad (35)$$

where

$$b = \sqrt{\frac{\omega_1}{\omega} - 1} \quad \text{and} \quad \mu = \frac{\epsilon_1}{4\epsilon_0}\sqrt{\frac{\omega_1}{\omega} - 1}.$$

Writing that the boundary conditions are satisfied, in O and A we have

$$a_1 + a_2 = a, \quad (36)$$

$$a_1 \exp jk_0\mu z_0 - a_2 \exp - jk_0\mu z_0 = 0. \quad (37)$$

Hence,

$$a_1 = \frac{a}{2}[1 - jtgk_0\mu z_0]$$

$$a_2 = \frac{a}{2}[1 + jtgk_0\mu z_0].$$

Two cases are of special interest:

$$k_0\mu z_0 = +\kappa\pi \qquad a_1 = a_2 = \frac{a}{2}.$$

Eq. (35) becomes

$$E_x = a \cos k_0\mu z \cos(\omega t - k_0 z) - ab \sin k_0\mu z \sin[(\omega_1 - \omega)t + (k_0 - k_1)z]. \quad (38)$$

For $z=0$ or $z=z_0$, the first term of (38) alone remains, the incident wave is transmitted unchanged, and no wave of pulsation $\omega_1-\omega$ issues.

$$k_0\mu z_0 = \frac{\pi}{2} + \kappa\pi.$$

System (36), (37) is degenerate, and there is no solution for it unless $a=0$. In this case with $a_1=a_2=a'/2$, (35) is written

$$E_x = a' \sin k_0\mu z \sin(\omega t - k_0 z) + a'b \cos k_0\mu z \cos[(\omega_1 - \omega)t + (k_0 - k_1)z]. \quad (39)$$

It is possible to reconcile this solution in O and A by the method shown in Fig. 5: a wave P_ω'' toward the right and a wave $P_{\omega_1-\omega}$ toward the left. It should be noted that the relation

$$\frac{P_\omega''}{\omega} = \frac{P_{\omega_1-\omega}}{\omega_1 - \omega} \quad (40)$$

is verified, as is readily seen in (39).

Of course, it is still necessary to find out *how* such a solution can be established in the perturbed medium (note that a' is arbitrary. However, it can be asserted that the system oscillates spontaneously on both pulsations ω and $\omega_1-\omega$.

One special case is that in which $\omega_1=2\omega$, $k_1=0$. This calls to mind the classical problem of a self-excited oscillator.[5]

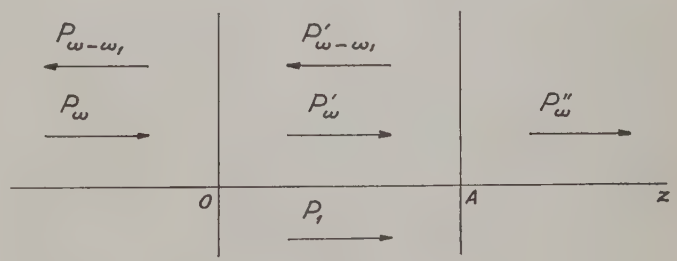

Fig. 4

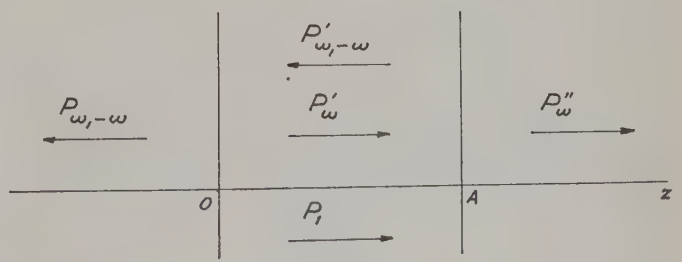

Fig. 5

[5] See paragraph 51 of [2].

Thus, in the case for which the relations

$$\begin{cases} \omega_1 > \omega \\ \dfrac{k_1}{k_0} = 2 - \dfrac{\omega_1}{\omega} \\ z_0 k_0 \dfrac{\epsilon_1}{4\epsilon_0}\sqrt{\dfrac{\omega_1}{\omega} - 1} = \dfrac{\pi}{2} + \kappa\pi \end{cases} \tag{41}$$

are satisfied, the element OA behaves as an oscillator at frequencies ω and $\omega_1-\omega$. For given values of ω_1 and k_1, this condition can arise fortuitously, since the domain allowed to the electromagnetic wave $(\omega_1 k_0)$ is generally considerable. These conditions are very similar to the condition of oscillation of the "carcinotron" tube.

Section IV

A. *Triple Root Case: Relation 1) or 3)*

The following is a case of triple degeneration.

$$X_1 = \Omega; \qquad \frac{k_1}{\omega_1} = \frac{k_0}{\omega_0}.$$

The three brackets of (12), (13) and (14) become zero, and coefficients a_0, a_1 and a_{-1} are of the same order. We must therefore consider (12), (13), and (14). In actual fact we shall examine not only the case where $k_1/\omega_1 = k_0/\omega$ but also neighboring cases, which will give an idea of the stability of the solution.

Let $X=1+\theta$; $X_1=\Omega+\theta_1$. The parameter

$$\theta_1 = \frac{k_1}{k_0} - \frac{\omega_1}{\omega}$$

is a measurement of the difference between the phase velocity of the unperturbed wave and that of the perturbation.

Eqs. (12), (13) and (14), which are in fact the fundamental equations of the problem, are written with these new variables, assuming that θ and θ_1 are small compared to unity:

$$\frac{\theta_1+\theta}{\Omega+1} a_1 - \frac{\sqrt{Z}}{2} a_0 = 0 \tag{42}$$

$$\theta a_0 - \frac{\sqrt{Z}}{2}(a_{-1} + a_{+1}) = 0 \tag{43}$$

$$\frac{\theta_1-\theta}{\Omega-1} a_{-1} - \frac{\sqrt{Z}}{2} a_0 = 0. \tag{44}$$

Eqs. (15) or (16), obtained by eliminating a_{-1}, a_0 and a_{+1} from these three equations, is written, with these new variables:

$$Z = 2\theta \frac{\theta^2 - \theta_1^2}{\theta - \theta_1\Omega}. \tag{45}$$

B. *Case $\Omega=\omega_1/\omega<1$*

Fig. 6 represents the function $Z=f(\theta)$ for case $\theta_1>$ zero. Case $\theta_1<0$ is deduced from the former by changing θ_1 to $-\theta_1$ and θ to $-\theta$ (symmetry with respect to the Z axis).

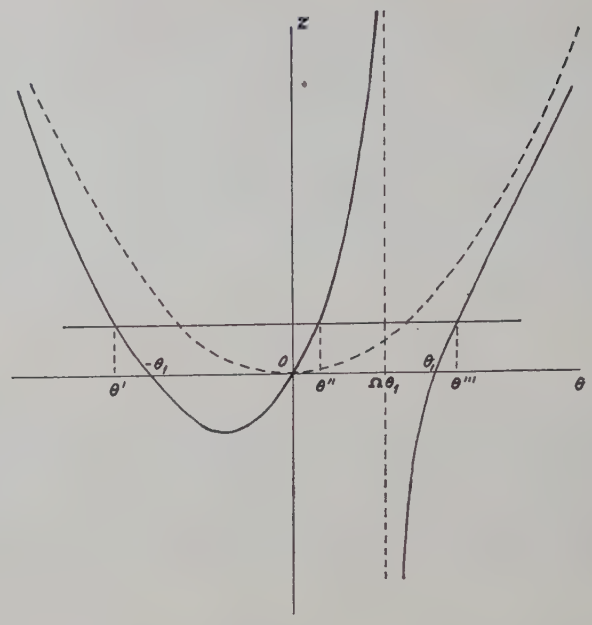

Fig. 6

For Z small and positive, there are three real roots θ', θ'' and θ''' for $Z=f(\theta)$. θ' is close to and less than $-\theta_1$; θ'' is close to zero and positive; θ''' is close to and greater than θ_1. If θ_1 tends toward zero, the solid curve blends with the parabola $Z=2\theta^2$ shown as a dashed line in Fig. 6, and the Z axis.

If θ_1 is small, the solutions $\theta_1 \neq 0$ are of a kind differing little from the solutions $\theta_1=0$—a group of slow waves, a group of fast waves, and a group with velocities very close to that of the unperturbed wave.

Let us therefore examine the case $\theta_1=0$. The two groups of fast and slow waves have for the value of k:

$$\frac{k}{k_0} = 1 + \alpha\frac{\epsilon_1}{2\sqrt{2}\epsilon_0} \qquad \text{with } \alpha = \pm 1. \tag{46}$$

The corresponding values of a are:

$$\frac{a_{-1}}{a_0} = \frac{\alpha}{\sqrt{2}}(1-\Omega) \tag{47}$$

$$\frac{a_{+1}}{a_0} = \frac{\alpha}{\sqrt{2}}(1+\Omega). \tag{48}$$

For the group of waves of the same velocity as the unperturbed wave $k=k_0$, we have for the solution of the system (42), (43), and (44): $a_0=0$, and $a_1+a_2=0$. The latter solution is of little interest since it does not agree with an incident wave of phase $\omega t-k_0 z$.

Therefore the two groups of waves described by the solutions (46), (47) and (48) must be used. All these waves are propagating in the same direction. Since their phase velocities are slightly different, they beat with one another. Actually, this produces a sinusoidal modulation of the amplitude at the various pulsations $\omega-\omega_1$; ω; $\omega+\omega_1$. The phase of this modulation is $k_0\mu z$ with $\mu=\epsilon_1/2\sqrt{2}\epsilon_0$.

Writing accord at O, we have for the field expression:

$$E_z = \cos k_0\mu z \exp -j(\omega t - k_0 z) + \frac{j}{\sqrt{2}} \sin k_0\mu z \cdot\left[\left(1-\frac{\omega_1}{\omega}\right)\exp -j[(\omega-\omega_1)t-(k-k_1)z] + \left(1+\frac{\omega_1}{\omega}\right)\exp -j[(\omega+\omega_1)t-(k+k_1)z]\right]. \quad (49)$$

The energy passes alternately from the vibration at frequency $\frac{\omega}{2\bar{u}}$ to the vibrations at frequencies $\frac{\omega-\omega_1}{2\bar{u}}$ and $\frac{\omega+\omega_1}{2\bar{u}}$.

C. Case $\Omega=\omega_1/\omega>1$.

In Fig. 7 the solid curve shows the variation of $Z=f(\theta)$ for $\theta_1>0$. The curve $\theta_1<0$ is deduced from the latter by symmetry with respect to the Z axis.

If $0<Z<\zeta$, or if $Z>\zeta'$, there are three real roots for θ. But if $\zeta>Z>\zeta'$, two of the real roots are transformed into complex roots.

Developing in the neighborhood of point A, we have:

$$X = 1+\frac{\theta_1}{\sqrt{3}}[1+\alpha j u], \quad (50)$$

with

$$\alpha = \pm 1; \qquad u^2 = \frac{2}{3}\left(\frac{Z}{z}-1\right); \qquad \zeta = \frac{4\theta_1^2}{3(\sqrt{3}\Omega-1)}$$

$$\Omega = \frac{\omega_1}{\omega}; \qquad \theta_1 = \frac{k_1}{k_0}-\frac{\omega_1}{\omega}; \qquad Z = \frac{\epsilon_1^2}{4\epsilon_0^2};$$

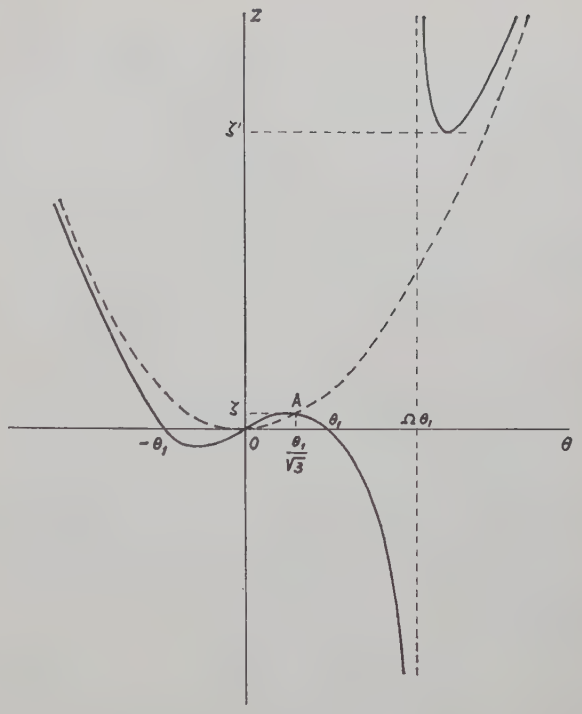

Fig. 7

the phase velocity of the exponential waves is always less than the phase velocity of the unperturbed wave, whether the perturbation phase velocity is lower or higher than the latter.

If Z is much greater than ζ, the value of k is no longer given by the approximation of (50) but is complex if $\zeta>Z>\zeta'$:

$$X = 1+v[1+\alpha j u]; \quad (54)$$

or

$$\frac{k}{k_0} = 1+\frac{1}{\sqrt{3}}\left(\frac{k_1}{k_0}-\frac{\omega_1}{\omega_0}\right)\left[1+\alpha\sqrt{\frac{2}{3}}\left(\frac{Z}{\zeta}-1\right)^{1/2}\right]. \quad (50')$$

The value of k is complex only if $Z>\zeta$, *i.e.*, assuming that 1 is small compared to $\sqrt{3}\Omega$.

$$\frac{\epsilon_1^2}{\epsilon_0^2} > 3\frac{\omega}{\omega_1}\left(\frac{k_1}{k_0}-\frac{\omega_1}{\omega}\right)^2. \quad (51)$$

Eq. (51) gives a threshold for the appearance of exponential solutions, tied to the depth of perturbation. This threshold is lower as ω_1 becomes greater than ω. It should be noted, however, that the solution is valid only if $\omega_1/\omega_1 \# k_0/\omega_0$.

The phase velocity V is the same if $\alpha=+1$ or $\alpha=-1$; it is given by:

$$\frac{1}{V} \# \frac{1}{v_0} + \frac{1}{\sqrt{3}}\frac{\omega_1}{\omega}\left(\frac{1}{v_1}-\frac{1}{v_0}\right). \quad (52)$$

Note that if

$$\begin{cases}\theta_1>0 & v_1<v_0 & v_1<V<v_0\\ \theta_1<0 & v_1>v_0 & V<v_0<v_1,\end{cases} \quad (53)$$

u and v must be calculated directly. But it can be stated that

$$\frac{\theta_1}{\sqrt{3}} < v < \frac{3\theta_1\Omega}{2}.$$

The relations expressed in (53) are still valid, and the exponential waves are always slower than the unperturbed wave.

A group of sinusoidal waves corresponding to the real root of $Z=f(\theta)$ must be associated with the two groups of exponential waves. The latter becomes

$$X \# 1-\theta_1-\frac{Z}{4\theta_1}(1+\Omega). \quad (55)$$

Verification is made of the fact that, since $\theta_1 \ll 1$, all the waves considered have positive phase velocities. The solution will therefore be obtained by bringing the fields into agreement in the plane $z=0$. We have

$$\left[\begin{array}{l} b_1 + b_2 + b_3 = a \\ b_1 \dfrac{\sqrt{3Z}}{2\theta_1} \dfrac{\Omega - 1}{\sqrt{3} - 1 - ju} + b_2 \dfrac{\sqrt{3Z}}{2\theta_1} \dfrac{\Omega - 1}{\sqrt{3} - 1 + ju} + b_3 \dfrac{\sqrt{Z}}{2\theta_1}(\Omega - 1) = 0 \\ b_1 \dfrac{\sqrt{3Z}}{2\theta_1} \dfrac{\Omega + 1}{\sqrt{3} + 1 + ju} + b_2 \dfrac{\sqrt{3Z}}{2\theta_1} \dfrac{\Omega + 1}{\sqrt{3} + 1 - ju} - b_3 \dfrac{2\theta_1}{\sqrt{Z}} = 0. \end{array}\right. \quad (56)$$

b_1, b_2 are the arbitrary coefficients affecting the groups of exponential waves $\alpha = +1$, $\alpha = -1$, and b_3 is the arbitrary coefficient of the group of sinusoidal waves. a is the coefficient of the incident wave. The group of equations in (56) is obtained by equating the field values for pulsations ω, $\omega - \omega_1$, $\omega + \omega_1$. The system in (56) of three equations with three unknowns has, in general, only one solution.

In the case $\theta_1 > 0$ it is the group of waves corresponding to $\alpha < 0$ with coefficient b_2, which increases exponentially; in the case $\theta_1 < 0$ it is the group of waves corresponding to $\alpha > 0$ with coefficient b_1. At first sight, there is no essential difference between the two types of solutions, except for an amplitude ratio which is different in the components at the various frequencies.

Section V

A. Physical Applications

The foregoing paragraphs have established a certain number of results which can find application, in particular, in the so-called domain of "parametric amplification."

Before passing to this domain, it is useful to recall a few features and conditions of the results obtained.

a) The application of the method of first order perturbations assumes, basically, that the neglected quantities do not influence the exact solution. In the cases dealt with, this assumes that ϵ_1/ϵ_0 is small, and that the components with pulsations $\omega + n\omega_1$ with $n > 1$ are negligible. In general, this approximation seems to be reasonable physically. This means that the spectrum decreases rapidly around pulsation ω.

This may not be the case for a Bragg interference of order greater than unity, described by the relation

$$\left(\frac{k_0 + nk_1}{\omega + n\omega_1}\right)^2 = \left(\frac{k_0}{\omega}\right)^2.$$

In fact, in an actual physical problem, it is necessary to take into consideration harmonics of high order.

b) It has been implicitly assumed that extraction of energy did not modify the perturbation. This can be true only for weak signals, or when it is possible to feed the medium at all points with energy of correct phase and amplitude. Otherwise, it would be necessary to consider the fact that the electromagnetic wave at ω would have some effect on the medium itself by weakening or strengthening the perturbation. (This is similar to the action of the perturbation on the electromagnetic wave by increasing or decreasing it.)

c) The cases examined have this in common—they all relate to Bragg interference of the first order. There is a clear feeling that it is in the case of Bragg interference that the interaction of the medium on the wave is strong, for it is then that the phase conditions which make the action cumulative are best obtained. A particularly striking example is that of cases 2) and 4) (Section III) for small values of ω_1/ω.

This has led to the exploration in plane k_1/k_0, ω_1/ω of two straight lines [cases 2) and 4)] and of a region around the first bisector [cases 1) and 3) and surroundings].

In order to exhaust the problem it would, in fact, be necessary to explore the whole plane. But then the question would be raised of the validity of the solutions obtained, which, it should be remembered, are only approximations.

B. Parametric Amplification

As was stated in Section I it is possible to approach the problems of parametric amplification by separating the difficulties. A pumping energy modifies the characteristics of the medium. Knowing the modification of the medium, an action on the signal is deduced. It is then unnecessary to introduce the pumping field in the equations. This is obvious in the case of an energy of a different character—mechanical for instance. Consider the case of an electromagnetic pumping energy: that is, the same kind as the signal.

Let E_1, H_1, E, H represent the pumping field of frequency $\omega_1/2\pi$ and signal field of frequency $\omega/2\pi$. By hypothesis, the Maxwell equations (2), (3), (4) and (5) and the boundary conditions are satisfied for the pumping field E_1, H_1 alone. In particular, (4) is written

$$\nabla \times \overline{H}_1 = \frac{\partial \epsilon \overline{E}_1}{\partial t}. \quad (57)$$

In (57) ϵ is a function of x, y, z and of the field E_1, H_1. In particular it can take the form described by (1).

It is now necessary to satisfy the Maxwell equations and the boundary conditions for the sum of the pumping and signal fields. But the Maxwell equations, as well as the boundary conditions, are linear. Since the pumping field already satisfies them, it is necessary and sufficient that the signal field satisfy them, provided that ϵ is formulated so that it can be determined by (57). This assumes that the addition of the signal field does not modify the value of ϵ. This condition, generally realized, can be described as an "approximation for small signals."

This being said, up to the moment and as far as we know, parametric amplification experiments have been performed only with lumped constants or with cavities. In the case of lumped constants, the circuits have always been tuned, which, as in the cavities case, is the same as repeating in time the action of the medium on the electromagnetic wave. More precisely, it is possible to pass easily from the case of a traveling wave to that of a cavity. Thus, as is well-known, in a cavity the field can generally be given the form of two traveling waves circulating in opposite directions so that the matching conditions may be obtained at the extremities. A transposition of the solutions found for traveling waves can therefore be made for cavity problems.

C.

Various analogies can be drawn from known cases of localized parametric amplification.

Up-converter: An input signal of frequency ω and "pumping" power of frequency ω_1 produce a signal of frequency $\omega+\omega_1$. The latter is amplified in power in the ratio $1+\omega_1/\omega$. This is what was found in Section III, B; in particular, see (22).

Down-converter: An input signal of frequency ω and "pumping" power of frequency ω_1 produce a signal of frequency $\omega-\omega_1$ (see Section III, D).

If $\omega L>\omega$, the resultant signal is diminished. Power loss is given by $1-\omega_1/\omega$ (see Section III, E).

If $\omega_1>\omega$, it is possible to obtain some amplification (see Section III, F). However, there is a tendency to instability; under certain conditions the system can break into oscillations, as in (41). As was already seen, this case approaches the conventional self-excited oscillator.

D.

The solution examined in Section IV should be compared to the operation of traveling wave tubes, especially in the case where $\omega_1>\omega$. (See the preceding paragraph.)

Thus, drawing an analogy between dielectric and electric current, we find that, as in the TWT case, it is in the neighborhood of equality of phase velocity of the cold wave and of the velocity of the electrons, and that it is possible to obtain exponential amplification. The amplified wave, sometimes designated "forced" wave, in TWT tubes always has a phase velocity which is less than the phase velocity of the "cold" wave [see (53)].

E.

It has been found (Section III, F) that under certain conditions described by (41) the perturbed medium may behave like an oscillator delivering energy at frequencies ω and $\omega_1-\omega$. It is interesting to point out that there is a strong analogy between the conditions in (41) and those which give the oscillating state for the UHF tube called "carcinotron" or backward wave oscillator.

VI. Conclusion

This investigation has made it possible to obtain the modes of action of a perturbation of the medium on a guided electromagnetic wave. This action is intense, especially when the so-called Bragg phase velocity conditions are obtained. It is then possible to have energy transfer into the electromagnetic wave.

In such a problem, the "boundary conditions" are as important as the solution of the propagation equation. In particular, the "accord conditions" between a perturbed and an unperturbed medium have set aside a certain number of solutions which could have been taken as actual amplifications. Such a state of affairs is found in certain plasma waves which cannot be "extracted" from the medium.

In the "approximation of small signals," it has been seen that the problem discussed is related to the problem of parametric amplification. Analogies have been found with cases of localized parametric amplification and with the conditions of traveling wave tubes and carcinotrons.

We do not claim to have completely dealt with parametric amplification for traveling waves, but it seems that this way of treating the problem may bring out the greatest number of related physical concepts. It appears that the complete solution of practical cases should be undertaken in accordance with the proposed scheme which makes it possible to separate the difficulties—action of the "pumping energy" on the medium, and action of the perturbed medium on the signal.

Acknowledgment

The author wishes to thank Harold Mintz of the Raytheon Company for his kind assistance in editing the English translation.

Bibliography

[1] J. C. Slater, "Interaction of waves in crystals," *Rev. Mod. Phys.*, vol. 30, sec. 2, p. 197; January, 1958.
[2] L. Brillouin and M. Parodi, "Wave Propagation in Periodic Media," Dunod and Masson, Paris, France.
[3] E. Whittaker and G. Watson, "Modern Analysis," Cambridge University Press, Cambridge, Eng.
[4] J. Stratton, "Electromagnetic Theory," McGraw-Hill Book Co., Inc., New York, N. Y.; 1941.
[5] H. Miyakawa, "Amplification and frequency conversion in propagating circuits," *Natl. Conv. Rec. Inst. Elec. Commun. Engrs., Japan*, p. 8; November, 1957.
[6] P. K. Tein and H. Suhl, "A traveling wave ferromagnetic amplifier," Proc. IRE, vol. 46, pp. 700–706; April, 1958.
[7] F. R. Morgenthaler, "Velocity modulation of electromagnetic waves," IRE Trans. on Microwave Theory and Techniques, vol. MTT-6, pp. 167–172; April, 1958.
[8] R. S. Engelbrecht, "A low noise nonlinear reactance traveling wave amplifier," presented at AIEE–IRE Solid State Device Res. Conf., Columbus, Ohio; June 18–20, 1958.
[9] P. K. Tien, "Parametric amplification and frequency mixing in propagating circuits," *J. Appl. Phys.*, vol. 29, pp. 1347–1357; September, 1958.
[10] K. Kurokawa and J. Hamasaki, "Mode theory of lossless periodically distributed parametric amplifiers," IRE Trans. on Microwave Theory and Techniques, vol. MTT-7, pp. 360–356; July, 1959.

Periodic and Guiding Structures at Microwave Frequencies*

A. F. HARVEY†

Summary—The paper reviews the properties of periodic and guiding structures which now play an important part in the operation of components, antennas, electron tubes and low-noise amplifiers. An account is first given of dispersive propagation in periodic-loaded lines, showing how the frequency characteristic breaks into pass and stop bands. The formation of forward- and backward-space harmonics and the effect of systematic modification of loading are examined. A description is then given of the various types of surface-wave structures including dielectric rods, dielectric-clad metals, and corrugated surfaces, as well as surface wave instruments and circuits. Practical slow-wave structures such as ladder lines, coupled cavities and helices are finally treated. The survey concludes with a bibliography.

List of Principal Symbols

(Rationalized mks Units are Used Unless Otherwise Indicated)

b = Linear dimension, meters.
c = Speed of light in vacuo = 2.997929×10^8 meters per second.
C = Capacitance, farads.
d = Linear dimension, meters.
E = Electric field, volts per meter.
H = Magnetic field intensity, ampere turns per meter ($=4\pi \times 10^{-3}$ oersted).
$H_n^{(1)}$ = Hankel function of the first kind and nth order.
$H_n^{(2)}$ = Hankel function of the second kind and nth order.
j = Operator, 90° rotational = $\sqrt{-1}$.
J_n = Bessel function of the first kind and nth order.
l = Length, meters.
l = Suffix for long.
L = Inductance, henry.
m = Integer.
n = Integer.
N = Number of resonators or elements.
p = Pitch of periodic structure, meters.
P = Power, watts.
Q_u = Unloaded Q factor.
r = Radial coordinate or suffix.
r_h = Radius of helix, meters.
r_1 = Radius of rod, meters.
R_s = Surface resistance, ohms.
s = Suffix for short.
t = Time, seconds.
u = Radial propagation coefficient = $a+jb$.
v_g = Group velocity of wave = $d\omega/d\beta$ meters per second.
v_p = Phase velocity of wave = ω/β meters per second.
w = Linear dimension, meters.
W_s = Total average stored energy per unit length, joules per meter.
x = Linear coordinate, meters or suffix.
X_s = Surface reactance, ohms.
y = Linear coordinate, meters or suffix.
Y_n = Bessel function of the second kind and nth order.
Y_0 = Characteristic admittance of transmission line, mhos.
Y_1 = Admittance of stub, mhos.
z = Axial linear coordinate, meters or suffix.
Z_c = Coupling impedance of circuit, ohms.
Z_0 = Characteristic impedance of transmission line, ohms.
Z_s = Surface impedance = R_s+jX_s ohms.
Z_{sh} = Shunt impedance of circuit, ohms per meter.
Z_w = Wave impedance of free space = 377 ohms.
Z_1 = Impedance of loading element, ohms.
α = Attenuation coefficient, nepers per meter.
β = Phase-change coefficient = $2\pi/\lambda_g$, radians per meter.
β_n = Value of β for nth space harmonic.
β_w = Value of β in free space.
γ = Propagation coefficient = $\alpha+j\beta$.
γ_n = Value of γ for nth space harmonic.
δ = Dielectric loss angle.
δ_s = Skin depth in a conductor = $2/(\omega\mu\mu_0\sigma)^{1/2}$ meters.
ϵ = Dielectric constant.
ϵ_0 = Electric space constant, $(1/36\pi)10^{-9}$ farads per meter.
θ = Angular coordinate or suffix.
λ = Free-space wavelength, meters.
λ_c = Cutoff wavelength of waveguide, meters.
λ_g = Guide wavelength, meters.
μ = Relative permeability.
μ_0 = Magnetic space constant, $4\pi \times 10^{-7}$ henry per meter.
ρ = Amplitude reflection coefficient.
σ = Conductivity, mhos per meter.
ϕ = Angular coordinate or suffix.
ψ_h = Pitch angle of helix.
ω = Angular frequency, radians per second.

* Manuscript received by the PGMTT, January 2, 1959; revised manuscript received July 27, 1959.
† Royal Radar Establishment, Malvern, Worcester, Eng.

Waves in Periodically-Loaded Lines

Dispersion

The propagation characteristics of a transmission line are modified [39] when the line is loaded with reactances connected in series or parallel, and spaced at regular intervals. The analysis of such periodic structures, familiar [30] in many branches of science, has been extended [50], [167], [233] to microwave transmission lines. An equivalent circuit treatment reveals a qualitative description of the various phenomena, providing a basis for exact analysis using Maxwell's theory.

Propagation along a transmission line, loaded as shown in Fig. 1, may be analyzed by Floquet's theorem [30], [233] which states that for a given mode of oscillation and frequency the wave function is multiplied by a constant complex factor $\exp(-\gamma p)$ on moving along the structure by one section or period. For propagation along the z-axis, the wave function can be written in the general form $\exp-(\gamma+2\pi nj/p)z$. It can be shown that in a structure without energy dissipation γ must be real or imaginary. If real, the exponentials for each value of n decrease with increasing z and attenuated waves result. If, on the other hand, γ is imaginary, putting

$$\beta_n = \beta_0 + 2\pi n/p, \tag{1}$$

the wave function becomes $\exp j(\omega t-\beta_n z)$, on inclusion of the time dependent term. This represents a progressive wave with angular frequency ω and wavelength $2\pi/\beta_n$, travelling along the z-axis with phase velocity $v_{pn}=\omega/\beta_n$.

The loaded line may be considered as a series of sections, each consisting of a portion of line of characteristic impedance Z_0 and a lumped impedance Z_1. The phase change across a section AC consists of the sum of the phase changes along a portion of line AB and across the lumped impedance BC. The equations of the frequency characteristics of this infinite loaded line may be determined by the usual analysis [271] of ladder lines. The phase change along a length of transmission line is $2\pi p/\lambda$, while the total phase change per section is $\beta_n p$ or $2\pi p/\lambda_g$ when n is considered zero. It can then be shown [167] that

$$\cos\frac{2\pi p}{\lambda_g} = \cos\frac{2\pi p}{\lambda} + j\frac{Z_1}{2Z_0}\sin\frac{2\pi p}{\lambda} \tag{2}$$

is the equation of the frequency characteristic. For a line loaded with series inductances L,

$$Z_1 = j\omega L \tag{3}$$

and the resulting (2) with $\omega L \simeq Z_0$ is plotted in Fig. 2. It will be seen that as ω is increased from zero to about two-thirds of $\pi c/p$ the value of β increases from zero to π/p. At this higher frequency, reflections set up at the inductors add in phase, resulting in a standing wave on the line with current antinodes at the inductors. For

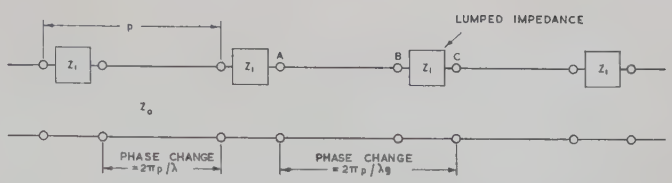

Fig. 1—Line loaded with lumped impedance.

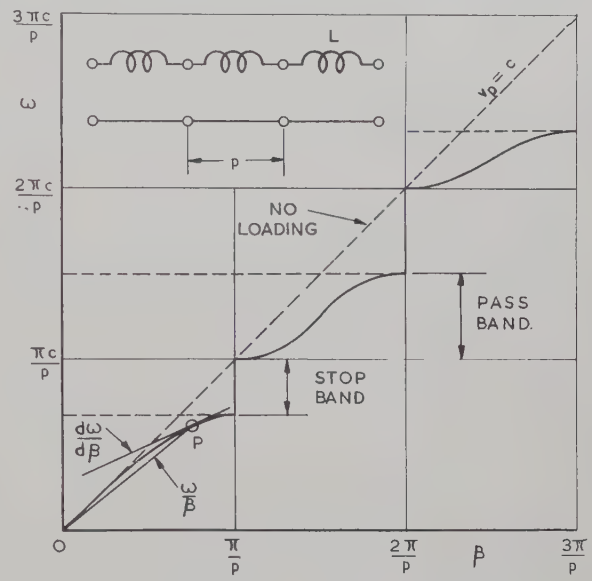

Fig. 2—Frequency characteristic for inductively loaded line.

higher frequencies a stop band occurs, the wave down the line being attenuated by successive reflections at the inductors while the total phase change remains constant at the value π. For smaller or larger values of L, the curves have similar shapes but follow the $v_p=c$ line to higher or lower frequencies, respectively. The curves always have zero slope at cutoff and propagation is possible at zero frequency. A second pass band begins when the phase change across each portion of the line (not including the inductor) becomes π; *i.e.*, when ω becomes $\pi c/p$. At this frequency there is no phase change across the inductor, a standing wave being produced with nodes at the inductor. With further increase in frequency, the phase constant increases until the phase change across each section of the line becomes 2π when a further stop band occurs. The widths of successive stop bands increase with frequency since they are dependent on the reactance ωL of the inductor. It will be seen that the phase velocity given by ω/β is less than c, except in the special case of standing waves with current nodes at the inductors when, as may be expected, it is equal to c.

For a line loaded with series capacitances C,

$$Z_1 = 1/j\omega C \tag{4}$$

and the resulting (2) with $(1/\omega C)\simeq 3Z_0$ is plotted in Fig. 3. Once again a series of stop and pass bands is obtained but in this case the widths of the stop bands

decrease with increasing frequency. The phase change across the capacitor is such that the phase velocity is greater than c, except when a standing wave with nodes at the capacitors occurs when it is equal to c. It should be observed that the transmission line now has a cut-off frequency below which no propagation occurs. The general shape of the curves is the same for other values of C, tending to the $v_p = c$ line for C large and to horizontal lines representing no propagation for C small. These dispersion curves for series capacitance are identical with those for shunt inductance loading while, by the principle of duality, the curves for shunt capacitance are identical with those already shown for series inductance.

Microwave transmission lines are often loaded with resonant circuits such as, for example, series stubs. If l is the length and Z_{01} is the characteristic impedance of such a stub, the loading impedance is

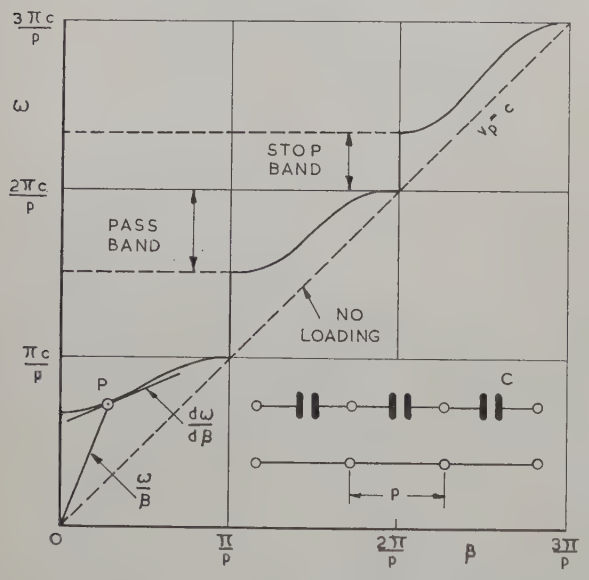

Fig. 3—Frequency characteristic for capacitively loaded line.

$$Z_1 = jZ_{01} \tan (2\pi l/\lambda). \tag{5}$$

The equation of the dispersion curves then becomes

$$\cos \frac{2\pi p}{\lambda_g} = \cos \frac{2\pi p}{\lambda} - \frac{Z_{01}}{2Z_0} \tan \frac{2\pi l}{\lambda} \sin \frac{2\pi p}{\lambda}. \tag{6}$$

The analysis is simplified without affecting the qualitative features if $Z_{01} = 2Z_0$, so that (6) becomes

$$\cos \frac{2\pi p}{\lambda_g} = \left[\cos \frac{2\pi(p+l)}{\lambda}\right] \Big/ \cos \frac{2\pi l}{\lambda} \tag{7}$$

which is plotted in Fig. 4 for $l/p \simeq 1.2$. At low frequencies the loading is inductive, but as ω increases a cutoff occurs when $\lambda_g = 2p$, a standing wave being produced with antinodes at the stubs. The frequency at which this cutoff occurs is less than the lowest or first resonant frequency of the loading reactor. This first resonance occurs when the effective length of the stub is $\frac{1}{4}\lambda$ and the attenuation in the guide is then infinite. From the cutoff frequency to the frequency at which the stub length is $\frac{1}{4}\lambda$, the phase change along one section of the guide remains at the value π.

At the resonant frequency, the loading on the guide changes from inductive to capacitive and the phase difference across a section changes by π. The phase change remains constant at zero until the next pass band is reached. At the beginning of the second pass band, the loading is capacitive with a corresponding frequency characteristic. When the effective length of the stub becomes $\frac{1}{2}\lambda$, it is again resonant with a node of electric field at the mouth of the resonator and $\lambda_g = \lambda$. For a higher frequency, the loading is inductive and a cutoff occurs at a frequency approaching the value for which the resonator length is $\frac{3}{4}\lambda$. The same cycle of events is repeated at all resonant lengths $(m\lambda + \frac{1}{2}\lambda)/2$ where m is a positive integer. At frequencies for which the effective length of the stub is $m\lambda/2$, the loading changes from capacitive to inductive and $\lambda_g = \lambda$.

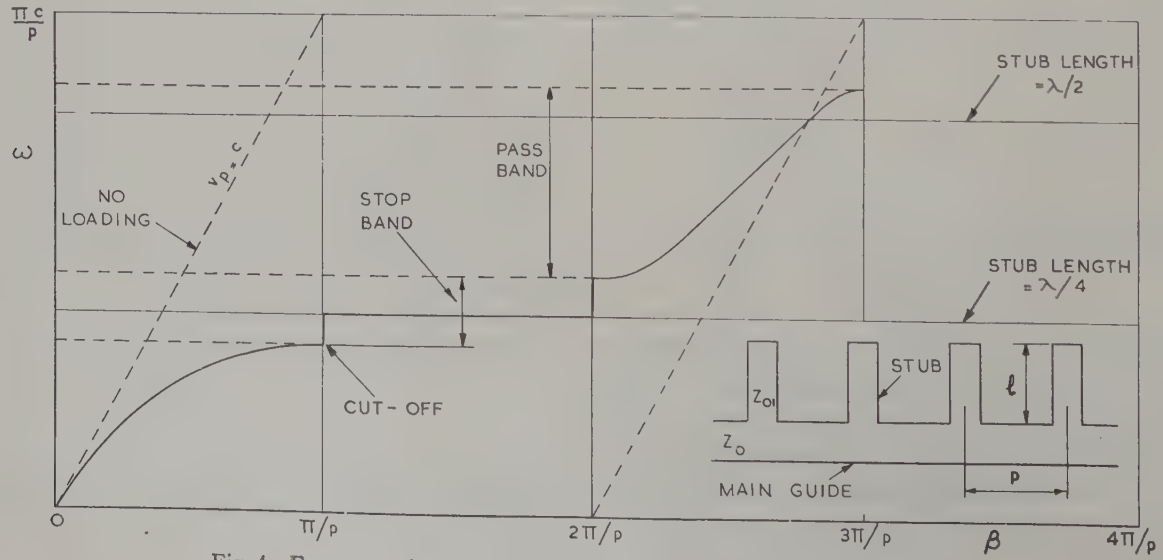

Fig. 4—Frequency characteristic for a parallel-plate line loaded with stubs.

At frequencies such that $\omega = m\pi c/p$, further cutoff values occur. The stop band associated with this type of cutoff is the same as that obtained with inductive or capacitive loading. No resonance occurs in the cavities and the phase change across a section of the guide remains constant throughout the stop band. On both sides of the stop band, the pass bands are either both inductive or both capacitive. In the former case, $\omega = m\pi c/p$ is a low-frequency cutoff for the pass band, and in the latter, it is a high-frequency cutoff. For example, if $l/p = 0.2$, the first stub resonance occurs at $\omega = 2.5\pi c/p$; before this frequency is reached, the dispersion curve shows inductive stop bands at both $\pi c/p$ and $2\pi c/p$.

The phase velocity $v_p = \omega/\beta$ for any point P on the dispersion curve is given by the slope of the line joining the point to the origin. The group velocity $v_g = d\omega/d\beta$ is given by the slope of the curve at the particular point. Provided that the attenuation coefficient is not too great, v_g is also the energy velocity [30] defined as the rate of flow of energy through a cross section of the guide to the energy stored per unit length, the ratio being averaged over one complete section. If Q_u relates to the resonance of the loaded line which is short-circuited at both ends, the attenuation in the pass bands is given in nepers per meter by [233]

$$\alpha = \omega/(v_g Q_u). \tag{8}$$

The dispersion or rate of variation of phase velocity with frequency may determine the useable bandwidth of a periodic structure in a practical device; it is given by

$$dv_p/d\omega = (v_p/\omega)(1 - v_p/v_g). \tag{9}$$

Information about the stop bands is obtained [167] by substituting $\cos(\beta - j\alpha)p$ for $2\pi p/\lambda_g$ in (6). The attenuation in nepers per section αp is then given by

$$\cos(\beta - j\alpha)p = \cos\frac{2\pi p}{\lambda} - \frac{Z_{01}}{2Z_0}\tan\frac{2\pi l}{\lambda}\sin\frac{2\pi p}{\lambda}. \tag{10}$$

The attenuation is zero near the edges and becomes infinite at the center of the resonance stop bands, but remains finite in the inductive and capacitive stop bands. The treatment given for the frequency characteristics has assumed that there is a nearly loss-free system and, moreover, the simple relation of (8) predicts infinite attenuation as the edges of the pass band are approached. These difficulties have been overcome by Butcher [36] who, in taking into account the effect of both conductor and dielectric losses, introduced a complex Q factor which can be used in the pass and stop bands.

Space Harmonics

The frequency characteristics given so far have been for the case when $n = 0$ in (1); that is, only one value of phase velocity has been given explicitly for a particular frequency. The instantaneous potential waveform along the guide is, however, not sinusoidal, but changes discontinuously across the loading impedances and can be described in terms of Fourier analysis as a sum of a series of space harmonics. The amplitudes of these harmonics depend on the form of the potential field which is controlled by the particular structure of the periodic guide. For example, the potential of a travelling wave on a parallel plate line with stubs of aperture b_1, assuming that the electric field strength is constant across the mouth, is given by [167]

$$\sum_n \left[\left(\sin\frac{1}{2}b_1\beta_n\right) \Big/ \frac{1}{2}b_1\beta_n\right] e^{j(\omega t - \beta_n z)}. \tag{11}$$

If β_0 is given the value $\pi/4p$, (1) gives

$$\beta_n = (\pi/4p) + (2\pi n/p). \tag{12}$$

The instantaneous waveforms of the harmonics corresponding to $n = -1, 0, +1$ are shown in Fig. 5(a).

The frequency characteristic of a periodic stub loaded structure which includes all space harmonics from $n = -2$ to $n = +3$ is shown by the full lines of Fig. 5(b). It will be seen that the phase velocities of the various harmonics are different and that those for $n = 0, +1, +2$, and $+3$ are positive, while those for $n = -1$ and -2 are negative. At the cutoff frequencies, for every space harmonic with positive phase velocity there is one with an equal and opposite phase velocity. Further investigation shows that the amplitudes of these pairs are also equal and therefore at a cutoff frequency, the guide can support only standing waves. If v_p is the phase velocity at a point A, geometrical considerations show that the phase velocity at corresponding points such as B, C, D, and E is given by $v_p p/(n\lambda_g + p)$.

The group velocities of all the space harmonics are seen to be equal for any given frequency and to have the same direction as that of the energy. For n negative, the phase velocity is always opposite in direction to the group velocity. Such space harmonics are termed reverse or backward waves and, in particular, it is possible to have periodic structures in which the fundamental is itself a reverse wave. The complete characteristic contains a range of upper branches corresponding to resonances of the stubs. Two conventions are in use for the numbering of these branches. In one, the fundamental is taken to be that space harmonic with the highest phase velocity, while in the second, which is adopted here, it is that harmonic which normally has the largest amplitude. In the latter case, with small loading, the characteristic tends to that of the transmission line.

If electromagnetic energy is propagated in both directions, then as shown by the dotted lines of Fig. 5(b), additional curves which represent waves with negative group velocity appear to complete the frequency characteristic. If the forward and backward energies are equal, standing waves are produced not only at the cutoff values but at all frequencies. This analysis may readily be extended from parallel plate lines to waveguides. The characteristic impedance is now given for any one mode of propagation by the ratio of the trans-

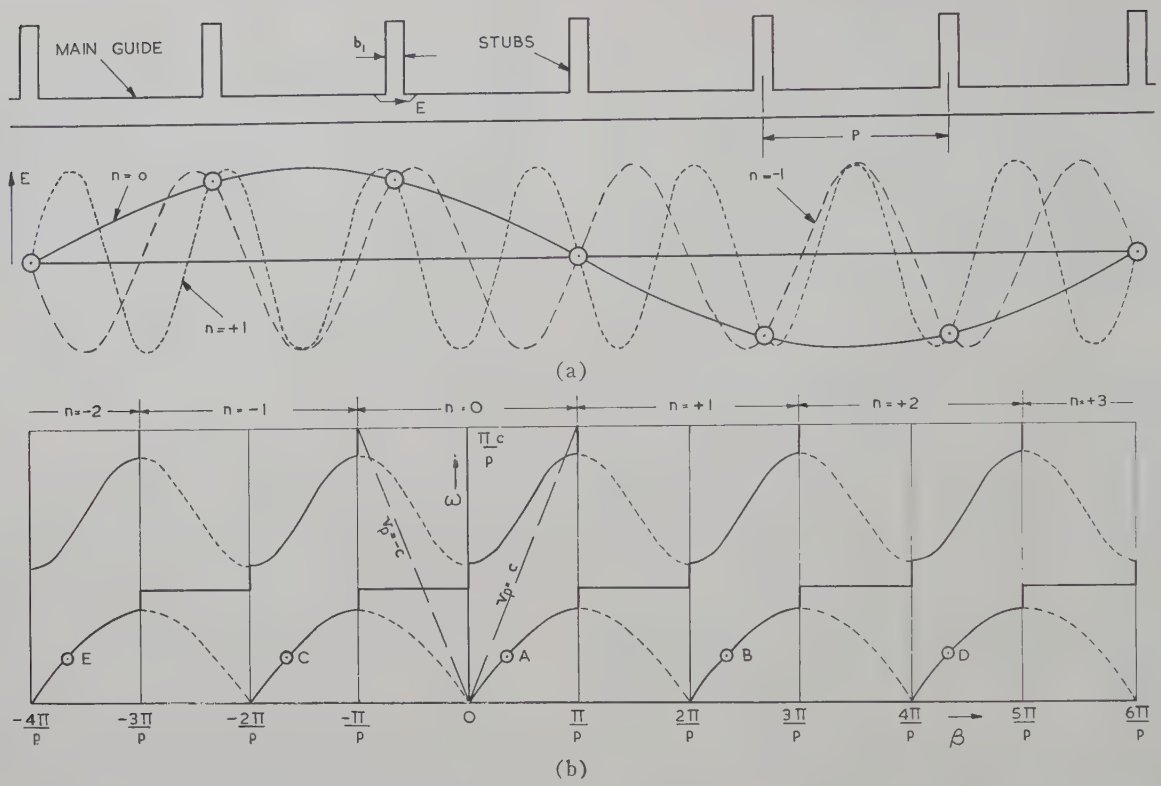

Fig. 5—Forward and backward space harmonics. (a) Stub structure and wave forms of the $n=-1$, 0, and $+1$ space harmonics. (b) Frequency characteristics of the $n=-2$ to $n=+3$ inclusive space harmonics.

verse electric to transverse magnetic field. The frequency characteristics will be similar to those given above except at low frequencies where the guide exhibits a cutoff.

It may be shown [167] that the longitudinal and transverse components of the electric field in the main guide oscillate in quadrature. For capacitive loading where $v_p > c$, the amplitudes vary in the transverse direction according to sine and cosine laws. For inductive loading where $v_p < c$, the transverse propagation constant is real and the amplitudes decay according to hyperbolic sine and cosine laws; these become exponential some distance from the loaded surface.

Multiply-Periodic Loading

Other properties of periodic structures emerge when the loading is systematically uneven [24], [256]. For example, in the structure shown in the inset of Fig. 6, which consists of series stubs of alternate length, it will be evident that the number of degrees of freedom of the system are now doubled and therefore there will be twice the number of branches in the frequency characteristic. Analysis of the equivalent circuit of this double-stub structure gives [167] the equation of the frequency characteristic as

$$\cos(4\pi p/\lambda_g) = \cos(4\pi p/\lambda) - (Z_{01}/2Z_0)\sin(4\pi p/\lambda)[\tan(2\pi l_l/\lambda) + \tan(2\pi l_s/\lambda)] + (Z_{01}^2/2Z_0^2)\sin^2(2\pi p/\lambda)\tan(2\pi l_l/\lambda)\tan(2\pi l_s/\lambda), \quad (13)$$

where $(4\pi p/\lambda_g)$ is the phase change across one complete section of the line (including a long and a short stub).

The frequencies at cutoff for $\beta=0$ and $\beta=\pi/p$ are given by

$$\cos(4\pi p/\lambda_g) = 1. \quad (14)$$

For $Z_{01}=2Z_0$, (13) then gives

$$\omega = \frac{m\pi c}{p}, \quad (15)$$

$$\omega = \frac{m\pi c}{p}\left\{1 + \frac{l_l}{p} + \frac{l_s}{p}\right\}. \quad (16)$$

The values of ω in (15) are the capacitive or inductive cutoff frequencies, being the beginning or end of a stop band. The values of ω in (16) which depend upon l_l and l_s give the cutoff frequencies when adjacent resonators are oscillating in antiphase.

The frequencies at cutoff for $\beta=\pi/2p$ are given by

$$\cos(4\pi p/\lambda_g) = -1, \quad (17)$$

and, for $Z_{01}=2Z_0$, (13) gives

$$\omega = \frac{\pi c}{2}\frac{2m+1}{p+l_l}, \quad (18)$$

$$\omega = \frac{\pi c}{2}\frac{2m+1}{p+l_s}. \quad (19)$$

These values of ω correspond to the occurrence of nodes at the long and short resonators, respectively. If the stubs are all of length l, the frequency for $\beta=\pi/2p$ is given from (7) by

$$\omega = \frac{\pi c}{2}\frac{2m+1}{p+l}. \quad (20)$$

Comparison of (20) with (18) and (19) shows that cutoff values of ω at $\beta=\pi/2p$ for the double-stub structure

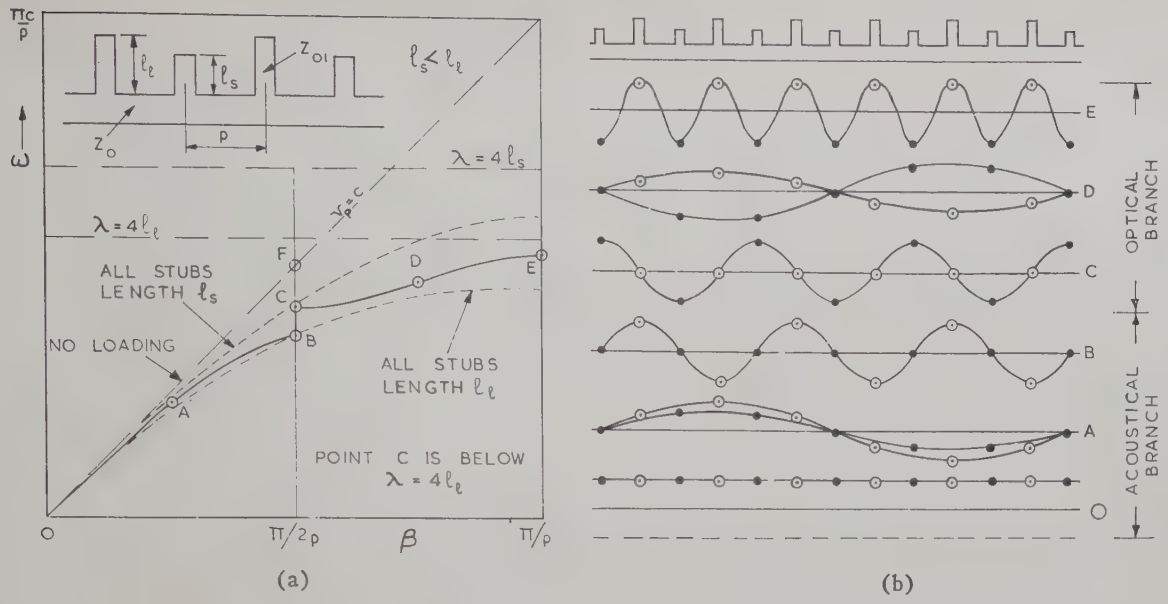

Fig. 6—Inductive double-stub structure. (a) Frequency characteristic. (b) Relative phases of the stubs.

occur at all points where the ordinate $\pi/2p$ cuts the curves of the two uniformly-loaded lines.

Thus the frequency characteristic of the double-stub periodic structure will be similar to that of the simple structure until the phase constant approaches the values at which the cutoffs occur. The characteristics will depart at these points since standing waves can occur with either nodes or antinodes at the modified resonators. These standing waves will have the same wavelength but different frequencies and will be displaced with respect to each other by $\frac{1}{4}\lambda_0$.

The useful properties of this structure occur when the ratio l_l/l_s is not too great, for instance, between 1 and 2. The frequency characteristic may then belong to two classes. In the first class shown in Fig. 6(a), the resonances of the stubs occur at a higher frequency than the two standing waves at B and C when $\beta=\pi/2p$. Therefore, in passing from one branch to the other, the loading remains inductive and there is no change in the phase coefficient at $\beta=\pi/2p$. As Z_{01} is reduced from the value $2Z_0$, the initial portion of the characteristic for all stub lengths tends to follow the $v_p=c$ line more closely and vice versa if Z_{01} is increased; the cutoff frequencies are also modified. From analogy with the characteristics of crystal lattices containing diatomic molecules, the lower curve is sometimes termed the acoustical branch and, as shown in Fig. 6(b), the phase of the oscillations in the resonators differs by less than $\frac{1}{2}\pi$ and tends to zero when β approaches zero. The upper curve is termed the optical branch and the phase of the neighbouring resonators differs by more than $\frac{1}{2}\pi$ and approaches π as β approaches π/p.

In the second class illustrated by Fig. 7, a resonance of the larger stub occurs between the two standing waves at $\beta=\pi/2p$ when $l_l \simeq \frac{1}{4}\lambda$ and results in a change from inductive to capacitive loading. The loading remains capacitive until a frequency is reached where $\lambda_0=\lambda$; *i.e.*, the phase velocity is equal to the free-space

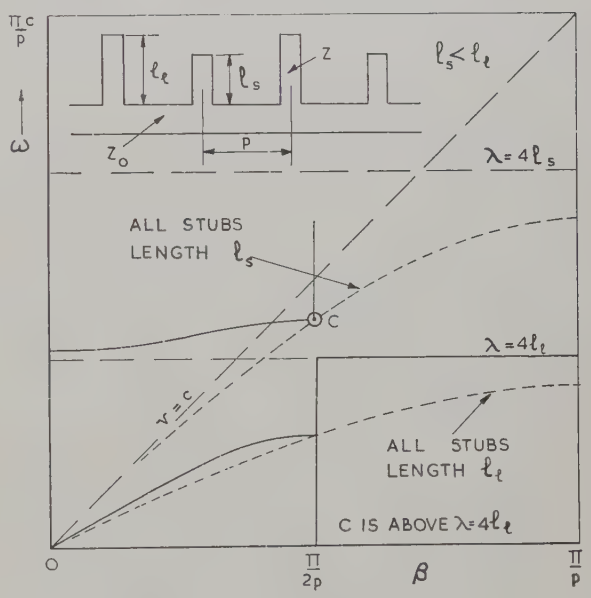

Fig. 7—Resonant double-stub structure.

velocity. At this frequency the capacitance of the small resonator and inductance of the larger resonator may be regarded approximately as a series resonant circuit. At a still higher frequency the loading is again inductive. For periodic structures with more than two lengths of stubs, the number of branches in the frequency characteristic will equal the number of different lengths of resonator; *i.e.*, the number of frequencies corresponding to a given phase constant is equal to the number of degrees of freedom associated with each section of the line. For example, in a structure in which there are three stubs per section and every third is modified, one of the many possible characteristics takes the form shown in Fig. 8. It has been shown [167] that under certain conditions and over a limited frequency range, the dispersion is small since the phase velocity is nearly constant.

Dielectric-Clad Metal Structures

Plane Waves Over Flat Surfaces

In conventional transmission systems, at microwave frequencies the electromagnetic energy is effectively confined to a closed region of space by means of conducting walls. Under certain conditions other types of transmission may exist in which the energy is not rigidly confined but rather is bound to a surface or structure. Such a guiding structure can support [32] three classes of waves: first, a continuous spectrum of propagating waves and second, a continuous spectrum of evanescent waves which are exponentially attenuated in the direction of propagation. The third class represents one or more surface waves which, by careful launching, can be made to predominate.

These surface waves [20], [190], [292], [293] are forms of electromagnetic energy which propagate without radiation along an interface between two media with different physical properties. The electromagnetic field extends to infinity in the transverse direction but the energy density decreases with distance so that, in practice, most of the energy of the wave is constrained to flow in the immediate neighborhood of the structure. The only flow of energy away from the interface is that required to supply the losses in the media concerned. The properties of these waves are governed by the surface impedance Z_s defined as the ratio of the tangential components of the electric and magnetic field vectors. In general, Z_s is complex, having both resistive and reactive components.

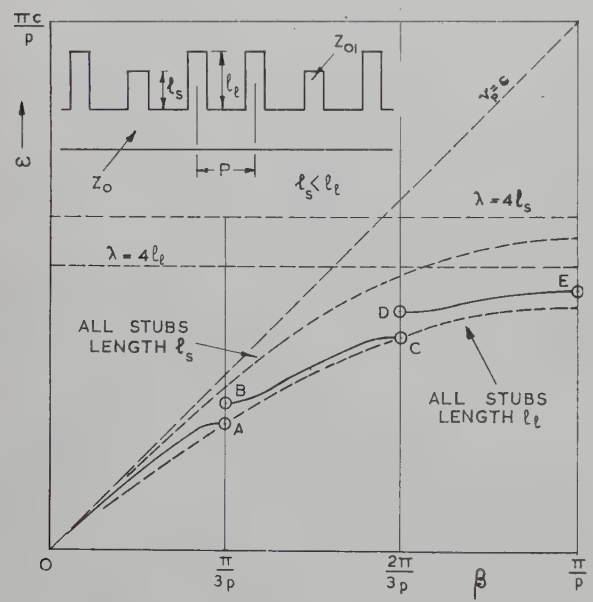

Fig. 8—Triple-stub multiply-periodic structure.

To comply with the conditions required for the support of surface waves, the interface must be straight in the direction of propagation of the wave but, transversely, it can take a variety of shapes and forms. The external medium is usually air, while the structure may consist of dielectric, either alone or in combination with a conductor, and metal surfaces provided with periodic corrugations. For example, a wave which travels without change of pattern over a flat surface bounding [6] two homogeneous media of different conductivity and permittivity was shown by Zenneck [291] to be a particular solution of Maxwell's equations. Such a wave is characterized [93] by the presence of a longitudinal component of the electric field vector; it is a TM wave.

Surface waves can be propagated [44], [239], [257] in plane or radial form over a dielectric-clad flat structure and in axial form along a cylinder. Such waves can also be supported by conical guides and, in particular, there are surface waves of various forms in between the axial and the radial variety. A typical flat surface is shown in Fig. 9(a) in which medium (*m*) is a metallic conductor, (*d*) is a dielectric slab, and (*a*) is air. For the dominant TM_0 plane wave travelling in the z direction with propagation coefficient γ, the three components of field required to satisfy the wave equation in the metal are given by Barlow and Cullen [15] as

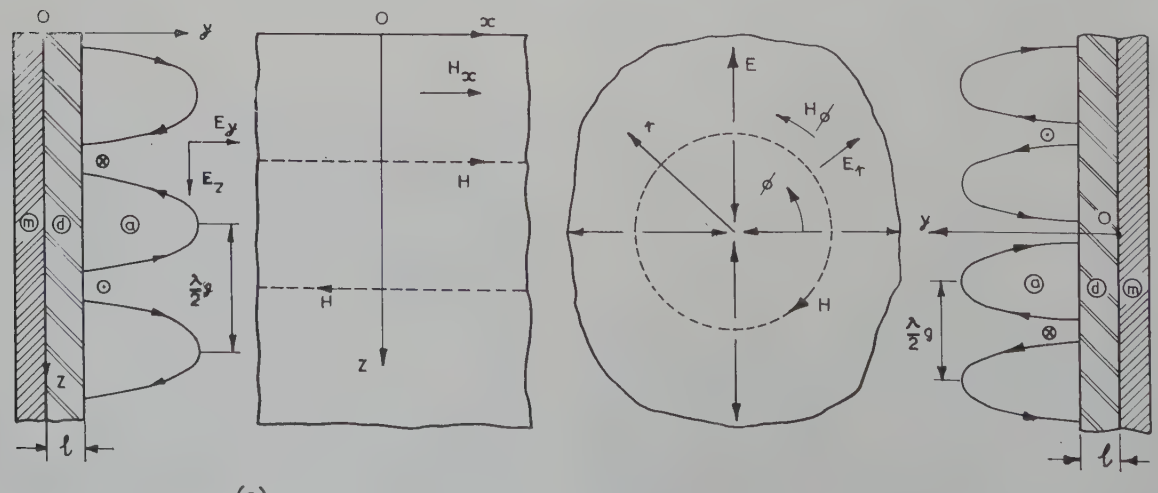

Fig. 9—Propagation over flat dielectric-clad surfaces. (a) Plane wave. (b) Radial wave. The properties of the media are (*m*) Metal, $\mu_m=\mu_0$, $\epsilon_m\epsilon_0$, σ_m, (*d*) Dielectric, $\mu_d=\mu_0$, $\epsilon_d\epsilon_0$, $\sigma_d=0$, and (*a*) Air, $\mu_a=\mu_0$, $\epsilon_a\epsilon_0$, $\sigma_a=0$.

$$H_{xm} = Ae^{u_m y}, \tag{21}$$

$$E_{zm} = A\left(\frac{u_m}{\sigma_m + j\omega\epsilon_m\epsilon_0}\right)e^{u_m y}, \tag{22}$$

$$E_{ym} = A\left(\frac{\Gamma}{\sigma_m + j\omega\epsilon_m\epsilon_0}\right)e^{u_m y}. \tag{23}$$

The factor $e^{(j\omega t - \gamma z)}$ is omitted for convenience and A is a constant. The propagation coefficient along the y-axis,

$$u_m = a_m + jb_m, \tag{24}$$

represents an attenuation a_m and phase change b_m for a wave travelling inwards from the surface where $y \leq 0$. Within this medium

$$\gamma^2 + u_m^2 = j\omega u_0(\sigma_m + j\omega\epsilon_m\epsilon_0). \tag{25}$$

In the external air medium the fields for $y \geq l$ are similarly given by

$$H_{xa} = Ae^{-u_a y}, \tag{26}$$

$$E_{za} = -A(u_a/j\omega\epsilon_0)e^{-u_a y}, \tag{27}$$

$$E_{ya} = A(\gamma/j\omega\epsilon_0)e^{-u_a y}. \tag{28}$$

Here

$$u_a = a_a - jb_a \tag{29}$$

because the field not only decays at the rate a_a with increasing transverse distance but also suffers a progressive phase change b_a for a wave travelling towards the surface. In this medium the propagation coefficients satisfy

$$\gamma^2 + u_a^2 = -\omega^2/c^2. \tag{30}$$

Within the solid dielectric there exists a standing wave whose magnetic field is given by

$$H_{xd} = A_d' \cosh u_d y + A_d'' \sinh u_d y \tag{31}$$

and in this medium

$$\gamma^2 + u_d^2 = -\epsilon_d\omega^2/c^2. \tag{32}$$

The conditions for matching the field components at the boundaries between the different layers yields

$$\tanh u_d l = -\left[\frac{1 + \left(\frac{j\omega\epsilon_d\epsilon_0}{\sigma_m + j\omega\epsilon_m\epsilon_0}\right)\left(\frac{u_m}{u_a\epsilon_d}\right)}{\frac{u_d}{u_a\epsilon_d} + \left(\frac{j\omega\epsilon_d\epsilon_0}{\sigma_m + j\omega\epsilon_m\epsilon_0}\right)\left(\frac{u_m}{u_d}\right)}\right]. \tag{33}$$

The impedance looking into the surface of the solid dielectric is

$$Z_s = R_s + jX_s = E_{za}/H_{xa} = -u_a/j\omega\epsilon_0. \tag{34}$$

In the case of a good conductor, the surface impedance has nearly equal real and imaginary parts and is given by

$$Z_m = R_m + jX_m = (1 + j)(\omega\mu_0/2\sigma_m)^{1/2}. \tag{35}$$

The total surface resistance in the case of loss in the dielectric is given by

$$R_s = R_m + R_d = R_m + (\beta_w l/\epsilon_d Z_w)\tan\delta. \tag{36}$$

This resistance therefore depends upon the conductivity of the metal if the dielectric is loss free. The surface reactance X_s is made up of one component arising from the metal and another,

$$X_d = \omega\mu_0 l(\epsilon_d - 1)/\epsilon_d, \tag{37}$$

for which the layer of solid dielectric is responsible. These two components are of the same order of magnitude when the thickness of the dielectric is about equal to the skin depth δ_s of the metal.

If l is assumed to be small so that $\tanh u_d l \simeq u_d l$ and $u_d l \ll 1$, (33) gives

$$u_a = a_a - jb_a = j\beta_w Z_s/Z_w. \tag{38}$$

In general, the higher the surface reactance and the higher the frequency, the greater the decay factor a_a so that the field becomes concentrated more closely in the immediate vicinity of the surface. Any increase of R_s increases the inclination of the wavefront at the surface, measured from the normal and this, in turn, increases the phase velocity along the interface. On the other hand, it may be anticipated by analogy with electric circuits that the corresponding phase velocity would be reduced by an inductive surface reactance and increased by a capacitive one.

In order to obtain the attenuation and phase-change coefficients along the surface in the direction of propagation, (29) and (30) are substituted in the expression for γ to give [137]

$$\alpha = \beta_w R_s X_s/Z_w^2, \tag{39}$$

$$\beta = \beta_w\left\{1 - \frac{1}{2}\left(\frac{R_s^2 - X_s^2}{Z_w^2}\right)\right\}. \tag{40}$$

If $\beta \simeq \beta_w$, the velocity of propagation becomes

$$v_p = c\left\{1 + \frac{1}{2}\left(\frac{R_s^2 - X_s^2}{Z_w^2}\right)\right\}. \tag{41}$$

Eq. (39) shows that α is proportional to R_s and X_s while (41) shows that $v_p > c$ if R_s is substantially greater than X_s, and vice versa. Values of loss and phase velocity have been calculated [12] for frequencies of 0.3–30 kmc for a dielectric with $\epsilon_d = 4$, $\tan\delta = 0.001$, and thicknesses of 0.1–10 mm. At 10 kmc a layer 0.5 mm thick gave a loss of 10^{-3} *db/m* and a phase velocity of 0.65 c.

Radial Waves Over Flat Surfaces

The geometry and field pattern of a wave propagating radially over a flat dielectric-clad metal surface are shown in Fig. 9(b). The field components in the metal, omitting the time factor $e^{j\omega t}$, are [15]

$$H_{\phi m} = Ae^{u_m y}H_1^{(2)}(-j\gamma r), \tag{42}$$

$$E_{rm} = -A\left(\frac{u_m}{\sigma_m + j\omega\epsilon_m\epsilon_0}\right)e^{u_m y}H_1^{(2)}(-j\gamma r), \quad (43)$$

$$E_{ym} = A\left(\frac{j\gamma}{\sigma_m + j\omega\epsilon_m\epsilon_0}\right)e^{u_m y}H_0^{(2)}(-j\gamma r), \quad (44)$$

with (24) and (25) as previously. In the external air medium,

$$H_{\phi a} = Ae^{-u_a y}H_1^{(2)}(-j\gamma r), \quad (45)$$

$$E_{ra} = A(u_a/j\omega\epsilon_0)e^{-u_a y}H_1^{(2)}(-j\gamma r), \quad (46)$$

$$E_{ya} = A(\gamma/\epsilon_0)e^{-u_a y}H_0^{(2)}(-j\gamma r) \quad (47)$$

with (29) and (30) as previously.

By comparing (21)–(23) and (42)–(44) or (26)–(28) and (45)–(47), it will be seen that the radial form of the modified Zenneck wave has the same field distribution in the y direction as the corresponding plane wave. Along the radial coordinate r, the wave propagates according to the Hankel function and, at large distances, the amplitude follows an exponential of the form $e^{-\Gamma r}/r^{\frac{1}{2}}$.

There is again a standing wave in the intervening medium and the surface impedance looking into the dielectric-clad metal is given by

$$Z_s = R_s + jX_s = -E_{ra}/H_{\phi a}. \quad (48)$$

The values of R_s, X_s as well as the attenuation and phase-change coefficients, are the same as for the plane wave.

Axial Cylindrical Waves

It was theoretically shown by Sommerfeld [244] that a straight cylindrical conductor of finite conductivity and having a smooth surface can act as a guide for electromagnetic waves. This surface wave propagation was shown to take place for infinite conductivity by Harms [109] provided that the surface of the metal is coated with a dielectric layer. Although higher-order modes are associated [13], [116] with this guide, attention is usually focused on the dominant TM_{00} mode. The geometry and field distribution of this wave are shown in Fig. 10; when the radius of the cylinder is increased to infinity, this axial wave becomes identical with the plane wave over a flat surface. Following the work of Goubau [94] the dielectric-coated wire has been extensively examined [22], [42], [54], [55], [58], [72], [89], [131], [133], [134], [136], [157], [210], [224] as a transmission line for microwave frequencies.

For propagation along the z-axis, the field components inside the metal, omitting the term $e^{(j\omega t-\gamma z)}$, are given by [15]

$$H_{\theta m} = A\left(\frac{\sigma_m + j\omega\epsilon_m\epsilon_0}{ju_m}\right)J_1(ju_m r), \quad (49)$$

$$E_{zm} = AJ_0(ju_m r), \quad (50)$$

$$E_{rm} = A(\gamma/ju_m)J_1(ju_m r), \quad (51)$$

with (24) and (25) for the flat surface. In the external air medium,

$$H_{\theta a} = A(\omega\epsilon_0/u_a)H_1^{(1)}(ju_a r), \quad (52)$$

$$E_{za} = AH_0^{(1)}(ju_a r), \quad (53)$$

$$E_{ra} = A(\gamma/ju_a)H_1^{(1)}(ju_a r), \quad (54)$$

with (29) and (30) as for the flat surface. The argument of the Hankel functions is imaginary and thus the external fields decay at a rate which becomes exponential for large radii.

The surface impedance looking into the dielectric sheath, with $r = r_1$, is

$$Z_s = R_s + jX_s = \frac{E_{za}}{H_{\theta a}} = \left(\frac{u_a}{\omega\epsilon_0}\right)\left[\frac{H_0^{(1)}(ju_a r_1)}{H_1^{(1)}(ju_a r_1)}\right] \quad (55)$$

which, when $r_1 \to \infty$, becomes $j(u_a/\omega\epsilon_0)$, the value for the flat surface given in (34). For cylinders of small diameter, the curvature of the equiphase surfaces near the wire has an important effect on the wave impedance which may change from being inductive at a great dis-

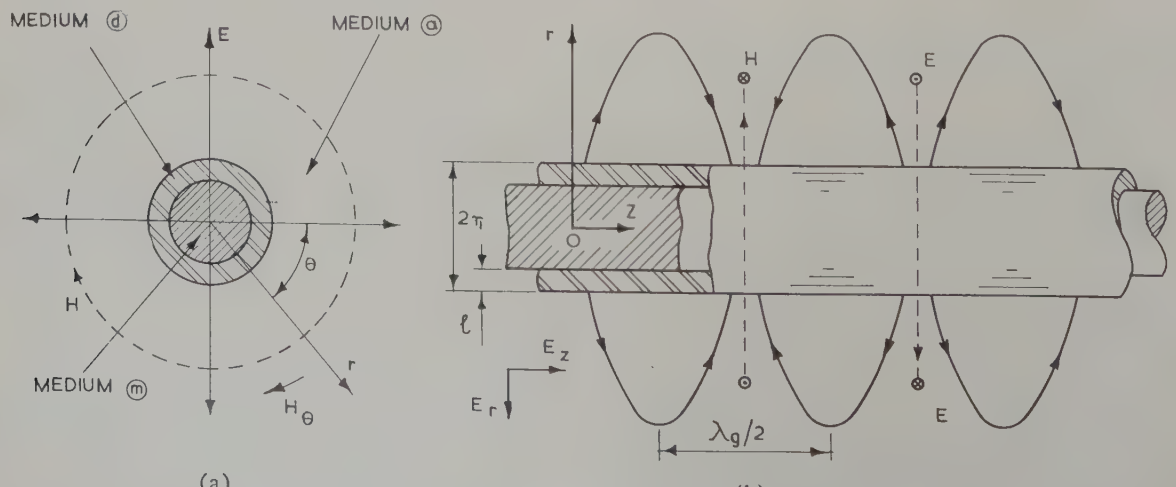

Fig. 10—Axial propagation on a dielectric-clad cylinder. The properties of the media are (m) Metal, $\mu_m = \mu_0$, $\epsilon_m\epsilon_0$, σ_m, (d) Dielectric, $\mu_d = \mu_0$, $\epsilon_d\epsilon_0$, $\sigma_d = 0$, and (a) Air, $\mu_a = \mu_0$, $\epsilon_a\epsilon_0 = \epsilon_0$, $\sigma_a = 0$.

tance from the wire to being capacitive near the wire. In fact, a bare copper wire which has a very small inductive component of impedance at its surface is a practical guide for the Sommerfeld surface wave at microwave frequencies.

Experiments on dielectric-coated wires have been reported at microwave frequencies [92], [95], [98], [211] including 3 kmc [99], 10 kmc [45], [145] and at ultra-high frequencies [198], [231]. The properties of the lines are found to agree closely with those predicted by theory. As an example [97], Fig. 11(a) shows the radius r_2 at which the field is 90 per cent of its maximum, the reduction $\delta v_p/v_p$ of phase velocity and the fraction $\delta W/W$ of the energy propagated in the dielectric layer, all as functions of the thickness of the layer. The wire radius was assumed to be 0.1 cm and the frequency was 3 kmc. The attenuation for wires coated with enamel, $\epsilon=3$, $\tan\delta=0.008$ is given in Fig. 11(b). A conductor for 35 kmc need only be 0.056-inch diameter with a thin coating of enamel.

Miscellaneous Surface Circuits

Transverse Corrugations

The surface reactance of a guide may be enhanced by coating it with an artificial dielectric such as a corrugated structure [27], [76], [121]. The flat surface shown in Fig. 12(a) was first examined by Cutler [64] who considered the corrugations as short-circuited parallel-plate stubs with an impedance given by (5). Assuming that the surface has infinite conductivity and omitting the factor $e^{j(\omega t-\beta z)}$, the field components in the air medium outside the grooves are given by

$$H_{xa} = jA(\beta_w/u_a Z_w)e^{-u_a y}, \tag{56}$$

$$E_{za} = Ae^{-u_a y}, \tag{57}$$

$$E_{ya} = -jA(\beta/u_a)e^{-u_a y}, \tag{58}$$

and (30) becomes

$$\beta^2 - u_a^2 = \beta_w^2 = \omega^2/c^2. \tag{59}$$

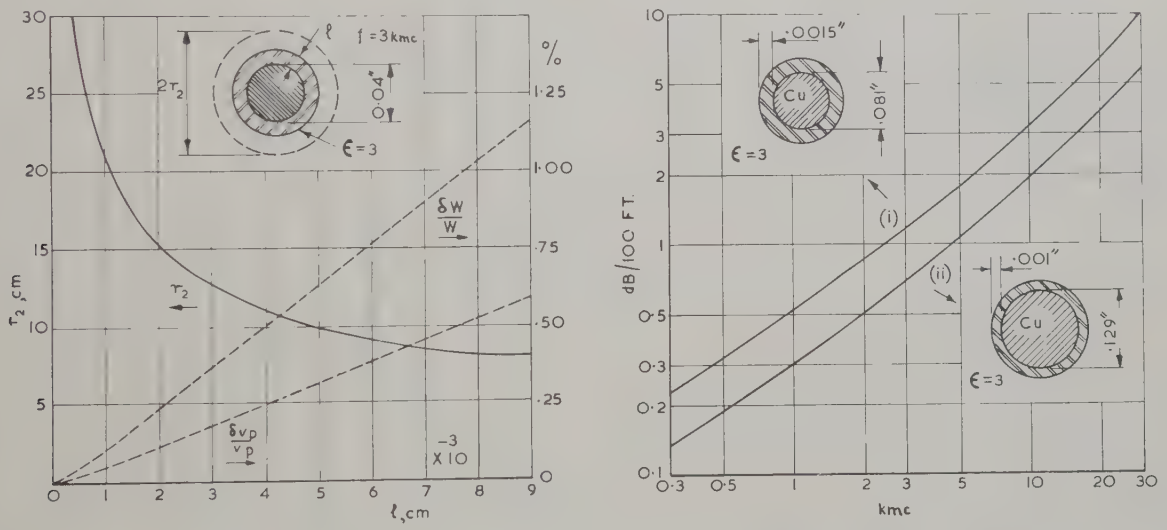

(a) (b)

Fig. 11—Properties of a dielectric coated wire. (a) 90 per cent field radius, change in phase velocity and propagation of energy stored in the dielectric. (b) Attenuation for two sizes of enamelled wire.

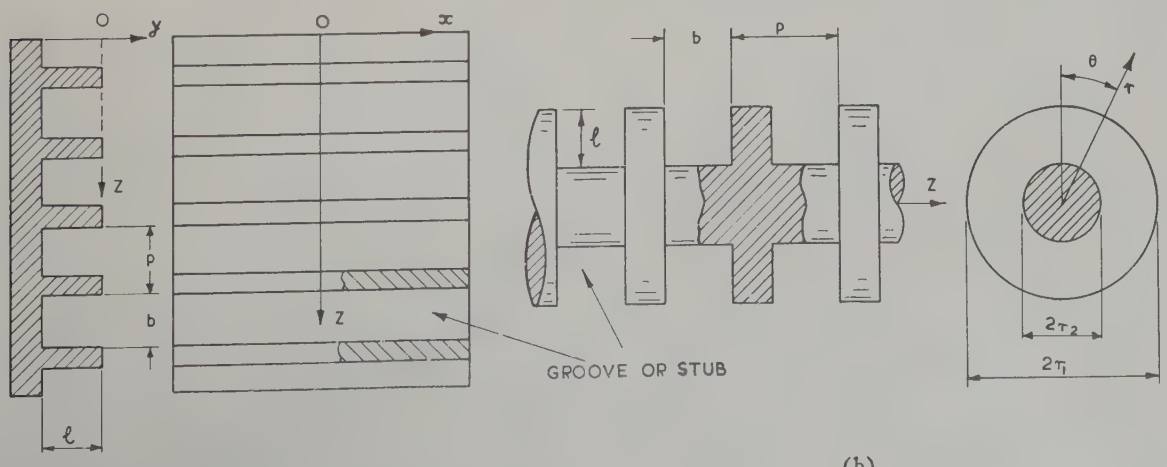

(a) (b)

Fig. 12—Propagation along corrugated surfaces. (a) Plane with parallel grooves. (b) Cylindrical with radial grooves.

The wave is a TM type since the magnetic field lies totally within the transverse plane.

Since the structure is periodic, the wave travelling along the surface consists of a fundamental plus space harmonics whose relative amplitudes are functions of stub width, length, and pitch. The surface impedance of the surface between the corrugations is zero, since E_{za} vanishes there. If the width of the stub is small compared with the guide wavelength, the surface impedance can be given its average value,

$$Z_s = -jZ_w(b/p) \tan (2\pi l/\lambda). \tag{60}$$

Matching this to the uniform surface impedance given by E_{za}/H_{xa} gives

$$u_a = \beta_w(b/p) \tan (2\pi l/\lambda). \tag{61}$$

This relation shows that propagation is possible in certain bands where u_a is positive, whereas, for other regions, u_a is negative and waves cannot be propagated. In the first pass band as l increases from 0 to $\frac{1}{4}\lambda$, the surface impedance is inductive and increases from zero to infinity. Moreover, the phase velocity varies from c to zero while the field intensity as a function of distance from the surface changes from a small to a large exponential decrease. Such results have been confirmed [213] by experiments on flat corrugated surfaces.

In the case of the corrugated cylinder in Fig. 12(b) the surface-wave field has components given by

$$E_{za} = AH_0^{(1)}(ju_a r), \tag{62}$$

$$E_{ra} = A(\beta/u_a)H_1^{(1)}(ju_a r), \tag{63}$$

$$H_{\theta a} = A(\beta_w/u_a Z_w)H_1^{(1)}(ju_a r), \tag{64}$$

with (59) as previously. If the dimensions are such that the field is caused by the principal wave only, the guide behaves as if it had a uniformly distributed surface impedance given by

$$Z_s = \frac{E_{za}}{H_{\theta a}} = \frac{u_a Z_w}{\beta_w} \frac{H_0^{(1)}(iu_a r)}{H_1^{(1)}(ju_a r)}. \tag{65}$$

The TEM wave impedance presented by the individual stub elements is given by [140]

$$Z_1 = -jZ_w \frac{Y_0(\beta_w r_2)J_0(\beta_w r_1) - J_0(\beta_w r_2)Y_0(\beta_w r_1)}{Y_0(\beta_w r_2)J_1(\beta_w r_1) - J_0(\beta_w r_2)Y_1(\beta_w r_1)}. \tag{66}$$

Here, again, a first-order approximation for the surface impedance includes a factor (b/p), but a more accurate empirical result,

$$Z_s = (b/p)Z_1(1 - \tfrac{1}{2}e^{-l/b} - \tfrac{1}{2}e^{-5l/b}), \tag{67}$$

is applicable for all values of surface parameters provided that $p < \frac{1}{4}\lambda$. The theoretical relations for the surface reactance have been supported by experiments of Barlow and Karbowiak [17] at 2.35 kmc and 9.4 kmc using resonant lines about 4 feet in length. The reactance as a function of stub width is shown in Fig. 13(a) while Fig. 13(b) shows the effect of varying either the length or pitch of the stubs.

Effect of Curvature

If the surface-wave structure is curved in the direction of propagation, radiation takes place. This phenomenon can be qualitatively examined [15], [20] by considering the adjacent equiphase planes between which the field is normally evanescent. On bending the structure, the planes diverge so that the spacing eventually becomes sufficient for them when considered as waveguides to allow propagation and hence radiation of energy. It may be visualized that increase of curvature would increase the radiation while enhancement of the surface reactance would, by confining the field more closely, reduce the radiation. This conception has been employed [19] to calculate the power radiated from a curved surface.

These azimuthal surface waves may be analyzed by finding [77], [117], [178] a solution of Maxwell's equations which represents their propagation. For a dielectric sheet, as in the inset of Fig. 14(a), bounded on the inside by a perfect conductor, the fields at a point r, θ, z may be constructed from cylindrical wave functions. Assuming that there is TM mode propagation and a dielectric constant of 4.0, the dotted lines in Fig. 14(a) give the dielectric thickness for various radii of bending. It will be observed that as the cylinder radius is decreased, a thicker dielectric film is required to maintain the same degree of trapping of the wave. However, for radii greater than a few wavelengths, the required film thickness is a slowly changing function of radius which smoothly approaches the plane value. An analysis for TE waves yields the full lines of Fig. 14(a) and, here again, many of the same considerations apply. A corrugated surface is shown in Fig. 14(b) where θ_p, θ_b are the angular stub pitch and width, respectively. The curves plotted again show that for radii of curvature exceeding several wavelengths, the value of λ/λ_g is almost independent of radius but depends chiefly on the corrugation geometry.

Launching and Other Devices

The important practical aspect of the efficient launching of surface waves may be ensured [162] by matching their field pattern with that of the launching device as closely as possible. The exponential decay of the fields above a plane surface does not approximate closely to the constant or sinusoidal distribution inside waveguides and parallel plate lines and the launching of a pure surface wave presents some difficulty. In an unpublished work, G. G. Macfarlane calculated that the range of the surface wave from a finite aperture h is restricted to a distance $h \csc \theta_0$ where θ_0 is the Brewster angle of the material. For a lossless dielectric coated surface, θ_0 is purely imaginary and the range is then infinite. Not all the energy goes into the surface wave because the finite aperture leads [15], [61] to an outward

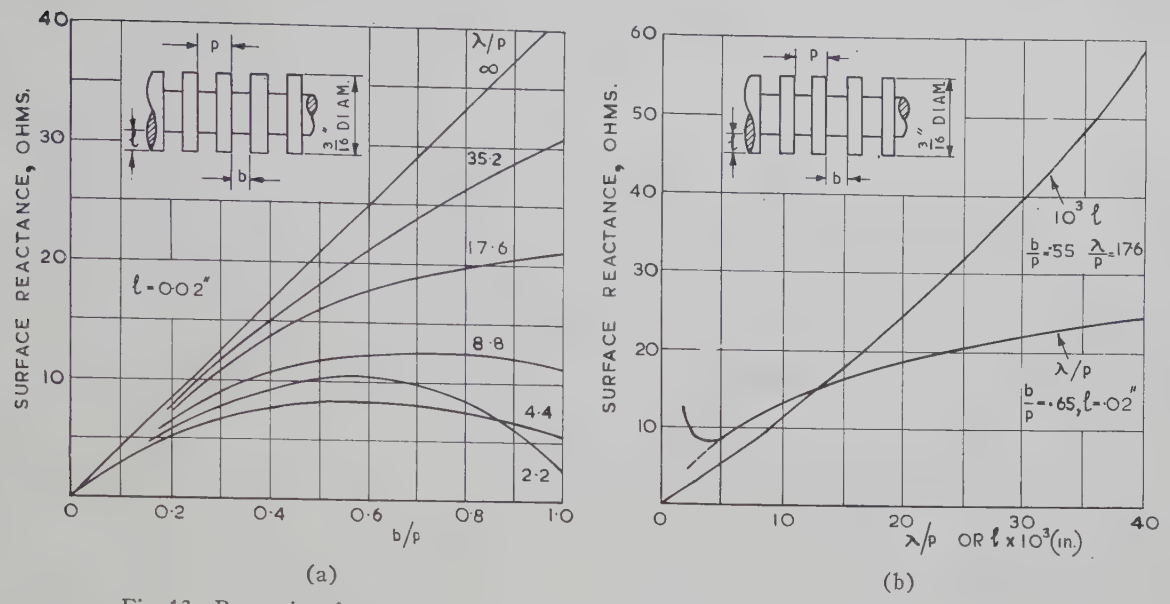

Fig. 13—Properties of a corrugated cylindrical surface. (a) Surface reactance vs groove width. (b) Surface reactance vs groove depth and number per wavelength.

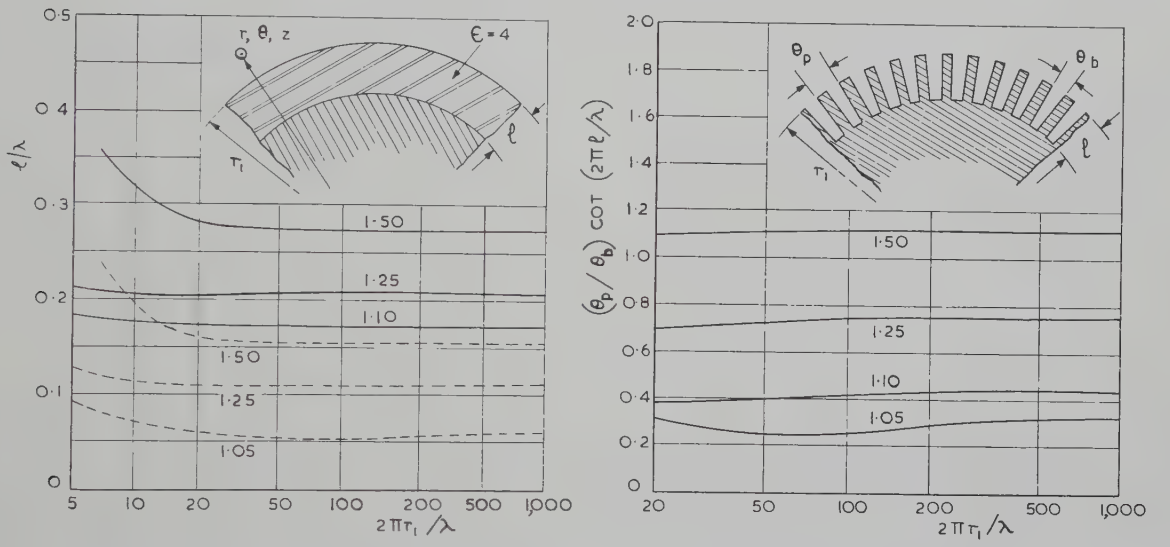

Fig. 14—Azimuthal waves on curved guiding surfaces. (a) Dielectric-clad metal, with TM (dotted line) and TE (full line) modes. (b) Corrugated surface, TM modes. The parameter marked on each curve is λ/λ_g.

travelling radiation wave which represents a loss of energy. The launching efficiency [143] is defined as the power in the desired mode divided by that supplied to the launcher.

The optimum conditions for launching surface waves over a flat structure have been extensively studied [87], [96], [168], [273]. In a typical theoretical and experimental investigation, Rich [208] employed the arrangement shown in Fig. 15 in which a 6-foot×1-foot brass sheet is coated with $\frac{1}{16}$-inch polystyrene. The frequency was 9.5 kmc and the vertical aperture of the flare could be restricted to various heights by a nonreflecting absorbing sheet. The efficiency of the launcher can be determined by first matching it to the surface when terminated by a resistive load. The latter is then replaced by a short circuit and the VSWR measured again; the launching efficiency is then equal to the voltage reflection coefficient. With aperture height of 1, 2, and 3 cm the efficiencies measured were respectively 30 per cent, 60 per cent, and 85 per cent, while from 5 cm, the efficiency flattened out to approach nearly 100 per cent asymptotically. Such results agree very closely with the theoretical values. A practical launcher [213] for a wave along a corrugated surface is shown in Fig. 16(a); two such devices, one for the input and the other for the output, give a power transmission ratio of 0.7.

The launching of a radial surface wave over a flat structure has also been the subject of investigation [28], [29]. In one series of experiments [81] the surface took the form of a large aluminium disk, 5-foot, 6-inch diameter and $\frac{3}{8}$-inch thick; it was electrically loaded to enhance its reactance by either a dielectric sheet or circumferential grooves. Radial slots were provided in the surface to enable probe measurements of field

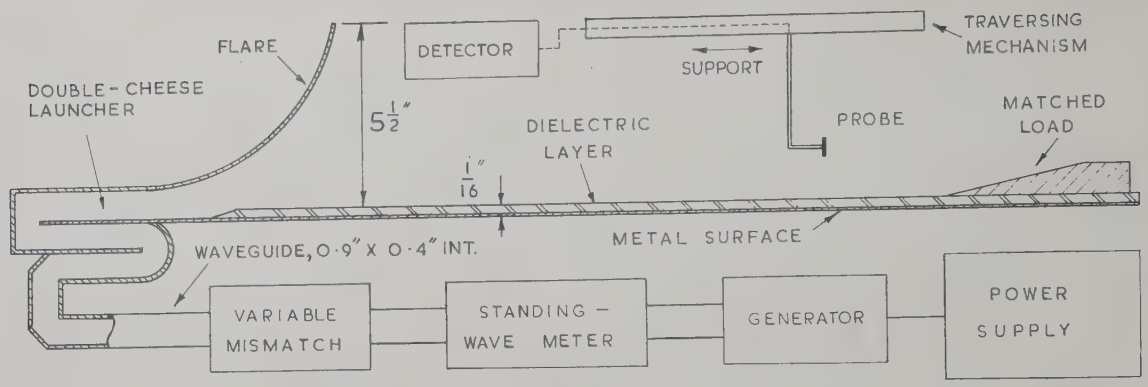

Fig. 15—Launching of waves over a dielectric surface. Frequency, 9 kmc; width of surface, 12 inches; dielectric-polystyrene, $\epsilon=2.5$.

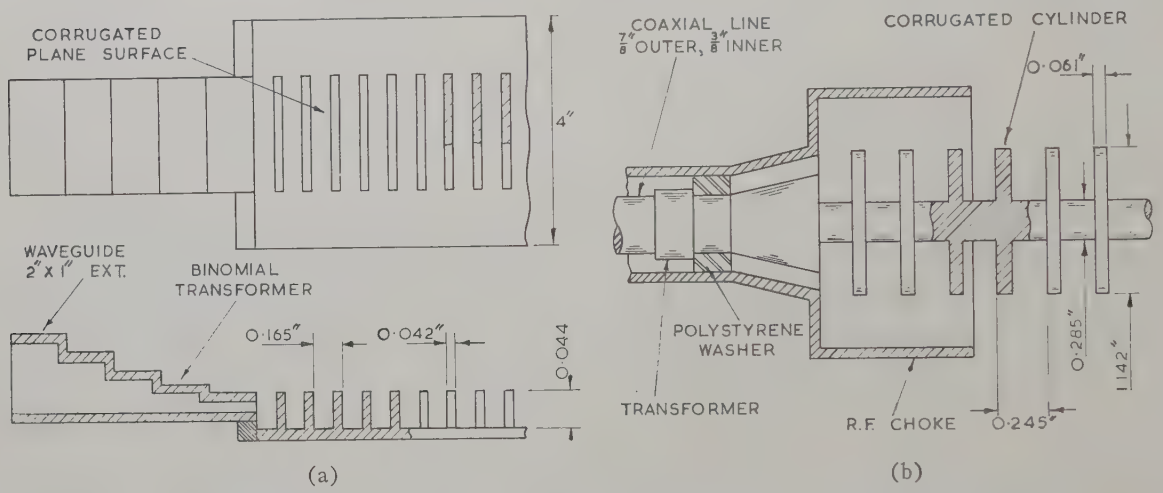

Fig. 16—Launching of waves over a corrugated surface. (a) Plane surface, frequency 5 kmc. (b) Cylindrical surface, frequency 3 kmc.

strength to be made. The launching was via a vertical dipole whose height above the surface was adjustable. At a frequency of 9.5 kmc, the launching efficiencies were as high as 80 per cent for a particular height of the dipole. Slot excitation has been shown [62] to be convenient, and efficient and the use of a circumferential slot in a conducting cylinder leads to symmetry of launching. In one arrangement [33] for 9.5 kmc, the slot is at the circumference of a radial line fed by a coaxial line within the cylinder.

Launching on a cylindrical-surface structure is facilitated because the Hankel function distribution of the radial field intensity approximates to the inverse radius law obeyed by fields inside a coaxial line. The wave is therefore usually [18], [74] launched by flaring the outer conductor of a coaxial line into a cone and continuing the inner conductor to form the transmission line. An alternative is to employ a tapered tube of solid dielectric slipped over the guide but, in either case, the surface wave tends to be contaminated by radiation from the launching device. As an example [213], Fig. 16(b) shows a corrugated cylinder fed from a rigid coaxial line; a typical value of launching efficiency is 90 per cent.

Practical data have been given [262] on surface-wave circuits and many instruments and components have been constructed. Simple corners can be made by employing [41] a large reflecting sheet situated at the intersection of the axes of the mating guides. Similar reflectors have been used to form surface-wave resonators. In one example [14], [16] for 9 kmc the short-circuited ends took the form of flat metal plates about 4-foot diameter and mounted at right angles to the guide. The energy was fed into the resonator by a small annular opening adjoining the guide at one end as shown in Fig. 17(a); the observed surface wave was very pure and thus measurement techniques are facilitated. It may be shown from (40) that

$$\frac{\lambda}{\lambda_g} \simeq 1 - \frac{1}{2}\left[\left(\frac{\lambda}{2\pi}\right)^2 (b^2 - a^2) + \left(\frac{\lambda}{2\pi}\right)^4 a^2 b^2\right] \qquad (68)$$

and, since the length of the circuit at resonance is an integral number of half-wavelengths, the velocity of propagation can be determined. The radial variation of the tangential magnetic field can be measured by a loop probe in the far end-plate of the resonator.

Neighbouring surface-wave lines can interact [173], [174] and thus impedances can be measured by re-

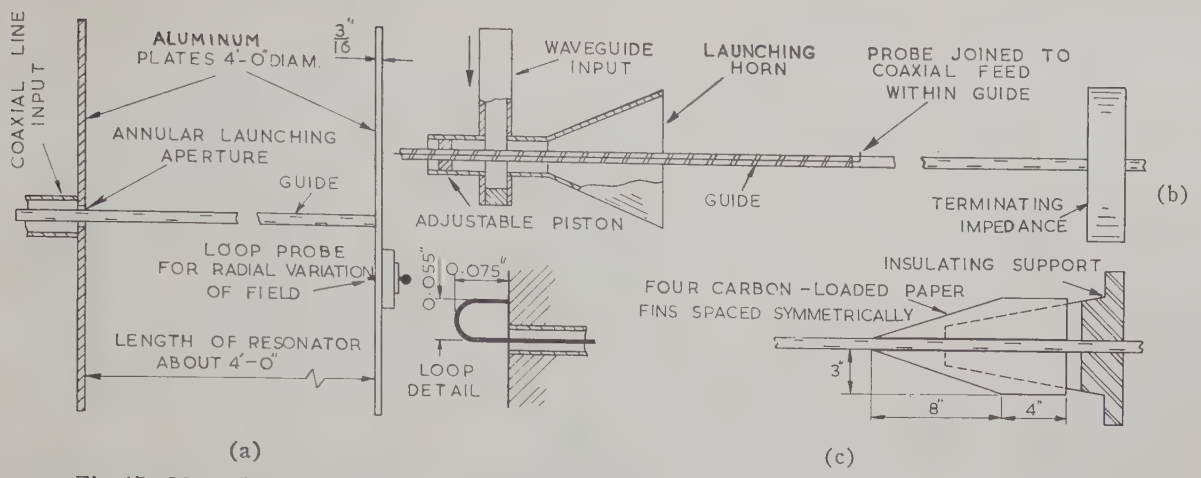

Fig. 17—Measuring apparatus for waves on cylindrical surfaces. Surface-wave resonator with loop detail. (b) Standing-wave meter for surface waves. (c) Matched termination, VSWR = 1.02.

flectometer techniques [226]. The loss of a surface-wave structure can also be measured [219] while the reflection-coefficient of a discontinuity can be determined by the Deschamps method [230]. Greater versatility is achieved by a standing-wave meter constructed in the surface-wave line itself and a typical example [16] is shown in Fig. 17(b). The surface waveguide consists of a metal tube through whose wall the probe projects slightly into the surrounding field. The energy extracted by the probe is taken to the detector via a coaxial line formed by an insulated wire drawn through the tubular guide. The probe projection is fixed and the whole guide with the probe is moveable while the field pattern remains stationary. A suitable matched termination is shown in Fig. 17(c).

Waves on Dielectric Lines

Plane Slabs

The waves considered so far have been TM modes propagating along a surface. In the case of a thick dielectric slab, higher modes may propagate and, depending upon the cross-sectional area of the guide, the proportion of energy flowing in the dielectric or in the external medium can be controlled. One such practical structure, the H-guide [255], consists of a dielectric slab between two parallel conducting strips. Provided that the dielectric has low loss, the attenuation of such a guide is not only less than that of the corresponding rectangular guide but decreases as the frequency increases.

Propagation of energy inside dielectric sheets [263] may be examined [220], [248], [288] by the use of Maxwell's equations, but an analysis depending on the breaking up of the wave into two criss-crossing components leads directly to the cutoff frequencies. Guidance takes place provided that these components are totally reflected at the dielectric/air interface. From Fig. 18(a), this means that the angle of incidence must be greater than the critical angle $\sin^{-1}\epsilon^{-1/2}$; that is,

$$\lambda/\lambda_g = \epsilon^{1/2}\sin\theta. \tag{69}$$

The wave impedance in the z direction is given for TE waves by

$$Z_{TE} = E_y/H_x = Z_w\epsilon^{-1/2}/\sin\theta, \tag{70}$$

and for TM waves by

$$Z_{TM} = E_x/H_y = Z_w\epsilon^{-1/2}\sin\theta. \tag{71}$$

The reflection coefficient for the transverse field component which is parallel to the interface is

$$\rho_{TE} = \frac{\epsilon^{1/2}\cos\theta + j(\epsilon\sin^2\theta - 1)^{1/2}}{\epsilon^{1/2}\cos\theta - j(\epsilon\sin^2\theta - 1)^{1/2}} \tag{72}$$

for the E_y component of TE waves and

$$\rho_{TM} = \frac{\epsilon^{-1/2}\cos\theta + j(\epsilon\sin^2\theta - 1)^{1/2}}{\epsilon^{-1/2}\cos\theta - j(\epsilon\sin^2\theta - 1)^{1/2}} \tag{73}$$

for the H_y component of TM waves. The imaginary terms in (72) and (73) represent an exponential decay of the fields outside the dielectric. The propagation coefficient in the x direction is real and given by

$$\gamma = -(2\pi/\lambda)(\epsilon\sin^2\theta - 1)^{1/2}. \tag{74}$$

The reflection coefficients always have a magnitude of unity and thus transverse standing waves are set up in the dielectric which are cosinusoidal for odd-numbered modes and sinusoidal for even-numbered modes. The electrical length ϕ of the standing wave from the midplane to the boundary for both TE_{0n} and TM_{0n} modes is given by

$$\phi = \cos^{-1}\left|(1+\rho)/2\right| + (n-1)\pi/2. \tag{75}$$

If λ_x is the transverse wavelength, Fig. 18(a) gives

$$\lambda/\lambda_x = \epsilon^{1/2}\cos\theta \tag{76}$$

and, therefore,

$$\lambda_x/l = 2\pi/\phi. \tag{77}$$

Combination of (76) and (77) gives

$$\lambda/2l = (\pi\epsilon^{1/2}\cos\theta)/\phi. \tag{78}$$

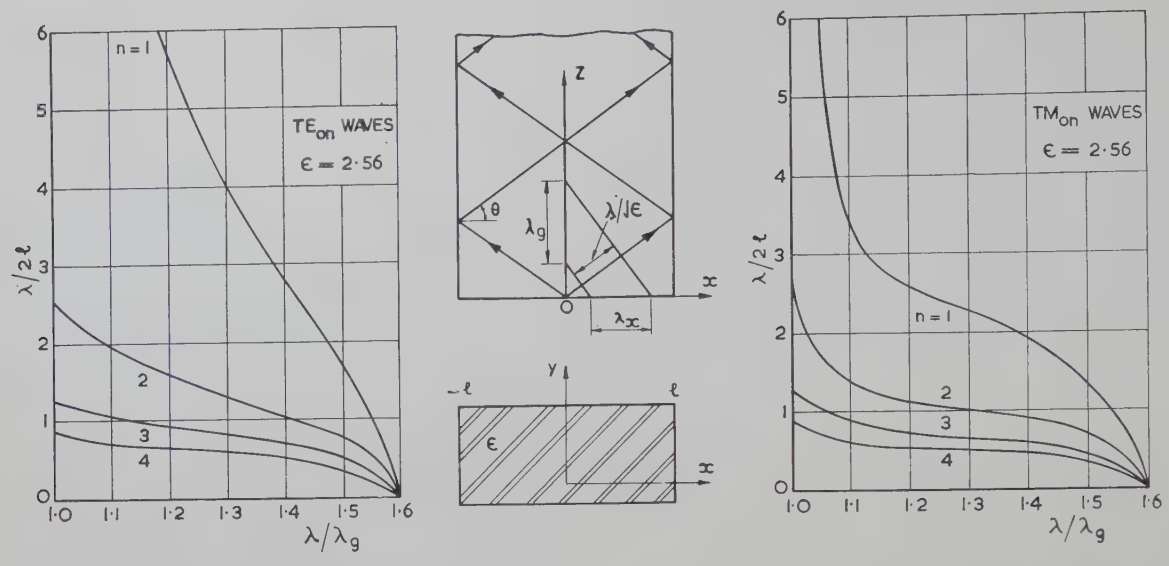

(a) (b) (c)

Fig. 18—Propagating modes in dielectric sheets. (a) Guide wavelength for TE_{0n} modes. (b) Geometry of the system. (c) Guide wavelength for TM_{0n} modes.

At cutoff, $\phi = 0$ and $\cos\theta = [(\epsilon-1)/\epsilon]^{1/2}$ so that

$$\frac{\lambda_c}{2l} = 2\frac{(\epsilon-1)^{1/2}}{n-1}. \tag{79}$$

Thus, for a given value of λ/λ_g, θ may be found from (69) and ϕ from (75) to give $\lambda/2l$ from (78). Values of $\lambda/2l$ vs λ/λ_g are plotted for polystyrene material with $\epsilon = 2.56$ in Figs. 18(b) and 18(c) for various TE and TM waves.

Cylindrical Rods

The theory of the nonradiative modes propagated along a dielectric rod was give by Hondros and Debye [115] and confirmed experimentally by Zahn [290] and Schriever [225]. Their study has a long history [53], [153], [209], [217], [218], [234] and is still the subject of extensive investigation [1], [127], [128], [249], [286]. A typical analysis [40], [78] assumes that there is a cylindrical coordinate system r, θ, z having its z-axis along the rod of radius r_1. The longitudinal components of the field vectors, omitting the factor $e^{(j\omega t-\gamma z)}$ are, inside the rod with $r<r_1$,

$$E_{zd} = A\cos n\theta J_n(u_d r), \tag{80}$$

$$H_{zd} = B\sin n\theta J_n(u_d r), \tag{81}$$

where

$$\gamma^2 - u_d^2 = -\epsilon\omega^2/c^2. \tag{82}$$

Outside the rod, with $r>r_1$,

$$E_{za} = C\cos n\theta H_n^{(1)}(ju_a r), \tag{83}$$

$$H_{za} = D\sin n\theta H_n^{(1)}(ju_a r), \tag{84}$$

with (30) as previously. Similar relations hold for the other field components. Eqs. (30) and (82) give

$$[(u_d^2 + u_a^2)/(\epsilon-1)]^{1/2} = \omega/c. \tag{85}$$

A further relation between u_d and u_a is obtained from the boundary conditions and thus enables these quantities to be obtained for given values of ω, n, and ϵ.

For $n=0$, the fields as shown in Fig. 19(a) are rotationally symmetrical and there are two solutions. One corresponds to a TM mode in which the magnetic lines of force are circles centered on the rod axis. The electric lines of force lie in the meridional planes through the rod axis; they go to infinity and asymptotically approach planes perpendiuclar to the rod that are spaced $\frac{1}{2}\lambda_g$ apart. The other solution corresponds to a TE mode in which the roles of the magnetic and electric field vectors are interchanged. If $n=1$, there is an unsymmetrical or "dipole" wave which may be roughly described as a sinuosidal dielectric polarization perpendicular to the rod and travelling along it. There is no cutoff frequency for this wave, which thus exists for thin rods or low frequencies.

The guide wavelength is given as a function of rod radius in Fig. 19(b) for the $n=0$ and $n=1$ modes, the free-space wavelength being 1.25 cm and $\epsilon=2.56$ for polystyrene. The attenuation coefficient is given in decibels per meter by

$$\alpha_d = 2729\epsilon(F/\lambda)\tan\delta, \tag{86}$$

where F is a dimensionless quantity plotted in Fig. 19(c). For large radii of the rod, F tends to its plane-wave value of $\epsilon^{-\frac{1}{2}}=0.625$ while for thin rods, it becomes smaller because a greater fraction of the energy resides in the external medium. Nonradiative modes similar to those discussed can also exist on dielectric tubes [264].

The $n=0$, TM mode on a dielectric rod can be launched [123] from the end of a TEM mode coaxial line or a TM mode circular waveguide [7]. The $n=0$, TE mode can be excited from a similar plate containing

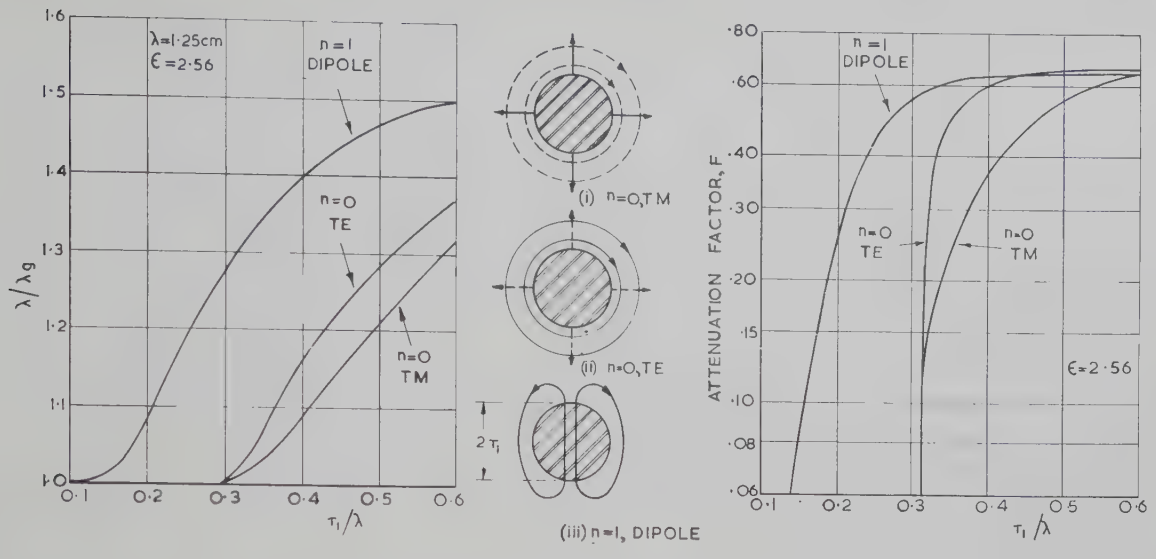

(b) (a) (c)

Fig. 19—Propagation along dielectric cylinders. (a) Field configurations of various modes. (b) Guide wavelength vs radius. (c) Attenuation vs radius.

slots which are suitably orientated and excited. The field configurations of the $n=1$, dipole, or HE_{11} mode are roughly similar to those of the TE_{11} mode in circular waveguide, and, thus, a suitable transition is one in which the dielectric rod, tapering from a point to minimize reflection, is inserted in the guide to fill the open end. The portion of the rod external to the guide may be further tapered to any size required. An experimental investigation [41] of this mode at 24 kmc showed that the guiding effect was retained even when the rod was only a fraction of a wavelength in diameter. With polystyrene material, the attenuation coefficient could be as small as 0.004 db/m, the values showing good agreement with (86). A length of the dielectric rod made resonant by supporting it between two plane mirrors 36-inches square, gave a maximum Q factor of 53,000. The propagation in the dielectric is, of course, altered by shielding [259] the rod by a metal tube.

In the case of TM modes supported by a lossy dielectric, it may be shown [18] that when the radius of the rod exceeds a certain value, the surface impedance is inductive and when it is less, the surface impedance is capacitive. For a perspex rod, $\epsilon=2.61$, radius 0.978 cm, the phase velocity at frequencies below 9.2 kmc was greater than the velocity of light.

Multiple Media

Surface waves may be propagated under more complicated conditions than those considered so far. In particular, the properties have been analysed of a cylindrical conductor embedded in two [122] or three [43] layers of coaxial dielectric. An analysis of surface wave propagation along several layers of different media has been given by Karbowiak [137] who showed that the surface impedance is then given by the sum of the surface impedances of the individual layers taken by themselves each over a perfectly conducting sheet. Furthermore, the impedance will remain the same even if one layer of the composite medium is split up into a number of thinner layers and intermixed with the others; it is the total thickness of any one medium that is important.

The analysis becomes difficult when the conductor is coated with a slab of magnetized ferrite. For thin slabs, the TM mode is dominant and if the applied steady field is perpendicular to the surface, it may be shown [195] that the phase velocity can be controlled by variation of its magnitude.

Provided that the dielectric coating on the conductor is thick enough, the higher order modes found in the case of the plain slab can propagate. The electric and magnetic fields have one or more half-sinusoidal variations in the dielectric but decay exponentially in the external air medium. The TM modes were given in an unpublished work by R. B. R. Shersby-Harvie by p_n, the $(n+1)$th solution of

$$\tan\left[2\pi p_n(\epsilon_d - 1)^{1/2}\frac{l}{\lambda}\right] = \epsilon_d\left(\frac{1}{p_n^2} - 1\right)^{1/2}. \quad (87)$$

The cutoff wavelength for the nth mode is given by

$$\lambda_c = 2l(\epsilon_d - 1)^{1/2}/n \quad (88)$$

and the corresponding guide wavelength is given by

$$\left(\frac{\lambda}{\lambda_g}\right)^2 = 1 + (\epsilon_d - 1)(1 - p_n^2). \quad (89)$$

Propagation is possible at all frequencies when $n=0$; this is the TM_0 mode previously considered for thin layers.

For TE modes, p_n is a solution of

$$\cot\left[2\pi p_n(\epsilon_d - 1)^{1/2}\frac{l}{\lambda}\right] = -\left(\frac{1}{p_n^2} - 1\right)^{1/2}. \quad (90)$$

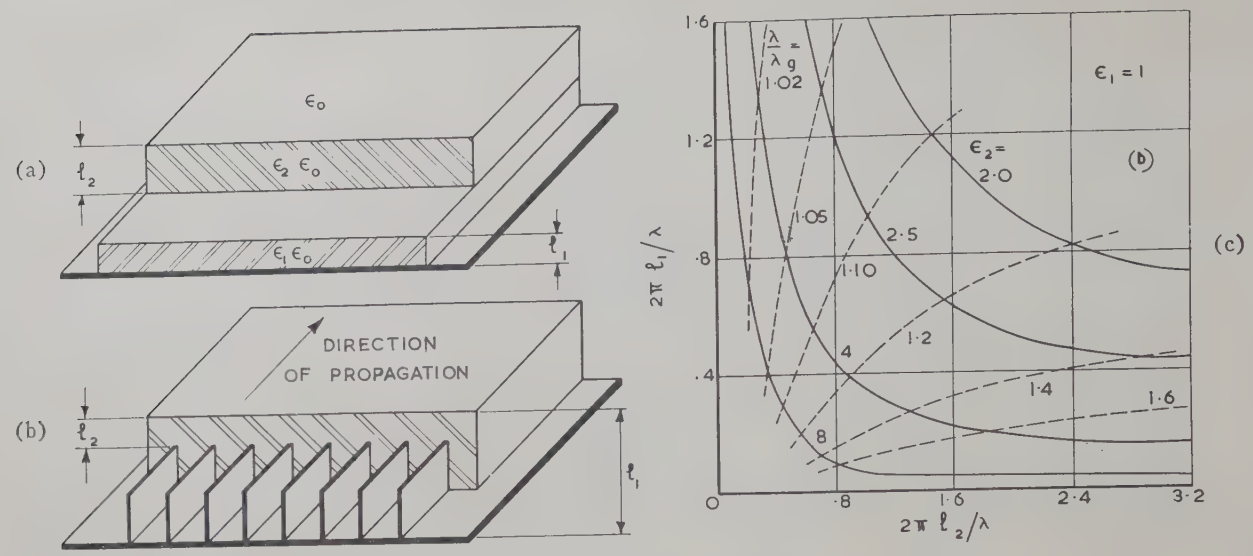

Fig. 20—Arbitrary-polarization surface-wave structures. (a) Double-dielectric slab. (b) Contours of equal phase velocity for TM and TE modes. (c) Single-dielectric slab with septa.

This has no real solutions if l is sufficiently small so that the lowest mode in this case has a cutoff wavelength. For the nth mode

$$\lambda_c = 4l(\epsilon_d - 1)^{1/2}/(1 + 2n) \tag{91}$$

and the corresponding guide wavelength is given by

$$\left(\frac{\lambda}{\lambda_g}\right)^2 = 1 + \left(\frac{\lambda_c}{4l}\right)^2 (1 + 2n)^2(1 - p_n)^2. \tag{92}$$

For some applications of surface-wave structures it is desirable to support a wave of arbitrary polarization; this means the combination of two principal polarization components with arbitrary amplitudes and phase. Propagation of such a wave over a surface-wave system requires that both TM and TE waves be supported and also possess the same propagation coefficient. The general equations for an n-layered slab have been given [75] and it has been shown [205] that the requirements for arbitrary polarization can be met by the double-layer earthed dielectric slab shown in Fig. 20(a). Typical contours of equal phase velocity for TM and TE waves on the slab-thickness plane are given [205] in Fig. 20(b); the lower slab is air filled, the parameters are λ/λ_g, and ϵ_2 is the dielectric constant of the upper slab.

A corrugated surface is unable to support a TE mode and thus an alternative medium for arbitrary polarization involves [108] the use of a "mode filter" consisting of septa embedded within a single dielectric slab whose initial thickness l and dielectric constant are adjusted for a given "trapping" of the TE mode. The septa shown in Fig. 20(c) are spaced considerably less than $\frac{1}{2}\lambda$ in the dielectric medium so that a wave with the electric field polarized parallel to them is reflected. The height $(l_1 - l_2)$ of the septa is chosen so that the TM mode is "trapped" to the degree desired. For example, with a slab of dielectric constant 2.5, an inverse velocity ratio (λ/λ_g) of 1.2 is obtained with a slab thickness $2\pi(l_1 - l_2)/\lambda = 1.0$ for the TM mode and $2\pi l_1/\lambda = 2.1$ for the TE mode. Such equal velocity surfaces are, of course, able to support circularly-polarized waves.

Image Lines

Surface-wave systems have found their main application in the antenna field [107] but the dielectric image line of King [146] shown in Fig. 21(a) has several advantages as a transmission line. This image line is essentially a dielectric rod supporting, as in field configuration (iii) of Fig. 19(a), the dipole mode in which a conducting sheet is placed in the plane of symmetry and normal to the electric field. Thus half the rod and the space surrounding it are replaced by an image in the conductor.

The polarization of such a line is uniquely determined while the phase-change coefficients are identical to those of the complete rod. The extent of the RF fields is determined by the ratio of rod radius to wavelength; if for example, this is 0.142, then 80 per cent of the power flows in a region of radius ten times that of the rod. For $\lambda = 1.25$ cm, a typical line in polystyrene would have a radius of 2 mm, the total width of the image plane being 10 cm.

The loss in the dielectric material is given by (86) but is supplemented by losses caused by radiation and the finite conductivity of the image plane. In the absence of artificial boundaries to the field, the radial component of the Poynting vector is purely imaginary and the radiation is zero. Loss caused by radiation does, however, occur in the presence of bends, obstacles and a finite image surface. The attenuation coefficient caused by conductor loss is given in decibels per meter by

$$\alpha_c = 69.5R_sF'/\lambda Z_a, \tag{93}$$

where F' is a factor which must be calculated [149] for

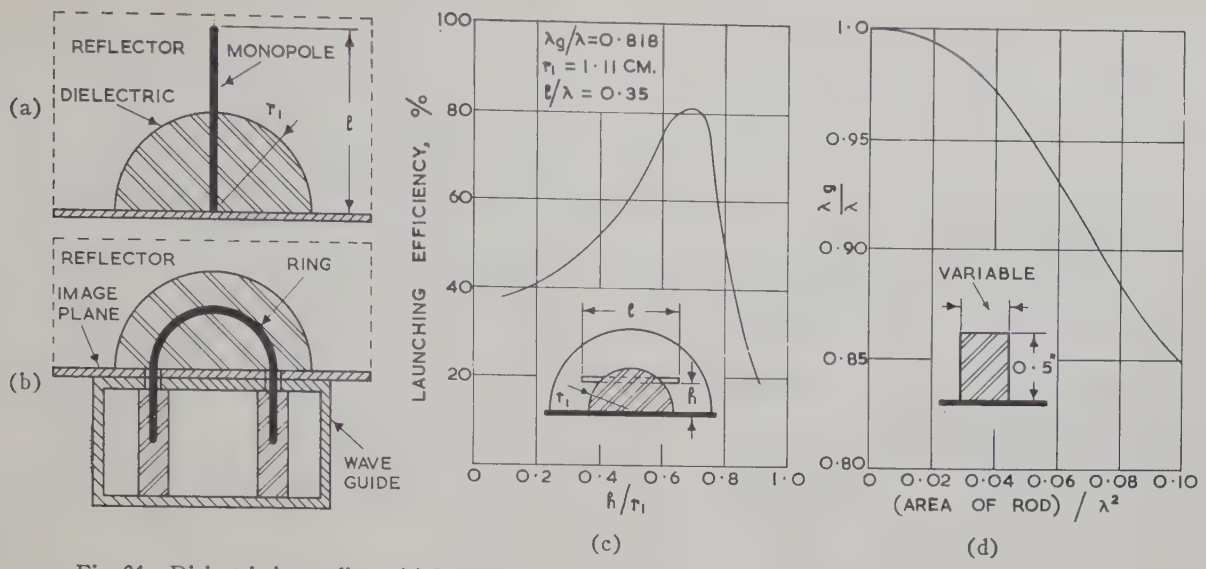

Fig. 21—Dielectric image lines. (a) Monopole launching. (b) Ring launching. (c) Efficiency of slot excitation. (d) Effect of varying the area of a rectangular rod. The frequency is 9.7 kmc.

the particular geometry. This loss is generally smaller than that caused by the dielectric except when the wave is only loosely bound to the line. For example, at 9.6 kmc the total attenuation coefficient in decibels per meter is 4.0 and 0.2 for values of r_1/λ of 0.4 and 0.15, respectively.

There are several methods of efficiently launching [73] a pure dipole mode on an image line. The monopole in Fig. 21(a) achieves an efficiency of 75 per cent provided that l/λ exceeds 0.15. It is necessary to position a reflecting plate about $\frac{1}{4}\lambda$ behind the monopole. As shown in Fig. 21(b), a ring excited from a rectangular waveguide achieves 75 per cent efficiency for r_2/λ between 0.1 and 0.2. The efficiency of resonant-slot excitation as a function of distance from the image plane is shown in Fig. 21(c).

The small dielectric cross sections used in the dipole mode do not permit any transverse resonances within the dielectric and the concentration of the field about the rod depends upon the volume of dielectric in regions of high electric field. The properties of the transmission system should therefore be insensitive to the exact shape of the dielectric cross section, but strongly dependent upon the total cross-sectional area occupied by the dielectric. Typical sections studied [147] at a frequency of 24 kmc were a half round, radius 0.066 inch, both in the normal and inverted positions, a 0.084-inch square, and a rectangle, 0.280 inch×0.030 inch, with either face in contact with the image plane. Such shapes, as well as recessed and twin lines, all show much the same dielectric loss and field confining effect. The rectangular shape does, however, lend itself to easy fabrication and Fig. 21(d) gives data [223] at 9.7 kmc for a particular sample.

Experiments [148] show that the system is insensitive to minor twists and imperfections in the dielectric rod while the surface finish of the image plane is not important. Such properties make the image line suitable [289] for millimeter wavelengths. Simple bends and corners can be made with moderate loss and low reflection. Semiconductor diodes may be coupled to the image line with an insulated metal pin to give a VSWR better than 1.2. A variable attenuator results when a thin resistive sheet is placed in a radial plane whose angle with respect to the image plane can be adjusted. Such devices as standing-wave meters and directional couplers can also be made in image line.

Coupled-Resonator Structures

Tape-Ladder Lines

Systems propagating slow electromagnetic waves are used extensively in practice and, although continuous dielectrics have a limited application, the majority employ periodic structures of various kinds [26], [106], [130]. The velocity of propagation in such structures must depend upon the particular application and may, for example, be c for linear electron accelerators [110], 0.1 c for electron-tube amplifiers [202] and 0.01 c for solid-state low-noise amplifiers [68]. Although bidimensional and tridimensional slow-wave structures have been examined [30], [182], only linear types will be considered in what follows.

The power P flowing along a slow-wave structure and W_s are related by

$$P/W_s = v_g. \tag{94}$$

If the electric field in the structure is of importance, then a practical parameter is the coupling impedance

$$Z_c = |E|^2/2\beta^2 P. \tag{95}$$

If the modulus of the magnetic field is effective, the performance is specified by the admittance

$$Y = |H|^2/2\beta^2 P. \tag{96}$$

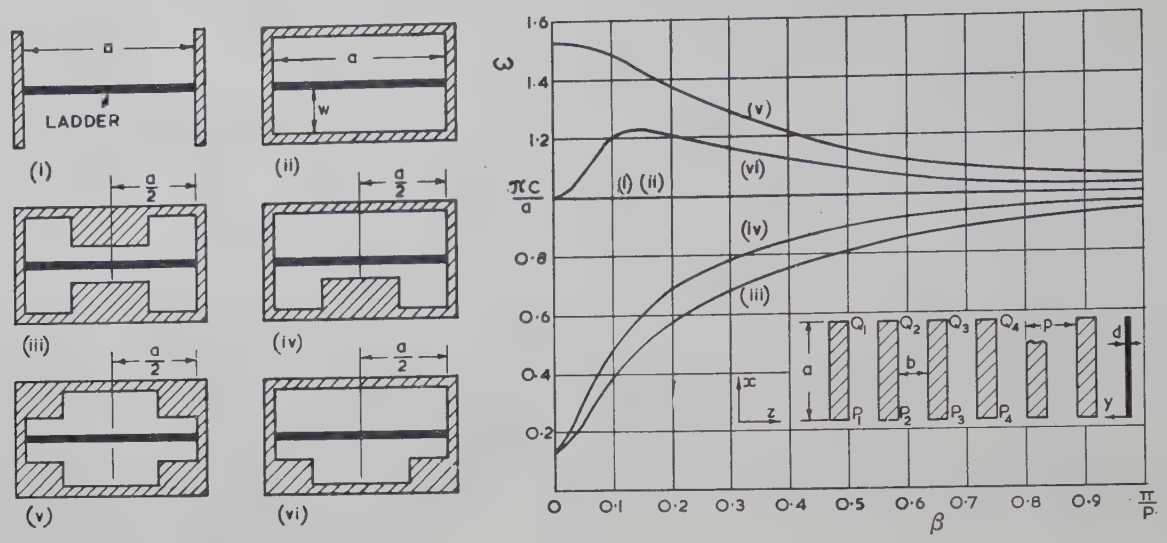

Fig. 22—Propagation along tape ladder lines. (a) Cross sections of lines. (b) Dispersion curves with ladder detail. Structures are (i) side wall, (ii) waveguide, (iii) double ridge, (iv) single ridge, (v) double tee and (vi) single tee.

Another parameter, the shunt impedance, is defined as

$$Z_{sh} = |E|^2/2\alpha P \tag{97}$$

and is related to the power dissipated per unit length because of ohmic losses.

A large class of slow-wave structures consists [21] of resonators of identical shape and size coupled together. The two basic types of coupling are pure inductive and pure capacitive, the magnitude of each component determining how the ω-β diagram of the uncoupled resonators is modified. For example, the ladder line consists, as shown in the inset of Fig. 22(b), of a periodic array of parallel straight conductors. Such a wire or tape structure can propagate a variety of TEM waves, each one corresponding to a different mode of excitation of the tapes; the simplest mode is that in which there is a phase change βp from one tape to the next.

$$V_m \text{ (or } I_m) = V_{m-1} \text{ (or } I_{m-1}) e^{-i\beta p}. \tag{100}$$

The characteristic impedance of a single conductor in the array may be defined by

$$Z_0(\beta p + 2n\pi) = V_m/I_m, \tag{101}$$

where n is caused by the periodicity of the structure.

The method of determining Z_0 found by Fletcher [85] is restricted to rectangular conductors and assumes that the component E_z of field is constant throughout the region between the tapes. The fields at the common boundaries of the other regions are then matched. The voltage on the nth conductor can then be obtained directly, and the current in the conductor can be found by integrating the tangential component of magnetic field around its periphery. With the ladder equally spaced from either ground plane and with dimensions as in Fig. 22, this method gives

$$\frac{Z_w}{Z_0} = \frac{4d}{b}\sin^2\left(\tfrac{1}{2}\beta p\right) + 4\left(1-\frac{b}{p}\right)\sin\left(\tfrac{1}{2}\beta p\right)\sum_{-\infty}^{+\infty}(-1)^n \times \coth\left\{\frac{w}{p}(bp+2n\pi)\right\}\frac{\sin\left\{\left(1-\frac{b}{p}\right)\left(\frac{\beta b}{2}+n\pi\right)\right\}}{\left(1-\frac{b}{p}\right)\left(\frac{\beta p}{2}+n\pi\right)}\cdot\frac{\sin\left\{\frac{b}{p}\left(\frac{\beta p}{2}+n\pi\right)\right\}}{\frac{b}{p}\left(\frac{\beta p}{2}+n\pi\right)}. \tag{102}$$

The dispersion curve and coupling impedance of the ladder structure can be calculated by assuming that the TEM-mode voltage on each wire is given by

$$V(x, y, z, t) = V(y, z)(Ae^{-i\beta_w x} + Be^{i\beta_w x})e^{i\omega t}, \tag{98}$$

where

$$\frac{\partial^2 V}{\partial_y{}^2} + \frac{\partial^2 V}{\partial_z{}^2} = 0. \tag{99}$$

The voltage and current on successive conductors in a given (y, z) plane are related by

Numerical values of the summation for practical geometries have been given by Walling [276]. If $w/p \to 0$, (102) simplifies to

$$\frac{Z_w}{Z_0} = \frac{4d}{b}\sin^2\left(\tfrac{1}{2}\beta p\right) + \frac{2p}{w}\left(1-\frac{b}{p}\right). \tag{103}$$

Leblond and Mourier [163] calculated Z_0 by using a quasi-electrostatic field distribution in the (y, z) plane, but this method requires a measured value of the capacitances between different parts of the structure. The

analysis also assumes that the conductors are thick enough in the direction normal to the plane of the ladder to ensure that each wire is shielded from all except its neighbours; for rectangular conductors the result reduces to (103).

Butcher [38] has exactly calculated the RF fields distributed around an array of thin tapes by a method which takes into account all the mutual couplings. This theory predicts in the practical case of equal tape and gap widths with $w = \infty$ that

$$\frac{Z_w}{Z_0} = 4 \sin \tfrac{1}{2}\beta p \tag{104}$$

which may be compared with (102). It was shown that the coupling impedance and the group velocity have a product which with certain provisos, is the same for a wide range of geometries. This "field distribution factor" of an array, using (94) and (95) is given by

$$F_d = \frac{v_g Z_c}{c Z_w} = \frac{\epsilon_0 |E|^2}{2\beta^2 W_s}. \tag{105}$$

In the case of space harmonics such that $1.5\pi < \beta < 2\pi$, the exact solution leads to much higher values for the coupling impedance than those given by the approximate methods.

The results of these methods are applied to practical structures by consideration of the geometry and boundary conditions. In Fig. 22(a) the tapes are short-circuited at either end by (i) two perpendicular conducting side walls or (ii) the opposing narrow walls of a rectangular waveguide. Whatever the value of β, this array can support TEM standing waves only at the frequency for which λ is twice the length of the tapes. The dispersion curves (i) and (ii) shown in Fig. 22(b) are thus horizontal lines and since the group velocity is always zero, the structure does not propagate. Both inductive and capacitive coupling are present but the amounts are just equal and cancel each other.

The tape-ladder line can be given a pass band with finite bandwidth by upsetting [37] the equality. The frequency corresponding to any value of β can be reduced by distorting the structure to the ridge shapes (iii) and (iv) of Fig. 22(a) which, in effect, reduces the cutoff frequency of the guides formed on either side of the ladder. The dispersion curves therefore have the forms labelled (iii) and (iv) in Fig. 22(b) and the structure now propagates energy. The frequency corresponding to any value of β can be increased by adopting the tee-shaped structures (v) and (vi) of Fig. 22(a), the corresponding dispersion curves being given in Fig. 22(b). The single tee curve behaves peculiarly because the cutoff frequency of the TE_{01} mode of the guide formed below the ladder is higher than the zero mode cutoff frequency set by the guide above the ladder and the first resonant frequency of the tapes. In both tee structures the fundamental is seen to have the phase and group velocities in opposite directions; it is thus a backward wave. The π-mode cutoff frequency of any of these ladder lines can be raised by using shorter tapes running between horizontal plates supported by the side walls [186]. The π-mode cutoff frequency is still approximately equal to the first resonant frequency of the short-circuited tapes and is thus inversely proportional to their length. This is a valuable technique for broadening the pass band of these structures while, moreover, energy can now be made to propagate down the undistorted rectangular waveguide.

The above analysis can be applied to a structure consisting of two parallel arrays. In this case, modes can exist with symmetric or antisymmetric field distributions; the former is usually of practical interest. Such multiple lines give [191] high coupling impedance, wide pass band, and low dispersion. Ash [11] has shown that propagation takes place along the ladder if the tapes are inclined or distorted in some way. Since there is now no need for ridge or tee sections, several ladder lines may be stacked together. Tape-ladder lines have proved to be a convenient means of achieving [68] group velocities of the order of 0.01 c.

If, in the ladder line of the inset of Fig. 22(b), P_1 is short-circuited to P_3 and Q_2 is short-circuited to Q_4, while P_2, P_4, Q_1, and Q_3 are open-circuited and so on down the array, the interdigital line [112], [164], [193], [279] of Fig. 23(a) is obtained. The period of the whole structure is $2p$, but it is also unchanged when it is moved along the z-axis through half a period and then reflected in the $x = 0$ plane. It is possible, therefore, to consider a mode for which the electric field at $(-x, y, z+p)$ differs from that at (x, y, z) only by a constant factor $e^{-j\beta p}$.

Taking into account the boundary conditions, the dispersion curve may be calculated as for the ladder line. The results [38] for thin tapes, for various values of b/p, are given in Fig. 23(b). The branch corresponds to a backward space harmonic but the complete dispersion curve can be obtained by displacing it by integral multiples of π/p along the β-axis and then reflecting all these branches in the ω-axis. The portions of the curve in which v_g tends to be greater than c lie in forbidden regions such that the phase velocity of one of the space harmonics also exceeds c. The exact dispersion curve of a completely open structure cannot pass through the forbidden regions because, if it did, the structure would radiate. For thick tapes, successive gaps are shielded from one another and the structure resembles a folded transmission line; the branches are given by

$$\pm \omega - 2\beta = 2n\pi/p \tag{106}$$

as shown by the dashed line of Fig. 23(b). For very wide gaps, the free-space wavelength has the value $4a$ as in the dotted line.

The meander line of Fig. 23(c) is constructed by short circuiting P_1 and P_2, Q_2 and Q_3, and P_3 and P_4, and so on down the array. The structure has a period of $2p$ and is able to propagate at frequencies down to zero. It may

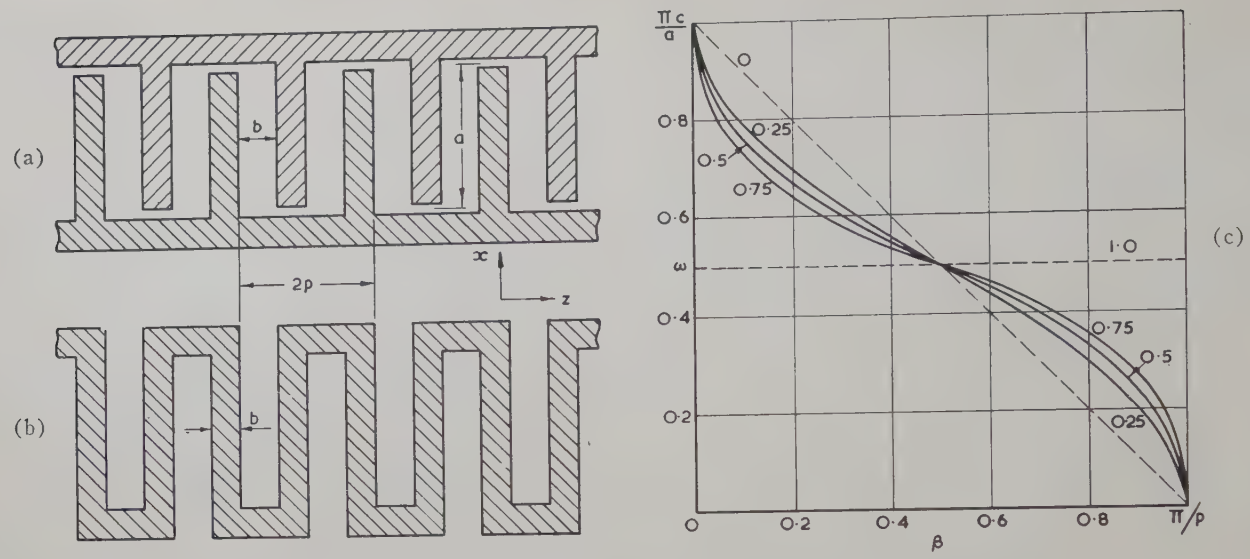

Fig. 23—Interdigital and meander structures. (a) Interdigital tape line. (b) Dispersion curves with parameter b/p. (c) Meander tape line.

be shown [38] by the use of Babinet's principle that the complete dispersion curve of a meander line with gap width $(p-b)$ and tape width b is the same as that of an interdigital line with gap width b and tape width $(p-b)$. For structures with thick tapes, the phase velocity of the nth space harmonic is given by

$$\frac{c}{v_{pn}} = 1 + \frac{a}{p} + \frac{\lambda}{2p}(2n-1) \tag{107}$$

and the group velocity is

$$v_g = \frac{c}{1 + a/p}. \tag{108}$$

Resonant Cavities

Slow-wave structures [65], [66] may employ resonant cavities coupled in various ways. If the amount of loading is small, the analysis can be based on a perturbation of a homogeneous transmission line. For example, Field [82] considered a coaxial line in which either the inner or outer conductor is provided with radial grooves [70], [242]. Such an inductively-loaded surface can support a TM-type slow wave, the phase velocity being governed by the depth of the stub. At 9 kmc the inner conductor is typically 0.686-inch diameter with disk thickness of 0.011 inch and spacing rather more. As with all corrugated structures, the field decays in the transverse direction and, in the example quoted, the field is effective to about 0.04 inch from the disc edges.

The structure of Fig. 24(a) is essentially a rectangular waveguide with one broad wall inductively loaded with series stubs. The dispersion curve resembles that of Fig. 2 except that there is a lower cutoff frequency caused by the unperturbed waveguide. A waveguide of square section can transmit two orthogonal modes with different velocities and, as such, is a broad-band means of producing [236] circularly polarized waves. In practical

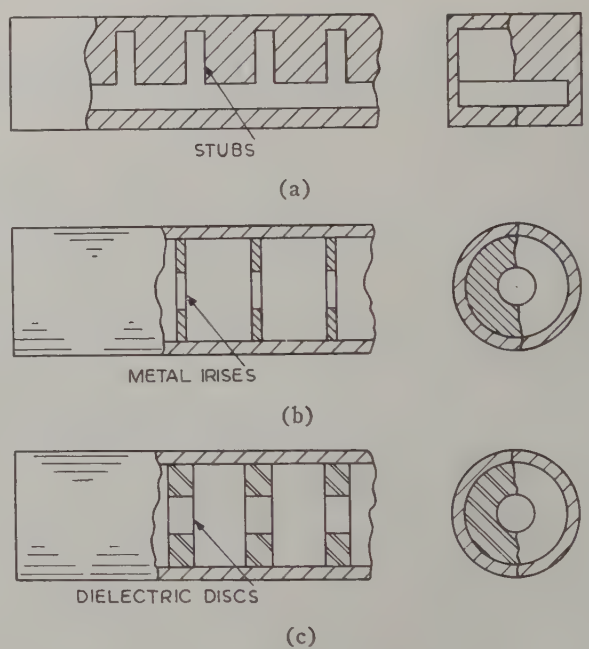

Fig. 24—Coupled-cavity slow-wave structures. (a) Stub resonators in rectangular guide. (b) Capacitive-coupled circular resonators. (c) Dielectric-disc loading of circular guide.

structures [135], [179], [265] for millimeter wavelengths the stubs have been milled in the ridge of a ridged waveguide.

The disk-loaded circular guide [144], [201] of Fig. 24(b) has been extensively employed in applications requiring $v_p = c$. The theory [31], [51], [69], [101], [102], [104], [105] of TM propagation is based on a matching of the fields at the mouths of the resonators. The dispersion [56], [245], [268], [269], [270] of this structure is rather pronounced but can be reduced at the expense of low coupling impedance by the use of large apertures in the disks. Data has been given on attenuation [57] and the theory has been confirmed by

experiment [103]. An alternative treatment assumes [165], [181], [233] that the circular waveguide is periodically loaded with shunt susceptances while an accurate estimation of the dispersion curve has been based [212] on a Fourier series representation. In some cases, lower attenuation is achieved by the use of dielectric disks [277], [278] as an anisotropic artificial medium.

Resonant-cavity slow-wave structures can be analysed [21] by consideration of the method of coupling. Pure inductive coupling is a scheme in which only H lines link the cavities. An example consists of a TE_{01} mode rectangular waveguide with transverse partitions spaced distance p apart. The dispersion curve is a horizontal frequency line corresponding to $\lambda_g = 2p$ which joins the points at $\beta = 0$ when the cavities oscillate in phase and at $\beta = \pi$ when they are out of phase. Narrow slots in the partitions cut centrally and parallel to the short sides of the guide allow inductive coupling, and consideration of the magnetic field distribution shows that the π mode is not affected whereas the zero mode is lowered until, as the slot widens, it reaches the cutoff frequency of the plain rectangular waveguide. The equivalent circuit of this structure is a transmission line periodically loaded with shunt inductances and the dispersion curve thus resembles that of Fig. 2.

Pure capacitive coupling exists in the disk-loaded circular waveguide, since E lines penetrate the small central aperture. In this case the zero mode is not disturbed while the other end of the pass band rises as the hole diameter increases to reach eventually the characteristic of a plain circular guide. The equivalent circuit of this structure is that of a line loaded with shunt capacitance and the dispersion curve resembles that of Fig. 1.

Mixed coupling is characterized by the presence of both E and H lines in the coupling mechanism. Again considering the disk-loaded circular waveguide, a slot cut in the periphery of the partitions will introduce inductive coupling. Investigation of the field perturbations caused by the central and peripheral apertures shows that the zero mode remains constant while the π mode is raised in frequency for the capacitive coupling, as previously observed, but lowered for the inductive coupling. If the structure initially has a central aperture, the addition of the inductive slot will decrease the capacitive pass band until, with equality of coupling, it becomes zero. Further increase in size of the inductive slot, which may be regarded as introducing positive mutual coupling, lowers the π-mode frequency. The fundamental component of the wave travelling through the structure now has negative phase velocity [48] and is thus a backward wave.

In disk-loaded circular guides employing an electron beam, less stringent requirements are placed on the central aperture if the coupling of the cavities is mainly by inductive slots. Forward-wave operation now requires, however, the use of the $n = +1$ space harmonic with consequent reduced coupling impedance. A forward-travelling fundamental may be set up by employing negative mutual coupling. Chodorow and Craig [47] achieved this by using different shapes for alternate cavities so that the magnetic field on opposite sides of the partition is in the same direction at the π mode but in the opposite direction for the zero mode. The cloverleaf structure [47], [91] of Fig. 25(a) is an example of such a design. The dispersion curve shows that the zero-mode frequency is depressed relative to the π mode. At $\beta p = \frac{1}{2}\pi$, a typical coupling impedance is about 130 ohms.

Negative mutual coupling can also be obtained [47] with the structure of Fig. 25(b) in which adjacent cavities are coupled by reversed loops. An extension of this principle is that with the addition of many loops around the entire structure, the metallic wall can then be omitted. The dispersion curve of such an interlaced structure, shown in Fig. 25(b), indicates that the fundamental is again a forward wave. For reference, the cutoff frequency of the TM_{01} mode in the unloaded guide is also given. The characteristics are modified [194] when the loop circuits are themselves resonant.

The characteristics of periodically loaded waveguides may be measured by a number of experimental methods [9], [79], 159], [247]. The properties of a matched input coupling [185] may be examined by terminating the slow-wave structure with a nonreflecting load and by making impedance measurements in the input transmission line. In one method [124], all reactive values of the impedance in the loaded guide were produced by sliding a metal shorting plug into it at various distances. The parameters of the coupling system were then determined by the well-known nodal shift method.

The frequency characteristic of a periodic guide may be determined from probe measurements when the far end is short circuited. Care must be taken in the location of the probe since it detects the total electric field of all the space harmonics whereas generally a determination of the wavelength of the fundamental space harmonic is all that is required. Another method makes use of the fact that the phase of the field inside the stub uniquely determines the fundamental wavelength in the line. Thus by measurement of the amplitudes of the fields at the back of each stub and plotting on a graph, the wavelength may be obtained. Greater accuracy was obtained [135] in measurements at 50 kmc by using a sliding base plate to carry the probe, the output of which was fed into a bridge comparison circuit.

One satisfactory method is to short circuit the transmission system at both ends and to search for the resonant frequencies of this structure. It is necessary that the short-circuiting plungers be at planes of symmetry of the system so that all space harmonics have zeros in the standing-wave pattern at the plungers. If this is not done, reactances, caused by other modes being excited at the ends of the structure, would result in the resonant frequencies being dependent to some extent on the

length of guide chosen. The condition for resonance is that there must be an integral number of half-wavelengths in the length of the guide so that for a structure of N resonators, β is given by

$$\beta = 2\pi/\lambda_g = n\pi/Np. \tag{109}$$

The resonant frequencies of the author's structure consisting of $N=6$ resonators are shown in Fig. 26; the relevant dimensions are given in the inset. It is seen that the modes form a group of $N+1$ frequencies in a restricted pass band where the modes are clustered in the neighbourhood of the two edges of the pass band and more widely spaced between. The edges of the pass band are the zero and π modes at which the phase changes from one section to the next are $\beta p=0$ and π, respectively. The group velocity may be found from the slope of the curve and therefore by using a measured value of unloaded Q factor, the attenuation is calculated from (8). A periodic waveguide may also be made resonant by bending it around in a circle so that the input connects to the output. In this case there must be an integral number of whole wavelengths in the length of guide and, once again, the continuous curves break up into a series of discrete points or modes. In both these types of resonators the separation of the resonances, especially near the π mode, can be increased by the use of systematically-modified loading reactances.

The field distribution, coupling impedance, and shunt impedance of a slow-wave structure are usually determined by perturbation techniques [3], [184]. As shown

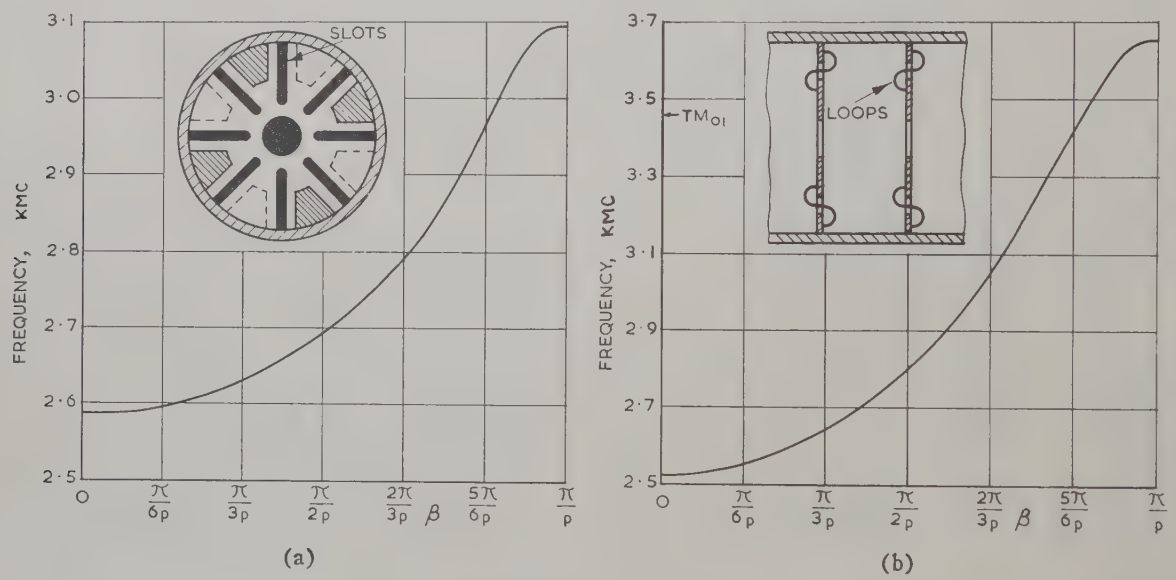

Fig. 25—Slow-wave structures with negative-mutual inductance coupling. (a) Re-entrant cavity with slot coupling. (b) Cavity with reversed-loop coupling.

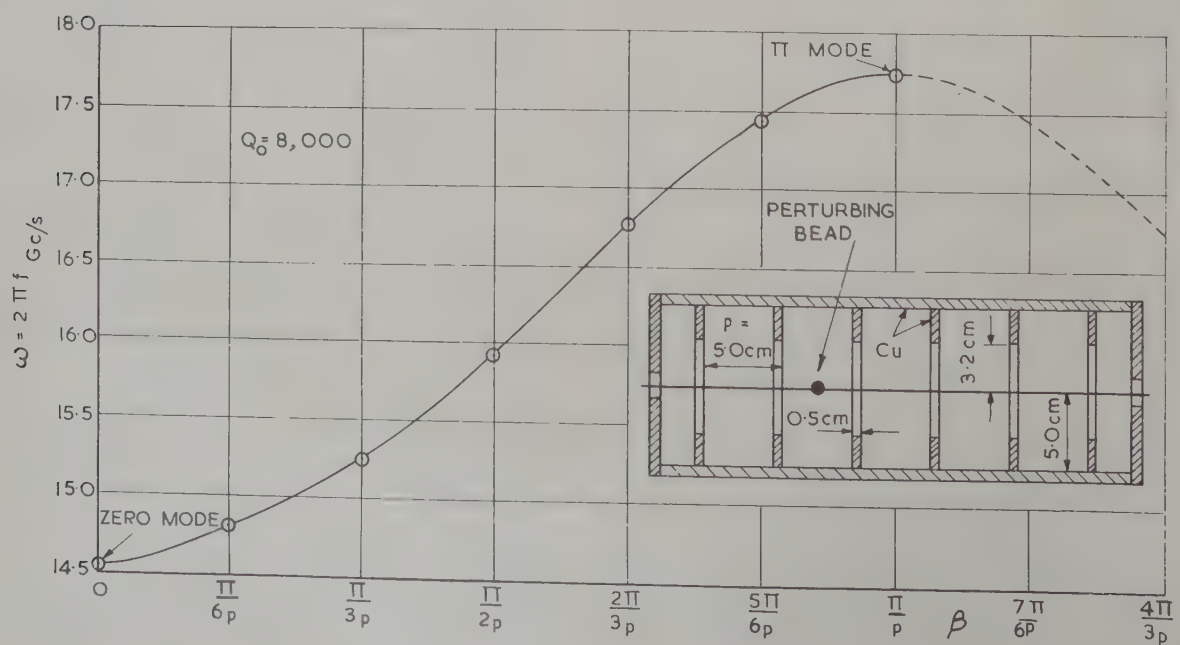

Fig. 26—Resonant frequencies of a short-circuited slow-wave structure.

in the inset of Fig. 26, a perturbing object such as a small dielectric or metal sphere is moved along a predetermined line as, for example, the direction of propagation. Observations are made on the changes in resonant wavelength for which Slater [233] gives the relation

$$\frac{d\lambda}{\lambda} = -\frac{1}{2}\frac{\int_{\Delta V}(\mu_0 H^2 - \epsilon_0 E^2)dV}{\int_V (\mu_0 H^2 + \epsilon_0 E^2)dV} \qquad (110)$$

where ΔV, V are, respectively, the perturbed and cavity volumes. The measurement is made absolute by determining the total stored energy by introducing [187] for, example, a small variable plunger in a region where H is zero and E constant. From knowledge of the phase velocity and field distribution, the coupling impedance may be calculated.

Helical Structures

Simple Helix

A widely-used slow-wave structure consists of a metallic conductor wound in the form of a helix with circular cross section. The propagation of electromagnetic waves on such helical structures was first studied by Pocklington [206] who assumed that there was a thin perfectly conducting wire. The solutions obtained predicted a travelling wave whose axial phase velocity is nearly c for low frequencies but reduces to $c \sin \psi_h$ for high frequencies. The latter result is equivalent to a wave with phase velocity c travelling along the wire. Under these circumstances it has been shown [138] that the wave possesses axial components of both electric and magnetic field and since it is evanescent over the wave front on the outside of the helix it may be regarded as an *EH* surface wave, *i.e.*, a mixture of TM and TE modes which contain roughly equal amounts of electric and magnetic energy. A pure *EH* wave may only exist as a travelling wave on a simple helix—two *EH* waves travelling in opposite directions result in an elliptically polarized *EH* surface wave whose plane of polarization rotates with position along the line.

Some basic properties emerge from the model applied by Ollendorf [188] and others [132], [150], [151], [202], in which the helix is replaced by an anisotropic sheet wound on a cylinder and conducting only in the ψ_h direction. This sheath model ignores the periodic structure of the actual helix as well as the finite size of the conductor. Sensiper [228] shows that solutions only exist for slow waves where $\beta > \beta_w$ and which represent modes characterized by different angular variations given by $e^{jm\theta}$. The usual $m=0$ wave shows large dispersion at low frequencies, but at higher frequencies, the phase and group velocities are nearly equal over a broad band. For modes where $m>1$ which occur when $2\pi r_h > \lambda$, the results are more complicated since there are now several waves per mode number. When these are plotted on an $\omega-\beta$ diagram it is observed that some branches have the phase and group velocities in opposite directions, corresponding with backward waves. The sheath model enables an estimate of the coupling impedance to be made but experiment [63] shows that this is about twice that possessed by practical structures.

The periodic nature of the helix is evident in analysis based on the tape model in which the conductor is considered to possess zero radial extent. The structures examined have included narrow tapes or wires [154], [155], [156], [197], [214], [215], [240], those with narrow gaps [266] and miscellaneous sections [49]. The developed tape helix [228] is shown in Fig. 27(a), practical structures having nearly equal gap and conductor widths. It is evident that

$$\cot \psi_h = 2\pi r_h / p. \qquad (111)$$

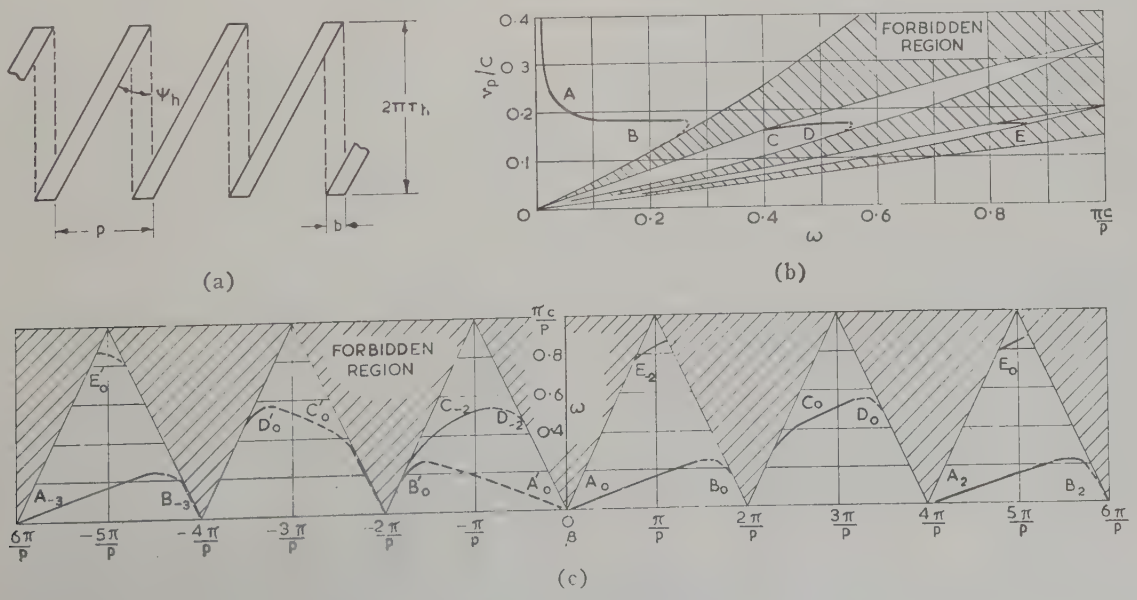

Fig. 27—Propagation along a tape helix. (a) Developed tape helix. (b) Phase velocity vs frequency. (c) Frequency characterisitc. Helix details are $\psi_h = 10°$, $\pi b/p = 0.1$.

The periodicity means that the wave function is characterized by a phase-change coefficient given by (1). Each angular mode of the helix now contains a complete set of space harmonics and, because of the close connection between translation and rotation in helical structures, the conditions for propagation require $m=n$. The exponential field relation then becomes

$$e^{-jn}[(2\pi/p)z - \theta]. \tag{112}$$

On applying the appropriate boundary conditions, analytical and graphical procedures give the results shown in Fig. 27(b) for the particular case of $\psi_h=10°$ and $\pi b/p=0.1$. The condition $\beta_n>\beta$ leads to the existence of forbidden regions which are associated [203] with coupling to fast waves [169] leading to radiation from the structure. No propagation takes place for the condition

$$\omega > \pi c/p \qquad \text{or} \qquad p < \tfrac{1}{2}\lambda. \tag{113}$$

The branches A to E correspond to different angular modes. If the helix is excited by a source at $z=0$, then for $z>0$ those waves with positive group velocity, indicated by full lines, can exist, whereas for $z<0$ those waves with negative group velocity, indicated by dotted lines, can occur.

For example, when $\omega<0.2\pi c/p$, propagation is possible with values of β_0 indicated by the branches A_0 and C_0 having positive phase velocities and B_0' having negative phase velocities. A few examples of the associated space harmonics marked with the appropriate subscript n, are also shown on the diagram; such harmonics have been observed experimentally [5], [280], [281]. The phase velocity [267] of the harmonics for various angular modes is given by

$$\frac{v_{pn}}{c} = \frac{\beta_w p/2\pi}{n + \beta_0 p/2\pi} \tag{114}$$

and values for various branches are given, as a function of ω, in Fig. 27(c). Eq. (114) shows, for example, that the first forward space harmonic is equivalent, as regards phase velocity, to the fundamental of a helix of radius $(2\pi r_h-\lambda)/2\pi$. Operation in such a harmonic allows [158] the use of a larger helix than with the usual fundamental mode.

Analysis of the power flow shows that a considerable fraction is carried by the space harmonics which explains the too-high coupling impedance given by the sheath-helix model. Butcher [38] extended his work on ladder lines to include calculation of the dispersion curves and coupling impedance of tape helices. Other studies of the helix have included power handling capacity [34] and attenuation [118], [222], [261]; the latter results have been extended [49] by the use of a correction factor to conductor shapes other than the thin tape.

Practical Modifications

Considerations arising in practical use require modification [161] of the simple helix. The effect of a dielectric has, for example, been examined [100] in the case of a spiral support for a coaxial line but most work [183], [189], [221], [240], [260] has been devoted to determining the change in characteristics of the metal helix in a continuous surround. In a comprehensive analysis, Tien [252] showed that the phase velocity and coupling impedance are reduced by a dielectric loading factor. This factor is typically 0.2–0.8 and can be raised by supporting the helix by tubes or wedges so that the main body of dielectric is away from the immediate vicinity of the helical surface.

Analysis with the sheath model suggests [251] that in certain circumstances small amounts of dielectric can reduce the dispersion of the helix. Experimental results of the attenuation of helices, both alone and in several types of dielectric support, have been quoted [196]. The frequency was in the range 2.6 to 3.6 kmc and the examined helices possesed diameters of 0.1 to 0.25 inch and wire to helix length ratios of 13 to 23. The helix attenuation was found to vary with the material, to increase linearly with frequency, and to have a flat maximum at a ratio of wire-diameter pitch of $\frac{1}{3}$. For a helix of 40 turns per inch with diameters 0.15-inch outside, 0.128-inch inside, the attenuation coefficients at 3 kmc for various materials and supports are given in Table I; the wire diameter was 0.011 inch. These results confirm that a fluted or similar support adds little to the helix losses.

TABLE I
ATTENUATION OF SUPPORTED HELICES

Type of Dielectric	Plain Tungsten Wire	Silver-Plated Tungsten Wire
	decibels per inch	decibels per inch
None	0.55	0.26
707 fluted glass tube	0.62	0.33
Quartz tube	0.75	0.42
707 plain glass tube	0.88	0.49

More complicated media which have been studied include attenuating layers [160], [284] and semiconductors [243]. Ferrites are of practical interest since the loss caused by this medium may be nonreciprocal in direction. Propagation along a helix surrounded by a ferrite sleeve has been analysed [250] in terms of a plane sheath model with nonreciprocal properties occurring under the condition of circumferential magnetization.

The properties of a helix with a coaxial inner conductor have been examined but the effect of an outer metallic sheath is more pronounced [8], [207], [229], [235], [283] since radiation from the helix is prevented. Under conditions of evanescent radial decay of the fields, the outer sheath has little effect unless it is very close or the frequency is low. For modes in which $v_p>c$ Stark [246] has shown that the fields have a radial dependence which oscillates outwards to the conducting

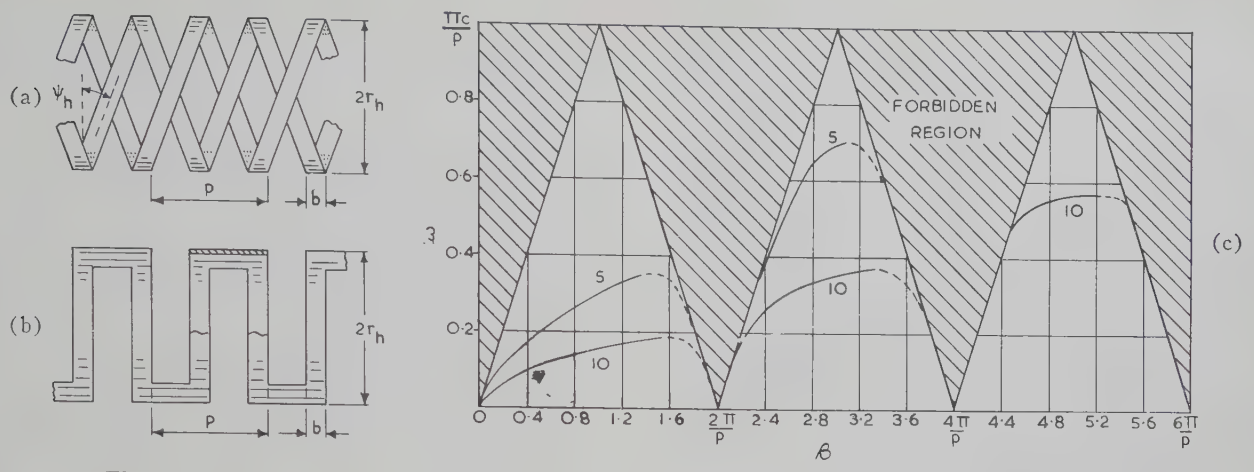

Fig. 28—Contra-wound helixes. (a) Twin tape helix. (b) Modified structure. (c) Frequency characteristic for helix with $2\pi b/p=1$ and cot ψ_h as parameter.

sheath in the manner noted in the case of capacitive loading of Fig. 4. In these "exceptional" regions the conditions resemble perturbed TE and TM modes of a coaxial line and circular waveguide.

If several helices each with the same pitch and radius are equally spaced in the axial direction, there results the multifilar helix [126], [238]. The curves of Fig. 27(b) still apply, but if N is the number of conductors the abscissa points $(-2\pi/p)$, 0, $(+2\pi p)$ and the ordinate point $\pi c/p$ are multiplied by N. According to the value of N, some of the space harmonic components will be missing.

The bifilar helix with $N=2$ has received much attention [86], [152], [175]. At low frequencies there is an extra mode present which is analogous to the TEM wave on a two-wire line. At any transverse plane the equal RF currents on the two tapes may thus be in-phase or out-of-phase. In the former case, odd space harmonics are zero and in Fig. 27(b) the solution corresponding to branch B_0 and the portion of branch C_0 along the forbidden boundary region disappear; the A_0 branch and the remaining portion of C_0 then join through the now-vanished forbidden region. In the out-of-phase case, the even space harmonics are zero. In either condition, the power carried by some of the unwanted components can be eliminated and a higher impedance for the desired modes is realized. The bifilar helix has received special study [280] regarding backward-wave per performance; in the push-pull mode it has substantially higher impedance [253] than the single helix.

As the pitch and diameter of a single helix are increased, the impedance of the fundamental is reduced [252], [253] while that of the $n=-1$ space harmonic is increased. Such an effect is undesirable in practice and may be eliminated by the contra-wound helix [46] which, as shown in Fig. 28(a), consists of two helices wound in opposite directions. An alternative version shown in Fig. 28(b) consists [25] of a spatial distortion which has the advantage of simplicity of construction. Single or multifilar helices are possible in both arrangements. Two modes, designated as the symmetric and antisymmetric, may be propagated and can be considered as arising from the combining of the single helix modes with different phases. In the former, the two modes are superimposed in phase and, in the latter, out of phase. In the symmetric mode, which is the one considered, the axial electric fields of the fundamental component add, and the resultant axial magnetic field, together with its associated stored energy, is zero. Thus the TE portion of the fundamental component is nonexistent so that the higher order space harmonics must have most of their energy in the magnetic or TE part of the field. This implies that the higher order space harmonics have small axial electric field components and, consequently, small impedance for backward waves.

The exponential term in the field equations now takes the form

$$\exp\{-j[(2\pi/p)(n+2n')z-m\theta]\}, \qquad (115)$$

where

$$\beta_{n,n'}=\beta_{0,0}+2\pi(n+2n')/p \qquad (116)$$

and is similar, if n' is omitted, to the single helix set of space harmonics. In Fig. 28(c), ω is plotted against β for two examples of twin helices with $2\pi b/p=1$, and cot $\psi_h=5$ and 10, respectively. The forbidden regions are the same as for the single helix, and the solution for cot $\psi_h=5$ has two branches, whereas that for cot $\psi_h=10$ has five, only three of which are shown. Measurements [25] on contra-wound helices show typically that there is an increase by a factor of 2 in the fundamental impedance and a reduction by a factor of 20 in the $n=-1$ space harmonic, as compared with the single helix. As expected from the diagrams, the phase velocities show increased dispersion over the single helix.

Numerous practical designs of helices have been developed [71], [84] for use at microwave frequencies. A typical example of 0.048-inch diameter copper wire, diameter of turn 0.25-inch and pitch 0.157-inch would have an axial velocity of 0.1 c, attenuation, 2 decibels per meter, and coupling impedance, 500 ohms. The ap-

plications of helices require measurement [184] of their essential properties and the design of broad-band transitions from coaxial and waveguide transmission lines. In experiments [282] on such devices, mercury formed a convenient and efficient moveable short circuit. Transitions from coaxial line [170], [287] may be via the inner conductor, the outer being continued for a short distance as a sheath surrounding the helix. The reflections caused by changes in pitch angle [200] are also relevant.

Coupling of power into and out of a helix at any particular point can be achieved [59] with an additional surrounding concentric helix. The coupling is strong when the helices have very nearly equal velocities of propagation when uncoupled and they are wound in opposite senses. These transitions resemble directional couplers, and modifications such as tapering or stepping can be employed. Complete power transfer can be affected over a distance of the order of one-helix wavelength (about 0.1λ). Coupled helices have no direct connection and thus the input or output circuit may be external to the device containing the main helix. The coupling conditions are modified in the presence of a dielectric or electron beam [272] and triangular as well as semicircular-re-entrant coupling helices have been developed [10]. A typical [166] helix coupler for frequencies of 1.7–2.3 kmc possessed a diameter ratio of 2.7 with an input VSWR of 1.3 and a directivity of 4 db. Such large diameter ratios lead to difficulty in matching and thus a third helix, intermediately placed and unconnected but contra-wound with respect to the other two, has been proposed and tested [180].

A helical structure may be made by spiralling [113] a rectangular waveguide. Such an arrangement has been analysed [274], [275] by considering a guide whose axis is uniformly curved and adopting the fiction that points at angular separation of 2π are not equivalent but differ in axial position by the pitch. If the rectangular guide propagating its dominant mode is orientated with its major dimension perpendicular to the axis of the structure, a TM_{01} mode is supported whereas the orthogonal orientation supports a TE_{01} mode. Such a structure is very dispersive [52] if coiled, for example, with a radius ratio of 5:1. Improvement results when there is coupling between turns as, for instance, in the extreme case of a coaxial line with helical grooves in one or both conductors. The properties now resemble those of the stub-loaded line provided that account is taken of circumferential as well as of axial propagation. A further modification entails the removal of the center conductor to form an open helical waveguide which has a low frequency cutoff.

Acknowledgment

The author is grateful to G. J. Rich, Dr. H. W. Duckworth, Dr. P. N. Butcher, Dr. A. E. Karbowiak and Prof. A. L. Cullen for helpful comments on the manuscript.

Bibliography

[1] M. Abele, "Theory of the Propagation of Electromagnetic Waves along a Dielectric Guide of Circular Section," Consiglo Nazionale Delle Richerche, Tipographia Del Senato, Rome, Italy; 1948.
[2] R. B. Adler, "Waves on inhomogenous cylindrical structures," Proc. IRE, vol. 40, pp. 339–348; March, 1952.
[3] A. W. Aikin, "Measurements in travelling-wave structures," *Wireless Engr.*, vol. 32, p. 230; 1955.
[4] A. I. Akhiezer, and Y. B. Faynberg, "Slow electromagnetic waves," *Uspekhi Fiz. Nauk*, vol. 44, p. 321;1951.
[5] C. P. Allen and G. M. Clarke, "Interpretation of wavelength measurements on tape helices," *Proc. IEE*, vol. 103, pt. C, pp. 171–176; March, 1956.
[6] C. M. Angulo, "Diffraction of surface waves by a semi-infinite slab," IRE Trans. on Antennas and Propagation, vol. AP-5, pp. 100–109; January, 1957.
[7] C. M. Angulo and W. S. C. Chang, "The excitation of a dielectric rod by a cylindrical waveguide," IRE Trans. on Microwave Theory and Techniques, vol. MTT-6, pp. 389–393; October, 1958.
[8] E. V. Anisimov and N. M. Sovetov, "The propagation of electromagnetic waves along a helical strip in a circular waveguide," *Zhur. Tekh.*, vol. 25, p. 1965; 1955.
[9] T. Ankel, "Investigation of the propagation of signals in dispersive media, using an acoustic model," *Z. Physik*, vol. 144, p. 120; 1956.
[10] E. A. Ash and J. D. Pattenden, "Modified transmission-line couplers for helice," *Proc. IEE*, vol. 105, pt. B, pp. 762–768; May, 1958.
[11] E. A. Ash, " A new type of slow-wave structure for millimetric wavelengths," *Proc. IEE*, vol. 105, pt. B, pp. 737–745; May, 1958.
[12] S. S. Attwood, "Surface-wave propagation over a coated plane conductor," *J. Appl. Phys.*, vol. 22, pp. 504–509; April, 1951.
[13] H. Awender and O. Lange, "The propagation of decimetre and centimetre waves along single metallic and dielectric wires," *Funktech. Monatshefte*, pt. 2, p. 5, 51; 1938.
[14] H. E. M. Barlow and A. E. Karbowiak, "An investigation of the characteristics of cylindrical surface waves," *Proc. IEE*, vol. 100, pt. III, pp. 321–328; November, 1953.
[15] H. E. M. Barlow and A. L. Cullen, "Surface waves," *Proc. IEE*, vol. 100, pt. III, pp. 329–347; November, 1953.
[16] H. E. M. Barlow and A. E. Karbowiak, "Proposed use of a cylindrical surface-wave resonator for the determination of the velocity of short electro-magnetic waves," *Brit. J. App. Phys.*, vol. 4, pp. 186–187; June, 1953.
[17] H. E. M. Barlow and A. E. Karbowiak, "An experimental investigation of the properties of corrugated cylindrical surface waveguides," *Proc. IEE*, vol. 101, pt. III, pp. 182–188; May, 1954.
[18] H. E. M. Barlow and A. E. Karbowiak, "An experimental investigation of axial cylindrical surface waves supported by capacitive surfaces," *Proc. IEE*, vol. 102, pt. B, pp. 313–322; May, 1955.
[19] H. E. M. Barlow, "The power radiated by a surface wave circulating around a cylindrical surface," *Proc. IEE*, vol. 106, pt. B, pp. 180–185; March, 1959.
[20] H. E. M. Barlow, "Surface waves," Proc. IRE, vol. 46, pp. 1413–1417; July, 1958.
[21] E. Belohoubek, "Propagation characteristics of slow-wave structures derived from coupled resonators," *RCA Rev.*, vol. 19, p. 283; 1958.
[22] T. Berceli, "Surface-wave propagation along coated wires," *Acta Tech. Acad. Science Hungaricae*, vol. 17, p. 269; 1957.
[23] F. Bertein and W. Chahid, "Production of slow electromagnetic waves by means of cylindrical current sheets," *Compt. Rend. Acad. Sci. (Paris)*, vol. 242, p. 2918; 1956.
[24] V. I. Bespalov and A. B. Gapanov, "Influence of inhomogeneities on the propagation of electromagnetic waves in periodic structures," *Radiotekh. i Elektron.*, vol. 1, p. 772; 1956.
[25] C. K. Birdsall and T. E. Everhart, "Modified contra-wound helix circuits for high power travelling wave tubers," IRE Trans. on Electron Devices, vol. ED-3, pp. 190–204; October, 1956.
[26] F. E. Borgnis, "Electric waves on delay lines," *Elektrotech. Z.*, vol. 79A, p. 383; 1958.
[27] F. E. Borgnis and C. H. Papas, "Electromagnetic waveguides," in "Encyclopedia of Physics," vol. 16; Springer-Verlag, Berlin, Ger.; 1958.
[28] D. B. Brick, "The radiation of a hertzian dipole over a coated conductor," *Proc. IEE*, vol. 120, pt. C, pp. 104–121; March, 1955.

[29] D. B. Brick, "The excitation of surface waves by a vertical antenna," PROC. IRE, vol. 43, pp. 221–727; June, 1955.
[30] L. Brillouin, "Wave Propagation in Periodic Structures," McGraw-Hill Book Co., Inc., New York, N. Y.; 1946.
[31] L. Brillouin, "Wave guides for slow waves," *J. Appl. Phys.*, vol. 19, p. 1023; 1948.
[32] J. Brown, "The types of waves which may exist near a guiding surface," *Proc. IEE*, vol. 100, pt. III, pp. 363–364; November, 1953.
[33] J. Brown and K. P. Sharma, "The launching of radial cylindrical surface waves by a circumferential slot," *Proc. IEE*, vol. 106, pt. B, pp. 123–128; March, 1959.
[34] J. H. Bryant and E. F. White, "Attenuation and power-handling capability of helical radio-frequency lines," IRE TRANS. ON MICROWAVE THEORY AND TECHNIQUES, vol. MTT-1, pp. 33–38; November, 1953.
[35] J. H. Bryant, "Some wave properties of helical conductors," *Elec. Commun.*, vol. 631, p. 50; 1954.
[36] P. N. Butcher, "A new treatment of lossy periodic waveguides," *Proc. IEE*, vol. 103, pt. B, pp. 301–306; May, 1956.
[37] P. N. Butcher, "A theoretical study of propagation along tape ladder lines," *Proc. IEE*, vol. 104, pt. B, pp. 169–176; March, 1957.
[38] P. N. Butcher, "The coupling impedance of tape structures," *Proc. IEE*, vol. 104, pt. B, pp. 177–187; March, 1957.
[39] G. A. Campbell, "On loaded lines in telephonic transmission," *Phil. Mag.*, vol. 5, p. 319; 1903.
[40] J. R. Carson, S. P. Mead, and S. A. Schelkunoff, "Hyperfrequency waveguides—mathematical theory," *Bell Sys. Tech. J.*, vol. 15, p. 310; 1936.
[41] C. H. Chandler, "An investigation of dielectric rod as wave guide," *J. Appl. Phys.*, vol. 20, pp. 1188–1192; December, 1949.
[42] S. K. Chatterjee and P. Madhaven, "Propagation of microwaves on a single wire," *J. Indian Inst. Sci.*, vol. 37 B, p. 200; 1955.
[43] S. K. Chatterjee and R. Chatterjee, "Propagation of microwave along a solid conductor embedded in three coaxial dielectrics," *J. Indian Inst. Sci.*, vol. 38 B, p. 157, 1956; vol. 39 B, p. 7, 1957.
[44] S. K. Chatterjee and R. Chatterjee, "Surface waveguides," *J. Inst. Telecommun. Engrs. (India)*, vol. 4, p. 90; 1958.
[45] P. Chavance and B. Chiron, "Experimental study of the transmission of centimetre waves along wire waveguides," *Ann. Télécommun.*, vol. 8, p. 367; 1953.
[46] M. Chodorow and E. L. Chu, "Cross-wound twin helices for traveling-wave tubes," *J. Appl. Phys.*, vol. 26, p. 33; January, 1955.
[47] M. Chodorow and R. A. Craig, "Some new circuits for high-power traveling wave tubes," PROC. IRE, vol. 45, pp. 1106–1118; August, 1957.
[48] M. Chodorow and E. J. Nalos, "The design of high-power traveling-wave tubes," PROC. IRE, vol. 44, pp. 649–659; May, 1956.
[49] C. M. Chu, "Propagation of waves in helical wave guides," *J. Appl. Phys.*, vol. 29, pp. 88–99; January, 1958.
[50] E. L. Chu and W. W. Hansen, "The theory of disk-loaded waveguides," *J. Appl. Phys.*, vol. 18, pp. 996; 1947.
[51] E. L. Chu and W. W. Hansen, "Disk loaded waveguides," *J. Appl. Phys.*, vol. 20, p. 280; 1949.
[52] G. M. Clarke, "Helical waveguides—closed, open and coaxial," *J. Brit. IRE*, vol. 18, pp. 359–361; June, 1958.
[53] A. G. Clavier and V. Altovsky, "Experimental researches on the propagation of electromagnetic waves in dielectric guides," *Elec. Commun.*, vol. 18, p. 8; 1940.
[54] P. J. M. Clavier, "Physical explanation of the surface wave on a dielectric-coated line," *Cables & Transmission*, vol. 7, p. 34; 1953.
[55] J. F. Colin, "Propagation of an electromagnetic wave guided by a metal surface with dielectric coating," *L'Onde Electrique*, vol. 31, p. 245; 1951.
[56] R. Combe, "Pass band and dispersion of waveguides loaded with circular irises," *Compt. Rend. Acad. Sci. (Paris)*, vol. 238, p. 1697; 1954.
[57] R. Combe, "Attenuation coefficient of waveguides loaded with circular irises," *Compt. Rend. Acad. Sci. (Paris)*, vol. 238, p. 2063; 1954.
[58] S. N. Contractor and S. K. Chatterjee, "Propagation of microwaves on a single wire: part 2," *J. Indian Inst. Sci.*, vol. 39 B, p. 52; 1957.
[59] J. S. Cook, R. Kompfner, and C. F. Quate, "Coupled helices," *Bell Sys. Tech. J.*, vol. 35, pp. 127–178; January, 1956.
[60] A. L. Cullen, "Waveguide field patterns in evanescent modes," *Wireless Engr.*, vol. 26, p. 317; 1949.
[61] A. L. Cullen, "The excitation of plane surface waves," *Proc. IEE*, vol. 191, pt. IV, p. 225; 1954.
[62] A. L. Cullen, "A Note on the excitation of surface waves," *Proc. IEE*, vol. 104, pt. C, pp. 472–474; September, 1957.
[63] C. C. Cutler, "Experimental determination of helical-wave properties," PROC. IRE, vol. 36, pp. 230–233; February, 1948.
[64] C. C. Cutler, "Electromagnetic Waves Guided by Corrugated Conducting Surfaces," Bell Telephone Labs., New York, N. Y., unpublished rept.; October, 1944.
[65] J. Dain, "Some fundamental aspects of slow wave propagation," *L'Onde Électrique*, vol. 37, p. 86; 1957.
[66] J. Dain, "The propagation of slow waves," *Electronic Engrg.*, vol. 30, pp. 388–393; June, 1958.
[67] W. Dallenback, "Travelling waves between two parallel diaphragm-loaded reflector planes," *Arch. elek. Übertragung*, vol. 7, p. 297; 1953.
[68] R. W. DeGrasse, "Slow-wave structures for unilateral solid-state maser amplifiers," 1958 WESCON CONVENTION RECORD, pt. 3, pp. 29–35.
[69] H. Derfler, "On the theory of disc-loaded waveguide," *Z. Ange. Math. Phys.*, vol. 6, p. 190; 1955.
[70] C. C. Dewey, P. Parzen, and T. M. Marchese, "Periodic waveguide travelling-wave amplifier for medium powers," PROC. IRE, vol. 39, pp. 153–159; February, 1951.
[71] W. J. Dodds and R. W. Peter, "Filter helix travelling-wave-tube," *RCA Rev.*, vol. 14, p. 502; 1953.
[72] L. Drozdowicz, "Guiding of an electromagnetic wave by a single conductor," *Przeglad Telekomun.*, vol. 1, p. 1; 1953.
[73] R. H. DuHamel and J. W. Duncan, "Launching efficiency of wires and slots for a dielectric rod waveguide," IRE TRANS. ON MICROWAVE THEORY AND TECHNIQUES, vol. MTT-6, pp. 277–284; July, 1958.
[74] R. B. Dyott, "The launching of electromagnetic waves on a cylindrical conductor," *Proc. IEE*, vol. 99, pt. III, pp. 408–413; November, 1952.
[75] H. Ehrenspeck, W. Gerbes, and F. J. Zucker, "Trapped wave antennas," 1954 IRE CONVENTION RECORD, pt. 1, pp. 25–30.
[76] R. S. Elliott, "On the theory of corrugated plane surfaces," IRE TRANS. ON ANTENNAS AND PROPAGATION, vol. AP-2, pp. 71–81; April, 1954.
[77] R. S. Elliott, "Azimuthal surface waves on circular cylinders," *J. Appl. Phys.*, vol. 26, pp. 368–376; April, 1955.
[78] W. M. Elsasser, "Attenuation in a dielectric circular rod," *J. Appl. Phys.*, vol. 20, pp. 1193–1196; December, 1949.
[79] B. Epsztein and G. Mourier, "Definition, measurement and character of the phase velocities in systems with periodic structure," *Ann. Radioelectricité*, vol. 10, p. 64; 1955.
[80] Y. N. Fel'd, "Infinite systems of linear algebraic equations connected with problems of semi-infinite periodic structures," *Compt. Rend. Acad. Sci. U.R.S.S.*, vol. 102, p. 257; 1955.
[81] W. M. G. Fernando and H. E. M. Barlow, "An investigation of the properties of radial cylindrical surface waves launched over flat reactive surfaces," *Proc. IEE*, vol. 103, pt. B, pp. 307–318; May, 1956.
[82] L. M. Field, "Some slow-wave structures for travelling wave tubes," PROC. IRE, vol. 37, pp. 34–40; January, 1949.
[83] L. M. Field, "Recent developments in traveling-wave valves," *Electronics*, p. 150; January, 1950.
[84] R. C. Fletcher, "Helix parameters used in travelling-wave tube theory," PROC. IRE, vol. 38, pp. 413–417; April, 1950.
[85] R. C. Fletcher, "A broad-band interdigital circuit for use in travelling-wave-type amplifiers," PROC. IRE, vol. 40, pp. 951–958; August, 1952.
[86] V. J. Fowler, "Analysis of helical transmission lines by means of the complete circuit equations," IRE TRANS. ON ANTENNAS AND PROPAGATION, vol. AP-2, pp. 132–143; October, 1954.
[87] B. Friedman, and W. E. Williams, "Excitation of surface waves," *Proc. IEE*, vol. 105, pt. C, pp. 252–258; March, 1958.
[88] C. Froese, and J. R. Wait, "Calculated diffraction patterns of dielectric rods at centimetre wavelengths," *Canad. J. Phys.*, vol. 32, p. 775; 1954.
[89] A. Fromageot, and B. Louis, "Propagation of electromagnetic waves along a conducting wire with thin dielectric covering," *Bull Soc. Franç., Electriciens*, vol. 1, p. 291; 1951.
[90] M. A. Gintsburg, "Surface waves on the boundary of a gyrotropic medium," *Zhur. Eksp. i Teoret. Fiz.*, vol. 34, p. 1635; 1958.
[91] J. F. Gittins, N. H. Rock, and A. B. J. Sullivan, "An experimental high-power pulsed travelling-wave tube," *J. Electronics and Control*, vol. 3, p. 267; 1957.
[92] G. Goubau, "Designing surface-wave transmission lines," *Electronics*, vol. 27, pp. 180–184; April, 1954.
[93] G. Goubau, "On the Zenneck surface wave," *Z. Angew. Phys.*, vol. 3, p. 103; 1951.
[94] G. Goubau, "Surface waves and their application to transmission lines," *J. Appl. Phys.*, vol. 21, pp. 1119–1128; November, 1950.

[95] G. Goubau, "Surface-wave transmission line," *Radio and TV News*, vol. 14, p. 10; 1950.
[96] G. Goubau, "On the excitation of surface waves," PROC. IRE, vol. 40, pp. 865–868; July, 1952.
[97] G. Goubau, "Single-conductor surface-wave transmission lines," PROC. IRE, vol. 39, pp. 619–624; June, 1951.
[98] G. Goubau, "Open wire lines," IRE TRANS. ON MICROWAVE THEORY AND TECHNIQUES, vol. MTT-4, pp. 197–200; October, 1956.
[99] A. C. Grace and J. A. Lane, "Surface-wave transmission lines," *Wireless Engr.*, vol. 29, p. 230; 1952.
[100] J. W. E. Griemsmann, "An approximate analysis of coaxial line with a helical dielectric support," IRE TRANS. ON MICROWAVE THEORY AND TECHNIQUES, vol. MTT-4, pp. 13–23; January, 1956.
[101] C. C. Grosjean, "Theory of circularly symmetric standing TM waves in terminated iris-loaded waveguides," *Nuovo Cim.*, vol. 2, p. 11; 1955.
[102] C. C. Grosjean, "Transformation of a frequency equation in corrugated waveguide theory," *Nuovo Cim.*, vol. 1, p. 174; 1955.
[103] C. C. Grosjean and V. J. Vanhuyse, "Experimental verification of a frequency equation for corrugated waveguides," *Nuovo Cim.*, vol. 1, p. 193; 1955.
[104] C. C. Grosjean, "Mathematical transformation of a system of equations appearing in the theory of TM wave propagation in corrugated guides," *Nuovo Cim.*, vol. 1, p. 439; 1955.
[105] C. C. Grosjean, "Note on the properties of two functions appearing in the theory of TM wave propagation through periodically iris-loaded guides," *Nuovo Cim.*, vol. 1, p. 1264; 1955.
[106] P. Guénard, O. Doehler, and R. Warnecke, "Properties of lines with periodic structures," *Compt. Rend. Acad. Sci. (Paris)*, vol. 235, p. 32; 1952.
[107] W. Gunn, "Application possibilities of a surface-wave mode," *Marconi Rev.*, vol. 15, p. 145; 1952.
[108] R. C. Hansen, "Single-slab arbitrary-polarization surface-wave structure," IRE TRANS. ON MICROWAVE THEORY AND TECHNIQUES, vol. MTT-5, pp. 115–120; April, 1957.
[109] F. Harms, "Electromagnetic waves on a wire with a cylindrical insulating sheath," *Ann. Phys.*, vol. 23, p. 44; 1907.
[110] A. F. Harvey, "Radio-frequency aspects of electro-nuclear accelerators," *Proc. IEE*, vol. 106, pt. B, pp. 43–57; January, 1959.
[111] L. Hatkin, "Analysis of propagating modes in dielectric sheets," PROC. IRE, vol. 42, pp. 1565–1568; October, 1954.
[112] J. Hirano, "Characteristics of interdigital circuits and their use for amplifiers," *Proc. IEE*, vol. 105, pt. B, pp. 780–785; May, 1958.
[113] B. T. Henoch, "Investigations of the disk-loaded and helical waveguide," *Kgl. Tek. Högskol. Handl.*, no. 129, p. 1; 1958.
[114] G. Hok, "Calculation of a waveguide loaded resonator for interdigital magnetrons," PROC. IRE, vol. 41, pp. 763–769; June, 1953.
[115] A. Hondros and P. Debye, "Electromagnetic waves in dielectric wires," *Ann. Physik*, vol. 32, p. 465; 1910.
[116] D. Hondros, "Electromagnetic waves on wires," *Ann. Physik*, vol. 30, p. 905; 1909.
[117] K. Horiuchi, "Surface-wave propagation over a coated conductor with small cylindrical curvature in direction of travel," *J. Appl. Phys.*, vol. 24, p. 961; 1953.
[118] T. Hosono, "Radio-wave propagation along a helix," *J. Inst. Elec. Commun. Engrs. (Japan)*, vol. 38, p. 34; 1955.
[119] K. Hübener, "Investigations on helical lines," *Nachrichtentech. Zeitung*, vol. 9, p. 581; 1956.
[120] J. F. Hull, G. Novick and B. D. Kumpfer, "A high-power delay line for a travelling-wave amplifier or oscillator," *Proc. NEC*, vol. 8, p. 313; 1952.
[121] R. A. Hurd, "The propagation of an electro-magnetic wave along an infinite corrugated surface," *Can. J. Phys.*, vol. 32, p. 727; 1954.
[122] R. A. Hurd, "Surface Waves on a Two-Layer Dielectric-Coated Wire," Natl. Res. Council of Canada, Ottawa, Ont., Publication No. 3187, p. 1; 1953.
[123] C. Jauquet, "Excitation of a transverse magnetic surface-wave propagated on a dielectric cylinder," *Ann. Télécommun.*, vol. 12, p. 217; 1957.
[124] E. T. Jaynes, "The concept and measurement of impedance in periodically loaded wave guides," *J. Appl. Phys.*, vol. 23, p. 1077; 1952.
[125] M. Jessel and R. Wallauschek, "Experimental study of propagation along a delay line in the form of a helix," *Ann. Télécommun.*, vol. 3, p. 291; 1948.
[126] H. R. Johnson, T. E. Everhart, and A. E. Siegman, "Wave propagation on multifilar helices," IRE TRANS. ON ELECTRON DEVICES, vol. ED-3, pp. 18–24; January, 1956.
[127] C. E. Jordan and A. B. McLay, "Diffraction of 3.2 cm electromagnetic waves by dielectric rods: part 3—lucite 1½ in.—diameter semicylinder, fields very close to surfaces," *Can. J. Phys.*, vol. 35, p. 1253; 1957.
[128] C. Jouget, "The surface wave on a dielectric cylinder: the method of launching it and its characteristics," *Rev. HF (Brussels)*, vol. 3, p. 283; 1956.
[128a] C. Jouget, "Excitation of a transverse magnetic surface wave propagated on a dielectric cylinder," *Ann. Télécommun.*, vol. 12, p. 217; 1957.
[129] M. Jouget, "Propagation in a dielectric transmission line," *Compt. Rend. Acad. Sci. (Paris)*, vol. 237, p. 1656; 1953.
[130] M. Jouget, "Waveguides with discontinuous structure," *Compt. Rend. Acad. Sci. (Paris)*, vol. 245, p. 297; 1957.
[131] H. Kaden, "Advances in the theory of waves on wires," *Arch. elek. Übertragung*, vol. 5, p. 399; 1951.
[132] Kaden, H. "A general theory of the helical line," *Arch. elek. Übertragung*, vol. 5, p. 534; 1951.
[133] H. Kaden, "Dielectric and metal waveguides," *Arch. elek. Übertragung*, vol. 6, p. 319; 1952.
[134] H. Kaden, "Recent research on the transmission of signals along metal and dielectric lines," *Fernmeldetech. Z.*, vol. 6, p. 432; 1953.
[135] K. Kamirijo, H. Hozumi, Y. Shibata, and Y. Fukushima, "Measurements of field patterns for a comb-type slow-wave structure," *Proc. IEE*, vol. 105, pt. B, pp. 890–892; May, 1958.
[136] M. D. Karasev and V. A. Apanasenko, "Surface waves propagated along a single cylindrical conductor," *Zhur. Tekh. Fiz.*, vol. 24, p. 662; 1954.
[137] A. E. Karbowiak, "Theory of composite guides: stratified guides for surface waves," *Proc. IEE*, vol. 101, pt. III, pp. 238–242; July, 1954.
[138] A. E. Karbowiak, "The E-H surface wave," *Wireless Engr.*, vol. 31, p. 71; 1954.
[139] A. E. Karbowiak, "The elliptic surface wave," *Brit. J. Appl. Phys.*, vol. 5, pp. 328–335; September, 1954.
[140] A. E. Karbowiak, "On the surface impedance of a corrugated waveguide," *Proc. IEE*, vol. 102, pt. B, pp. 501–502; July, 1955.
[141] A. E. Karbowiak, "Microwave propagation in anisotropic waveguides," *Proc. IEE*, vol. 103, pt. 3, pp. 139–144; March, 1956.
[142] H. Kaufman, "Bibliography of nonuniform transmission lines," IRE TRANS. ON ANTENNAS AND PROPAGATION, vol. AP-3, pp. 218–220; October, 1955.
[143] A. F. Kay and F. J. Zucker, "Efficiency of surface wave excitation," 1955 IRE CONVENTION RECORD, pt. 1, pp. 1–5.
[144] E. Kettel, "A waveguide with phase velocity $v<c$ for the E_{10}-wave," *Frequenz*, vol. 3, pp. 73–00; Month, 1949.
[145] D. G. Kiely, "Experiments with single-wire transmission lines at 3 cm wavelength," *J. Brit. IRE*, vol. 13, pp. 194–199; April, 1953.
[146] D. D. King, "Dielectric image line," *J. Appl. Phys.*, vol. 23, pp. 699–700; June, 1952.
[147] D. D. King, "Properties of dielectric image lines," IRE TRANS. ON MICROWAVE THEORY AND TECHNIQUES, vol. MTT-3, pp. 75–81; March, 1955.
[148] D. D. King, "Circuit components in dielectric image lines," IRE TRANS. ON MICROWAVE THEORY AND TECHNIQUES, vol. MTT-3, pp. 35–39; December, 1955.
[149] D. D. King and S. P. Schlesinger, "Losses in dielectric image lines," IRE TRANS. ON MICROWAVE THEORY AND TECHNIQUES, vol. MTT-5, pp. 31–35; January, 1957.
[149a] H. S. Kirschbaurn and R. Tsu, "A study of a serrated ridge waveguide," IRE TRANS. ON MICROWAVE THEORY AND TECHNIQUES, vol. MTT-7, pp. 142–148; January, 1959.
[150] W. Klein, "The delay line as a component of valves," *Arch. Elektrotech.*, vol. 40, p. 280; 1952.
[151] W. Klein, "The dimensions of helices in travelling wave tubes," *Arch. elek. Übertragung*, vol. 10, p. 261; 1956.
[152] H. Kleinwachter and H. Weiss, "Bifilar line with large flexibility and rapid diminution of radial field for the transmission of hyperfrequencies," *L'Onde Électrique*, vol. 32, p. 46; 1952.
[153] A. Klemt, "Contribution to the propagation of electromagnetic waves along dielectric wires," *Funktech. Monatshefte*, vol. 4, p. 122; 1939.
[154] S. K. Kogan, "The propagation of waves along an endless helix," *Compt. Rend. Acad. Sci. U.R.S.S.*, vol. 66, p. 867; 1949.
[155] S. K. Kogan, "The excitation of a helical conductor," *Compt. Rend. Acad. Sci. U.R.S.S.*, vol. 74, p. 487; 1950.
[156] S. K. Kogan, "Theory of helical lines," *Compt Rend. Acad. Sci. U.R.S.S.*, vol. 107, p. 541; 1956.

[157] E. T. Kornhauser, "Propagation on dielectric coated wires," *J. Appl. Phys.*, vol. 22, p. 525; April, 1951.
[158] J. Koyama, "An application of the spatial-harmonic wave on a large-diameter helix," *Proc. IEE*, vol. 105, pt. B, pp. 412–414; May, 1958.
[159] R. L. Kyhl, "The use of non-Euclidean geometry in measurements of periodically loaded transmission lines," IRE Trans. on Microwave Theory and Technique, vol. MTT-4, pp. 111–115; April, 1956.
[160] G. Landauer, "The helical line with a coaxial cylindrical attenuating layer," *Arch. elek. Übertragung*, vol. 11, p. 267; 1957.
[161] P. Lapostalle, "Helices for travelling-wave valves: effect of supports, attenuation: parasitic modes," *Ann. Télécommun.*, vol. 12, p. 34; 1957.
[162] J. D. Lawson, "A method of launching surface waves," Proc. IRE, vol. 44, p. 111; January, 1956.
[163] A. Leblond and G. Mourier, "Investigation of lines with periodic bar structure for VHF valves: parts 1 and 2," *Ann. Radioélectricité*, vol. 9, pp. 180, 311; 1954.
[164] A. Leblond, "Investigation of an interdigital line operating in the vicinity of the π mode," *Ann. Radioélectricité*, vol. 10, p. 83; 1955.
[165] J. Levy, "Transmission of electromagnetic guided waves through a series of symmetrical and equidistant obstacles," *Câbles & Transmission*, vol. 1, p. 103; 1947.
[166] P. A. Lindsay and K. D. Collins, "Some aspects of the design of a helical coupler for a travelling-wave tube operating in the 2Gc/s band," *Proc. IEE*, vol. 105, pt. B, pp. 756–761; May, 1958.
[167] A. W. Lines, G. R. Nicoll, and A. M. Woodward, "Some properties of waveguides with periodic structures," *Proc. IEE*, vol. 97, pt. III, pp. 263–276; July, 1950.
[168] Y. T. Lo, "Electromagnetic field of a dipole source above a grounded dielectric slab," *J. Appl. Phys.*, vol. 25, pp. 733–740; July, 1954.
[169] L. N. Loshakov and E. B. Ol'derogge, "Fast waves in a coaxial helical line," *Radiotekhnika*, vol. 12, p. 25; 1957.
[170] C. O. Lund, "Broadband transition from coaxial line to helix," *RCA Rev.*, vol. 11, p. 133; 1950.
[171] P. Mallach, "Investigations on dielectric waveguides in rod or tube form," *Fernmeldetech. Z.*, vol. 8, p. 8; 1955.
[172] D. Marcuse, "A new type of surface waveguide with bandpass properties," *Arch. elek. Übertragung*, vol. 11, p. 146; 1957.
[173] D. Marcuse, "Investigation of the energy exchange and the field distribution for parallel surface-wave transmission lines," *Arch. elek. Übertragung*, vol. 10, p. 117; 1956.
[174] A. A. Meyerhoff, "Interaction between surface-wave transmission lines," Proc. IRE, vol. 40, pp. 1061–1065; September, 1952.
[175] V. S. Mikhalevski, "Theory of twin-helix coaxial line," *Radiotekh. i Elektron.*, vol. 1, p. 1309; 1956.
[176] M. A. Miller, "Propagation of electromagnetic waves over plane surface with anisotropic homogeneous boundary conditions," *Compt. Rend. Acad. Sci. U.R.S.S.*, vol. 87, p. 511; 1952.
[177] M. A. Miller, "Elektromagnetic surface waves in rectangular channels," *Zhur. Tekh. Fiz.*, vol. 25, p. 1972; 1955.
[178] M. A. Miller and V. I. Tolanov, "Electromagnetic surface waves, guided by a boundary with small curvature," *Zhur. Tekh. Fiz.*, vol. 26, p. 2755; 1956.
[179] S. Millman, "A spatial-harmonic travelling-wave amplifier for six-millimeters wavelength," Proc. IRE, vol. 39, pp. 1035–1943; September, 1951.
[180] B. Minakovic, "The coupling of three coaxial helices," *Proc. IEE*, vol. 105, pt. B, pp. 769–778; May, 1958.
[181] R. G. Mirimahov and G. I. Zhileiko, "A new type of waveguide with diaphragms," *Radiotekh. i Elektron.*, vol. 1, p. 1374; 1956.
[181a] R. A. Moore and R. E. Beam, "A duo-dielectric parallel-plane waveguide," *Proc. NEC*, vol. 12, p. 689; 1956.
[182] G. Mourier, "Bi-dimensional and Tri-dimensional periodic structure circuits," *L'Onde Électrique*, vol. 37, p. 86; 1957.
[183] M. Muller, "Dielectric in the field of helical lines," *Die Telefunken-Rohre*, no. 4, p. 100; 1953.
[184] R. Müller, "Measurement of the coupling impedances of delay lines," *Arch. elek. Übertragung*, vol. 10, p. 424; 1956.
[185] R. Müller, "Reflection of electromagnetic waves at inhomogeneous boundary surfaces with a periodic structure perpendicular to the electric vector," *Arch. elek. Übertragung*, vol. 7, p. 492; 1953.
[186] L. B. Mullett and B. G. Loach, "Waveguide systems with negative phase velocities," *Nature*, vol. 169, p. 1011; 1952.
[187] E. J. Nalos, "Measurement of circuit impedance of periodically loaded structures by frequency perturbation," Proc. IRE, vol. 42, pp. 1508–1511; October, 1954.
[188] F. Ollendorf, "The Theoretical Foundations of High-Frequency Technique," Springer-Verlag, Berlin, Ger.; 1926.
[189] S. Olving, "Electromagnetic wave propagation on helical conductors embedded in dielectric medium," *Chalmers Tek. Högskol. Handl.*, no. 156, p. 1; 1955.
[190] H. Ott, "Surface waves," *Arch. elek. Übertragung*, vol. 5, p. 343; 1951.
[191] P. Palluel and J. Arnaud, "Results on delay lines for high-power travelling-wave tubes," *Proc. IEE*, vol. 105, pt. B, p. 727; May, 1958.
[192] F. Paschke, "Investigation of an interdigital delay line," *Arch. elekt. Übertragung*, vol. 10, p. 195; 1956.
[193] F. Paschke, "A note on the dispersion of interdigital delay lines," *RCA Rev.*, vol. 19, p. 418; 1958.
[194] A. F. Pearce, "A structure, using resonant coupling elements, suitable for a high-power travelling-wave tube," *Proc. IEE*, vol. 105, pt. B, pp. 719–726; May, 1958.
[195] R. L. Pease, "On the propagation of surface waves over an infinite grounded ferrite slab," IRE Trans. on Antennas and Propagation, vol. AP-6, pp. 13–20; January, 1958.
[196] R. W. Peter, J. A. Ruetz and A. B. Olson, "Attenuation of wire helices in dielectric supports," *RCA Rev.*, vol. 13, p. 558; 1952.
[197] R. S. Phillips, "The electromagnetic field produced by a helix," *Quart. Appl. Math.*, vol. 8, p. 229; 1950.
[198] G. Piefke, "On the theory of Harms-Goubau single-wire transmission lines for metre wavelengths," *Arch. elek. Übertragung*, vol. 9, p. 81; 1955.
[199] G. Piefke, "Wave propagation in a diaphragm-type and a corrugated waveguide," *Arch. elek. Übertragung*, vol. 12, p. 26; 1958.
[200] G. Piefke, "Reflection in helical lines at a change in the helix pitch," *Arch. elek. Übertragung*, vol. 9, pp. 269, 402; 1955.
[201] G. Piefke, "Wave propagation in a disk line," *Arch. elek. Übertragung*, vol. 11, p. 49; 1957.
[202] J. R. Pierce, "Circuits for travelling wave tubes," Proc. IRE, vol. 37, pp. 510–515; May, 1949.
[203] J. R. Pierce and P. K. Tien, "Coupling of modes in helices," Proc. IRE, vol. 42, pp. 1389–1396; September, 1954.
[204] J. R. Pierce, "Propagation in linear arrays of parallel wires," IRE Trans. on Electron Devices, vol. ED-2, pp. 13–14; January, 1955.
[205] R. E. Plummer and R. C. Hansen, "Double-slab arbitrary-polarization surface-wave structures," *Proc. IEE*, vol. 104, pt. C, pp. 465–471; September, 1957.
[206] H. C. Pocklington, "Electrical oscillations in wires," *Proc. Cambridge Phil. Soc.*, vol. 9, p. 324; 1897.
[207] K. Pöschl, "Wave propagation along a helix with a cylindrical outer conductor," *Arch. elek. Übertragung*, vol. 7, p. 518; 1953.
[208] G. J. Rich, "The launching of a plane surface wave," *Proc. IEE*, pt. III, pp. 237–246; March, 1955.
[209] R. D. Richtmyer, "Dielectric resonators," *J. Appl. Phys.*, vol. 10, p. 391; 1939.
[210] T. E. Roberts, "Theory of the single-wire transmission line," *J. Appl. Phys.*, vol. 24, pp. 57–67; January, 1953.
[211] T. E. Roberts, "An experimental investigation of the single-wire transmission line," IRE Trans. and Antennas and Propagation, vol. AP-2, pp. 46–56; April, 1954.
[212] P. N. Robson, "A note on the Fourier series representation of the dispersion curves for circular iris-loaded waveguides," *Proc. IEE*, vol. 105, pt. B, pp. 69–72; January, 1958.
[213] W. Rotman, "A study of single-surface corrugated guides," Proc. IRE, vol. 39, pp. 952–949; August, 1951.
[214] E. Roubine, "Investigation of electromagnetic waves guided by helical conductors," *Compt. Rend. Acad. Sci. (Paris)*, vol. 232, p. 1748; 1959; and, *Ann. Télécommun.*, vol. 7, pp. 206, 262, and 310; 1952.
[215] E. Roubine, "The helical circuit used in travelling wave tubes," *L'Onde Electrique*, vol. 27, p. 203; 1947.
[216] N. M. Rust, "Surface-wave transmission line," *Wireless Engr.*, vol. 27, p. 270; 1950.
[217] H. Ruter and O. Schriever, "Electromagnetic Waves in Dielectric Wires," Schriften Naturwissenschaften Verlag Schleswig-Holstein, Ger., vol. 16, p. 2; 1915.
[218] J. Saphores and L. Brillouin, "General properties of dielectric guides and cables," *Elec. Commun.*, vol. 16, p. 346; 1938.
[219] E. H. Scheibe, B. G. King, and D. L. Van Zeeland, "Loss measurements of surface-wave transmission lines," *J. Appl. Phys.*, vol. 25, pp. 790–797; June, 1954.
[220] S. A. Schelkunoff, "Electromagnetic Waves," D. Van Nostrand Co., Inc., New York, N. Y.; 1943.
[221] W. P. Schestopalow, "Theory of a waveguide containing a spiral, partly filled with a dielectric," *Nachr. Tech.*, vol. 4, p. 425, 1954; and *Zhur. Tekh. Fiz.*, vol. 22, p. 414, 1952.

[222] G. Schiefer, "The attenuation of the helical wire line," *Arch. elek. Übertragung*, vol. 11, p. 35; 1957.
[223] S. P. Schlesinger and D. D. King, "Dielectric image lines," IRE TRANS. ON MICROWAVE THEORY AND TECHNIQUES, vol. MTT-6, pp. 291–299; July, 1958.
[224] H. M. Schmidt, "Cylindrical surface-wave guides," *Z. Angew. Phys.*, vol. 3, p. 272; 1951.
[225] O. Schriever, "Electromagnetic waves in dielectric conductors," *Ann. Physik*, vol. 63, p. 645; 1920.
[226] G. Schulten, "Novel method for measuring impedance on surface-wave transmission lines," PROC. IRE, vol. 47, pp. 76–77; January, 1959.
[227] F. Sellberg, "Theoretical investigation of some closed delay structures for high-power travelling-wave tubes," *Proc. IEE*, vol. 105, pt. B, pp. 730–735; May, 1958.
[228] S. Sensiper, "Electromagnetic wave propagaiton on helical structures (a review and survey of recent progress)" PROC. IRE, vol. 43, pp. 149–161; February, 1955.
[229] R. Servant and P. Londette, "First results of a polarimetric study, with microwaves, of asymmetric metal resonators," *J. Phys. Radium*, vol. 14, p. 79S; 1953.
[230] K. P. Sharm, "An investigation of the excitation of radiation by surface waves," *Proc. IEE*, vol. 106, pt. B, pp. 116–122; March, 1959.
[231] C. E. Sharp and G. Goubau, "A UHF surface-wave transmission line," PROC. IRE, vol. 41, pp. 107–109; January, 1953.
[232] A. A. Sharshanov and K. N. Stepanov, "Electromagnetic wave propagation in an almost periodic waveguide," *Zhur. Tekh. Fiz.*, vol. 27, p. 1474; 1957.
[233] J. C. Slater, "Microwave Electronics," D. Van Nostrand Co. Inc., New York, N. Y.; 1950.
[234] K. E. Slevogt, "Propagation of decimetre waves along a dielectric line," *Hochfreq. und Elek.*, vol. 59, p. 1; 1942.
[235] W. Sichak, "Coaxial line with helical inner conductor," PROC. IRE, vol. 42, pp. 1315–1319; August, 1954.
[236] A. J. Simmons, "Phase shift by periodic loading of waveguide and its application to broad-band circular polarization," IRE TRANS. ON MICROWAVE THEORY AND TECHNIQUES, vol. MTT-3, pp. 18–21; December, 1955.
[237] N. N. Smirnov, "Propagation of waves along an infinitely long helix," *Compt. Rend. Acad. Sci. U.R.S.S.*, vol. 108, p. 243; 1956.
[238] N. N. Smirnov, "Dispersive properties of multifilar helices," *Compt. Rend. Acad. Sci. U.R.S.S.*, vol. 110, p. 212; 1956.
[239] V. Y. Smorgonskii, "Calculation of the phase and group velocity of surface waves," *Radiotekhnika*, vol. 10, p. 25; 1955.
[240] W. Sollfrey, "Wave propagation on helical wires," *J. Appl. Phys.*, vol. 22, pp. 905–910; July, 1951.
[241] E. G. Solov'ev, "Circular and rectangular waveguides with longitudinal diaphragms," *Zhur. Tech. Fiz.*, vol. 25, p. 707; 1955.
[242] E. G. Solov'ev, "Propagation of electromagnetic waves between two circular cylindrical surfaces in the presence of longitudinal periodically spaced diaphragms," *Radiotekhnika (Moscow)*, vol. 11, p. 57; 1956.
[243] E. G. Solov'ev and L. V. Belows, "Theory of helical line surrounded by a cylindrical semi-conducting envelope," *Radiotekhnika (Moscow)*, vol. 11, p. 31; 1956.
[244] A. Sommerfeld, "Propagation of electromagnetic waves along a cylindrical conductor," *Ann. Physik und Chemie*, vol. 67, p. 233; 1899.
[245] N. M. Sovetov, "Dispersion characteristic of a disk loaded waveguide," *Zhur. Tekh. Fiz.*, vol. 24, p. 1907; 1954.
[246] L. Stark, "Lower modes of a concentric line having a helical inner conductor," *J. Appl. Phys.*, vol. 25, pp. 1155–1162; September, 1954.
[247] H. Seyskal, "Experimental study of delay-lines," *L'Onde Electrique*, vol. 37, p. 86; 1957.
[248] J. A. Stratton, "Electromagnetic Theory," McGraw-Hill Book Co., Inc., New York, N. Y.; 1941.
[249] M. K. Subbarao and A. B. McLay, "Diffraction of 3.2 cm. electromagnetic waves by dielectric rods: part 1—lucite and tenite 1 in. diameter cylinders," *Can. J. Phys.*, vol. 34, p. 546; 1956.
[250] H. Suhl and L. R. Walker, "Topics in guided wave propagation through gyromagnetic media: part II—transverse magnetization and the nonreciprocal helix," *Bell Sys. Tech. J.*, vol. 33, pp. 939–986; July, 1954.
[251] D. T. Swift-Hook, "Dispersion curves for a helix in a glass tube," *Proc. IEE*, vol. 105, pt. B, pp. 747–755; May, 1958.
[252] P. K. Tien, "Traveling-wave-tube helix impedance," PROC. IRE, vol. 41, pp. 1617–1623; November, 1953.
[253] P. K. Tien, "Bifilar helix for backward wave oscillations," PROC. IRE, vol. 42, pp. 1137–1143; July, 1954.
[254] F. J. Tischer, "H-guide—a new microwave concept," *Electronic Ind. Tele-Tech.*, vol. 15, p. 50; 1956.
[225] F. J. Tischer, "H-guide, A waveguide for microwaves," 1956 IRE CONVENTION RECORD, pt. 5, pp. 44–47.
[256] S. E. Tsimring, "Variational calculation method for waveguides with periodic inhomogeneities: part 1," *Radiotekh. i Elektron.*, vol. 2, p. 3; 1957.
[257] H. Uchida and S. Nishida, "Surface and Space Waves on the Surface-Wave Transmission Line," Res. Insts., Tohuku University, Japan, Sci. Rept. 6B, p. 217; 1955.
[258] H. Uchida, S. Nishida, H. Uda, and H. Nagasawa, "The Shunt Reactive Element on the Surface-Wave Transmission line," Res. Insts., Tohuku University, Japan, Sci. Rept. 6B, p. 229; 1955.
[259] H. Uchida, S. Nishida, and H. Shioya, "Shielded Dielectric Waveguide," Res. Insts., Tohuku University, Japan, Sci. Rept. 8B, p. 7; 1956.
[260] K. Udagawa, "Propagation of electromagnetic waves in helical circuits coaxially surrounded by a dielectric tube," *J. Inst. Elec. Commun. Engrs. (Japan)*, vol. 35, p. 85; 1952.
[261] K. Udagawa, "On the attenuation characteristics of electromagnetic waves in helical circuits," *J. Inst. Elec. Commun. Engrs. (Japan)*, vol. 35, p. 342; 1952.
[262] T. Umehara, "Design charts for surface-wave transmission lines," *J. Inst. Elec. Commun. Engrs. (Japan)*, vol. 37, p. 425; 1954.
[263] H. G. Unger, "Transfer of energy by dielectric guides," *Fernmeldetech. Z.*, vol. 8, p. 438; 1955.
[264] H. G. Unger, "Dielectric tubes as waveguides," *Arch. elek. Übertragung*, vol. 8, p. 241; 1954.
[265] L. A. Vainshtein, "Surface electromagnetic waves on a comb structure," *Zhur. Tekh. Fiz.*, vol. 26, p. 385; 1956.
[266] S. A. Vakin, "Propagation of electromagnetic waves along an infinite helical slit," *Compt. Rend. Acad. Sci. U.R.S.S.*, vol. 84, p. 37; 1952.
[267] B. Valtersson, "Phase velocity in helical waveguides," *L'Onde Électrique*, vol. 37, p. 843; 1957.
[268] V. J. Vanhuyse, "On the (β_0, k) diagrams for circularly symmetric TM waves in infinite iris-loaded waveguides," *Nuovo Cim.*, vol. 1, p. 447; 1955.
[269] V. J. Vanhuyse, "On the proper frequencies of terminated waveguides," *Physica*, vol. 21, pp. 269, 603; 1955.
[270] V. J. Vanhuyse, "On the resonance frequencies and the field configurations in terminated corrugated waveguides," *Physica*, vol. 21, p. 829; 1955.
[271] R. E. Vowels, "Matrix methods in the solution of ladder networks," *J. IEE*, vol. 95, pp. 40–50; January, 1948.
[272] G. Wade and N. Rynn, "Coupled helices for use in travelling-wave tubes," IRE TRANS. ON ELECTRON DEVICES, vol. ED-2, pp. 15–24; July, 1955.
[273] J. R. Wait, "Excitation of surface waves on conducting stratified, dielectric-clad and corrugated surfaces," *J. Res. Natl. Bur. Standards*, vol. 59, p. 365; 1957.
[274] R. A. Waldron, "Theory of the helical waveguide of rectangular cross section," *J. Brit. IRE*, vol. 17, p. 577; 1957.
[275] R. A. Waldron, "A helical coordinate system and its applications in electromagnetic theory," *Quart. J. Mech. Appl. Math.*, vol. 11, pt. 4, pp. 438–461; November, 1958.
[276] J. C. Walling, "Interdigital and other slow wave structures," *J. Electronics*, vol. 3, p. 239; 1957.
[277] G. B. Walker and N. D. West, "Mode separation at the π-mode in a dielectric loaded waveguide," *Proc. IEE*, vol. 104, pt. C, pp. 381–387; September, 1957.
[278] G. B. Walker, "Dielectric loading for U.H.F. valves," *Proc. IEE*, vol. 105, pt. B, pp. 717–718; May, 1958.
[279] R. Warnecke, O. Doehler and P. Guenard, "On delay lines in the form of combs or interdigital structures and their equivalent circuits," *Compt. Rend. Acad. Sci. (Paris)*, vol. 231, p. 1220; 1950.
[280] D. A. Watkins and E. A. Ash, "The helix as a backward-wave circuit structure," *J. Appl. Phys.*, vol. 25, pp. 782–790; June, 1954.
[281] D. A. Watkins and A. E. Siegman, "Helix impedance measurements using an electron beam," *J. Appl. Phys.*, vol. 24, pp. 917–922, July, 1953; vol. 25, p. 133, January, 1954.
[282] W. H. Watson, "The experimental determination of equivalent networks for a coaxial line to helix junction," IRE TRANS. ON ELECTRON DEVICES, vol. ED-3, pp. 149–152; July, 1956.
[283] W. H. Watson and J. R. Whinnery, "Study of a plane short on a shielded helix," IRE TRANS. ON ELECTRON DEVICES, vol. ED-2, pp. 34–36; October, 1955.
[284] S. E. Webber, "Calculations of wave propagation of a helix in the attenuation region," IRE TRANS. ON ELECTRON DEVICES, vol. ED-1, pp. 35–39; August, 1954.

[285] H. Weber, "The dimensions of loaded waveguides for the H_{10} mode," *Telefunken Zeitung*, vol. 27, p. 44; 1954.
[286] M. T. Weiss and E. M. Gyorgy, "Low-loss dielectric waveguides," IRE Trans. on Microwave Theory and Techniques, vol. MTT-2, pp. 38–44; September, 1954.
[287] R. E. White, "Coaxial-to-helix transducers for travelling-wave-tubes," *Elec. Commun.*, December, 1953; also 1953 IRE Convention Record, pt. 10, pp. 42–45.
[288] R. M. Whitmer, "Fields in nonmetallic waveguides," Proc. IRE, vol. 36, pp. 1105–1109; September, 1948.
[288a] E. Wild, "Electromagnetic waves in nearly periodic structures," *Quart. J. Mech. Appl. Math.*, vol. 10, p. 322; 1957.
[289] J. C. Wiltse, "Some characteristics of dielectric image lines at millimetre wavelengths," IRE Trans. on Microwave Theory and Techniques, vol. MTT-7, pp. 65–69; January, 1959.
[290] H. Zahn, "Detection of electromagnetic waves in dielectric wires," *Ann. Physik*, vol. 49, p. 907; 1916.
[291] J. Zenneck, "On the propagation of plane electromagnetic waves along a flat conductor and its application to wireless telegraphy," *Ann. Physik*, vol. 23, p. 846; 1907.
[292] F. J. Zucker, "Theory and application of surface waves," *Nuovo Cim.*, vol. 9, (supplement), p. 450; 1952.
[293] F. J. Zucker, "The guiding and radiation of surface waves," *Proc. of the Symposium on Modern Advances in Microwave Techniques*, Polytechnic Inst. of Brooklyn, Brooklyn, N. Y.; 1954.

Design of Mode Transducers*

L. SOLYMAR† and C. C. EAGLESFIELD†

Summary—**The propagation of the electromagnetic wave in a gradual transducer is discussed. It is shown that the incident mode and the geometry of the transducer determine the outgoing mode. Inverting this theorem, a method is suggested for the design of the transducer's surface for cases in which the desired modes in the uniform waveguides are given.**

The application of the method is illustrated in three examples.

I. Introduction

IN the design of a microwave transmission system it is often necessary to connect two uniform waveguides of different cross section by means of a nonuniform waveguide (subsequently referred to as a transducer). The transducer can be used for two different purposes: 1) to transform the same mode from one waveguide into another waveguide of different size; and 2) to transform a certain mode of one waveguide into a predetermined mode of the other waveguide.

The best example for the first type is a transducer between two rectangular waveguides of different size. The requirement is to transform efficiently the H_{01} mode in a specified bandwidth. All the solutions naturally employ a transducer whose cross section is everywhere rectangular. Similarly, the cross section of a transducer between two circular waveguides of different diameter is always circular. The problem in these cases is how to vary the size of the cross section. This field is well explored, and for certain cases optimum solutions have been obtained.

* Manuscript received by the PGMTT, July 6, 1959; revised manuscript received, August 17, 1959.
† Standard Telecommun. Labs. Ltd., Harlow, Essex, Eng.

The design of a transducer of the second type (generally called a mode transducer) is incomparably more complicated, since the shape of the cross section is varying. Although mode transducers have been used since the earliest days of microwave transmission, no systematic procedure seems to have been developed for the design of the required cross sections. The existing mode transducers were designed by physical intuition.

The aim of the present paper is to suggest a systematic design method. For the better understanding of the basic phenomena, the properties of a given transducer are first analyzed. It is shown that the incident mode and the surface of a sufficiently gradual transducer determine the outgoing mode. In the third section the inverse problem is dealt with, *i.e.*, choosing the surface of the transducer when the desired modes in the uniform waveguides are given.

II. The Propagation of the Electromagnetic Wave in a Sufficiently Gradual Transducer

Let us consider the following arrangement of waveguides (see Fig. 1). The uniform waveguide A extends from $z=-\infty$ to $z=0$, the transducer from $z=0$ to $z=L$ and the uniform waveguide B from $z=L$ to $z=\infty$.

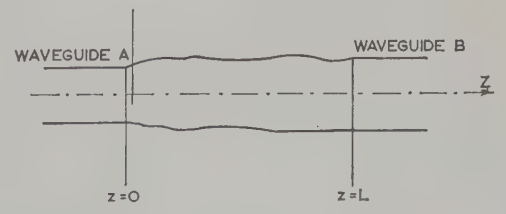

Fig. 1.

The transducer has the following properties:

a) The equation of the surface is differentiable as a function of z.

b) A plane perpendicular to the z axis cuts the surface in a single closed curve.

c) The cross sections [denoted by $S(z)$] at $z=0$ and $z=L$ are equal to those of the uniform waveguides A and B, respectively; *i.e.*, $S(O)=S^A$ and $S(L)=S^B$.

The propagation of an electromagnetic wave in this waveguide system can be studied with the aid of the equivalent circuit concept.

As is known,[1] a uniform waveguide can be represented by a set of uniform transmission lines, where each transmission line corresponds to a mode. The impedance and the propagation coefficient of the transmission line can be expressed by the eigenfunctions (cross-sectional wave functions) and eigenvalues (cutoff wave numbers) of the uniform waveguide. A wave can separately propagate on any of the transmission lines.

Propagation in a waveguide of gradually varying cross section can also be represented by the same picture of a number of transmission lines,[2,3] but now each line has gradually varying characteristics and there is a coupling between the lines. The coupling coefficients and the characteristics of the transmission lines can be expressed by the eigenfunctions and eigenvalues of a uniform waveguide, whose cross section is identical with that of the nonuniform waveguide at z. However, if the transducer is sufficiently gradual, the coupling between the transmission lines can be neglected.[4]

Thus, if a single mode enters the transducer from waveguide A it will travel along one of the transmission lines and emerge at the end as a single mode of waveguide B. However, at this stage of the argument it is not at all clear which mode of waveguide B will be excited; in order to discover this, the transducer has to be studied step by step. This can be done in principle (and in practice numerically) by determining the eigenfunctions and eigenvalues at a number of successive cross sections of the transducer; thus, the continuity of the transmission lines is determined in particular that of the transmission line which is terminated in the incident mode. The investigated cross sections must be spaced sufficiently close, so that the continuity can be clearly established.

If we write $t_m{}^A$ for the incident mode and refer to the transmission line on which it travels as the mth transmission line, and if $\psi_m(x, y, z)$ is the corresponding gradually varying eigenfunction, then the requirements on ψ_m are as follows:

1) It is differentiable as a function of z.
2) $\psi_m(x, y, 0)=\psi_m{}^A$, where $\psi_m{}^A$ is the eigenfunction of the $t_m{}^A$ mode in waveguide A.
3) $\psi_m(x, y, L)=\psi_m{}^B$, where $\psi_m{}^B$ is the eigenfunction of the excited mode in waveguide B (denoted by $t_m{}^B$).
4) It satisfies the two-dimensional wave equation for all values of z.
5) It satisfies the boundary conditions on the boundary of every cross section.

We must note here that as a direct consequence of the equivalent circuit of the transducer, the $t_m{}^B$ mode belongs to the same family (H or E) as the $t_m{}^A$ mode.

Summarizing the conclusions of this section, we state that if the geometry of a sufficiently gradual transducer and the incident mode are given, the outgoing mode may be determined with the aid of the $\psi_m(x, y, z)$ function.

However, the above treatment is not completely general. In a few special cases, spurious modes will be present in waveguide B even for a very gradual transducer. These exceptions are discussed in the Appendix.

III. Outline of the Design Method

We now invert the problem; instead of starting with an existing transducer and deducing $\psi_m(x, y, z)$, we lay down the required $t_m{}^A$ and $t_m{}^B$ modes, construct the eigenfunction of the mth transmission line, and design the transducer.

Knowing $\psi_m{}^A$ and $\psi_m{}^B$ it is always possible to construct a function ψ_a which satisfies conditions 1)–4). (A particular method of this construction will be given in a later section.) ψ_a becomes the eigenfunction of the mth transmission line, if it satisfies condition 5) as well as conditions 1)–4). Thus, the surface of the transducer must be designed in such a way that the boundary conditions for ψ_a are satisfied at every cross section. If the transducer furthermore satisfies conditions a)–c), then according to the analysis of the previous section, the transducer transforms the $t_m{}^A$ mode of waveguide A into the desired $t_m{}^B$ mode of waveguide B.

The Equation of Possible Boundaries

If both $t_m{}^A$ and $t_m{}^B$ belong to the family of the E modes, then the equation of the possible boundaries is given simply as follows:

$$\psi_m(x, y, z) = 0. \tag{1}$$

If both $t_m{}^A$ and $t_m{}^B$ are H modes, then the normal derivative of the eigenfunction should vanish at the boundary. Denoting by $f(x, y)=0$ the equation of the boundary curve at a given z, it must satisfy the following partial differential equation:

$$\frac{\partial \psi_m}{\partial x}\frac{\partial f}{\partial x}+\frac{\partial \psi_m}{\partial y}\frac{\partial f}{\partial y}=0. \tag{2}$$

[1] N. Marcuvitz, "Waveguide Handbook," McGraw-Hill Book Co., Inc., New York, N. Y., pp. 3–7; 1948.

[2] S. A. Schelkunoff, "Conversion of Maxwell's equations into generalised telegraphist's equations," *Bell Sys. Tech. J.*, vol. 34, pp. 995–1045; September, 1955.

[3] G. Reiter, "Connection of Two Waveguides by a Waveguide of Variable Cross-Section," M.S. thesis in applied mathematics, University Eotvos Lorand, Budapest, Hungary; June, 1955.

[4] L. Solymar, "Spurious mode generation in nonuniform waveguide," IRE Trans. on Microwave Theory and Techniques, vol. MTT-7, pp. 379–383; July, 1959.

In a practical case it is generally sufficient to construct the boundary curve by finding graphically the orthogonal trajectories of the (ψ_m = constant) electric lines.

Construction of $\psi_m(x, y, z)$

The eigenfunction of the mth transmission line can be constructed in an infinite number of ways. We shall choose it for most of the subsequent examples in a simple mathematical form as follows:

$$\psi_m(x, y, z) = g_1(z)\psi_m{}^A + g_2(z)\psi_m{}^B \tag{3}$$

where

$$g_1(0) = 1, \qquad g_1(L) = 0$$
$$g_2(0) = 0, \qquad g_2(L) = 1 \tag{4}$$

and both $g_1(z)$ and $g_2(z)$ are monotonic differentiable functions. ψ_m—constructed in this way—obviously satisfies conditions 1)–3). A simple (but not the only possible) way of meeting condition 4) is to make the eigenvalues (cutoff wave numbers) of the $t_m{}^A$ and $t_m{}^B$ modes equal. This implies a certain relation between the dimensions of waveguides A and B which may not be convenient. In practical devices, this can be overcome by a preliminary taper in which the dimensions of waveguide A (or B) are changed gradually, where the shape is kept the same.

An interesting special case arises when the eigenfunction of the $t_m{}^A$ and $t_m{}^B$ modes is the same, although the cross sections of the uniform waveguides are different. Then an obvious choice for the eigenfunction of the mth transmission line is

$$\psi_m = \psi_m{}^A = \psi_m{}^B. \tag{5}$$

Mode Purity

A disadvantage of the method is that we cannot perform the design for a specified mode purity. Because of the coupling (neglected in the design) between the transmission lines, spurious modes will always be present. After the transducer has been constructed, the power in the spurious modes is calculable[3] although the calculations are very laborious.

The mode purity will also depend on frequency, but since the transducer is built up by gradual change the purity of the desired mode cannot change violently with frequency. However, when the frequency is increased, the power in the spurious modes generally increases[4,5] due to the decrease in the difference of the propagation coefficients. Nevertheless, this increase in the power of the spurious modes is small within the normally required bandwidth and is unlikely to affect the performance.

[5] B. Z. Katzenelenbaum, "On the Theory of Nonuniform Waveguides with Slowly Changing Parameters," presented at the Congres International Circuits et Antennes Hyperfrequences, Paris, France; October, 1957.

Examples

We shall illustrate the design method in three examples.

The first example is a transducer between two uniform waveguides having cross sections which are, respectively, a section of a circle and a whole circle. The electric lines of the desired modes (both are H modes) are shown in Figs. 2(a) and 2(c). (The density of the lines

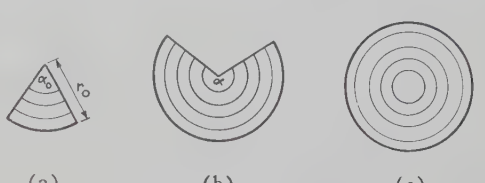

(a) (b) (c)

Fig. 2.

in these and subsequent drawings is not related to the intensity of the electric field). In this case, the eigenfunctions of both modes are the same. The simplest choice for the eigenfunction of the mth transmission line is in the form of (5). Then

$$\psi_m = J_0\left(3.83\frac{\rho}{r_0}\right) \tag{6}$$

where

J_0 = zero order Bessel function,
ρ = the radial polar coordinate, and
r_0 = the radius of the circle.

The boundary of an intermediate cross section must be chosen in such a way that the boundary conditions are fulfilled for ψ_m. It may be easily shown that the normal derivative of (5) vanishes on the boundary of any section of a circle of radius r_0. Hence, the cross section of the transducer is chosen as a section of a circle of radius r_0, whose central angle is a monotonic function of z satisfying the conditions $\alpha(0) = \alpha_0$ and $\alpha(L) = 2\pi$.

This type of transducer is in common use.[6] The example simply shows that, using this method, we arrive at the same transducer.

We wish, however, to emphasize the fact that this is not the only solution. If we choose a different ψ_m we arrive at a different transducer. Another possible choice of ψ_m [it obviously satisfies conditions 1)–4)] is, for example,

$$\psi_m = J_0\left(3.83\frac{\rho}{r(z)}\right) \tag{7}$$

where $r(z)$ is a slowly varying function of z, $r(0) = r(L) = r_0$. An intermediate cross section of this transducer is a section of a circle of radius $r(z)$.

[6] A. C. Beck, "Measurement Techniques for Multimode Waveguides," presented at the Symposium on Modern Advances in Microwave Techniques, New York, N. Y.; November, 1954.

A further choice of ψ_m might result in a transducer in which none of the intermediate cross sections is a section of a circle, and which nevertheless produces an arbitrarily pure mode at the output, provided that the transducer is sufficiently gradual.

There is no doubt that an engineer will prefer the transducer designed in the first way (it is very likely that for a given length that transducer produces the purest mode), but it is worthwhile to note that, depending on the choice of ψ_m, an infinity of solutions exists.

Our second example is a mode transducer from the H_{02} mode of a rectangular waveguide into the H_{01} mode of a circular waveguide. Mode transducers between these two modes were designed a long time ago.[7] We wish to suggest an alternative solution.

ψ_m is chosen in the form of (3). The ratio of the diameter of the circle (denoted by d) to the width of the rectangle (denoted by a) is $d/a=1.22$, determined from the equality of the cutoff wave numbers. The height of the rectangular waveguide is chosen to be equal to the diameter of the circular waveguide. Thus, the eigenfunction of the mth transmission line may be expressed as follows:

$$\psi_m(x, y, z) = g_1(z) \cos\frac{2\pi}{a}y + g_2(z)J_0\left(\frac{2\pi}{a}\sqrt{x^2+y^2}\right) \quad (8)$$

where x, y, z are Cartesian coordinates.

In this case, the intermediate cross sections of the transducer cannot be determined by simple considerations. Either a numerical solution of the differential equation (2) is necessary, or the following graphical method can be used.

The ψ_m=constant curves representing the lines of electric intensity are plotted in Fig. 3 for given values of $g_1(z)$ and $g_2(z)$. A possible boundary intersects perpendicularly these electric lines. A further consideration is that the resulting surface between the prescribed cross sections should be a smooth one. Taking account of these requirements, Fig. 4 shows four cross sections (initial, two intermediate, and final) of the transducer designed. One can see from the changing picture of the electric lines how the H_{02} mode of the rectangular waveguide is transformed into the H_{01} mode of the circular waveguide.[8]

Let us choose for the third example a mode transducer, which—although it has no practical importance at the moment—illustrates how powerful the method is.

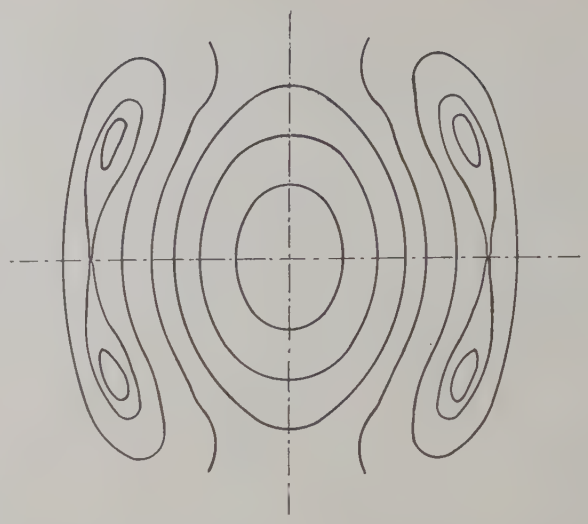

Fig. 3—The ψ_m=constant curves, $g_1(z)=0.246$, $g_2(z)=0.8$.

The cross sections of the two uniform waveguides (rectangle and isosceles right-angled triangle) to be connected and the electric lines of the desired modes may be seen in Figs. 5(a) and 5(e). The mode in the triangular waveguide is the same as an H_{11} mode in a square waveguide.

In this case— in our opinion—intuition fails and the cross sections of the transducer cannot be guessed, while the application of the proposed design method leads to a direct result.

The height of the rectangle (denoted by b) is chosen to be equal to the sides of the triangle. The equality of the eigenvalues is assumed by the choice $w=b/\sqrt{2}$, where w is the width of the rectangle. Constructing the eigenfunction of the mth transmission line in the same way as before, we obtain

$$\psi_m(x, y, z) = g_1(z) \cos\frac{\pi y}{w} + g_2(z) \cos\frac{\pi x}{w\sqrt{2}} \cos\frac{\pi y}{w\sqrt{2}} \cdot \quad (9)$$

Three intermediate cross sections of the transducer may be seen in Figs. 5(b), (c), and (d). Having seen these figures, one can imagine how the transducer works; *i.e.*, the application of the method helps to build up a deeper physical insight.

IV. Conclusion

It has been shown that for a gradual transducer the outgoing mode $t_m{}^B$ can be determined from the incident mode $t_m{}^A$ (exceptions are treated in the Appendix). The gradually changing field configuration in the transducer is represented by an appropriately chosen function, the eigenfunction of the mth transmission line. When this theorem is inverted, the eigenfunction of the mth transmission line is determined from the incident and outgoing modes, and with its aid the surface of the transducer is also determined.

[7] C. G. Montgomery, R. H. Dicke, and E. M. Purcell, "Principles of Microwave Circuits," McGraw-Hill Book Co., Inc., New York, N. Y., p. 340; 1948.

[8] A transducer of this type has been constructed and tested by Dr. Y. Klinger. It is 3 inches long, $\frac{5}{8}$ inch diameter at the circular end. Preliminary measurements at the wavelength 9 mm indicate a power level in the desired H_{01} circular mode of about 95 per cent.

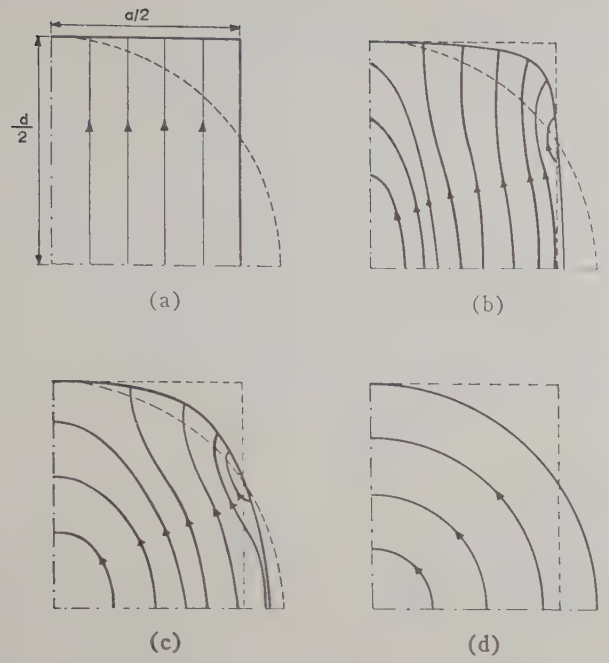

Fig. 4—Four cross-sections of a transducer from the $H_{02}^{\square}$ mode to the $H_{01}^{\circlearrowleft}$ mode. (a) $g_1(z)=1$, $g_2(z)=0$; (b) $g_1(z)=0.739$, $g_2(z)=0.4$; (c) $g_1(z)=0.246$, $g_2(z)=0.8$; (d) $g_1(z)=0$, $g_2(z)=1$.

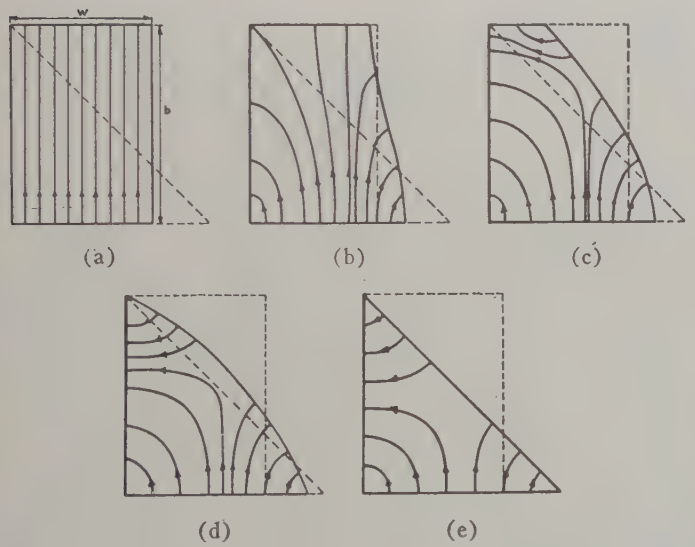

Fig. 5—Five cross-sections of a transducer from the $H_{01}^{\square}$ mode to the $H_{11}^{\circlearrowleft}$ mode. (a) $g_1(z)=1$, $g_2(z)=0$; (b) $g_1(z)=0.6$, $g_2(z)=0.4$; (c) $g_1(z)=0.37$, $g_2(z)=0.63$; (d) $g_1(z)=0.2$, $g_2(z)=0.8$; (e) $g_1(z)=0$, $g_2(z)=1$.

Three examples have been worked out to illustrate the design procedure. The electric lines in intermediate cross sections are plotted; these show how the transducer works.

The paper presents a systematic approach to the design of mode transducers, but certainly leaves many questions unanswered, a few of which are listed here.

1) In choosing a ψ_m, does a transducer exist between the required cross sections of the uniform waveguides for which ψ_m is the eigenfunction of the mth transmission line?
2) Which is the best choice of ψ_m?
3) When choosing ψ_m in the form (3), what is the best choice of $g_1(z)$ and $g_2(z)$?

The answers to these questions do not seem to be simple ones, but there is no reason to suppose that the optimum design (in one or other sense) of mode transducers is prohibitive.

Appendix

There are two types of cases when the conclusions of Section II are not valid. Both are consequences of degeneracy.

1) If a mode at a certain cross section of the transducer can be represented as the superposition of two modes which have the same cutoff wave numbers, then, because of a change in the boundary, the two components might separate (in the equivalent circuit this means that a transmission line is split into two). This may happen, for example, with a (not circularly symmetrical) mode in a circular pipe. If the circular waveguide is deformed into an elliptical waveguide, and the deformation does not take place along one of the axes of symmetry, then two separate modes with different velocities will propagate in the elliptical waveguide.[9]

2) If in the equivalent circuit of the transducer there exists another transmission line whose cutoff wave number agrees with that of the mth transmission line for every value of z, and these two transmission lines are coupled, then this coupling can never be neglected. The power is fluctuating between these two transmission lines.[10] This happens, for example, in a bent circular waveguide, where the H_{01} and E_{11} modes (each representing a transmission line) have the same cutoff wave number and are coupled through the boundary.

It is unlikely that in the design of a mode transducer either of these cases will arise. Nevertheless, it must be borne in mind that these effects can cause the failure of the method.

Acknowledgment

The authors wish to thank L. Lewin, Dr. Y. Klinger, and Dr. A. E. Karbowiak for many interesting discussions. Acknowledgment is also made to Standard Telecommunication Laboratories for permission to publish the paper.

[9] L. J. Chu, "Electromagnetic waves in elliptic hollow pipes of metal," *J. Appl. Phys.*, vol. 9; September, 1938.
[10] S. E. Miller, "Coupled wave theory and waveguide applications," *Bell Sys. Tech. J.*, vol. 33, pp. 661–719; May, 1954.

UHF Resonator with Linear Tuning*

B. H. WADIA† AND R. L. SARDA†

Summary—A novel method of tuning a transmission-line type resonator is described. The first-order theory of such a resonator is derived and presented in the form of design curves which indicate an extremely good tuning linearity. Experiments with a resonator designed on this principle agree with theory.

I. Introduction

A tunable resonant device, in which frequency varies linearly with mechanical motion, promises a large number of advantages in applications such as wavemeters, ganged resonators, and mechanically swept oscillators where such a characteristic could permit vernier frequency dials, one-point calibration, and easier alignment and adjustment. Resonant circuits which are in general use (LC circuits, resonant lines, re-entrant cavities) depart greatly from linearity when used over a large frequency range. Attempts are often made to improve linearity by special measures and auxiliary devices such as cams, link motions, specially shaped tuning rods and plates; among the more sophisticated devices of this type, we may mention the developments of Ginzton and Salisbury,[1] and Brot and Soulard.[2] However, these methods are not linear "in principle" but are made so by special design. A resonant system which can indicate linearity or near linearity in its basic conception is likely to be even more valuable.

This paper describes a simple method of tuning which exhibits good linearity over a wide frequency range. In essence, it involves two quarter-wave resonant transmission line sections which are coupled together at their open ends by a series capacitor. By a common mechanical motion, the length of one section is increased while that of the other is reduced by the same amount in such a way that the combined length remains the same. This causes one section of line to tune up its frequency curve while the other tunes down and the nonlinearities of the two sections effectively cancel each other. By a proper choice of the characteristic impedances of the two sections, one can vary the tuning range, the rate of tuning, and the region of approximate linearity. This principle is quite neatly applied to two quarter-wave coaxial lines placed "back-to-back" so as to form a doubly re-entrant cavity as shown in Fig. 1(a); tuning is accomplished by the movement of the capacitive gap relative to the outer conductor. The theory and the design curves for this type of tuning are derived and show that good linearity can be obtained over as large a tuning range as 1.5:1. Experimental evidence is given in support of the theory. The study also includes a consideration of the higher order modes and the Q of the structure.

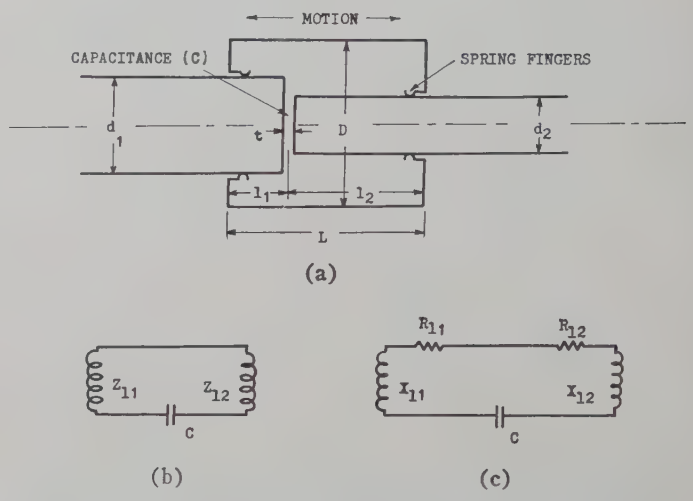

Fig. 1—(a) Schematic diagram of the resonant system. (b) Idealized and lossless equivalent circuit. (c) Ideal equivalent circuit with losses.

In connection with previous work, we may mention an article by Barrow and Mieher[3] which gives extensive experimental data on re-entrant cavities. The article deals with various modes which interplay in a re-entrant cavity as it passes from a perfect cylinder to a perfect coaxial line. In the process, the authors give brief data on the resonant frequencies of the cavity with various gap positions. It is interesting to note its similarity with the data presented in our work. However, Barrow and Mieher do not proceed to analyse the system nor to consider it as a method of linear tuning as is done in the present paper. The article came to the attention of the authors after the principle of back-to-back tuning had been established.

II. Principle of Back-to-Back Tuning

Consider two coaxial line sections each shorted at one end with their open ends brought together. If the diameters of their outer conductors are equal and if a narrow capacitive gap is left at the junction between their center conductors, a doubly re-entrant resonant cavity results. Fig. 1(a) shows such a structure and its major dimensions. In general, the diameters (d_1 and d_2) of the two portions of the center conductor on either side of the capacitive gap may be different; they are,

* Manuscript received by the PGMTT, June 12, 1959.
† Central Electronics Engrg. Res. Inst., Pilani, Rajasthan, India.
[1] E. L. Ginzton and F. L. Salisbury, "Ultra-high-frequency wavemeter," U. S. Patent No. 2,503,256; April, 1950.
[2] C. Brot and A. Soulard, "Cavity with linear tuning for meter and decimeter wavelengths," *Compt. Rend. Acad. Sci. (Paris)*, vol. 243, pp. 1848–1850; December, 1956.
[3] W. L. Barrow and W. W. Mieher, "Natural oscillations of electrical cavity resonators," Proc. IRE, vol. 28, pp. 184–191; April, 1940.

however, mechanically joined together to keep the gap distance constant. Tuning of the cavity consists in making the outer shell capable of axial motion relative to the center conductor assembly so that the capacitive gap changes position and the lengths of the two coaxial lines on either side of the capacitive gap are altered by the same amount—one increases and the other decreases in length. If l_1 and l_2 are the lengths of the two sections and Z_{01} and Z_{02} are their characteristic impedances, the ideal and lossless equivalent circuit of the resonator will be as shown in Fig. 1(b). The impedances of the two lines in question seen at the capacitive gap will be

$$Z_{l_1} = jZ_{01} \tan \frac{2\pi l_1}{\lambda},$$

$$Z_{l_2} = jZ_{02} \tan \frac{2\pi l_2}{\lambda};$$

both are normally inductive.

A. The Resonance Equation

For resonance

$$\frac{1}{2\pi fC} = Z_{01} \tan \frac{2\pi l_1}{\lambda} + Z_{02} \tan \frac{2\pi l_2}{\lambda}.$$

By appropriate re-arrangement

$$\frac{1}{\left(\frac{2\pi fL}{v_0}\right)\left(\frac{CZ_{01}v_0}{L}\right)} = \tan\left[\left(\frac{2\pi fL}{v_0}\right)\left(\frac{l_1}{L}\right)\right] + \left(\frac{Z_{02}}{Z_{01}}\right) \tan\left[\left(\frac{2\pi fL}{v_0}\right)\left(1 - \frac{l_1}{L}\right)\right],$$

where v_0 = velocity of light.

It is noted that the bracketed quantities are dimensionless and constitute normalized variables. A simpler form of the equation results as

$$\frac{1}{f_n C_n} = \tan f_n l_{1n} + Z_n \tan f_n(1 - l_{1n}) \qquad (1)$$

where

$$f_n = \text{normalized resonant frequency} = \frac{2\pi fL}{v_0}, \qquad (2)$$

$$l_{1n} = \text{normalized length} = \frac{l_1}{L}, \qquad (3)$$

$$C_n = \text{normalized impedance} = \frac{CZ_{01}v_0}{L}, \qquad (4)$$

$$Z_n = \text{normalized impedance} = \frac{Z_{02}}{Z_{01}}. \qquad (5)$$

In order to examine the tuning characteristics, the above equation must be solved to yield f_n as a function of l_{1n} for representative values of the design parameters Z_n and C_n. From the nature of the above equation it would at first appear that the relation between f_n and l_{1n} could hardly be linear and indeed in the rigorous sense it is not so; attempts to convert (1) to a linear form by some appropriate approximation did not yield neat results. However, solution and plotting of (1) shows that a significant portion of the curve differs only slightly from the linear, and this is borne out by subsequent experimentation. It must be admitted that, in spite of the nonlinear appearance of (1), faith in the ultimate linearity of tuning was maintained by a certain amount of intuitive reasoning based on the fact that the two component lines of the resonator are operating back-to-back; while one is increasing in length, the other is being reduced—thus giving a chance for the nonlinearities on either side of the gap to neutralize each other.

B. Solution of the Resonance Equation

By treating Z_n and C_n as parameters, (1) reduces to an implicit transcendental relation between f_n and l_{1n} for each set of values of Z_n and C_n and can be solved by well-known graphical methods. For each value of l_{1n} from 0 to 1, the two sides of the equation are separately plotted with f_n as abscissa; the intersection of the two curves gives the solution of f_n for each l_{1n}. Fig. 2 pertains

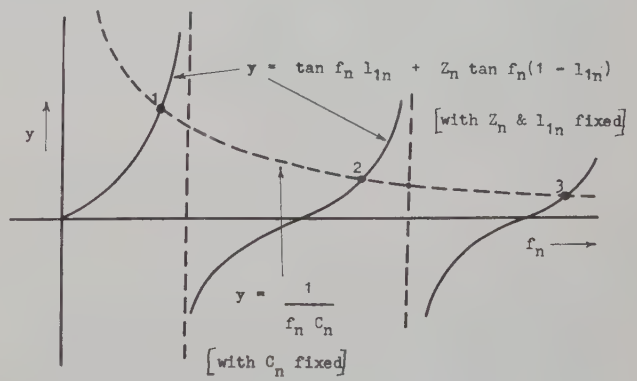

Fig. 2—Method of solution of the resonance equation.

to this process of graphical solution. It must be noted that the terms on the right hand side of the equation are periodic and that there will be a large number of possible solutions according to the branch on which the intersection occurs. We shall discuss this point again later, but for the moment we limit ourselves to the solution on the first branch of the curve, thus considering only the case of "quarterwave" operation for each of the two component lines. This is the lowest or dominant mode and is of major practical importance.

The solutions obtained for this fundamental mode are given in Fig. 3(a), (b), (c), and (d) in the form of a series of universal design curves. These curves and the normalized variables defined in (2), (3), (4) and (5) give us the tools for designing these types of resonators in the desired frequency range. The loci of the maxima are also obtained by equating the derivative to zero and solving the resulting equation.

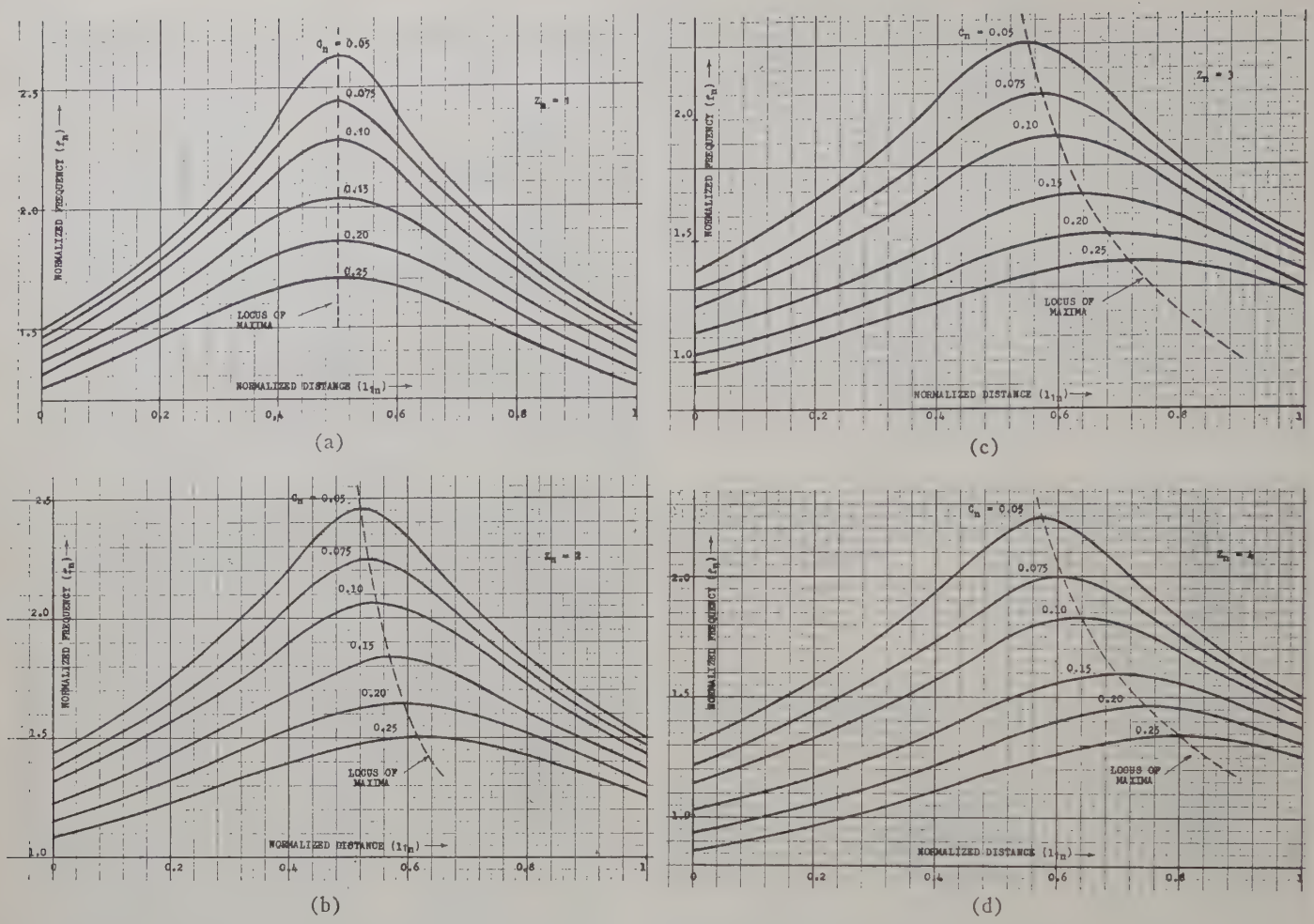

Fig. 3—Universal design curves for various values of Z_n and C_n.

An examination of these curves shows the following properties:

1) Good linearity is obtained except near the maximum of the curve.
2) For values of Z_n other than unity, better linearity and more gradual tuning can be obtained over a greater range on one side of the curve than on the other.
3) The tunable range is reduced while linearity improves as value of C_n increases.
4) From symmetry considerations, it should be clear that for Z_n less than unity, the curves are lateral inversions of the corresponding cases for their reciprocals.
5) For $l_{1n}=0$ or 1 the cavity resembles a singly reentrant cavity of length L and characteristic impedance Z_{02} or Z_{01} respectively.

C. Higher Order Modes

We have thus far restricted ourselves to the discussion of the simplest mode in the cavity, *i.e.*, the transmission line mode with nearly quarterwave variation in each coaxial section. It would be worthwhile to study the possibility of other modes to see whether they behave linearly and to assure that there is no likelihood of interference between the useful mode and the higher orders.

That higher order longitudinal modes are possible can easily be seen from the periodic nature of the tangent functions and from Fig. 2, where several intersections are indicated. A physical picture can also be obtained by noting that the resonance condition is determined by the impedances looking into both lines at the plane of the capacitive gap; the requisite impedances on either side may be obtained by modes which are not necessarily of the fundamental type. The number of possibilities for satisfying the resonance condition is therefore infinite for each position of the capacitive gap.

For a proper understanding of such higher modes, a solution for some typical values of parameters was obtained for the mode which appears next after the dominant, *i.e.*, as given by the second intersection (shown in Fig. 2). Fig. 4 shows a comparison of the normal tuning curve with the tuning curve for this next solution when $Z_n=3$ and $C_n=0.05$. It is noted that the new curve is far from regular; also that, fortunately, considerable frequency separation occurs, and there is no harmonic relation between the modes. We are therefore fairly safe in assuming good mode-separation properties.

Higher order modes of the circumferential type are

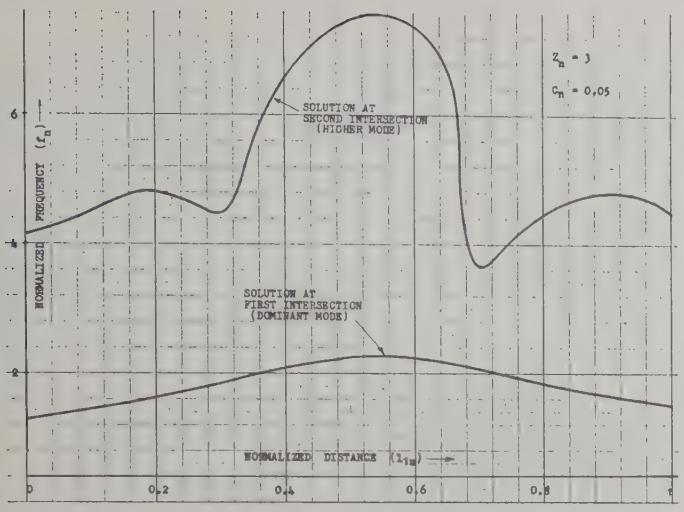

Fig. 4—Comparison of the next higher mode with the dominant for $Z_n=3$, and $C_n=0.05$.

also possible as in all cylindrically symmetric structures. However, if care is taken to keep the circumference of the cavity sufficiently less than one wavelength in the operating range, the cavity can be essentially free from circumferential mode interference.

Two simple checks can be made to assure that any given design is operating in the required fundamental mode:

$\pi D \ll \lambda$ for circumferential modes

$2L < \lambda$ for longitudinal modes

at the highest operating frequency.

III. Calculation of Q

If we take into account the small losses occurring in the cylindrical conducting walls, the equation of input impedance of the left side line can be rewritten as

$$Z_{l_1} = R_{l_1} + jX_{l_1} = Z_{01} \tanh \gamma_1 l_1$$

where

$\gamma_1 = \alpha_1 + j\beta_1$,
α_1 = loss factor in nepers per meter (small),
β_1 = phase constant in radians per meter

provided we neglect the losses at the shorting end and at the capacitive gap.

By standard algebraic methods, the real and the imaginary parts of the above equation can be separated to give

$$R_{l_1} = Z_{01}\alpha_1 l_1 \sec^2 \beta_1 l_1$$

$$X_{l_1} = Z_{01} \tan \beta_1 l_1.$$

We assume that α_1 is quite small so that terms with $\alpha_1^2 l_1^2$ are neglected and $\tan \alpha_1 l_1 \approx \alpha_1 l_1$. This assumption is justified for cavities with inner surfaces of high conductivity materials.

The value of α_1 is given by the usual skin effect formula[4]; for a silver plated cavity

$$\alpha_1 = \frac{6.68 \times 10^{-10}\sqrt{f}\left(\frac{D}{d_1}+1\right)}{D \log_e \frac{D}{d_1}}.$$

But since

$$Z_{01} = 60 \log_e \frac{D}{d_1} \quad \text{and} \quad f_n = \frac{2\pi f L}{v_0},$$

hence

$$\alpha_1 = 2.774 \times 10^{-4}\sqrt{\frac{f_n}{L}} \cdot \frac{\left(\frac{D}{d_1}+1\right)}{Z_{01}D}. \tag{6}$$

The resistive and reactive components of Z_{l_1} become

$$R_{l_1} = 2.774 \times 10^{-4}\sqrt{\frac{f_n}{L}} \cdot \frac{\left(\frac{D}{d_1}+1\right)}{D/L} l_{1n} \sec^2 f_n l_{1n}$$

$$X_{l_1} = Z_{01} \tan f_n l_{1n}$$

and similar expressions hold for the right-side coaxial line.

The equivalent circuit of Fig. 1(b) can be modified to include the resistive components as shown in Fig. 1(c). An expression for the unloaded Q is then simply given by

$$Q_0 = \frac{X_{l_1} + X_{l_2}}{R_{l_1} + R_{l_2}}.$$

But we note that

$$X_{l_1} + X_{l_2} = Z_{01} \tan f_n l_{1n} + Z_{02} \tan f_n(1 - l_{1n}) = \frac{Z_{01}}{f_n C_n}.$$

Hence

$$Q_0 = \frac{Z_{01}\left(\frac{D}{d_1}\right)L^{1/2}}{2.774 \times 10^{-4} f_n^{3/2} C_n \left[\left(\frac{D}{d_1}+1\right) l_{1n} \sec^2 f_n l_{1n} + \left(\frac{D}{d_2}+1\right)(1 - l_{1n}) \sec^2 f_n(1 - l_{1n})\right]}.$$

[4] W. Jackson, "High Frequency Transmission Lines," Methuen and Co. Ltd., London, Eng., p. 50; 1951.

IV. Experimental Results

A. Cavity Design

In most cases, cavity design begins with a knowledge of the desired tuning range around a given center frequency. From the normalized curves in Fig. 3, one curve with the appropriate linear tuning range and slope is chosen; this determines the values of the parameters Z_n and C_n. The value of L is then determined by applying (2) to the center frequency; knowing L, the product $Z_{01}C$ in (4) is fixed from the chosen value of C_n. The value of C is generally determined by the bounds of the design problem such as the required gap distance or the capacity of the tube electrodes in case of oscillator cavities; hence Z_{01} gets defined. The rest of the design requires only the determination of the diameters d_1, d_2, and D for the appropriate characteristic impedances keeping in mind that larger diameters give better Q_0, while a possibility of circumferential modes limits the average circumference to less than the lowest wavelength.

A cold test model of a cavity with a range of 1100 to 1900 mc was designed to test the principles outlined above. The curves of $Z_n=3$ were chosen due to their reasonable linearity consistent with good tuning range. The mechanical structure of the cavity is shown in Fig. 5. The two center conductors are supported with the requisite spacing by being clamped to an outside frame which forms the base of the whole structure. The outer cylinder is mounted concentric to these conductors and it slides over the center conductor assembly. Accurate linear motion is imparted to the outer cylinder by means of a micrometer head having threads with one millimeter pitch; there are two hundred circumferential divisions, and motion adjustability of nearly 10^{-4} cm is thereby derived. An inherent backlash of about 0.005 cm exists; hence care is taken to make all adjustments in one direction only. The important dimensions of the cavity are $L=4.967$ cm, $D=4.0$ cm, $d_1=3.0$ cm, $d_2=1.75$ cm, and t is adjustable. The zero position on the micrometer scale corresponds to the case when the inner conductor d_1 is flush with the left wall of the cavity.

The feeding-in of the RF signal is in a completely symmetric manner. A tiny probe protrudes through the center of one of the inner conductors at the capacitive gap and delivers the RF signal to the cavity from an ordinary flexible coaxial cable which is brought in along the middle of the tube forming the center conductor d_1.

B. Frequency Measurements

Measurements were first made on the cavity before plating and installation of spring fingers in order to assure that the cavity configuration was as close as possible to the theoretical design. As will be shown later, these changes lead to a perturbation of the frequency. For this experiment, the bearing surfaces were made to the best possible sliding fit and properly aligned in all respects to ensure a good contact. A standard method[5] was used for obtaining the curve of resonant frequency vs cavity scale reading for two gap distances [0.42 cm which corresponds to approximately $1\mu\mu f(C_n=0.1)$, and 0.21 cm which gives twice as much capacity $(C_n=0.2)$].

Fig. 6 shows the measurements (curves B) as well as the calculations (curves A) of tuning characteristics for these two gap spacings; it is noted that the measured curves exhibit an appreciably linear behavior, perhaps slightly better than the theoretical curves. For comparison, a tuning curve (curve D shown dotted) is also computed for the usual type of singly re-entrant cavity (*i.e.* the capacitance terminated coaxial line) in the same general range; the improvement in linearity by back-to-back tuning becomes quite apparent. By fitting the best

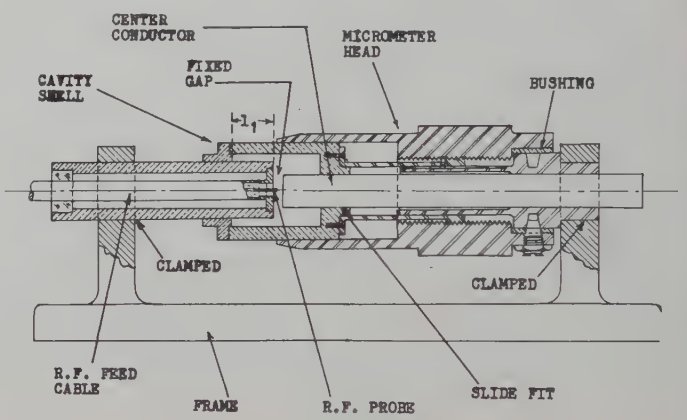

Fig. 5—The experimental resonator.

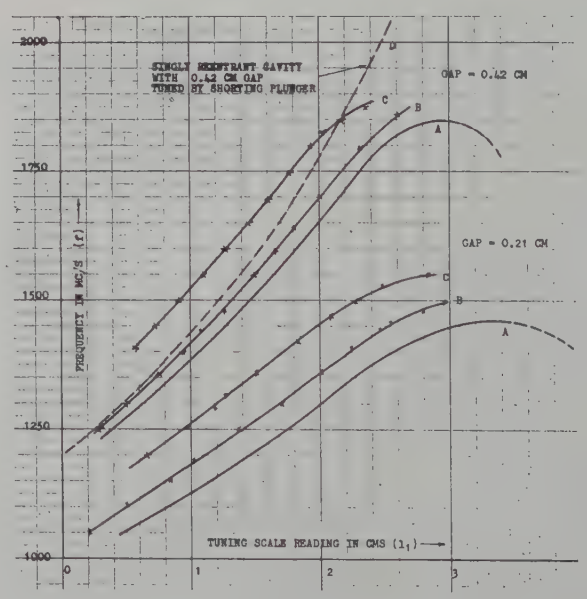

Fig. 6—Comparison of measured and calculated readings for gap distances of 0.42 cm $(C_n=0.1)$ and 0.21 cm $(C_n=0.2)$. A gives calculated values; B gives measured values without spring fingers; C gives measured values with spring fingers and silver plating.

[5] E. L. Ginzton, "Microwave Measurements," McGraw-Hill Book Co., New York, N. Y., pp. 413–417; 1957.

straight line through our measured values, it can be checked that departure from linearity is much less than 1 per cent for the whole range. For the larger capacitance value, the linearity appears to be further improved, although the tuning range is much reduced.

It is noticed that the measured curves have shifted upwards and leftwards from the calculated curves for both values of gap distance. An inquiry into the possible reasons for this difference between theory and experiment yields a better insight into short-comings of the first order theory.

1) A small systematic error is introduced due to the finite thickness of the capacitive gap. In the experiment, the micrometer scale is referenced from the left wall of the cavity and, in any given position, measures the distance from the wall to the end plate of the larger central conductor. Where the gap thickness is truly negligible this would not cause an error, but for appreciable gap width (0.42 cm and 0.21 cm in our experiment) the distance l_1 should be measured to the center line of the gap as the appropriate reference; hence all measured readings would be shifted to the right by half the gap width.
2) Consider the RF field configuration near the gap as sketched in Fig. 7. Our design did not take into account the effects of the "fringe" fields on the capacity at the gap but merely assumed a lumped capacitance of the ideal parallel-plate-type calculated from the average area of the end surfaces of the two center conductors. In practice, the "effective" capacitance under RF operation is different and is determined by the field lines exchanged between the two center conductors. Hence the lines terminating on the outer cylinder indicate a reduced effective capacitance. Resonance would therefore be indicated at a slightly higher frequency.
3) Due to the same fringing effect, the effective lengths of the coaxial lines have changed. This is shown by the distance marked A on Fig. 7 which is the distance from the gap center to the surface of revolution which separates the fields of the left-hand coax from the fields of the righthand coax. It is easily seen that the direction of the error is such as to explain the differences between theory and experiment.

A little thought will show that the errors due to 2) and 3) will be larger for larger values of Z_n and for narrower gaps, since the differences in diameters of the two central conductors, as will a narrower gap, will cause the actual capacitance value to differ considerably from that calculated on the average area basis.

In preparation for a proper measurement of Q_0, spring-fingers were subsequently installed at the sliding contacts and the RF surfaces were plated with a coat of about 20 microns of silver. Frequency measurements were repeated in order to assess the change caused by these additions; these measured curves are also shown in Fig. 6 (marked *C*). It is clear that these changes have caused a perturbation of nearly 100 mc in the frequency due to the reduction in volume and the consequent change in the resonant structure; however, linearity is not at all impaired.

C. Measurement of Q

The first order formula for calculating the Q_0 of this cavity was derived in Section III. When applied to the present design, a curve of Q_0 vs the tuning position can be calculated; such a curve is shown in Fig. 8. It is of interest to note the general trend of the curve which indicates a similarity in general form to the slope of the tuning curve. We see that Q_0 is reasonably high in the region of interest to us (namely the linear tuning region on the left hand side) and that it shows a slight rise with frequency; the rapid fall in the region beyond the linear range is of little consequence since the cavity is not intended for use in that region.

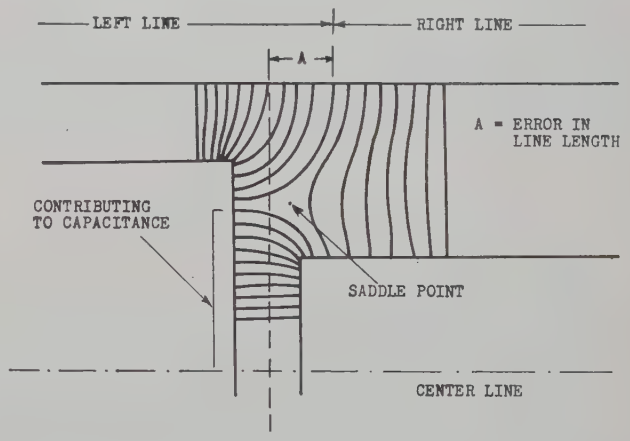

Fig. 7—Probable configuration of electric field lines near the gap.

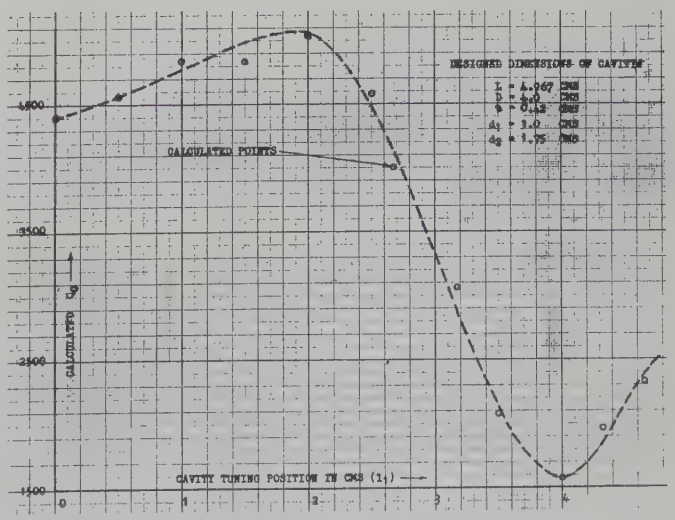

Fig. 8—Calculated Q_0 of the resonant system.

Practical measurements of unloaded Q_0 for a gap distance of 0.42 cm were carried out using the impedance method,[5] and are shown in Table I together with the corresponding calculated values.

TABLE I
COMPARISON OF CALCULATED AND MEASURED VALUES OF Q_0

Measured frequency in megacycles per second	Tuning position in centimeters	Measured Q_0	Corresponding theoretical Q_0
1500	0.85	1125	4700
1600	1.55	1280	4950
1800	1.8	1720	5100
1870	2.50	900	4400
1690	3.49	575	2100

As can be expected, the measured values of the unloaded Q_0 are about 25 per cent of the theoretical values. This difference is a usual one in case of Q_0 measurements and is due to losses which are not accountable by the simple theory. Losses at the shorting end, imperfect spring contacts, unpolished surfaces, dirt, scratches, capacitance losses at the gap, no losses etc., account for this difference.

V. Conclusion

The first-order theory of back-to-back tuning has been derived and shown to agree reasonably well with the experimental results. Both theory and experiment show that the resonator tuning characteristic obtainable by this method is linear for all practical purposes over a large frequency range. By appropriate design, various frequency ranges and tuning slopes can be obtained. The theoretically expected values of unloaded Q_0 are in the vicinity of 4500, while in actual practice values around 1200 are obtained in the useful range of linear tuning.

The method is, in general, applicable to any form of resonant system where quarter-wave line sections can be employed. For instance, for frequencies in the VHF range, the method can be applied with Lecher lines; in the UHF range, coaxial-type lines are more convenient. The presence of a capacitive gap makes the system especially adaptable where interaction with an electron beam is intended. Due to the simple construction, convenient size, nonharmonic modes, and good mode separation, this method should hold promise of valuable application over a wide frequency spectrum.

VI. Acknowledgment

The authors gratefully acknowledge the valuable help of Dr. H. D. Doolittle of Machlett Laboratories, Inc., Springdale, Conn., for initiating the idea and giving a start to the investigation; and also the assistance of B. Rama Krishna Rao and Ravindra Babu (both of this Institute) in making the many measurements and plots.

Equivalent Circuits for Small Symmetrical Longitudinal Apertures and Obstacles*

ARTHUR A. OLINER†

Summary—**Formulas based on small aperture and small obstacle theory are presented for the determination of equivalent circuits for symmetrical longitudinal apertures and obstacles. These formulas are then applied to several examples of practical interest, including aperture discontinuities in trough waveguide and an obstacle array of interest to anisotropic radomes.**

I. Introduction

THE evaluation of equivalent circuits for waveguide discontinuities often involves the solution of a boundary value problem of considerable complexity. For the class of so-called "small" apertures and obstacles, however, this evaluation becomes particularly simple when the problem is properly phrased. A small aperture or obstacle is one which is located far from the guide walls and whose dimensions are small compared to a wavelength. Under these conditions, the distortion of the field lines in the vicinity of such a small aperture or obstacle, due to some specified excitation, is essentially independent of the cross-sectional shape of the containing waveguide, and depends only on the nature of the excitation and the physical shape of the aperture or obstacle. The quantity which characterizes the aperture or obstacle and which is a function only of its physical geometry and the type of incident excitation is the *polarizability*; since the aperture or obstacle is small compared to wavelength, the polarizability may be determined under static conditions. The function of small aperture or obstacle theory is then to relate the polarizability to the location of the aperture or obstacle within the containing waveguide and to the appropriate

* Manuscript received by the PGMTT, August 28, 1959. The major portion of this work was performed at the Microwave Research Institute of the Polytechnic Institute of Brooklyn under Contract No. AF-19(604)-2031, sponsored by the Air Force Cambridge Research Center.

† Microwave Research Institute, Polytechnic Institute of Brooklyn, Brooklyn, N. Y.

incident mode in a fashion such that the equivalent circuit parameters may be readily evaluated. The value of this method lies not only in the simple phrasing of the problem that is permitted, but also in the fact that the resulting solutions are useful considerably beyond the strict limitations indicated in the preceding.

Small aperture theory was first formulated by Bethe,[1,2] and was soon afterwards rephrased by Marcuvitz[3] in a more compact form particularly suitable for equivalent circuit evaluations. Transverse apertures (*i.e.*, apertures located in a metal plate which is coincident with a waveguide cross-section plane) have been treated by many workers, both with regard to the power coupled through the hole and in terms of its shunt equivalent circuit. It has also been long recognized that the shunt equivalent circuit for a small transverse obstacle may be obtained by Babinet equivalence considerations from the results for a corresponding small transverse aperture.

For *longitudinal* apertures (located in a top or side wall of a waveguide and employed to couple power between two neighboring waveguides) the picture is not as complete. Bethe[2] presents formulas for the power coupled between two adjacent waveguides, and these formulas have been used, for example, in directional coupler designs. Expressions for the scattering matrix elements in multimode waveguide have also been derived[4,5] via simple extensions of Bethe's work. Marcuvitz[6] presents equivalents circuits which were obtained by small aperture methods for several examples of waveguides coupled by longitudinal apertures. Despite the existence of these solutions, general small aperture formulas for the equivalent circuit parameters do not appear anywhere and are not available.

In Section II-B of this paper, general expressions are presented for the equivalent circuit parameters of a certain class of small longitudinal apertures, these expressions being deduced from a knowledge of the scattering matrix elements. The longitudinal apertures considered here are restricted to symmetrical apertures coupling identical waveguides; this restricted class applies to a wide number of cases of practical interest, as is indicated later.

In contrast to the case of longitudinal apertures, small obstacle theory applicable to *longitudinal obstacles* has not been exploited heretofore. Formulas are presented in Section II-C of this paper which permit the ready evaluation of the equivalent circuits of small longitudinal obstacles which are symmetrical.[7] Since it is felt that the derivations of these expressions and those for longitudinal apertures are in themselves of lesser interest than the results, and since the derivations do not contain any new features and are somewhat lengthy, they are not included here.

Several applications of the small longitudinal aperture and longitudinal obstacle expressions presented in Section II are also included here. These applications serve partly to illustrate the use of these relations, but are also of interest in themselves and were solved originally in answer to a need. In Section III, the small aperture formulas are applied first to a round hole located in the center fin of trough waveguide, and then to an array of holes coupling two parallel plate waveguides. It is pointed out there that the latter case is of particular value in its use in a transverse resonance procedure, and can be applied, for example, to top wall directional couplers in rectangular waveguide, or to a periodic array of holes in trough waveguide. The small obstacle formulas are applied in Section IV first to a circular disk in rectangular waveguide, where the distinctions between longitudinal and transverse orientations of the disk are determined, and then to the case of a plane wave incident at an angle on a two-dimensional array of longitudinal rods. The latter problem is of interest in a study of anisotropic radomes, since this configuration discriminates between incident waves of parallel and perpendicular polarization.

II. Small Aperture and Small Obstacle Formulas

A. Preliminary Relations and Definitions of Terms

The incident mode in the waveguide containing the aperture or obstacle may be characterized by transverse mode functions $\boldsymbol{e}$ and $\boldsymbol{h}$ and by a longitudinal scalar function ϕ or ψ. These functions and their normalizations are the same as those in the "Waveguide Handbook;"[8] expressions for these functions for conventional waveguides are also presented there.[9] The scalar function ϕ and ψ are proportional to longitudinal components of electric and magnetic field, respectively, so that $\phi=0$ for H (or TE) modes and $\psi=0$ for E (or TM) modes. When the mode functions and the scalar functions are normalized in the manner

$$\iint_{\text{cross section}} \boldsymbol{e}\cdot\boldsymbol{e}^* dS = \iint_{\text{cross section}} \boldsymbol{h}\cdot\boldsymbol{h}^* dS = 1, \quad (1)$$

and

$$\iint_{\text{cross section}} \phi\phi^* dS = 1/k_c^2, \qquad \iint_{\text{cross section}} \psi\psi^* dS = 1/k_c^2, \quad (2)$$

[1] H. A. Bethe, "Lumped Constants for Small Irises," M.I.T. Rad. Lab., Cambridge, Mass., Rept. No. 43-22; March, 1943.
[2] H. A. Bethe, "Theory of Side Windows in Waveguides," M.I.T. Rad. Lab., Cambridge, Mass., Rept. No. 43-27; April, 1943.
[3] N. Marcuvitz, "Waveguide Circuit Theory: Coupling of Waveguides by Small Apertures," Microwave Res. Inst., Polytechnic Inst. of Brooklyn, Rept. No. R-157-47, PIB-106; 1947.
[4] H. A. Judy and D. J. Angelakos, "Mode Selective Directional Couplers," Electronics Res. Lab., University of California, Berkeley, Ser. No. 60, Issue No. 19; September, 1954.
[5] L. B. Felsen, "Analysis of Circular Waveguide Modes," Microwave Res. Inst., Polytechnic Inst. of Brooklyn, Second Quarterly Rept., R-394.6-55, PIB-327.6; February, 1955.
[6] N. Marcuvitz, "Waveguide Handbook," Rad. Lab. Ser., McGraw-Hill Book Co., Inc., New York, N. Y., vol. 10; 1951. See for example, Sections 6.6, 6.8–6.10, 7.2–7.5.
[7] L. B. Felsen of the Polytechnic Institute of Brooklyn has independently derived a small obstacle formulation which applies also to unsymmetrical obstacles.
[8] Marcuvitz, *op. cit.*, Section 1.2.
[9] *Ibid*, Chap. II.

where $k_c(=2\pi/\lambda_c)$ is the cutoff wave number of the given mode; then the characteristic impedance Z_0 and the characteristic admittance Y_0 are equal to the wave impedance and admittance, respectively, *i.e.*,

$$Z_0 = 1/Y_0 = \begin{cases} \dfrac{\kappa}{\omega\epsilon} & \text{for E modes} \\ \dfrac{\omega\mu}{\kappa} & \text{for H modes} \end{cases} \tag{3}$$

where $\kappa(=2\pi/\lambda_g)$ is the propagation wave number.

It is convenient to employ the symbols e_z and h_z to represent the longitudinal field components; their relation to ϕ and ψ are

$$e_z = -j\frac{Y_0}{\omega\epsilon}k_c^2\phi \tag{4}$$

$$h_z = -j\frac{Z_0}{\omega\mu}k_c^2\psi. \tag{5}$$

Since the incident mode field does not vary much over a small aperture or obstacle, the value of the incident field is taken to be that at the center of the aperture or obstacle, and this particular value of the field is denoted by the subscript 0.

In small aperture theory, the behavior of the aperture is dependent on the magnetic and electric polarizabilities, M and P, which respond, respectively, to the tangential component(s) of magnetic field and the normal component of electric field at the aperture. These polarizabilities are a function of the shape and size of the aperture only, and expressions are available for the polarizabilities of apertures of simple shapes, such as a circle, ellipse, or long slit.[10] Numerical values for other shapes have been obtained experimentally by Cohn[11,12] using an electrolytic tank, thereby enhancing the usefulness of small aperture theory. Cohn has also derived a simple correction formula[13] for the magnetic polarizability in the case of larger apertures.

The behavior of a small obstacle is sensitive to the tangential component(s) of electric field and the normal component(s) of magnetic field at the obstacle. The respective polarizabilities are designated in this paper as P^{ob} and M^{ob}. For a planar obstacle, the numerical values of P^{ob} and M^{ob} are equal to those of M and P, respectively, for an aperture identical in size and shape to the obstacle. Such an equivalence is generally deduced via Babinet equivalence considerations, involving a factor of 4, but we choose to place this factor in the expressions for the equivalent circuit parameters rather than in the polarizability expressions directly. Expressions for certain nonplanar obstacles of simple shape are scattered throughout the literature.[14,15]

Since the apertures and obstacles treated in this paper are all symmetrical and lossless, only two independent parameters are required for their circuit representation. The reactance and susceptance representations are shown pictorially by the tee and pi networks of Fig. 1. The parameters are related to the reactance and susceptance matrix elements by

$$\begin{aligned} X_a &= X_{11} - X_{12},\ X_b = X_{12} \\ B_a &= B_{11} - B_{12},\ B_b = B_{12}. \end{aligned} \tag{6}$$

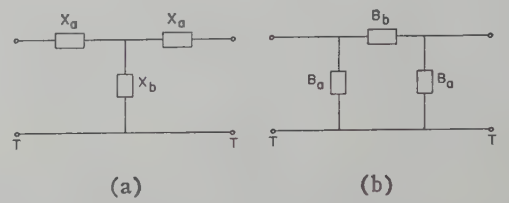

Fig. 1—(a) Tee equivalent network. (b) Pi equivalent network.

In the small aperture or obstacle limit, the reactance and susceptance parameters are very simply related, *i.e.*,

$$\begin{aligned} X_a' &= -\frac{1}{2B_b'} \\ X_b' &= -\frac{1}{2B_a'}, \end{aligned} \tag{7}$$

where the prime denotes the parameter normalized to the appropriate characteristic impedance or admittance. Relations (7) state in essence that the shunt effect and the series effect of the networks are independent in this limit.

In a scattering matrix representation of a symmetrical aperture or obstacle, only parameters S_{11} and S_{12} are independent. Furthermore, one can write for small apertures or obstacles

$$S_{12} = 1 + \sigma. \tag{8}$$

Element S_{12} should actually be expressed as

$$S_{12} = \frac{1}{1-\sigma},$$

so that $|S_{12}|^2 < 1$, but in the small aperture or obstacle limit $\sigma \ll 1$. Elements S_{11} and σ are related to the pi network parameters in this limit as

$$\begin{aligned} jB_b' &= \frac{1}{S_{11} - \sigma} \\ jB_a' &= -\tfrac{1}{2}(S_{11} + \sigma), \end{aligned} \tag{9}$$

[10] C. G. Montgomery, R. H. Dicke, and E. M. Purcell, "Principles of Microwave Circuits," Rad. Lab. Sers., McGraw-Hill Book Co., Inc., New York, N. Y., vol. 8, p. 178; 1948.

[11] S. B. Cohn, "Determination of aperture parameters by electrolytic-tank measurements," PROC. IRE, vol. 39, pp. 1416–1421; November, 1951.

[12] S. B. Cohn, "The electric polarizability of apertures of arbitrary shape," PROC. IRE, vol. 40, pp. 1069–1071; September, 1952.

[13] S. B. Cohn, "Microwave coupling by large apertures," PROC. IRE, vol. 40, pp. 696–699; June, 1952.

[14] C. Susskind, "Obstacle type artificial dielectrics for microwaves," *J. Brit. IRE*, vol. 12, p. 49; 1952.

[15] M. M. Z. Kharadly and W. Jackson, "The properties of artificial dielectrics comprising arrays of conducting elements," *Proc. I.E.E.* (London), Pt. III, vol. 100, pp. 199–212; July, 1953.

or

$$S_{11} = -j\left[B_a' + \frac{1}{2B_b'}\right]$$

$$\sigma = -j\left[B_a' - \frac{1}{2B_b'}\right]. \tag{10}$$

B. Symmetrical Longitudinal Apertures Coupling Identical Waveguides

Longitudinal apertures may be used to couple two waveguides either in a tee junction fashion or when placed parallel to each other. In either case, an appropriate equivalent circuit representation is chosen, and by small aperture theory the parameters of the equivalent circuit are related to the geometry of the coupling aperture and the coupled waveguides. Equivalent circuits for several specific examples of these two types are presented by Marcuvitz.[6]

When the two coupled waveguides are identical and are arranged parallel to each other, the form of the equivalent circuit becomes particularly simple. This special case corresponds to many practical situations; it occurs, for example, in various directional coupler applications and in strip line and trough waveguide discontinuities. The longitudinal aperture discussion in this paper is restricted to this class of structures.

Two typical cases which arise in the coupling of two parallel identical waveguiding regions are illustrated in Fig. 2. The coupling behavior for arbitrary field excitation may be expressed in terms of two orthogonal modal situations, one for which the excitations from the two separate waveguides are in phase and the second for which they are out of phase. When the field excitations in the separate waveguides are opposite to those indicated in Fig. 2, the surface common to the two identical waveguide regions becomes an electric wall and the presence of the coupling aperture is not felt. The equivalent circuit for this excitation degenerates into a straight-through connection for each waveguide separately, with no coupling between them.

When the excitations in the separate waveguides are as shown in Fig. 2, the aperture surface becomes a magnetic wall and the equivalent circuit is now nontrivial. Since the two halves of these structures are identical to each other, the reflection coefficients for each half are equal and are the same as the reflection coefficient for both halves taken together. The complete electrical behavior for this excitation is thus obtained by choosing a pi or tee network representation, of the form of Fig. 1, for either half of the structure.

It may be desirable to have available a single equivalent circuit appropriate to both excitations, or, equivalently, to an arbitrary excitation. In that case, a form such as that shown in Fig. 3 may be used; as seen, the circuit consists of two pi networks, back to back, bridged across by an additional element equal to $-B_a$. When the excitation is such as to produce a magnetic wall in the

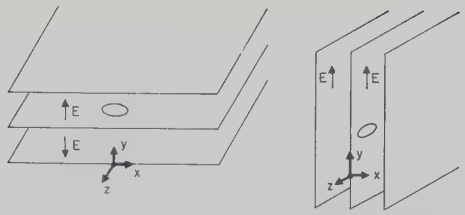

(a) (b)

Fig. 2—Longitudinal aperture coupling of identical waveguides. (a) E plane (top wall) coupling. (b) H plane (side wall) coupling.

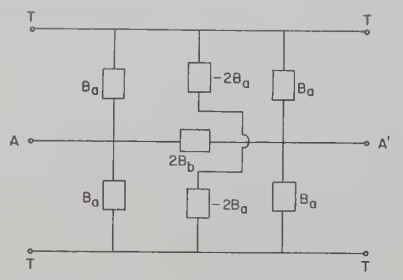

Fig. 3—Equivalent circuit for longitudinal aperture coupling two identical waveguides, valid for arbitrary excitation.

aperture, an open circuit is produced along the line $A-A'$ in Fig. 3, so that the circuit breaks up into two separate pi networks, back to back, and element $-B_a$ does not contribute. When the excitation is such as to produce an electric wall in the aperture, a short circuit occurs along $A-A'$ and the additional element $-B_a$ cancels the remaining elements to produce straight-through connections in the separate waveguides.

E Plane (Top Wall) Coupling: The structure appropriate to this situation was indicated in Fig. 2(a). The waves in both of the constituent waveguides propagate along the z direction, and the principal axes of the symmetrical coupling aperture are assumed to lie along the x and z axes. In small aperture theory, the coupling by the aperture is sensitive to the H_x, H_z, and E_y components of the unperturbed fields in the constituent waveguides. The expressions for the equivalent circuit parameters will therefore contain the M_x, M_z, and P_y polarizabilities in the general case. Only two parameters, B_a and B_b, are needed to specify the complete equivalent network, either in pi form for the "magnetic wall" excitation or in the form of Fig. 3 which is valid for arbitrary excitation. It can be shown that small aperture expressions for these two parameters, normalized to the characteristic admittance Y_0 of either of the identical coupled waveguides, are

$$\frac{1}{B_b'} = -\omega\mu Y_0 2M_x h_{x0} h_{x0}^* \tag{11}$$

$$B_a' = \omega\mu Y_0 M_z h_{z0} h_{z0}^* - \omega\epsilon Z_0 P_y e_{y0} e_{y0}^*. \tag{12}$$

The polarizabilities M and P have been discussed in the previous section, Y_0 and Z_0 are defined in (3), and the mode functions are defined with respect to their nor-

malizations in (1), (2), (4), and (5). The subscript 0 denotes the value of the mode function at the center of the aperture, and the asterisk means the complex conjugate. In the normalizations defined by (1) and (2), the integrations are performed over *either* of the two identical waveguides, but not over both. One sees from (11) and (12) that B_b' is always inductive, while B_a' can be either inductive or capacitive.

H Plane (Side Wall) Coupling: A structure corresponding to coupling of this type is shown in Fig. 2(b). Again, the power flow in both of the constituent waveguides is in the z direction, and the principal axes of the coupling aperture lie along the y and z directions. In the most general case, which might arise for some higher mode, the coupling would be responsive to the H_y, H_z, and E_z components of the unperturbed fields in the separate waveguides. For this case the expressions for B_a' and B_b' would be given by (11) and (12) upon replacement of M_x and P_y by M_y and P_x. Often, however, this type of coupling occurs when E_x and H_y are both zero in the unperturbed waveguides. Then (11) and (12) reduce to

$$\frac{1}{B_b'} \approx 0 \tag{13}$$

$$B_a' = \omega\mu Y_0 M_z h_{z0} h_{z0}^*. \tag{14}$$

It is seen from (13) and (14) that *to this order* the equivalent circuit reduces to a simple shunt capacitance. The other elements are actually nonvanishing but generally can be neglected; they correspond to higher order (multipole) contributions.[16]

C. Symmetrical Longitudinal Obstacles

A typical small symmetrical longitudinal obstacle and an equivalent circuit for it in pi form are shown in Fig. 4(a) and (b). Since the obstacle is symmetrical, only two parameters suffice to characterize it completely. In small obstacle theory, the electrical behavior of the obstacle is responsive to the tangential component(s) of electric field and the normal component(s) of magnetic field at the obstacle. As mentioned in Section II-A, the respective obstacle polarizabilities are designated in this paper as M^{ob} and P^{ob}.

The direction of propagation in the waveguide is denoted by z, with x and y referring to the cross-section coordinates. With these coordinates, small obstacle expressions for the parameters of the equivalent network of Fig. 4(b) may be shown to be

$$B_a' = 2\omega\epsilon Z_0[M_x{}^{ob} e_{x0} e_{x0}^* + M_y{}^{ob} e_{y0} e_{y0}^*] - 2\omega\mu Y_0[P_z{}^{ob} h_{z0} h_{z0}^*] \tag{15}$$

$$\frac{1}{B_b'} \doteq 4\omega\mu Y_0[P_x{}^{ob} h_{x0} h_{x0}^* + P_y{}^{ob} h_{y0} h_{y0}^*] - 4\omega\epsilon Z_0[M_z{}^{ob} e_{z0} e_{z0}^*]. \tag{16}$$

[16] For example, see N. Marcuvitz, *op. cit.*, pp. 379 (2), and 380 (6).

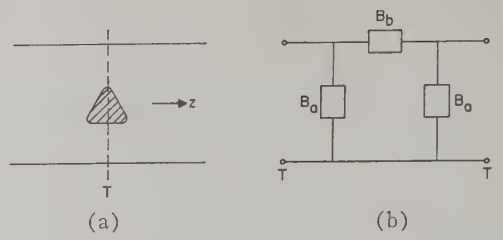

Fig. 4—Symmetrical longitudinal obstacle. (a) Geometry. (b) Typical equivalent circuit.

The various quantities appearing in (15) and (16) have been defined and discussed in Section II-A. In particular, attention is called to the remarks concerning the polarizabilities. The transverse mode functions $\boldsymbol{h}$ and $\boldsymbol{e}$ have been discussed above in their vector form; the components employed in (15) and (16) are related to the vector form in the evident manner

$$\boldsymbol{h} = h_x \mathbf{x}_0 + h_y \mathbf{y}_0, \quad \boldsymbol{e} = e_x \mathbf{x}_0 + e_y \mathbf{y}_0, \tag{17}$$

where $\mathbf{x}_0$ and $\mathbf{y}_0$ are unit vectors.

Since expressions (15) and (16) are valid for any small symmetrical, but otherwise general, obstacle, they should also apply to a transverse planar obstacle of the type shown in Fig. 5(a). The equivalent circuit for this transverse obstacle is purely shunt, as seen in Fig. 5(b). Since the obstacle is now responsive to E_x, E_y, and H_z, only the $M_x{}^{ob}$, $M_y{}^{ob}$, and $P_z{}^{ob}$ polarizability components will be nonvanishing. One then finds from (15) and (16) for a *transverse planar obstacle:*

$$\frac{1}{B_b'} = 0,$$

$$B' = 2B_a' = 4\omega\epsilon Z_0[M_x{}^{ob} e_{x0} e_{x0}^* + M_y{}^{ob} e_{y0} e_{y0}^*] - 4\omega\mu Y_0[P_z{}^{ob} h_{z0} h_{z0}^*]. \tag{18}$$

Result (18) is simply a rephrasing in the notation of this paper of the well-known result for a transverse planar obstacle. The factor of 4 arises because the numerical values for M^{ob} and P^{ob} are equal to those of M and P, respectively, for a transverse aperture identical in size and shape to the obstacle.

III. Applications of Small Aperture Formulas

A. Circular Hole in Trough Waveguide

The small aperture expressions are here employed to evaluate the equivalent circuit parameters of a circular hole located in the center fin of trough waveguide. The geometry is illustrated in Fig. 6(a). For the round hole this type of calculation is usually very good except when the hole is very large or almost in contact with the side wall, or is near to the edge of the fin. Since the trough waveguide is symmetrical, and therefore nonradiating, and since the hole is located on the center fin, the equivalent circuit for the hole is purely reactive. Due to the shape of the hole, the circuit is also symmetrical, and may be chosen in the form of the pi network of Fig. 6(b). It will be seen, as implied by Fig. 6(b), that the series element B_b is always inductive

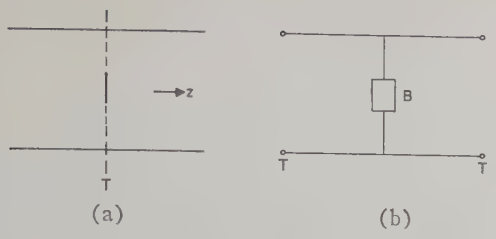

Fig. 5—Planar transverse obstacle. (a) Geometry. (b) Equivalent circuit.

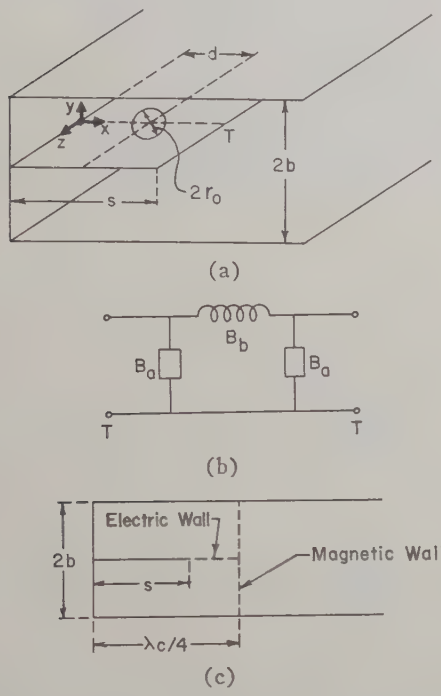

Fig. 6—Circular hole in center fin of trough waveguide. (a) Geometry. (b) Equivalent circuit. (c) Rectangular waveguide approximation to trough waveguide.

while the shunt arms B_a may be inductive or capacitive depending on the location of the hole (value of d).

The relation between the electric fields in the upper and lower portions of the trough waveguide in its usual mode of operation is that indicated in Fig. 2(a). Consequently, (11) and (12) are the appropriate expressions to use for the determination of B_a' and B_b'. Before these expressions can be applied, however, one must have knowledge of the polarizabilities M and P, the quantities Y_0 and Z_0, and expressions for the mode functions.

For the case of a circular hole, the polarizabilities are

$$M_x = M_z = \frac{4}{3} r_0^3$$

$$P_y = \frac{2}{3} r_0^3, \tag{19}$$

where r_0 is the radius of the hole. Since the dominant mode in trough waveguide is an H (or TE) mode, the appropriate relations for Y_0 and Z_0 are, from (3),

$$Z_0 = \frac{1}{Y_0} = \frac{\omega\mu}{\kappa}, \tag{20}$$

where $\kappa(=2\pi/\lambda_g)$ is the propagation wave number.

Because the rigorous mode functions for trough waveguide are somewhat involved, a simple approximation is employed here which is expected to be quite accurate. The lumped effect of the field distribution away from the edge of the fin can be very well approximated by replacing the fin edge with its associated fringing field by an additional width of fin and a magnetic wall (open circuit) at the end of this extension, as shown in Fig. 6(c). The structure then becomes two half-sections of rectangular waveguide, one on top of the other, coupled by the circular hole. The amount by which the center fin is extended can be obtained from the knowledge of the available value for the cutoff wavelength,[17,18] since, as shown in Fig. 6(c), the original fin width plus the extension must be equal to $\lambda_c/4$.

The mode functions h and e can now very readily be obtained from the equivalence of Fig. 6(c) and the normalization relations (1) and (2). Noting that the origin of coordinates is taken at the junction of the fin with the side wall, we find from an integration over one of the two halves of the structure that relations (1) and (2) yield

$$e(x) = h(x) = 2\sqrt{\frac{2}{b\lambda_c}} \sin\left(\frac{2\pi x}{\lambda_c}\right) \tag{21}$$

$$\psi(x) = \frac{\lambda_c}{\pi}\sqrt{\frac{2}{b\lambda_c}} \cos\left(\frac{2\pi x}{\lambda_c}\right), \tag{22}$$

using $\lambda_c = 2\pi/k_c$.

The equivalent circuit parameters for the circular hole can now be found by employing relations (19)–(22) and (5) in expressions (11) and (12). Noting that the center of the hole is located at $x = d$, we obtain after simplification

$$B_b' = -\frac{3b\lambda_g}{k_c(4r_0)^3 \sin^2 k_c d} \tag{23}$$

$$B_a' = \frac{\lambda_g(2k_c r_0)^3 \cos^2 k_c d}{3\pi^2 b}\left[1 - \frac{1}{2}\left(\frac{k}{k_c}\right)^2 \tan^2 k_c d\right] \tag{24}$$

where $k_c = 2\pi/\lambda_c$, $k = 2\pi/\lambda$. We also note that k must exceed k_c for propagation. Results (23) and (24) were originally derived as byproducts in an analysis of periodic structures in trough waveguide.[19]

From (24), one sees that B_a' can be capacitive or inductive, depending upon the frequency and the location of the hole. The inductive contribution is greater if the hole is located nearer to the fin edge. For an appropriate hole location, $B_a' = 0$, and the equivalent circuit be-

[17] A. A. Oliner, "Theoretical developments in symmetrical strip transmission line," Proc. Symp. on Modern Advances in Microwave Techniques, Polytechnic Institute of Brooklyn, Brooklyn, N. Y., pp. 387–390; November, 1954.

[18] K. S. Packard, "The cutoff wavelength of trough waveguide," IRE Trans., vol. MTT-6, pp. 455, 456; October, 1958.

[19] A. A. Oliner and W. Rotman, "Periodic structures in trough waveguide," IRE Trans. on Microwave Theory and Techniques, vol. MTT-7, pp. 134–140, (3) and (4); January, 1959.

comes a *pure series inductance.* This condition is, of course, given by

$$k = \sqrt{2}k_c \cot k_c d, \tag{25}$$

or

$$d = \frac{1}{k_c} \cot^{-1}\left(\frac{k}{\sqrt{2}k_c}\right). \tag{26}$$

We also note that it is possible at a given frequency or for a given hole location to obtain a *reflectionless* discontinuity. From (10), *i.e.*, from $S_{11}=0$, we see that a unity VSWR occurs when

$$k = \sqrt{\frac{2}{3}}\,\frac{k_c}{\sin k_c d} \tag{27}$$

or, alternatively, when

$$d = \frac{1}{k_c} \sin^{-1}\left[\sqrt{\frac{2}{3}}\,\frac{k_c}{k}\right]. \tag{28}$$

At these values of k or d the hole introduces only phase shift.

Numerical values for a typical case are presented in Fig. 7. The following dimensions [see Fig. 6(a)] have been taken: $2b=1.00$ inch, $s=1.00$ inch, $r_0=0.25$ inch, $\lambda=3.50$ inches; the wavelength chosen corresponds roughly to midband operation. Fig. 7 presents B_a' and B_b' as a function of the location of the hole on the fin. For these dimensions, one finds $d=0.617$ inch and $d=0.485$ inch to be the hole locations such that the equivalent circuit is pure series and the hole is nonreflecting, respectively. Fig. 7 also includes a curve of VSWR vs hole location.

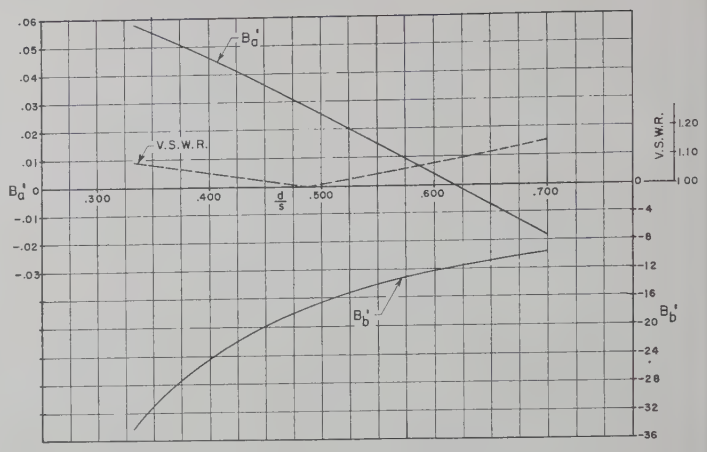

Fig. 7—Network parameter values for circular hole in trough waveguide.

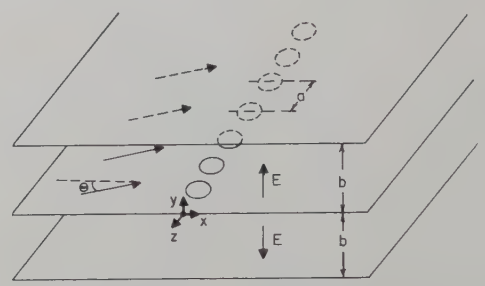

Fig. 8—Wave incident at angle θ on array of holes coupling parallel plate waveguides.

B. Array of Holes Coupling Parallel Plate Waveguides

In this section, small aperture expressions are employed to obtain the equivalent circuit parameters for an array of holes which couples two identical parallel plate waveguides. The geometry of the configuration is shown in Fig. 8. As shown, the waves in the parallel plate guides have oppositely directed electric fields and are incident on the array of holes at an angle θ with respect to the x direction. Because of the symmetry of the structure and the excitation, the equivalent circuit can be expressed in pi form and the parameters can be determined by the use of (11) and (12). The equivalent circuit, in fact, will be seen to be of the form of Fig. 6(b), with the series element always inductive and the shunt elements capacitive or inductive, depending on the angle θ of incidence.

The real value in the solution of this problem lies not in the direct phrasing of it, as given above, but in its application to the transverse resonance analysis of a number of waveguiding structures possessing a longitudinal array of holes. For example, if metal plates are placed at the sides of the structure in Fig. 8, one has a *top wall directional coupler in rectangular waveguide.* The use in a transverse resonance procedure of the equivalent circuit for the array of holes permits the determination of the properties of the coupler. A second example is an *array of longitudinal holes in trough waveguide.* Again, the results of this section are employed in a transverse resonance procedure.[20]

The TEM waves incident at angle θ are viewed in this analysis as being equivalent to H (or TE) waves incident normally (in the x direction) on the array of holes. The use of this technique simplifies the determination of the mode functions. The propagation wave number κ is related to angle θ as

$$\kappa = k \cos \theta, \tag{29}$$

and all field components experience an exponential variation of the form $\exp(-jk_z z)$, where

$$k_z = k \sin \theta. \tag{30}$$

Due to the periodicity of the array of holes, the modes in the vicinity of the array possess fields which are also periodic.[21] When the holes are sufficiently closely spaced together, the higher modes are nonpropagating. The mode functions for the dominant mode, normalized to a unit cell of the array, are then obtained by integrating over a unit cell in either the upper or lower portion of the configuration in the manner of (1) and (2). One finds, as a result,

[20] *Ibid.*, see Section II-B., pp. 137–138.
[21] Marcuvitz, *op. cit.*, pp. 88, 89.

$$h_z(z) = e_y(z) = \frac{1}{\sqrt{ab}} e^{-ik_z z}, \tag{31}$$

$$\psi(z) = \frac{1}{k_z\sqrt{ab}} e^{-ik_z z}, \tag{32}$$

where $k_c = k_z$. On use of (5) and (20), since the dominant mode is an H (or TE) mode, (31) and (32) become

$$h_z h_z^* = e_y e_y^* = 1/ab \tag{33}$$

$$h_x h_x^* = \left(\frac{k_z}{\kappa}\right)^2 1/ab. \tag{34}$$

When (33), (34), and (20) are used in relations (11) and (12), with x and z interchanged, expressions for the pi network parameters become

$$B_b' = -\frac{ab}{2\kappa M_z} \tag{35}$$

$$B_a' = \frac{1}{ab\kappa}\left[M_z k_z^2 - P_y k^2\right], \tag{36}$$

where M_x, M_z, and P_y are the magnetic and electric polarizabilities for an individual hole. In some cases, close proximity of the holes to each other may produce mutual coupling effects which will alter the polarizability values.

When the problem is phrased in terms of waves incident at angle θ, (35) and (36) become, on use of (29) and (30),

$$B_b' = -\frac{ab}{2kM_z\cos\theta} \tag{37}$$

$$B_a' = \frac{k}{ab\cos\theta}\left[M_x \sin^2\theta - P_y\right]. \tag{38}$$

One sees from (38) that B_a' can be either capacitive or inductive depending on θ.

When the equivalent circuit is to be used in a transverse resonance context, propagation actually occurs in the z direction so that in (35) and (36) k_z become the propagation wave number ($=2\pi/\lambda_g$) and κ becomes the transverse wave number k_t. Moreover, to be useful in a transverse resonance context, (35) and (36) must involve k_t but not k_z. Since k_t and k_z are related via

$$k^2 = k_t^2 + k_z^2,$$

(35) and (36) become

$$B_b' = -\frac{ab}{2k_t M_z} \tag{39}$$

$$B_a' = \frac{1}{abk_t}\left[(M_z - P_y)k^2 - M_z k_t^2\right]. \tag{40}$$

It is significant that B_a' involves the free space wave number k in addition to k_t. As a result, the transverse wave number will be frequency dependent, a property characteristic of periodic structures.

IV. Applications of Small Obstacle Formulas

A. Circular Disk in Rectangular Waveguide

As a simple illustration of the use of small obstacle expressions, the equivalent circuit of a centered circular metallic disk in rectangular waveguide can be examined for different orientations of the disk. For example, consider the disk located longitudinally and then transversely, as shown in Figs. 9(a) and (b).

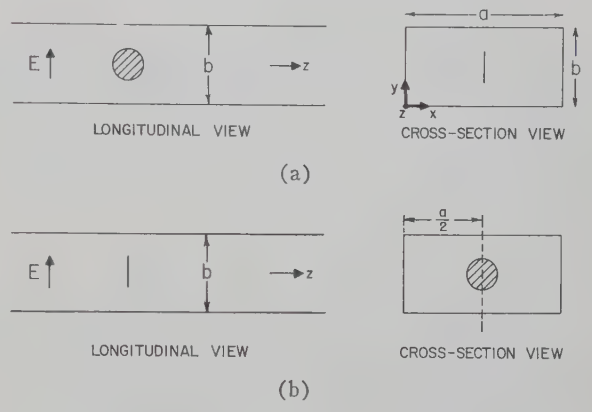

Fig. 9—Circular disc in rectangular waveguide. (a) Longitudinally oriented disc. (b) Transversely oriented disk.

The polarizabilities of the circular disk are

$$M_y{}^{ob} = M_z{}^{ob} = \frac{4}{3} r_0{}^3 \tag{41}$$

$$P_x{}^{ob} = \frac{2}{3} r_0{}^3 \tag{42}$$

for the longitudinal orientation; for the transverse orientation of Fig. 9(b), $M_z{}^{ob}$ and $P_x{}^{ob}$ should be replaced by $M_x{}^{ob}$ and $P_z{}^{ob}$, respectively. The dominant mode in rectangular waveguide is an H (or TE) mode, so that its characteristic impedance has the form (20); the corresponding transverse mode functions are[22]

$$h_x(x) = e_y(x) = \sqrt{\frac{2}{ab}} \sin\frac{\pi x}{a}. \tag{43}$$

The longitudinal magnetic field has a cos ($\pi x/a$) dependence, and is therefore zero at the center of the disk and can be neglected.

The parameters B_a' and B_b' of the pi network equivalent [see Fig. 4(b)] of the longitudinally oriented circular disk are found by employing (41), (42), (43), and (20) in relations (15) and (16). One finds then that

$$B_a' = \frac{4\pi}{3}\frac{(2r_0)^3}{ab}\frac{\lambda_g}{\lambda^2} \tag{44}$$

$$\frac{1}{B_b'} = \frac{4\pi}{3}\frac{(2r_0)^3}{ab\lambda_g}. \tag{45}$$

[22] *Ibid.*, Section 2.2.

When these same expressions are inserted into (18) one obtains the following result for the shunt element B' [see Fig. 4(a)] of the transversely oriented circular disk:

$$B' = \frac{8\pi}{3} \frac{(2r_0)^3}{ab} \frac{\lambda_g}{\lambda^2}. \tag{46}$$

When the two equivalent circuits are compared, it is seen that the total shunt effect of each is identical, due to the electric field component parallel to the disk, while for the longitudinal orientation an additional series capacitive element is present, resulting from the component of magnetic field normal to the disk. Since the shunt and series elements have the same sign, one sees from relation (10) that the VSWR introduced by the longitudinal orientation is greater than that produced by the transverse orientation.

B. Array of Longitudinal Rods in Free Space

The infinite two-dimensional array of longitudinal rods to be analyzed is described in Fig. 10. A plane wave of so-called parallel polarization is shown in Fig. 10(a) to be incident on the array of rods at angle θ with respect to the z direction. With such a polarization a component of electric field is set up parallel to the conducting rods, so that the rods exert a significant effect on the wave. For perpendicular polarization, on the other hand, a component of magnetic field would be created parallel to the rods and the wave would be negligibly affected if the rods were thin. Such a longitudinal array of rods thus serves to discriminate between the two polarizations.

For the polarization shown in Fig. 10(a), the total field consists of H_y, E_x, and E_z components. The plane wave incident at angle θ thus may be viewed as an E (or TM) mode incident along the z direction, with characteristic impedance Z_0 given by (3) as

$$Z_0 = \frac{1}{Y_0} = \frac{\kappa}{\omega\epsilon}, \tag{47}$$

with

$$\kappa = k \cos\theta. \tag{48}$$

When the spacing between successive rods is less than half a free-space wavelength, all the higher modes are nonpropagating. The mode functions of the dominant mode, which is the incident wave, normalized to the unit cell of dimensions a by b, are found by integrating over the unit cell according to (1) and (2). On use of (4), the mode functions may be written as

$$e_x(x) = h_y(x) = \frac{1}{\sqrt{ab}} e^{-jkx \sin\theta} \tag{49}$$

$$e_z(x) = -j \frac{\tan\theta}{\sqrt{ab}} e^{-jkx \sin\theta} \tag{50}$$

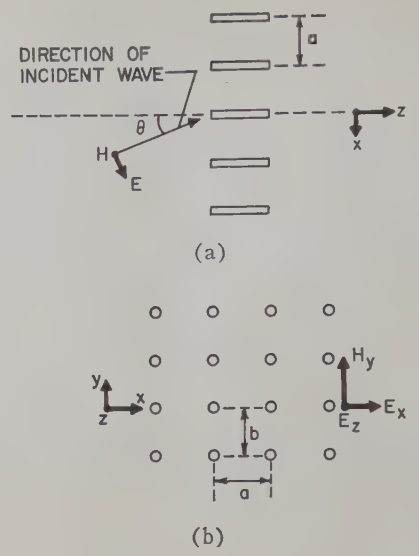

Fig. 10—Plane-wave incident on infinite two-dimensional array of longitudinal rods in free space. (a) Side view. (b) Cross-section view.

since

$$k_c = k_x = k \sin\theta. \tag{51}$$

For simplicity, we assume that the rods are thin so that the only non-negligible polarizability is $M_z{}^{ob}$, *i.e.*, the rods are sensitive only to the longitudinal component of electric field. Under these conditions, the equivalent circuit parameters can be evaluated via expressions (15) and (16), using (47), (49), and (50). One finds that[23]

$$B_a' = 0$$

$$-\frac{1}{B_b'} = X' = \frac{8\pi M_z{}^{ob}}{ab\lambda} \frac{\sin^2\theta}{\cos\theta}. \tag{52}$$

Result (52) states that the equivalent circuit consists only of a series inductance, the value of which is proportional to the polarizability. It is of interest that the element is inductive rather than capacitive, since an array of similar rods transversely oriented would be characterized by a shunt capacitive equivalent circuit. An analogous situation arises in connection with slots whose length is smaller than that required for resonance. Such a transverse slot in rectangular waveguide is inductive, while the equivalent circuit for this slot cut in the top wall of rectangular waveguide (a "longitudinal shunt slot") is a shunt capacitance.

Acknowledgment

The writer wishes to thank the Technical Research Group, Inc., for permission to report the material on the array of longitudinal rods.

[23] This result was obtained by the writer for the Technical Research Group in 1955 as part of consulting services on anisotropic radomes.

On the TE_{n0} Modes of a Ferrite Slab Loaded Rectangular Waveguide and the Associated Thermodynamic Paradox*

A. D. BRESLER†

Summary—It has been known for some time that the secular equation for the TE_{n0} modes of a perfectly conducting rectangular waveguide loaded with a transversely magnetized dissipationless full height ferrite slab located against one of the narrow walls of the waveguide admits the possibility of the existence of only a single propagating mode (transporting energy in one direction only). In this paper, it is established that if we admit the existence of a passive dissipationless uniform waveguide supporting only a single propagating mode we are led inescapably to a thermodynamic paradox. A uniqueness theorem is cited to establish that, for the waveguide described above, the paradox is associated with the TE_{n0} mode set alone. This conclusion motivates a thorough study of the secular equation for the TE_{n0} modes of this waveguide. This study is initiated by an investigation into the properties of the TE_{n0} surface waves guided along a plane interface separating a transversely magnetized dissipationless ferrite from free space. It is shown that two oppositely directed surface waves are guided along this interface. These two surface waves are admitted in different finite ranges of the parameter values which never coincide and which may or may not overlap. Each of the two surface waves has both a high- and a low-frequency cutoff and, in general, both a high and a low dc magnetic field cutoff. The propagation constant of one of the surface waves becomes infinite at the low field (high-frequency) cutoff. The next step in the analysis consists of an examination of the behavior of these surface waves on finite thickness ferrite slabs located in different environments. It is shown that when one of the two interfaces bounding the slab approaches a short circuit the infinite propagation constant noted above behaves in a peculiar discontinuous fashion. Next, the TE_{n0} mode secular equation of the slab loaded rectangular waveguide is analyzed and information is developed leading to a description of the behavior of the propagation constants of all the propagating TE_{n0} modes. This analysis reveals that the possibility of the existence of only a single propagating mode is associated only with the surface wave mode of this waveguide. A resolution for the thermodynamic paradox is proposed based on the discontinuous behavior of one of the infinite propagation constants associated with this surface wave mode. It is shown that with a properly chosen secular equation for the waveguide under consideration there are always an even number of TE_{n0} propagating modes, half of which transport energy in one direction, half in the other. This demonstration is based, in part, on an analysis leading to relations between the direction of the power flow associated with a propagating mode and the derivative of its propagation constant with respect to the dc magnetic field.

* Manuscript received by the PGMTT, April 6, 1959; revised manuscript received, September 2, 1959. Parts of this paper were presented at the IRE-URSI meeting, Washington, D. C., April, 1958. It is based, in part, on the author's dissertation submitted to the Polytechnic Institute of Brooklyn, Brooklyn, N. Y., in partial fulfillment of the requirements for the degree of Doctor of Engineering. The work on which this paper is based was done while the author was a member of the staff of the Microwave Res. Inst. of the Polytechnic Institute of Brooklyn, and was supported by the Air Force Cambridge Res. Center under contract AF-19(604)-2301.

† Jasik Laboratories, Inc., 100 Shames Dr., Westbury, N. Y.

Introduction—The Thermodynamic Paradox

THIS PAPER is concerned with a study of the TE_{n0} modes[1] of a perfectly conducting rectangular waveguide loaded with a full height ferrite slab located against one of the narrow walls of the waveguide. The ferrite slab is uniformly magnetized in the transverse direction indicated in Fig. 1. As part of this study, we will examine the properties of the TE_{n0} surface wave modes guided along the plane interfaces separating transversely magnetized ferrite slabs from free space. While these studies are of interest in their own right, they also have a further significance which will now be made evident by a statement of their motivation.

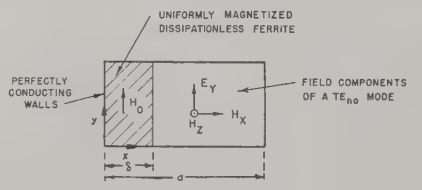

Fig. 1—Ferrite slab loaded rectangular waveguide (slab against waveguide wall).

Some time ago, Lax and Button[2] pointed out a curious phenomenon associated with the spectrum of the waveguide whose cross section is shown in Fig. 1. They found that the secular equation determining the propagation constants of the TE_{n0} modes of this waveguide admitted the possibility of the existence of only a single propagating mode (transporting energy in one direction only). The obvious implication is that this waveguide can be used to construct an ideal one way transmission system. If this were really possible, it would constitute a clear violation of the basic laws of thermodynamics. In

[1] These modes are characterized by the absence of any variation along the direction of the dc magnetic field, H_0, and by the fact that the electric field is parallel to H_0. The locations of the conducting planes normal to the y direction are therefore of no significance. For a description of the field components see, *e.g.*, H. Seidel, "Ferrite slabs in transverse electric mode waveguide," *J. Appl. Phys.*, vol. 28, pp. 218–226; February, 1957.

[2] B. Lax and K. J. Button, "Theory of new ferrite modes in rectangular waveguide," *J. Appl. Phys.*, vol. 26, pp. 1184–1185; September, 1955. Also, "Theory of ferrites in rectangular waveguide," IRE Trans. on Antennas and Propagation, vol. AP-4, pp. 531–537; July, 1956.

an attempt to resolve this difficulty, it has been argued[3,4] that the power flow in the reverse direction takes place via the cutoff (nonpropagating) modes and that therefore no thermodynamic difficulty actually exists. We will now show that the cutoff modes do not provide a satisfactory mechanism for the resolution of the paradox. This demonstration will not be restricted to the special case of the waveguide described previously.

To establish that the existence of a passive dissipationless uniform waveguide supporting only a single propagating mode does indeed constitute a violation of the basic thermodynamic laws, we note the following. First, we recall that in a dissipationless waveguide only the propagating modes (considered individually) carry power.[5] The cutoff modes take part in the mechanism of energy transport only through the coupling between two modes associated with complex conjugate propagation constants.[5] Now, consider the junction of the two dissimilar uniform waveguides illustrated in Fig. 2. In an earlier paper,[6] the author has shown that when this structure is excited from the empty waveguide side the fields to the right of the junction plane will consist of a superposition of only those modes which, if propagating, transport energy to the right (*i.e.*, along $+z$) or, if cut off, decay exponentially with increasing z. Thus, only one of the two modes associated with a pair of complex conjugate propagation constants is excited at the junction plane and therefore the cutoff modes play no role in the transport of energy away from the junction. Finally, suppose that the waveguide to the right of the junction plane supports only a single propagating mode which (without loss of generality) is assumed to transport energy to the right. The incident wave shown in Fig. 2 would then excite this single propagating mode along with an infinity of cutoff modes which all decay with increasing z. Therefore, for $z \gg z'$ and increasing, the fields in the waveguide approach ever more closely to the propagating mode fields.

Now let a short circuit termination be introduced into the waveguide at some $z \gg z'$. Since there are no propagating modes which carry power to the left, only cutoff modes will be excited at the short circuit. The amplitude coefficients of these cutoff modes will be determined from the requirement that the net tangential electric field at the short circuit must equal zero. Admittedly, some power transfer now takes place via the coupling between pairs of cutoff modes which decay with equal attenuations in opposite directions along z.[5] To demonstrate that this power transfer mechanism cannot provide a proper power balance, we first assume the converse; *i.e.*, we assume that the net power flow through the transverse plane just to the left of the short circuit is equal to zero. This net power flow may be written as $P_0+\Sigma P_i$ where P_0 is the power flow associated with the single propagating mode and ΣP_i is the net power flow resulting from cutoff mode coupling. Each term in ΣP_i is proportional to the product of the amplitude coefficients of a pair of cutoff modes characterized by complex conjugate propagation constants one of which is excited at the junction plane, the other at the short circuit.[5,6] Now suppose that the short circuit is moved a distance $n\lambda_{g0}$ (n is an integer, λ_{g0} is the guide wavelength associated with the propagating mode) further away from z'. The fields incident on the short circuit in the two locations are almost identical. Thus, for either location, the set of modes excited at the short circuit constitutes a modal representation (in terms of a complete eigenfunction set) of a transverse electromagnetic field whose electric field component must be almost exactly the negative of the propagating mode transverse electric field incident on the short circuit. Since the two short circuit positions are separated by $n\lambda_{g0}$, this latter field has equal amplitudes at the two short circuit positions. Therefore, the amplitude coefficients of the cutoff modes excited at the short circuit are practically identical for the two locations. In traversing the distance between the two short-circuit positions, the cutoff modes excited at z' are attenuated by the factor $\exp(-\alpha_i n\lambda_{g0})$ where $\alpha_i > 0$ is the attenuation constant of the ith mode. Thus, if we now compute the net power flow through the transverse plane just to the left of the new short-circuit position, we find that P_0 is unchanged while each term in ΣP_i is reduced by the factor $\exp(-\alpha_i n\lambda_{g0})$. Therefore $P_0+\Sigma P_i$ is now unequal to zero. We must therefore conclude that power transfer via cutoff mode coupling cannot provide the proper power balance. Thus, when we introduce the short circuit termination we are faced with a situation wherein we are continuously pumping energy into a reactive termination and no means exists for returning all of this energy to the source. This clearly constitutes a violation of the basic laws of thermodynamics. We are therefore led to assert that a passive dissipationless uniform waveguide cannot support but a single propagating mode.

We are now faced with the problem of reconciling this assertion with the known results cited earlier for the waveguide in Fig. 1. In this connection, it is important to recognize that when the discontinuity problem posed

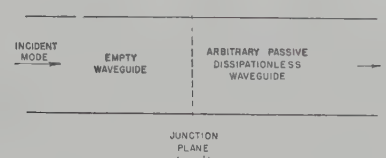

Fig. 2—Junction of two dissimilar uniform waveguides.

[3] B. Lax, Chairman, "Combined panel session on propagation in doubly-refracting media and future directions for research in electromagnetic wave theory in modern physics," IRE TRANS. ON ANTENNAS AND PROPAGATION, vol. 4, pp. 567–577 (esp. 573–576); July, 1956.

[4] M. L. Kales, "Topics in guided wave propagation in magnetized ferrites," PROC. IRE, vol. 44, pp. 1403–1409; October, 1956. The discussion referred to appears on p. 1408.

[5] A. D. Bresler, G. H. Joshi, and N. Marcuvitz, "Orthogonality properties for modes in passive and active uniform waveguides," *J. Appl. Phys.*, vol. 29, pp. 794–799; May, 1958.

[6] A. D. Bresler, "The far fields excited by a point source in a passive dissipationless anisotropic waveguide," IRE TRANS. ON MICROWAVE THEORY AND TECHNIQUES, vol. 7, pp. 282–287; April, 1959.

in Fig. 2 is that for an infinite rectangular waveguide which is empty for $z<z'$ and which, for $z>z^1$, is loaded with a ferrite slab as in Fig. 1, then the paradox arises even though it is the TE_{n0} mode set of the slab loaded waveguide which has only a single propagating mode. This conclusion is based on a uniqueness theorem established by the author[7] which states that if the fields which excite the two waveguides are independent of y (see Fig. 1) and are completely characterized by a single non-zero component of electric field directed along y, then the boundary value problem which has been posed is actually a two dimensional problem and the total field in the structure can be completely described in terms of this single component of electric field. Thus, when the incident mode indicated in Fig. 2 is, *e.g.*, the TE_{10} mode of the empty rectangular waveguide, only TE_{n0} modes will be excited at the junction plane and we therefore may not look outside the TE_{n0} mode set to resolve our difficulty.

In casting about for a basis for resolving this paradox, we reject the approach advanced by Seidel[8,9] which involves the assumption of an "intrinsic loss" for a lossless ferrite medium and into which he introduces arguments based on a consideration of the atomic model from which the ferrite properties are deduced. Our attitude is that such arguments seek to answer an electromagnetic question by considerations outside the framework in which the problem is posed. To be more specific, our attitude is that we are concerned solely with the solutions to the Maxwell equations in a region containing an anisotropic medium for which we are given the permeability dyadic. We do not need to know the atomic model from which this dyadic has been deduced. We do know that this dyadic satisfies the restrictions imposed by the linearity, passivity, losslessness and time reversibility requirements.[6,10] Under these circumstances, if the solutions to the Maxwell equations give rise to thermodynamic difficulties, the source of the difficulties must be sought in the electromagnetic problem, not in the atomic model.

As a consequence of the considerations outlined above a thorough analysis of the TE_{n0} modes of the waveguide illustrated in Fig. 1 was undertaken. As a result of this analysis, we will establish that with a properly chosen secular equation for the waveguide in Fig. 1 there are always an even number of TE_{n0} propagating modes, half of which transport energy in one direction, half in the other. This will dispose of the thermodynamic paradox associated with this structure. To accomplish this task, we will first show that the possibility of the existence of only a single propagating mode is associated only with the surface wave mode, *i.e.*, the "ferrite-dielectric" mode identified by Lax and Button.[2] In the discussion which follows, we will first examine the properties of this surface-wave mode. This mode represents a true surface phenomenon in that the amplitudes of its fields decay exponentially away from the ferrite-empty space interface on both sides of the interface. Therefore, the essential properties of this surface wave mode will be determined from a study of its behavior in the ferrite loaded parallel plate waveguide, whose cross section is shown in Fig. 3.

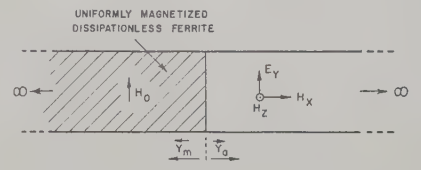

Fig. 3—Ferrite loaded parallel plate waveguide.

Definitions and Preliminary Considerations

All field components are assumed to have the (suppressed) time dependence exp $(-i\omega t)$ where ω is the radian frequency. Since we will be concerned exclusively with TE_{n0} modes, all field components are independent of y. Since these modes propagate along z, the z dependence for all field components in either the empty or ferrite loaded regions is taken as exp $(i\kappa z)$. The dependence on x differs in the two regions. This dependence is taken as exp $(\pm ik_{xa}x)$ in the empty regions and exp $(\pm ik_{xm}x)$ in the ferrite loaded regions. We adopt the convention that both k_{xa} and k_{xm} satisfy the restrictions $k_x>0$ if real and Im $k_x>0$ if imaginary. The wave numbers κ and k_x are related via[1]

$$\kappa^2 = k^2 - k_{xa}^2 = k^2\epsilon\nu_1 - k_{xm}^2 \tag{1}$$

where $k^2=\omega^2\mu_0\epsilon_0$, μ_0 and ϵ_0 are, respectively, the permeability and permittivity of free space, ϵ is the (relative) scalar dielectric constant of the ferrite and ν_1, the (relative) effective permeability parameter for transverse magnetization, will be defined more precisely below.

For the time dependence indicated above, the (relative) permeability tensor for a gyromagnetic ferrite subjected to a uniform internal magnetic field applied along y takes the form[11]

$$\mu_{zxy} = \begin{pmatrix} \mu_1 & i\mu_2 & 0 \\ -i\mu_2 & \mu_1 & 0 \\ 0 & 0 & 1 \end{pmatrix} \tag{2}$$

where the subscripts on μ indicate the cyclic order employed in the tensor representation. For a dissipationless ferrite, the dependence of $\mu_{1,2}$ on frequency, dc magnetic field (H_0), and saturation magnetization of the ferrite $(4\pi M_s)$ is given by[11]

[7] A. D. Bresler, "On the Discontinuity Problem at the Input to an Anisotropic Waveguide," D.E.E. dissertation, Polytechnic Institute of Brooklyn, Brooklyn, N. Y.; June, 1959. The dissertation has also appeared as Res. Rept. No. R-716-59 of the Microwave Res. Inst. of the Polytechnic Inst. of Brooklyn.

[8] Seidel, *op. cit.*

[9] "Round-table discussion on design limitations of microwave ferrite devices," IRE Trans. on Microwave Theory and Techniques, vol. 6, pp. 104–111; January, 1958.

[10] B. S. Gourary, "Dispersion relations for tensor media and their application to ferrites," *J. Appl. Phys.*, vol. 28, pp. 283–288; March, 1957.

[11] H. Suhl and L. R. Walker, "Topics in guided wave propagation through gyromagnetic media," *Bell Sys. Tech. J.*, vol. 33, pp. 579–660; May, 1954.

$$\mu_1 = \frac{1 - \sigma(\rho + \sigma)}{1 - \sigma^2} \qquad \mu_2 = \frac{\rho}{1 - \sigma^2} \tag{3}$$

where

$$\rho = \frac{\gamma(4\pi M_s)}{\omega} \qquad \sigma = \frac{\gamma H_0}{\omega} \tag{4}$$

and γ is the magnitude of the gyromagnetic ratio.[12] Note that ρ and σ are defined so that at a fixed frequency ρ is a constant of the material while σ is proportional to the dc magnetic field. Eqs. (3) are valid only for saturated ferrites, *i.e.*, only when H_0 exceeds that value required to produce saturation. Since the dc permeability of most ferrites is very large, the value of σ required for saturation is very small.[11] Thus, whenever results are stated for $\sigma = 0$ these are understood to be valid when σ approaches zero but remains larger than the value required for saturation. Since H_0 and $4\pi M_s$ must have the same algebraic sign, it follows that the product $\rho\sigma$ is always positive. Therefore, a reversal of the dc magnetic field changes the sign of μ_2 but does not affect μ_1.

For modes which propagate in a direction perpendicular to the dc magnetic field, it is convenient to express all results in terms of the elements of the inverse $\underline{\mu}$ tensor

$$\underline{\mu}^{-1} = \begin{pmatrix} \frac{1}{\nu_1} & -i\frac{1}{\nu_2} & 0 \\ i\frac{1}{\nu_2} & \frac{1}{\nu_1} & 0 \\ 0 & 0 & 1 \end{pmatrix} \tag{5}$$

where

$$\nu_1 = \frac{\mu_1^2 - \mu_2^2}{\mu_1} = \frac{1 - (\rho + \sigma)^2}{1 - \sigma(\rho + \sigma)}$$
$$\nu_2 = \frac{\mu_1^2 - \mu_2^2}{\mu_2} = \frac{1 - (\rho + \sigma)^2}{\rho}. \tag{6}$$

It is evident that a reversal of the dc magnetic field changes the sign of ν_2 but does not affect ν_1. The parameters $\mu_{1,2}$ and $\nu_{1,2}$ are sketched in Fig. 4 as functions of σ for fixed ρ. These sketches therefore illustrate the behavior of the permeability as a function of the dc magnetic field for a fixed ferrite at a fixed frequency.

Certain features of the curves in Fig. 4 deserve comment. First, since (3) and (6) are valid only for saturated ferrites, we should not be disturbed by the fact that the curves based on these equations do not indicate an isotropic medium at $\sigma = 0$. On the other hand, Fig. 4 makes evident that the ferrite becomes an isotropic dielectric as σ approaches infinity. Next, we remark that at $\sigma = 1$, *i.e.*, at the ordinary "gyromagnetic resonance," the parameters $\nu_{1,2}$ do not display any resonance or, indeed, any sort of unusual behavior. We will find that the point $\sigma = 1$ has no significance for the surface wave phenomena. Finally, two special values of σ, σ_2, and σ_5 are indicated in Fig. 4. At the latter, ν_1 becomes infinite. At the former, ν_1 and ν_2 both become zero, their ratio remaining finite.

[12] $\gamma = 5.6\pi$ for H_0 expressed in kilo-oersted, $4\pi M_s$ in kilogauss and frequency in kmc.

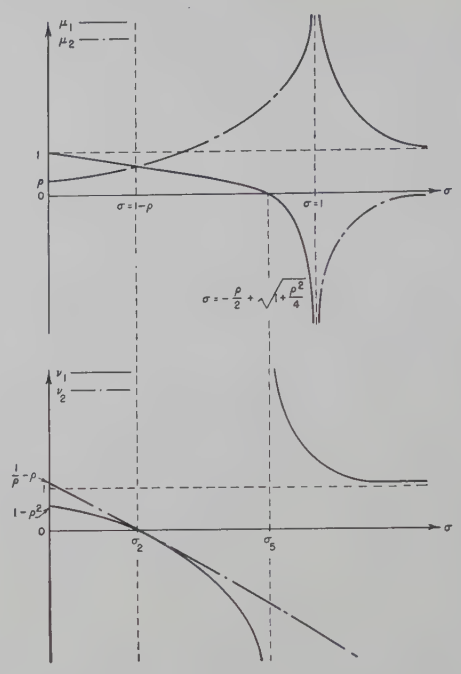

Fig. 4—Ferrite permeability parameters.

Surface Waves at a Single Interface

To obtain the secular equation determining the surface-wave propagation constants, we employ a transverse resonance procedure. For the structure in Fig. 3, this requires a knowledge of the admittances $\overrightarrow{Y_a}$ and $\overleftarrow{Y_m}$. The former is simply the input admittance of an infinite transmission line for a TE_{n0} mode of an empty parallel plate waveguide. If we choose to normalize the fields so that the admittance for the TEM mode of this waveguide is unity, then $\overrightarrow{Y_a}$ becomes

$$\overrightarrow{Y_a} = \frac{k_{xa}}{k}. \tag{7}$$

We recall that the input admittance to an infinite modal transmission line corresponds to the ratio of the amplitudes of the transverse (to x) magnetic and electric fields of that mode which propagates outward to infinity, *i.e.*, in this case, of the mode whose dependence on x is given by $\exp(ik_{xa}x)$. We obtain the admittance $\overleftarrow{Y_m}$ via a similar requirement for the ferrite loaded waveguide. Thus, we define $\overleftarrow{Y_m}$ as the ratio of the amplitudes of the transverse (to x) magnetic and electric fields for a mode whose x dependence is $\exp(-ik_{xm}x)$. The admittance $\overleftarrow{Y_m}$ is then obtained as[1]

$$\overleftarrow{Y} = \frac{k_{xm}}{k\nu_1} - i\frac{\kappa}{k\nu_2}. \tag{8}$$

The secular equation is now obtained from the transverse resonance requirement

$$\overrightarrow{Y}_a + \overleftarrow{Y}_m = 0 = q_a + \frac{q_m}{\nu_1} - i\frac{\theta}{\nu_2} \tag{9}$$

where we have introduced the normalized wave numbers

$$q_a = \frac{k_{xa}}{k} \qquad q_m = \frac{k_{xm}}{k} \qquad \theta = \frac{\kappa}{k}. \tag{10}$$

As it stands, the secular equation (9) is ambiguous because of the quadratic nature of the relationships in (1). This ambiguity is resolved by recognizing that the fields of a surface-wave mode must decay exponentially away from the interface on both sides of the interface. Therefore, we require that Im $q_a > 0$ and Im $q_m > 0$. Substitution from (1) into (9) now yields the following as the secular equation in terms of θ only:

$$\sqrt{1-\theta^2} + \frac{1}{\nu_1}\sqrt{\epsilon\nu_1 - \theta^2} - i\frac{\theta}{\nu_2} = 0$$

subject to

$$\begin{cases} \theta^2 > 1 & \operatorname{Im}\sqrt{1-\theta^2} > 0 \\ \theta^2 > \epsilon\nu_1 & \operatorname{Im}\sqrt{\epsilon\nu_1 - \theta^2} > 0. \end{cases} \tag{11}$$

Since this is an algebraic equation, its solutions are readily obtained in closed form and are subject to exhaustive analysis. In the following, we give the results of such an analysis omitting most of the details of the required algebraic manipulations which, while complicated in detail, are quite straightforward.[7,13]

Solutions to (11) are obtained by squaring twice to obtain a quadratic equation in θ^2. When ν_1 and ν_2 are eliminated via (6) the solution to this quadratic is obtained as

$$\theta_\pm^2 = \frac{1}{2\rho(u^2-1)}\left\{(u^2-1)[\rho-(\epsilon-1)u] + \frac{\rho^2}{4}(\epsilon+1)u \pm \sqrt{\left[(u^2-1)-\frac{\rho^2}{4}\right]\left[(\epsilon-1)^2(u^2-1)-\frac{\rho^2}{4}(\epsilon+1)^2\right]}\right\} \tag{12}$$

where $u = \frac{1}{2}\rho + \sigma$. The plus or minus subscript associated with θ^2 distinguishes the solution with the corresponding algebraic sign preceding the radical (understood to be positive). Note that the solutions to the biquadratic given here do not necessarily provide solutions to (11). Such solutions result only when the restrictions indicated in (11) are satisfied. Moreover, when a particular θ^2 given by (12) does provide a solution to (11), it will satisfy the latter equation with only one or the other of $\theta = \pm\sqrt{\theta^2}$. Thus, the restrictions on the sign of the imaginary part of q_a and q_m serve to determine the algebraic sign of θ appropriate to the particular solution.

A sketch of $\theta_\pm^2$ as a function of σ with ρ held fixed is given in Fig. 5. We will now establish that only those values of $\theta_\pm^2$ lying on the solid line segments of the curves in Fig. 5 represent surface-wave solutions. In this discussion, we will make use of the information contained in the equations in Table I, where certain values of σ are distinguished and defined in terms of the fixed parameters ρ and ϵ. It is readily verified that, for $\rho > 0$ and $\epsilon > 1$, $\alpha > \beta$ implies $\sigma_\alpha > \sigma_\beta$ except that σ_3 may be $\gtrless \sigma_4$. Since the product of ρ and σ is always positive, it is sufficient to consider only $\rho > 0$ and $\sigma > 0$. Note that if ρ and σ are both replaced by their negatives, *i.e.*, if the dc magnetic field is reversed, the only effect on the solutions indicated in (12) is to interchange θ_+^2 and θ_-^2. The restriction to $\rho > 0$, $\sigma > 0$ means that if any σ_α in Table I is found to be negative for $\rho > 0$, then that value of σ is no longer significant, *i.e.*, can no longer be obtained with the given ferrite at the given frequency.

From the information given in (12), Table I, and Fig. 5, it follows that surface-wave mode solutions may occur only in the interval $0 < \sigma < \sigma_5$. To justify this statement, we note that $\theta_\pm^2$ are both equal to or less than zero for all $\sigma > \sigma_6$ so that the restriction in (11) is not satisfied. In the interval $\sigma_5 < \sigma < \sigma_6$, $\theta_\pm^2$ are both complex. Surface-wave modes with complex propagation constants are not admissible. This is evident from the following considerations. If a complex θ is a solution of (11) then its complex conjugate, θ^*, must also be a solution. Suppose that the q_a and q_m associated with θ are such that Im $q_a > 0$ and Im $q_m > 0$ so that θ represents an admissible surface wave-mode. It follows that q_a^* and q_m^*, associated with θ^*, are characterized by Im $q_a^* < 0$ and Im $q_m^* < 0$. Therefore, θ^* cannot be the propagation constant of an admissible surface-wave mode. It can be shown[5] that, in a dissipationless waveguide, complex modal propagation constants must occur in complex conjugate pairs. Therefore, since we cannot admit θ as a proper surface-wave solution and exclude θ^*, we exclude all complex θ from further consideration.

The outstanding feature to be observed in the range $\sigma < \sigma_5$ is the infinite θ_+^2 solution which obtains for $\sigma \to \sigma_3$. This infinity is not associated with any peculiarity in the ferrite parameters since both $\nu_{1,2}(\sigma_3)$ are finite and non-zero. Thus, this infinity might be described as a "waveguide resonance" as opposed to a "medium resonance."[14] Since a surface-wave solution must satisfy the restriction $\theta^2 > 1$, it follows that the infinite propagation

[13] A. D. Bresler, "TE_{n0} Surface Waves at Ferrite-Air Interfaces," Polytechnic Institute of Brooklyn, Brooklyn, N. Y., Microwave Research Institute, Memorandum R-723-59; February 28, 1959.

[14] The existence of this infinite solution in a ferrite slab loaded rectangular waveguide and its characterization as a "waveguide resonance" is noted by H. Seidel in ref. 1. Seidel gives the condition for the existence of this resonance as $\omega_3 = \frac{1}{2}\gamma(B_0 + H_0)$ where $B_0 = H_0 + 4\pi M_s$. This is exactly equivalent to $\sigma_3 = 1 - \frac{1}{2}\rho$. For the benefit of readers more familiar with descriptions of critical points in terms of B_0 and H_0 we take this opportunity to point out that σ_2 and σ_5 are exactly equivalent to $\omega_2 = \gamma B_0$ and $\omega_5 = \gamma\sqrt{B_0 H_0}$, respectively.

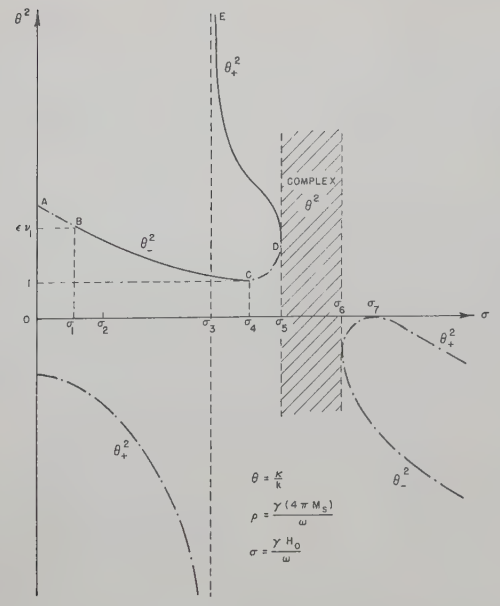

Fig. 5—$\theta_\pm^2$ as a function of σ with ρ fixed.

constant at σ_3 may be associated with a surface-wave solution only for $\sigma \to \sigma_3$ from above. It is readily demonstrated that θ_+^2 has only the single zero shown in Fig. 5 at σ_7 and that θ_-^2 has no zeros. In Table I it is indicated that θ_-^2 passes through a minimum at σ_4 and that its value there is always one. With this information, we conclude that surface-wave solutions may occur only on the curve passing through the points labeled A through E in Fig. 5.

We now assert that surface-wave mode solutions are obtained only on the segments BC and DE (the solid line segments) of the curve in Fig. 5. Moreover, we assert that θ_-^2 on BC represents a solution such that $\theta_- > 1$ whereas θ_+^2 on DE represents a solution such that $\theta_+ < -1$. In the following, we will give only a brief outline of the analysis required to justify these assertions.[13] To facilitate the discussion which follows we rewrite (11) as

$$\theta = \nu_2 \left| \sqrt{\theta^2 - 1} \right| + \frac{\nu_2}{\nu_1} \left| \sqrt{\theta^2 - \epsilon\nu_1} \right| . \qquad (13)$$

The "admissible" solutions of this equation must, of course, still satisfy the restrictions $\theta^2 > 1$ and $\theta^2 > \epsilon\nu_1$. This version of the secular equation makes evident that only one of the two square roots of either θ_+^2 or θ_-^2 may be an admissible surface-wave solution. Now, in the interval $0 < \sigma < \sigma_5$, θ_-^2 is a single valued continuous func-

TABLE I

σ	$\theta_\pm^2$	ν_1	ν_2
$\sigma = 0$	$\theta_\pm^2 = \dfrac{(\epsilon-3)\rho + \rho^2 \pm 2\sqrt{(\epsilon-1)^2 + \epsilon\rho^2}}{\rho(\rho^2-4)}$	$1-\rho^2$	$\dfrac{1}{\rho} - \rho$
$\sigma_1 \approx -\rho + \sqrt{1 - \rho\sqrt{\dfrac{\epsilon}{\epsilon-1}}}$ $\left(\dfrac{\rho}{\epsilon-1} \ll \dfrac{\epsilon\rho^2}{\epsilon+1} < 1\right)$	$\theta_-^2 = \epsilon\nu_1 \approx \dfrac{\epsilon\sqrt{\epsilon}}{\sqrt{\epsilon} + \sqrt{(\epsilon-1) - \rho\sqrt{\epsilon(\epsilon-1)}}} > 1$	$\nu_1 > \dfrac{1}{\epsilon}$	$\nu_2 > \dfrac{1}{\epsilon}$
$\sigma_2 = 1 - \rho$	$\theta_\pm^2 = \dfrac{2(\epsilon-1) - \epsilon\rho \pm 2\sqrt{(\epsilon-1)^2 + \epsilon\rho}}{\rho(\rho-4)}$	0	0
$\sigma_3 = 1 - \dfrac{\rho}{2}$	$\theta_+^2 = \infty$ $\theta_-^2 = \left[\dfrac{4 + (\epsilon+1)\rho}{2\sqrt{4(\epsilon+1)\rho}}\right]^2 \geq 1$	$-\dfrac{4+\rho}{\rho}$	$-\dfrac{4+\rho}{4}$
$\sigma_4 = -\dfrac{\epsilon}{\epsilon-1}\cdot\dfrac{\rho}{2} + \sqrt{1 + \dfrac{1}{4}\left(\dfrac{\epsilon\rho}{\epsilon-1}\right)^2}$	$\theta_-^2 = 1$ $\left(\dfrac{d}{d\sigma}\theta_-^2 = 0\right)$		
$\sigma_5 = -\dfrac{\rho}{2} + \sqrt{1 + \dfrac{\rho^2}{4}}$	$\theta_+^2 = \theta_-^2 = \dfrac{1}{2} + \sqrt{\dfrac{1}{4} + \dfrac{1}{\rho^2}} \geq 1$	∞	$-\dfrac{\rho}{2} - \sqrt{1 + \dfrac{\rho^2}{4}}$
$\sigma_6 = -\dfrac{\rho}{2} + \sqrt{1 + \left(\dfrac{\epsilon+1}{\epsilon-1}\cdot\dfrac{\rho}{2}\right)^2}$	$\theta_+^2 = \theta_-^2 = \dfrac{1}{2} - \sqrt{\dfrac{1}{4} + \dfrac{1}{\rho^2}\left(\dfrac{\epsilon-1}{\epsilon+1}\right)^2} \leq 0$		
$\sigma_7 = -\dfrac{\epsilon-2}{\epsilon-1}\cdot\dfrac{\rho}{2} + \sqrt{1 + \dfrac{1}{4}\left(\dfrac{\epsilon\rho}{\epsilon-1}\right)^2}$	$\theta_+^2 = 0$ $\left(\dfrac{d}{d\sigma}\theta_+^2 = 0\right)$	ϵ	

tion of σ. Therefore, if θ_-, one of the square roots of θ_-^2, is a proper solution of (13) in one part of this interval but not in another part, the change must occur either where $\theta_-^2=1$ (at point C) or where $\theta_-^2=\epsilon\nu_1$ (at point B). In the interval $\sigma_3<\sigma<\sigma_5$, θ_+^2 is also a single-valued continuous function of σ and, moreover, is always greater than both 1 and $\epsilon\nu_1$ in this interval. Therefore, if one of the square roots of θ_+^2 provides a proper surface-wave solution at any point of the segment DE, it must provide a proper solution at all points of this segment. Finally, we observe that if $\theta(\sigma)$ represents a proper surface-wave solution in some continuous interval in σ then either $\theta>1$ or $\theta<-1$ throughout this interval. With these observations, the significance of the successive steps in the analysis outlined in the next paragraph should be evident.

The first step in the analysis is to consider the behavior of (13) in the limit as $\theta_+^2\to\infty$. If ν_1 and ν_2 are eliminated from (13) by substituting their known values at σ_3, given in Table I, it becomes evident that, for $\theta_+^2\to\infty$, $\theta_+\to-\infty$ is a proper surface-wave solution near point E (*i.e.*, as $\sigma\to\sigma_3$ from above). It then follows that $\theta_+<-1$ must be a proper surface-wave solution throughout the segment DE. An independent verification of this conclusion may be obtained by demonstrating that, in the neighborhood of point D, points on DE are proper solutions with $\theta_+<-1$, whereas points on CD are not proper solutions. This implies that surface-wave solutions do not exist on the segment CD. The next step in the analysis is to show that $\theta_-(\sigma_3)>1$ is a proper surface-wave solution if and only if $(\epsilon+1)\rho>4$. Since $\sigma_4\gtrless\sigma_3$ according as $(\epsilon+1)\rho\gtrless4$, this verifies the conclusion that points on CD do not represent proper solutions. In addition, it shows that points on BC, with $\theta_->1$, do represent admissible surface-wave mode solutions. Point B is defined by the requirement that $\theta_-^2(\sigma_1)=\epsilon\nu_1(\sigma_1)$. This requirement is satisfied with $\sigma_1>0$ for all ρ less than some upper bound. For sufficiently large ϵ, in particular, for the range of ϵ values characteristic of most ferrites, the upper bound is given by $\rho_u\approx0.6$. Thus, the final step in the analysis is to show that $\theta_-^2(0)$ does not provide a proper surface-wave solution when ρ is sufficiently small. From this we conclude that, when $\sigma_1>0$, points on AB do not represent proper surface-wave mode solutions.

The conclusions we have drawn from the analysis described above are summarized in Fig. 6(a) where we indicate the behavior of the surface-wave mode propagation constants as a function of σ, *i.e.*, as a function of the dc magnetic field at a fixed frequency. To obtain analogous results applicable when the dc magnetic field is fixed and the frequency is varied, we introduce the variables

$$\Omega=\frac{1}{\sigma}=\frac{\omega}{\gamma H_0},\qquad m=1+\frac{\rho}{\sigma}=1+\frac{4\pi M_s}{H_0}\geq1 \quad (14)$$

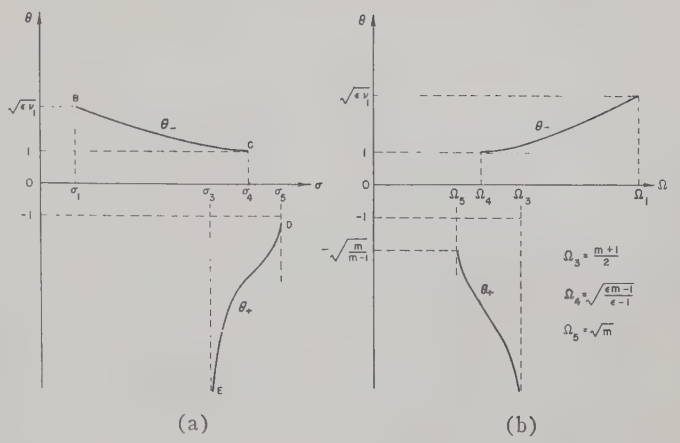

Fig. 6—Surface wave propagation constants. (a) ρ=constant, ω=constant, $\sigma\sim H_0$. (b) H_0=constant, $m=1+\rho/\sigma$=constant, $\Omega=1/\sigma\sim\omega$.

where m is independent of frequency and, for fixed H_0, Ω is directly proportional to the frequency. Expressions for $\nu_{1,2}$ as functions of Ω and m instead of ρ and σ are readily obtained and the entire analysis may be repeated. Most of the required information can be obtained by direct substitution into the result of the earlier analysis and a reinterpretation of these results for m fixed and Ω as the variable. The results of this new analysis are shown in Fig. 6(b). The surface-wave cutoff points $\Omega_{3,4,5}$ are defined there in terms of m and ϵ. For $\epsilon>1$ and $m>1$, all these cutoff points are finite and non-zero. The two frequency ranges in which surface waves are permitted will overlap, *i.e.*, $\Omega_3>\Omega_4$, when $(\epsilon-1)m>(\epsilon+3)$. In the earlier analysis, the low-field cutoff point σ_1 was obtained from the solution of a quartic equation. The expression for σ_1 given in Table I is an approximate solution of this quartic valid subject to the assumptions indicated in Table I in connection with the expression for σ_1. In the present analysis, it is possible to obtain an exact expression for Ω_1 since the quartic equation for σ_1 transforms to a quadratic equation in Ω_1^2. The solution of this biquadratic which corresponds to the requirement $\theta_-^2=\epsilon\nu_1$ is

$$\Omega_1^2=\frac{\alpha+\sqrt{\alpha^2-4(\epsilon-1)(\epsilon m-1)m^3}}{2(\epsilon-1)}$$

where

$$\alpha=(3\epsilon-1)m^2-(2\epsilon+1)m+\epsilon. \quad (15)$$

For all $\epsilon>1$, Ω_1^2 is finite so that this high-frequency cutoff point always occurs. This is consistent with the results of our earlier analysis since, for any ferrite, ρ approaches zero as ω goes to infinity.

Fig. 7 shows computed curves of θ as a function of σ for values of ρ and ϵ chosen to cover the range of values characteristic of most ferrites at X band.[15] Note that an

[15] S. Sensiper, "Resonance loss properties of ferrites in the 9-kmc region," PROC. IRE, vol. 44, pp. 1323–1342; October, 1956.

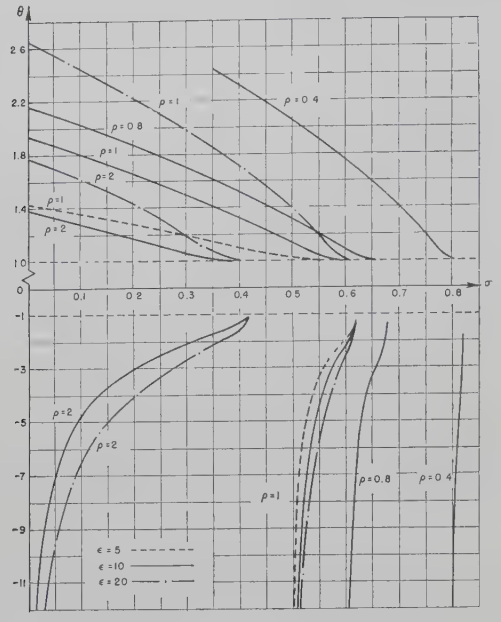

Fig. 7—Propagation constants for surface waves at a ferrite-air interface (for fixed frequency).

expanded scale has been employed for $\theta > 1$. The curves in Fig. 7 make it evident that, for fixed ρ and σ, $|\theta|$ increases with increasing ϵ and that, for ϵ and σ fixed, $|\theta|$ decreases with increasing ρ. The only positive directed ($\theta > 1$) surface wave which exhibits a low-field cutoff point is that for $\rho = 0.4$. This is consistent with the requirement indicated earlier that ρ be less than approximately 0.6 for this cutoff point to make its appearance.

To conclude this section, we note that we have shown that two oppositely directed TE_{n0} surface-wave modes are guided along a plane interface separating a dissipationless anisotropic (transversely magnetized) ferrite from free space. The two surface waves exist in different finite ranges of the parameter values. These two ranges never coincide and may or may not overlap. In contrast to the behavior of more familiar surface-wave phenomena, the surface waves here under consideration always exhibit both high- and low-frequency cutoff points (for fixed dc magnetic field). In addition, at a fixed frequency, each of the two surface waves cuts off for sufficiently high dc magnetic field and may or may not (depending on the parameter values) also cut off for sufficiently low dc magnetic field. The propagation constant of one of the two surface waves becomes infinite at the low-field (high-frequency) cutoff point. The behavior of this infinite propagation constant, when the guiding surface is located in different environments, will be the major subject of discussion in the next section.

Surface Waves on Ferrite Slabs

In this section we will be concerned with the TE_{n0} surface waves guided along finite thickness ferrite slabs located as indicated in Fig. 8. The secular equations determining the surface-wave propagation constants are again obtained via the transverse resonance procedure described above. For this purpose we employ, in addi-

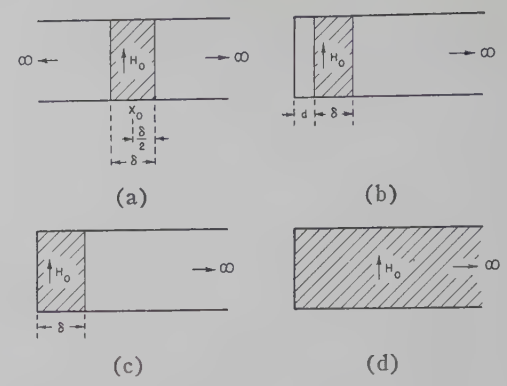

Fig. 8—Ferrite loaded parallel plate waveguides. (a) Ferrite slab in free space. (b) Ferrite slab near a short circuit. (c) Ferrite slab at a short circuit. (d) Ferrite filled semi-infinite waveguide.

tion to the admittances defined in (7) and (8), the impedance transfer formulas given by Morgenthaler[16] for TE_{n0} modes in ferrite media. We will be interested primarily in the surface-wave solutions with large θ. With this in mind we let

$$q_a = iQ_a \qquad q_m = iQ_m. \tag{16}$$

From (1) and (10) it follows that the wave numbers θ, Q_a, and Q_m are related through

$$\theta^2 = 1 + Q_a^2 = \epsilon\nu_1 + Q_m^2. \tag{17}$$

Thus, for finite ν_1, $\theta^2 \to \infty$ implies $Q_a^2 \to \infty$ and $Q_m^2 \to \infty$. For each of the structures in Fig. 8(a), (b), (c) the empty region extends to infinity. We must therefore require that $Q_a > 0$.

Before writing down the secular equation for the ferrite slab in free space [see Fig. 8(a)], it is instructive to predict some of the features of this equation. Suppose we choose to write the transverse resonance equation in terms of the admittances at x_0, the midpoint of the slab. With this choice, the total admittance is given as the sum of the admittances $\overrightarrow{Y}(x_0; H_0)$ and $\overleftarrow{Y}(x_0; H_0) = \overrightarrow{Y}(x_0; -H_0)$. Thus, while each of these admittances depends on the direction of H_0, their sum is independent of this direction. We therefore expect that the secular equation will be an even function of ν_2^2. Also, since reversing the direction of H_0 is equivalent to a 180° rotation about the x axis, the secular equation must contain only even powers of θ. These requirements are evidently satisfied by the secular equation

$$Q_a^2 + \frac{2Q_aQ_m}{\nu_1}\coth k\delta Q_m + \frac{Q_m^2}{\nu_1^2} - \frac{\theta^2}{\nu_2^2} = 0. \tag{18}$$

For a sufficiently thick slab, *i.e.*, for $k\delta Q_m$ sufficiently large, the two interfaces should behave independently. That this is the case is verified by noting that in the thick slab limit (18) becomes

[16] F. R. Morgenthaler, "Transverse impedance transformation for ferromagnetic media," Proc. IRE, vol. 45, p. 1407; October, 1957. The time dependence assumed in this reference is exp ($j\omega t$) not, as in this paper, exp ($-i\omega t$). Note that the term following the plus sign in the numerator of the right hand side of (4) of this reference has been omitted. The omitted term is simply the quantity j.

$$\left(Q_a + \frac{Q_m}{\nu_1} + \frac{\theta}{\nu_2}\right)\left(Q_a + \frac{Q_m}{\nu_1} - \frac{\theta}{\nu_2}\right) = 0. \quad (19)$$

This equation shows clearly that each interface of a thick slab supports a pair of surface waves whose propagation constants are either those in Fig. 6 (for the interface at $x=\frac{1}{2}\delta$) or the negatives of those in Fig. 6. With certain minor modifications,[13] this conclusion is valid for any slab thickness throughout most of the range in which the surface waves propagate. The conclusions noted above are summarized in the sketches in Fig. 9. Note that the curves labeled *RH* in Fig. 9 are practically identical with those in Fig. 6(a) except in the immediate vicinity of σ_5. Note also that the low-field cutoff point (σ_1') indicated in Fig. 9 is not simply related to the corresponding point (σ_1) in Fig. 6(a).

The behavior of the infinite propagation constants will play a significant role in the discussions which follow. For this reason, it is pertinent to establish that, for any slab thickness, θ approaching both $\pm\infty$ are proper solutions of (18) for $\sigma\rightarrow\sigma_3$ from above. We recall that ν_1 is finite in the neighborhood of σ_3 and therefore $\theta^2\rightarrow\infty$ implies $\theta^2\approx Q_a{}^2\approx Q_m{}^2\rightarrow\infty$. Thus, for θ approaching either $\pm\infty$, (18) may be approximated by

$$\coth k\delta|\theta| = -\frac{\nu_1}{2}\left(1 + \frac{1}{\nu_1{}^2} - \frac{1}{\nu_2{}^2}\right) = h(\sigma) \quad (20)$$

where, since Q_a must be positive, we have replaced Q_a by $|\theta|$ and, since $Q_m \coth k\delta Q_m > 0$ for $Q_m \gtrless 0$, we have replaced this term by $|\theta| \coth k\delta|\theta|$. Therefore, $\theta\rightarrow\pm\infty$ are both allowed solutions when $h(\sigma)\rightarrow 1$ from above or, as is evident from Fig. 10(a), as $\sigma\rightarrow\sigma_3$ from above.

In turning now to the analysis of the structure in Fig. 8(b) we are, in effect, asking the following question. What is the effect on the surface waves guided along a ferrite slab of locating one side of the slab near a short circuit? So long as we are interested only in the region in which $|\theta|$ is very large, the answer must be that the short circuit will have very little effect since the surface waves are very tightly bound to the two interfaces. In particular, we certainly expect that for any $d\neq 0$ the surface-wave propagation constants must still approach both $\pm\infty$ as $\sigma\rightarrow\sigma_3$ from above. To verify that this is indeed the case, we employ the transverse resonance procedure described earlier to obtain

$$Q_a{}^2 \coth kdQ_a + (1 + \coth kdQ_a)\frac{Q_aQ_m}{\nu_1}\coth k\delta Q_m + (1 - \coth kdQ_a)\frac{Q_a\theta}{\nu_2} + \frac{Q_m{}^2}{\nu_1{}^2} - \frac{\theta^2}{\nu_2{}^2} = 0 \quad (21)$$

as the secular equation for the waveguide shown in Fig. 8(b). It is immediately evident that as $Q_a\rightarrow\infty$ with $d\neq 0$ this equation reduces to (18). This verifies the assertion made above concerning the infinite solutions to (21) in the neighborhood of σ_3. Suppose now that the right hand interface of the structure in Fig. 8(b) is allowed to recede to infinity. The surface waves which the resulting structure would support would be those of the left-hand interface modified by the presence of the short circuit. It is evident that in this case we would find, for any $d\neq 0$, that there still exists an infinite solution ($\theta\rightarrow+\infty$ only) as $\sigma\rightarrow\sigma_3$ from above. On the other hand, if we set $d=0$ and so obtain the structure in Fig. 8(d) the surface waves must vanish completely since, as can readily be shown,[13] this structure will not support a surface wave. The discontinuous behavior noted here implies that a similar discontinuous behavior will be found in the comparison of the behavior of the surface waves for the structures in Figs. 8(b) and 8(c).

When the ferrite slab is against the short circuit [see Fig. 8(c)], the secular equation is obtained by setting $d=0$ in (21). This yields[2,17]

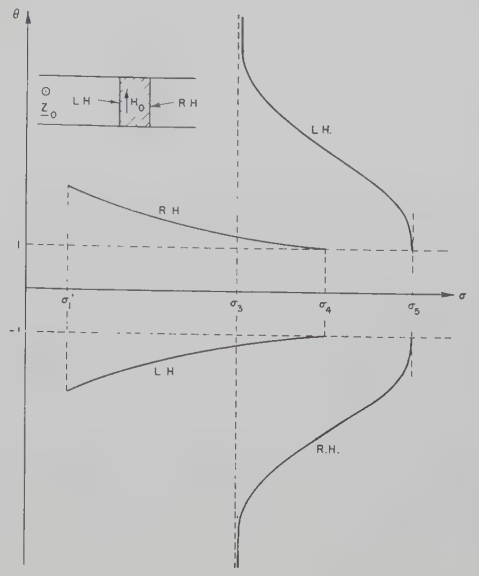

Fig. 9—Propagation constants for surface waves on a ferrite slab in free space.

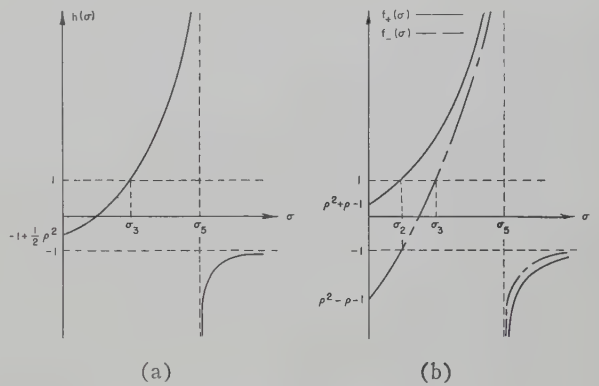

Fig. 10—The functions of $h(\sigma)$ and $f_\pm(\sigma)$.

(a) $h(\sigma) = -1 + \frac{1}{2}\frac{\rho^2}{1-\sigma(\rho+\sigma)}$. (b) $f_\pm(\sigma) = \frac{(\rho+\sigma)^2 \pm \rho - 1}{1-\sigma(\rho+\sigma)}$.

When the ferrite slab is against the short circuit [see Fig. 8(c)], the secular equation is obtained by setting $d=0$ in (21). This yields[2,17]

[17] R. L. Pease, "On the propagation of surface waves over an infinite grounded ferrite slab," IRE Trans. on Antennas and Propagation, vol. 6, pp. 13–21; January, 1958. Pease discusses the solutions to this equation in the thin slab approximation.

$$Q_a + \frac{Q_m}{\nu_1} \coth k\delta Q_m - \frac{\theta}{\nu_2} = 0. \qquad (22)$$

To investigate the infinite solutions of this equation, we proceed as we did in connection with (20) and, for $|\theta| \to \infty$, approximate this equation by

$$\coth k\delta |\theta| = \pm \frac{\nu_1}{\nu_2} - \nu_1 = f_\pm(\sigma) \qquad (\theta \to \pm\infty). \qquad (23)$$

The $\pm$ sign which appears in this equation (associated with $\theta \to \pm\infty$) results from replacing θ by $\pm|\theta|$ according as $\theta \gtrless 0$. It is evident from (23) that $\theta \to \pm\infty$ are allowed solutions of (22) only for $f_\pm(\sigma) \to 1$ from above. Sketches of these two functions are shown in Fig. 10(b). An examination of these sketches makes evident that $\theta \to \infty$ will be a solution for $\sigma \to \sigma_2$ from above whereas the solution $\theta \to -\infty$ occurs, as before, for $\sigma \to \sigma_3$ from above.

We have now arrived at the major result of this section. We saw earlier that when the ferrite slab was arbitrarily close to but not at the short circuit, *i.e.*, in the limit as $d \to 0$, there were two infinite solutions allowed, both occurring for $\sigma \to \sigma_3$ from above. These two infinite solutions are shown in Fig. 11(a). On the other hand, when the ferrite slab is at the short circuit, *i.e.*, at the limit $d = 0$, there are still two infinite solutions, but the $\theta \to +\infty$ solution is suddenly found at $\sigma \to \sigma_2$ from above instead of $\sigma \to \sigma_3$ from above. The two infinite solutions in this case are shown in Fig. 11(b). The discontinuous behavior of the $\theta \to +\infty$ solution is evident from a comparison of Fig. 11(a) and (b). This discontinuous behavior will play a significant role in the discussions which follow.

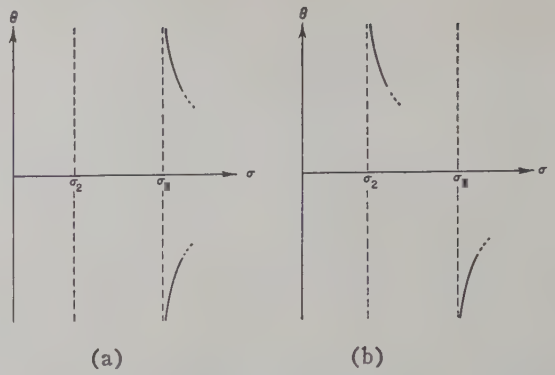

(a) (b)

Fig. 11—Infinite propagation constants for surface waves on a ferrite slab near a short circuit. (a) $d \to 0$. (b) $d = 0$.

The TE_{n0} Propagating Modes of the Slab Loaded Rectangular Waveguide

The secular equation determining the propagation constants of the TE_{n0} modes of the waveguide in Fig. 1 is[2,16]

$$q_a \cot K(1 - \Delta)q_a + \frac{q_m}{\nu_1} \cot K\Delta q_m - \frac{\theta}{\nu_2} = 0 \qquad (24)$$

where the dimensionless parameters K and Δ are defined as

$$K = ka = 2\pi \frac{a}{\lambda}; \qquad \Delta = \frac{\delta}{a} \qquad (0 \leq \Delta \leq 1). \qquad (25)$$

For the propagating modes, θ is real while $q_{a,m}$ may be either real or imaginary. Since the secular equation is an even function of both q_a and q_m we may, without loss of generality, prescribe that these be positive when they are real and that Im q_a, $q_m > 0$ when they are imaginary.

Very little has been published concerning the complete set of propagating mode solutions of (24). Some data has been given for a few special choices of the parameter values.[2] In addition, for thin slabs, perturbation formulas are available[15,18] in which the solutions to (24) are obtained as first-order perturbations about the propagation constants of the empty waveguide.

The analysis which follows is confined to the behavior of the propagation constants at a fixed frequency as a function of the dc magnetic field and the normalized slab thickness. It is convenient to assume that this fixed frequency is such that $\pi < K < 2\pi$, *i.e.*, such that the empty waveguide propagates only the TE_{10} mode. It will become evident as we proceed that this does not seriously restrict the generality of the conclusions we will draw.

Since the secular equation (24) is transcendental, we cannot obtain its solutions in closed form. The results presented below were obtained by a combination of analytical and graphical investigations, the details of which are given elsewhere.[7] In the following, the discussion will be primarily descriptive rather than deductive.

The propagating TE_{n0} modes of the waveguide in Fig. 1 are of two kinds, a "surface-wave mode" bound to the interface at $x = \delta$ and the "ordinary waveguide modes." The latter are the modes whose properties can be understood (except for the effect of the ferrite anisotropy) by assigning to the ferrite slab an equivalent dielectric constant of $\epsilon\nu_1$. We expect that, except for $\Delta \to 1$, the characteristics of the surface-wave mode will be very similar to those described earlier for the waveguide in Fig. 8(c). It is therefore not surprising that, by following the procedure employed in connection with (23), we again find that for $\theta^2 > \epsilon\nu_1$ (so that q_a and q_m are both imaginary for $\theta^2 \to \infty$) there are precisely two infinite θ solutions and that these occur as follows: (a) $\theta \to +\infty$ as $\sigma \to \sigma_2$ from above; (b) $\theta \to -\infty$ as $\sigma \to \sigma_3$ from above.

To justify the statement that $\epsilon\nu_1$ plays the role of an effective dielectric constant in determining the properties of the ordinary waveguide modes, we point out, first, that the relationship between θ^2 and q_m^2 involves only $\epsilon\nu_1$. Further, we note that the modal propagation

[18] B. Lax, K. J. Button, and L. M. Roth, "Ferrite phase shifters in rectangular waveguide," *J. Appl. Phys.*, vol. 25, pp. 1413–1421; November, 1954.

constants for the completely filled ferrite loaded waveguide (*i.e.*, for $\Delta=1$) are given by[19]

$$\theta = \pm\sqrt{\epsilon\nu_1 - \left(\frac{n\pi}{K}\right)^2} \qquad n = 1\ 2\ 3\cdots. \tag{26}$$

Finally, we note that the only place in which ν_2 has appeared so far is in the linear term in θ in the secular equation (24). In the isotropic limit, *i.e.*, for $\nu_2\to\infty$, this secular equation reduces to one which is very similar to the one which would apply for a dielectric slab with dielectric constant $\epsilon\nu_1$. Now, for $\pi<K<2\pi$, the empty waveguide ($\Delta=0$) propagates only a single pair of modes (two TE_{10} modes, one in each direction along z). It is evident from (26) that the number of pairs of modes propagated by the completely filled waveguide depends on $\epsilon\nu_1$. For $\nu_1<0$, no modes may propagate, and therefore increasing the slab thickness will tend to cut off the modes which propagate at $\Delta=0$. This will also be true for $\nu_1>0$, but $\epsilon\nu_1<(\pi/K)^2$. On the other hand, for $\epsilon\nu_1$ positive and large, the completely filled waveguide will propagate many pairs of modes and therefore increasing the slab thickness should have the tendency to increase the number of propagating modes. We recall that ν_1 approaches infinity in the neighborhood of σ_5. From the remarks above, we conclude that, except for the surface-wave mode, the slab loaded waveguide must become completely cut off as $\nu_1\to-\infty$, *i.e.*, as $\sigma\to\sigma_5$ from below. On the other hand, we expect to find a large number of propagating modes for $\nu_1\to+\infty$, *i.e.*, as $\sigma\to\sigma_5$ from above.

It was noted earlier that, subject to the restriction $\theta^2>\epsilon\nu_1$, there are precisely two infinite θ solutions to (24). The indicated restriction need not apply when $\nu_1\to+\infty$. Suppose then we assume that ν_1 and θ^2 are both large, but such that $\epsilon\nu_1-\theta^2>0$. In this case, for $\Delta\neq0$ and $\Delta\neq1$, we may approximate (24) by

$$\left(1\mp\frac{1}{\nu_2}\right)|\theta| + \frac{1}{\nu_1}\sqrt{\epsilon\nu_1-\theta^2}\cot K\Delta\sqrt{\epsilon\nu_1-\theta^2} = 0 \qquad (\theta\gtrless 0). \tag{27}$$

This equation is satisfied by many (large) values of θ, both positive and negative. The solutions are located approximately at the poles of the cotangent function. Finally, in the limit as $\nu_1\to\infty$, $\theta^2\to\infty$, subject to $\epsilon\nu_1-\theta^2>0$, we find an infinity of positive and negative infinite solutions for θ. These solutions represent surface waves which are bound to the ferrite-air interface on the air side only. The existence of such surface waves was ignored in the discussions above since these were concerned with surface waves which could exist on a single isolated interface. Since we have now determined the admitted infinite θ solutions for both $\theta^2>\epsilon\nu_1$ and $\theta^2<\epsilon\nu_1$ (with $\Delta=0$ and $\Delta=1$), these must constitute the complete set of infinite solutions.

The restrictions $\Delta\neq0$ and $\Delta\neq1$, noted in the preceding paragraph, do not represent a meaningless quibble. To see why this is so we note that the surface-wave modes cannot exist for either $\Delta=0$ or $\Delta=1$. How does the surface wave mode disappear as $\Delta\to0$ and $\Delta\to1$? One way in which this can be accomplished is to have the surface-wave mode disappear via $\theta^2\to\infty$. To investigate this possibility, we note that when $|\theta|\to\infty$ and $\Delta\to0$ (the product $\Delta|\theta|$ remaining finite and nonzero) the secular equation (24) may be approximated by

$$\coth K\Delta|\theta| = \pm\frac{\nu_1}{\nu_2} - \nu_1 = f_\pm(\sigma) \qquad (\theta\gtrless 0). \tag{28}$$

Similarly, when $|\theta|\to\infty$ and $\Delta\to1$ (the product $[1-\Delta]|\theta|$ remaining finite and non-zero), the secular equation (24) may be approximated by

$$\coth K(1-\Delta)|\theta| = \pm\frac{1}{\nu_2} - \frac{1}{\nu_1} = g_\pm(\sigma) \qquad (\theta\gtrless 0). \tag{29}$$

We therefore conclude that, for $\Delta\to0$, infinite solutions for θ exist only when $f_\pm(\sigma)\geq1$ while, for $\Delta\to1$, such solutions are admitted only when $g_\pm(\sigma)\geq1$. Examination of Figs. 10(b) and 12 makes evident that the infinite solutions under consideration can occur only as follows:

range of σ	$\sigma_2<\sigma<\sigma_3$	$\sigma_3<\sigma<\sigma_5$
for $\Delta\to0$	$\theta\to+\infty$	$\theta\to\pm\infty$
for $\Delta\to1$	$\theta\to-\infty$	no infinities.

(30)

The next step in the analysis is concerned with the determination of the conditions for cutoff. For $\theta=0$, the secular equation (24) becomes

$$\cot K(1-\Delta) + \frac{\sqrt{\epsilon\nu_1}}{\nu_1}\cot K\Delta\sqrt{\epsilon\nu_1} = 0. \tag{31}$$

The values of ν_1 required for cutoff are readily determined at those values of Δ for which $\cot K(1-\Delta)$ is either zero or infinite as follows:

for $\Delta = 1 - m\pi/K$,

$$\nu_1 = \frac{n^2}{\epsilon}\left(\frac{K}{\pi} - m\right)^{-2};$$

for $\Delta = 1 - (2m+1)\pi/2K$,

$$\nu_1 = \frac{(2n+1)^2}{4\epsilon}\left(\frac{K}{\pi} - \frac{2m+1}{2}\right)^{-2} \text{ and } \nu_1\to-\infty. \tag{32}$$

In each case, $m=0,\ 1,\ 2,\cdots$ up to the largest integer for which $\Delta\geq0$ and $n=0,\ 1,\ 2,\cdots$. Fig. 13 shows sketches of the values of ν_1 at cutoff as a function of Δ for $K=1.52\pi$ and $\epsilon=10$.[20] Points which were actually

[19] P. S. Epstein, "Theory of wave propagation in a gyromagnetic medium," *Rev. Mod. Phys.*, vol. 28, pp. 3–17; January, 1956.

[20] The value chosen for K is appropriate for, RG 52/U rectangular waveguide (inner dimensions 0.4 inch×0.9 inch) at 10 kmc.

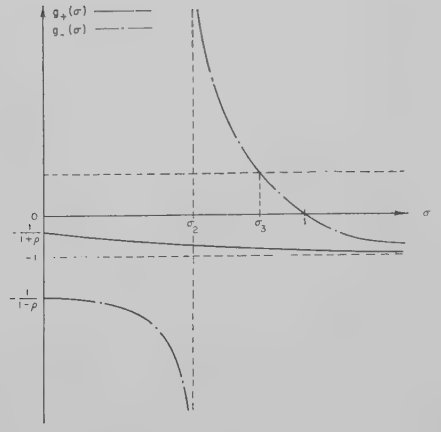

Fig. 12—The functions $g_{\pm}(\sigma)$.

$$g_{\pm}(\sigma) = \pm\frac{1}{\nu_2} - \frac{1}{\nu_1} = -\frac{(\sigma \pm 1)(\rho + \sigma \pm 1)}{(\rho + \sigma)^2 - 1}.$$

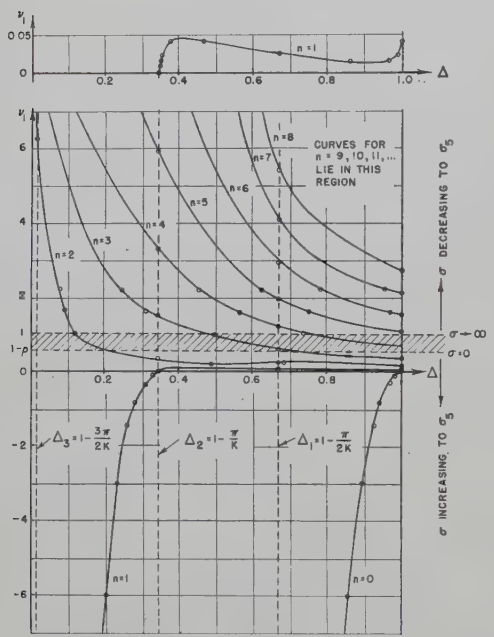

Fig. 13—ν_1 at cutoff ($\theta=0$) as a function of slab thickness ($K = 1.52\pi$, $\epsilon = 10$).

computed are indicated by the small circles. The curves are numbered according to the order of the modes of the completely filled waveguide starting with $n=1$ for the first mode which cuts off at a positive (non-zero) value of ν_1. The additional $n=0$ (or $\nu_1=0$) solution at $\Delta=1$ is identified as being associated with the surface-wave mode. Points on the curves labeled $n=2$, 3, 4 which lie in the shaded band are of no significance since values of ν_1 in the interval $1-\rho<\nu_1<1$ do not occur. The bottom of this band ($\nu_1=1-\rho$) corresponds to $\sigma=0$, the top ($\nu_1=1$) to $\sigma\rightarrow\infty$. Since the cutoff characteristics depend on ν_1 only, a scale of numerical values for σ need not be given unless we choose to specify ρ. Therefore, in Fig. 13 we content ourselves with merely indicating the directions in which σ increases from zero to σ_5 and decreases from infinity to σ_5.

There is a strong temptation to interpret the curves in Fig. 4 as follows. The mode corresponding to any one curve is either propagating or cut off according to whether the point representing the values of ν_1 and Δ lies "above" or "below" the curve.[21] While this interpretation does provide a rough idea of the conditions required for a particular mode to propagate, it is not strictly valid. The interpretation would be completely valid if the θ vs σ characteristics for fixed Δ (or, equivalently, the θ vs Δ characteristics for fixed σ) were symmetrical about the $\theta=0$ axis and were such that the poles of the derivative of θ with respect to σ always coincided with $\theta=0$. The need for these reservations becomes apparent from an examination of the results indicated in, *e.g.*, Fig. 17. Also, we remark that the curves in Fig. 13 give no indication of the erratic behavior of the solutions to (31) in the limit as $\Delta\rightarrow 0$. Therefore, they should not be used as a basis for a discussion of the cutoff characteristics in the immediate vicinity of $\Delta=0$.

The segment of the $n=1$ curve shown with an expanded ν_1 scale at the top of Fig. 13 reveals that $\Delta(\nu_1)$ for cutoff is multivalued for small positive $\epsilon\nu_1$. Presumably, this may also be the case for other values of n in the range of sufficiently small $\epsilon\nu_1$. The significance of this multivalued character becomes evident from a study of Figs. 14 and 15.[22] The curves in Fig. 14 are for $\nu_1<0$ so that the only propagating modes are the surface wave mode ($n=0$) and the perturbed empty waveguide mode ($n=1$). The curves for both modes exhibit only the single cutoff predicted in Fig. 13. The manner in which the surface-wave mode disappears for $\Delta\rightarrow 0$ and $\Delta\rightarrow 1$ is consistent with the information given in (30). When ν_1 takes on small positive values corresponding to values of σ in the interval $0<\sigma<1-\rho$ the surface wave mode is still admitted for $\Delta\neq 0$, 1. The empty waveguide still propagates only the TE_{10} mode and, for sufficiently small ν_1, the completely filled waveguide does not support any propagating modes. Now, it is evident from (30) that infinite solutions for θ are no longer admitted with either $\Delta\rightarrow 0$ or $\Delta\rightarrow 1$. Therefore, the only way in which the surface-wave mode can disappear at $\Delta=0$ and $\Delta=1$ is to have the θ vs Δ curve for this mode close on itself. This is precisely what happens in the curves labeled *a* and *b* in Fig. 15. In closing on itself, the θ vs Δ curve passes through $\theta=0$ twice. Thus, the three values of Δ at which Fig. 13 predicts that θ will equal zero are all accounted for. As ν_1 is increased, the two separate θ vs Δ curves join to form a single continuous curve. This situation is illustrated by curve *c* of Fig. 15. When ν_1 is increased further to a value such that the completely filled waveguide will support one pair of propagating modes, the single curve *c* splits at $\Delta=1$ to become the two continuous curves labeled *d*.

[21] In this connection, the adjective "above" is to be interpreted as implying "above and/or to the left of" for curves which vanish via $\nu_1\rightarrow -\infty$ and "above and/or to the right of" for the curves on which ν_1 tends to $+\infty$.

[22] Data for these curves was obtained by a graphical procedure described by Bresler (ref. 7).

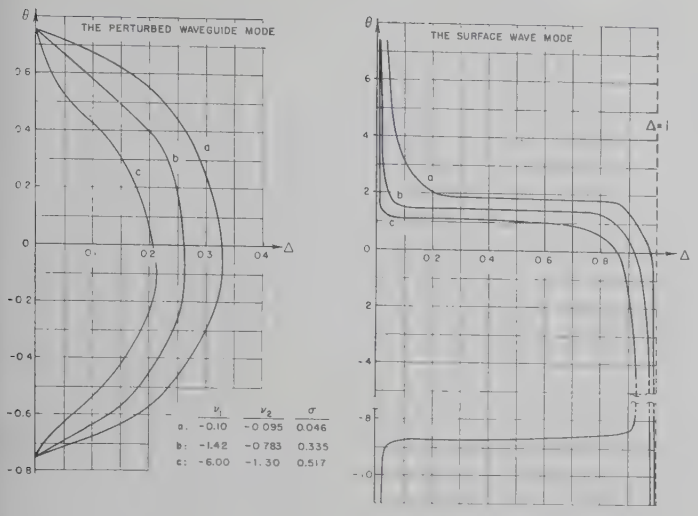

Fig. 14—Propagation constants as functions of the slab thickness ($K = 1.52\pi$, $\epsilon = 10$, $\rho = 1$).

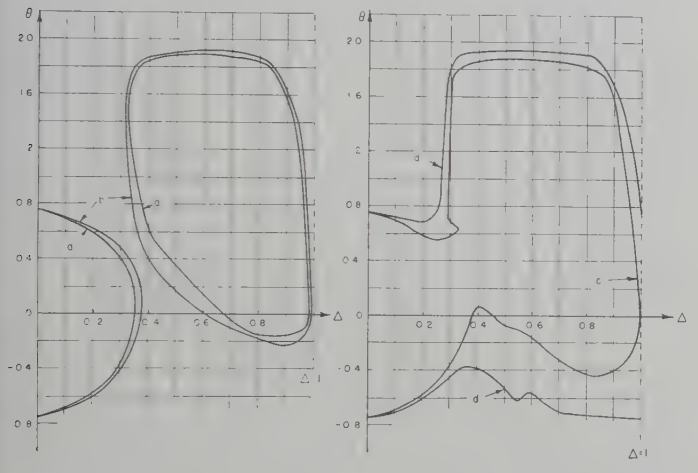

Fig. 15—Propagation constants as functions of the slab thickness ($K = 1.52\pi$, $\epsilon = 10$, $\rho = 0.8$).

(a) $\sigma = 0.190$, $\nu_1 = 0.0245$, $\nu_2 = 0.0249$.
(b) $\sigma = 0.1877$, $\nu_1 = 0.0300$, $\nu_2 = 0.0305$.
(c) $\sigma = 0.1822$, $\nu_1 = 0.0433$, $\nu_2 = 0.0444$.
(d) $\sigma = 0.1567$, $\nu_1 = 0.100$, $\nu_2 = 0.106$.

When ν_1 is increased still further beyond the values employed in Fig. 15, additional propagating modes appear at $\Delta = 1$ and will propagate for all values of Δ down to approximately the cutoff value given in Fig. 13. As soon as ν_1 becomes reasonably large, the surface wave mode is no longer propagated by the ferrite-air interface, and therefore we are no longer required to account for either its presence or the manner of its disappearance at $\Delta = 0, 1$. Sketches of a typical set of θ vs Δ curves for a reasonably large value of $\epsilon\nu_1$ are shown in Fig. 16.

The sketches shown in Fig. 17 illustrate the behavior of θ as a function of σ for fixed Δ. Certain essential features of these sketches (data concerning the surface-wave mode, the behavior at cutoff and the infinities in θ) follow directly from the results given above. Two other essential features (the slopes of the curves at $\theta = 0$ and the absence of maximum and minimum points)

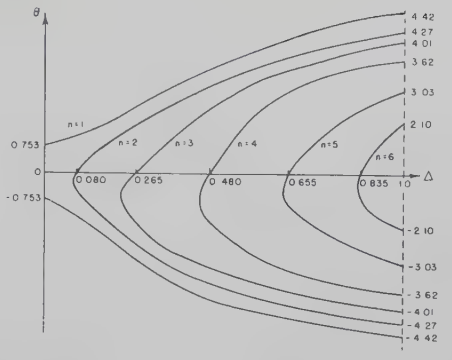

Fig. 16—Sketches of θ vs Δ for $K = 1.52\pi$, $\epsilon = 10$, $\nu_1 = 2$.

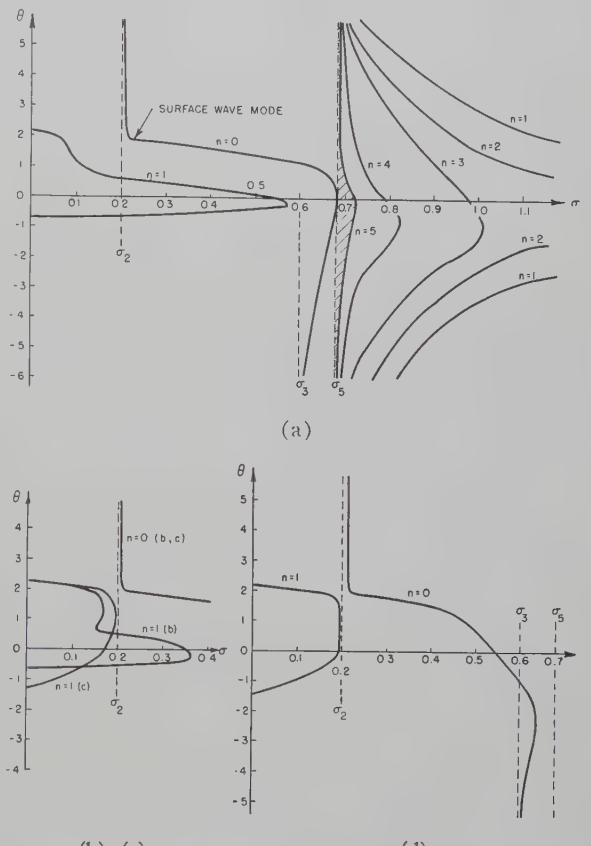

Fig. 17—Sketches of θ vs σ for $K = 1.52\ \pi$, $\epsilon = 10$, $\rho = 0.8$.
(a) $\Delta \approx 0.2$. (b) $\Delta \approx 0.3$. (c) $\Delta \approx 0.5$. (d) $\Delta \approx 0.9$.

will be justified by the analysis presented in the next section.

The sketches in Fig. 17 are proportioned to correspond roughly to $K = 1.52\pi$, $\epsilon = 10$ and $\rho = 0.8$. In Fig. 17(a), the region between the σ_5 ordinate and the $n = 5$ curve is shaded to indicate that this region contains an infinity of propagating modes for each of which $\theta \rightarrow \pm\infty$ as $\sigma \rightarrow \sigma_5$ from above. The region corresponding to $\sigma > \sigma_5$ is not reproduced in Fig. 17(b), (c), (d) since the basic characteristics of the θ vs σ curves in this interval do not change with Δ. In the interval $0 < \sigma < \sigma_5$ the $n = 0$ and $n = 1$ curves are shown for four different values of Δ. The remainder of this paragraph is devoted to a simplified explanation for the behavior exhibited by

these sketches. For the values of ρ and ϵ involved, an isolated ferrite-air interface would support a surface wave with $\theta > 1$ throughout the interval $0 < \sigma < \sigma_4$ where $\sigma_4 > \sigma_2$. With the finite thickness slab, the effect of placing the slab against a short circuiting wall is to convert the σ_2 ordinate into a barrier which the θ vs σ curve for the surface wave may not cross and at which $\theta \rightarrow + \infty$ as $\sigma \rightarrow \sigma_2$ from above. However, a study of Fig. 17 reveals that even with the smallest value of Δ employed (*i.e.*, when the effect of the short circuit should be most pronounced) the surface wave reasserts itself as σ approaches zero and distorts the $n=1$ curve so that part of this curve constitutes a continuation of the gently sloping portion of the $n=0$ curve. As Δ is increased so that the effect of the short circuit is diminished, the gap in the surface-wave characteristic between the $n=0$ and $n=1$ curves is likewise diminished. The gap does not disappear completely because the infinity at σ_2 is required for any finite slab thickness.

The Power Flow Associated with the Propagating Modes

In an earlier paper[6] the author employed a matrix formulation for the Maxwell equations to deduce a relationship between the power flow associated with a propagating mode in an arbitrary dissipationless uniform waveguide and the frequency derivative of the propagation constant of this mode. For our purposes here, we require an analogous relationship involving the derivative of θ with respect to σ when ρ and ω (or k) are held constant. By a procedure which parallels that employed in connection with (18) through (24) of the paper just cited,[6] it can be shown that the required relationship is

$$2P_\alpha\theta_\alpha' = \iint_S \boldsymbol{H}_\alpha^* \cdot \boldsymbol{\mu}' \cdot \boldsymbol{H}_\alpha dS \tag{33}$$

where θ_α is the (normalized) propagation constant of a particular propagating mode, P_α is the (real) power flow associated with this mode, $\boldsymbol{H}_\alpha$ is the total magnetic field of this mode, $\boldsymbol{\mu}$ is the tensor permeability of the ferrite slab, the prime superscript indicates the derivative with respect to σ and the required integration is to be carried out over the cross section, S, of the waveguide. P_α is defined so that it is positive for power flow along $+z$. The result in (33) is obtained when the modes are normalized in the manner indicated in the reference cited earlier.[6] Also, to obtain (33), we must exploit the fact that the boundary conditions at the waveguide walls, the (scalar) permittivity of the ferrite and both the (scalar) permeability and permittivity associated with the empty waveguide regions are all independent of σ.

For the TE_{n0} modes, $\boldsymbol{H}_\alpha$ has nonzero components only in the plane transverse to y (*i.e.*, to H_0). Therefore, for these modes, we introduce the subscript T to distinguish quantities confined to this transverse plane and rewrite (33) as

$$2P_\alpha\theta_\alpha' = \iint_S H_{T\alpha}^* \cdot \boldsymbol{\mu}_T' \cdot H_{T\alpha} dS. \tag{34}$$

For a dissipationless ferrite, $\boldsymbol{\mu}_T$ is a hermitian matrix, and therefore its derivative with respect to σ is also hermitian. Moreover, it is readily verified that (for fixed ρ and k) this derivative is negative definite when ρ is positive. It then follows from (34) that for the TE_{n0} modes here under consideration

$$P_\alpha\theta_\alpha' < 0 \qquad \text{for} \qquad \rho > 0 \tag{35}$$

so that, for positive ρ, $P_\alpha \gtrless 0$ according as $\theta_\alpha' \lessgtr 0$. Furthermore, we see that P_α may equal zero only at the poles of θ_α'. This means that the power flow associated with a propagating mode can change direction only where θ_α' is infinite. A further important interpretation of (35) is the recognition that θ_α' can not equal zero unless P_α becomes infinite. There is no difficulty in excluding the latter possibility in the case of closed waveguides, and we therefore conclude that $\theta_\alpha' = 0$ cannot occur; *i.e.*, that the θ *vs* σ curves cannot exhibit maximum or minimum points.

In the sketches in Fig. 17 we have indicated that the poles of θ_α' do not ordinarily occur where $\theta_\alpha = 0$. This statement is verified by noting that P_α is zero only at the poles of θ_α' whereas it can be shown that[7] at $\theta_\alpha = 0$

$$P_\alpha = -\frac{\nu_1^2}{K\nu_2}\left(\frac{\sin K\Delta\sqrt{\epsilon\nu_1}}{\sqrt{\epsilon\nu_1}}\right)^2. \tag{36}$$

Thus, for $\theta_\alpha = 0$, we find that $P_\alpha \gtrless 0$ according as $\nu_2 \lessgtr 0$. It then follows from (35) that, at $\theta_\alpha = 0$, $\theta_\alpha' \gtrless 0$ according as $\nu_2 \gtrless 0$. The availability of this last result eliminated a good deal of the guesswork which would otherwise have been involved in connection with the sketches in Fig. 17.

Conclusion—Resolution of the Thermodynamic Paradox

It is evident from Fig. 17 that the possibility of the existence of only a single TE_{n0} propagating mode for the waveguide in Fig. 1 arises only from the fact that there is a nonvanishing interval between the values of σ at which $\theta \rightarrow + \infty$ and $\theta \rightarrow - \infty$ for the surface-wave mode. It is further evident that if this interval did not exist there would always be an even number of propagating modes. The results obtained in the preceding section, in particular, that in (35), make evident that this even number of propagating modes would always divide so that half transported energy in one direction along z, half in the other. This observation clears the way for the resolution of the thermodynamic paradox. It is reasonable to expect that the discontinuous behavior illustrated in Fig. 11 will also be evident for the surface-wave modes of the waveguides in Figs. 1 and 18. To verify this conjecture we note that the secular equation for the TE_{n0} modes of the latter waveguide is[18]

$$q_a \cot K(1-\Delta-D)q_a + \frac{q_m}{\nu_1}\cot K\Delta q_m - \frac{\theta}{\nu_2} + \frac{\tan KDq_a}{q_a}\left\{\left[\frac{q_m}{\nu_1}\cot K\Delta q_m + \frac{\theta}{\nu_2}\right]q_a \cot K(1-\Delta-D)q_a - \frac{q_m^2}{\nu_1^2} - \frac{\theta^2}{\nu_2^2}\right\} = 0 \qquad (37)$$

where $D=d/a$. The reader may verify that for any $d\neq 0$, however small, this equation admits both $\theta\rightarrow\pm\infty$ as solutions for $\sigma\rightarrow\sigma_3$ from above, and does not admit $\theta\rightarrow+\infty$ as a solution in the neighborhood of σ_2. He may then further verify that, except for the discontinuity already referred to, all other solutions of (37) pass continuously into solutions of (24) in the limit as $d\rightarrow 0$. It will then be evident that in the limit as $d\rightarrow 0$, the sketches in Fig. 17 serve to describe all the modes of the waveguide in Fig. 18 except the $n=0$ mode. A study of Fig. 11 makes evident that the θ vs σ curve for the $n=0$ mode of the waveguide in Fig. 18 will be that illustrated in Fig. 19. Finally, when we combine the results given in Figs. 17 and 19, we see that for any $d\neq 0$ and, in particular, in the limit as $d\rightarrow 0$, the waveguide in Fig. 18 will always support an even number of propagating TE_{n0} modes. To establish that this conclusion is valid for values of K outside the range $\pi<K<2\pi$, we need only recall that the locations of the infinities in θ are independent of K.

The conclusion to which we are led is now evident. We have seen that if we accept the solutions of the secular equation (24) as constituting the correct description of the propagating TE_{n0} modes of the waveguide in Fig. 1, then we are led inescapably to a thermodynamic paradox. On the other hand, for any $d\neq 0$ and, in particular, in the limit as $d\rightarrow 0$, the solutions of the secular equation (37) do not, *a priori*, give rise to any thermodynamic difficulties associated with the TE_{n0} spectrum of the waveguide in Fig. 18. These considerations lead us to assert that the TE_{n0} mode propagation constants for the waveguide in Fig. 1 must be obtained from the solutions of the secular equation (37) in the limit $d\rightarrow 0$ and not from the secular equation (24), *i.e.*, not from the secular equation which obtains at the limit $d=0$. We assert further that when this is done there will no longer exist any basis for construction of a thermodynamic paradox associated with the waveguide in Fig. 1.

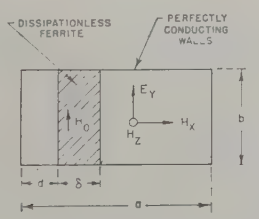

Fig. 18—Ferrite slab loaded rectangular waveguide (slab away from waveguide wall).

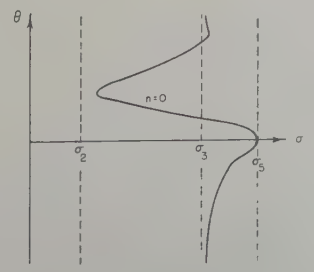

Fig. 19—θ vs σ for the surface wave mode of the waveguide in Fig. 18.

The conclusion just stated may be criticized on the grounds that while it tells us how to avoid thermodynamic difficulties, it does not tell us why such difficulties are encountered. Anticipating such criticism, we offer the following remarks in our defense. The problem we have been considering is an idealization of a physical reality. Let us recall some of the idealizations which were implicit in our formulation of the problem. Thus, we have been considering absolutely dissipationless waveguides bounded by perfectly conducting walls and loaded with uniformly magnetized homogeneous ferrite slabs contained within sharply defined planar boundaries. All these idealizations are widely employed in the formulation of electromagnetic problems and we accept them on the basis of the implicit assumption that the solutions to these idealized problems represent the behavior of a physical system in an appropriate limiting sense. To speak of the ferrite slab in Fig. 18 as being against the waveguide wall is to describe a physical situation for which we can not ordinarily distinguish between the mathematical descriptions $d=0$ and the limit as $d\rightarrow 0$. Given two different but equally acceptable mathematical idealizations for a physical situation, we are often called upon to distinguish between these idealizations by the physical content of the solutions to the problem which they yield. Thus, in our problem, we find that the two idealizations $d=0$ and $d\rightarrow 0$ lead to distinctly different solutions. Without asking why this difference arises, we are justified in choosing between them on the basis that the idealization which leads to a thermodynamic paradox must be discarded.

Acknowledgment

The author wishes to express his gratitude to his thesis adviser, Prof. N. Marcuvitz, for his guidance and assistance. Also, the author is indebted to his colleagues at the Microwave Research Institute, in particular to Prof. J. Shmoys, for their numerous helpful discussions and criticisms. Finally, thanks are due to Miss J. Spector for her perseverance in carrying out the tedious computations.

L-Band Ferromagnetic Resonance Experiments at High Peak Power Levels*

E. SCHLÖMANN†, J. H. SAUNDERS†, AND M. H. SIRVETZ†

Summary—Ferromagnetic resonance absorption at high peak power levels has been observed at 1300 mc in yttrium-gadolinium garnets and in a nickel ferrite-aluminate. In agreement with theoretical predictions, the critical field characterizing the onset of nonlinear effects, in a series of yttrium-gadolinium garnet disks of a given shape, was found to be very sensitively dependent on the gadolinium content. Similarly, for samples of a given composition, the critical field strength was sensitively dependent on the shape of the sample in agreement with theoretical predictions. At moderate power levels the susceptibility varies linearly with the square of the RF magnetic field strength over an appreciable range. This result can be understood in terms of an extension of Suhl's theory. The results can be used to predict the high power performance of these materials when used in isolators.

I. Introduction and Theory

In many important applications of ferrite devices high peak and average power levels are encountered. With Curie temperatures of the order of 200°C, and suitable provision for cooling, it would seem that isolators can be developed to handle any average power of interest (up to tens of kilowatts). With respect to peak power levels, on the other hand, the situation is not so simple, and it is known that the response of ferrite materials becomes nonlinear above a certain critical level[1,2] which for a given frequency depends on the linewidth, the saturation magnetization, and the shape of the specimen.

These effects manifest themselves as a reduction of the absorption at resonance and, under certain conditions, as an increase of the absorption away from resonance. The nonlinear effects usually set in at a fairly well defined threshold, and their presence very often interferes with the performance of ferrite devices such as isolators, phase shifters, and circulators. It is, therefore, important to investigate the possibilities of reducing the nonlinear effects.

The general features of the observed phenomena can be understood quite well in terms of a theory developed by Suhl.[3,4] According to this theory the nonlinear effects are due to the fact that certain spin waves become excited as soon as the amplitude of the uniform mode (which is driven by the applied microwave field) exceeds a certain critical value. Two possible mechanisms can be distinguished. For one of them, the unstable spin waves have half the frequency of the applied signal; for the other, they have the same frequency as the applied signal. We shall refer to these two mechanisms as nonlinear of first and second order. It has been shown by Suhl[3,4] that the first order effect has an inherently lower threshold than the second order effect (*i.e.*, it sets in at a lower value of the amplitude of the uniform mode, hence a lower power level). It has also been shown by Suhl,[3,4] however, that the first order effect can be suppressed if the experimental conditions are such that all spin wave frequencies are higher than half the signal frequency. For spheroidal samples this condition is realized at resonance if the signal frequency exceeds a "characteristic frequency"

$$\omega_c = 2\gamma 4\pi M_s N_\perp. \tag{1}$$

Here γ is the gyromagnetic ratio, M_s the saturation magnetization and $N_\perp$ the transverse demagnetizing factor of the sample (equal to $\frac{1}{3}$ for a sphere). At frequencies higher than this value only the second order effect can produce a change in the susceptibility at resonance and the first order effect gives rise to a "subsidiary" absorption peak at field strengths below those required for resonance. If the sample is biased for resonance, the critical RF field strength at which the nonlinear effects set in is, according to Suhl,

$$\begin{aligned} h_{\text{crit}} &= \Delta H \cdot \frac{\Delta H_k}{4\pi M} F \qquad \text{if } \omega < \omega_c \\ &= \Delta H \cdot \sqrt{\frac{\Delta H_k}{4\pi M_s}} \qquad \text{if } \omega > \omega_c. \end{aligned} \tag{2}$$

Here ΔH is the observed linewidth (total width of the resonance curve at half its maximum height) and ΔH_k a linewidth characteristic of the unstable spin waves. ΔH_k is believed to represent the intrinsic losses of the material, whereas very often ΔH is determined to a large extent by line broadening processes which arise from inhomogeneities such as the randomness in the distribution of the various magnetic ions over the available sites in the spinel lattice,[5] polycrystallinity,[6,7] and surface roughness.[8] The constant F in (2) is of the order

* Manuscript received by the PGMTT, August 3, 1959.

† Research Div., Raytheon Co., Waltham, Mass.

[1] R. W. Damon, "Relaxation effects in the ferromagnetic resonance," *Rev. Mod. Phys.*, vol. 25, pp. 239–245; January, 1953.

[2] N. Bloembergen and S. Wang, "Relaxation effects in para- and ferromagnetic resonance," *Phys. Rev.*, vol. 93, pp. 72–83; January, 1954.

[3] H. Suhl, "The nonlinear behavior of ferrites at high microwave signal levels," Proc. IRE, vol. 44, pp. 1270–1284; October, 1956.

[4] H. Suhl, "The theory of ferromagnetic resonance at high signal powers," *J. Phys. Chem. Solids*, vol. 1, no. 1, p. 209; 1957.

[5] A. M. Clogston, H. Suhl, L. R. Walker, and P. W. Anderson, "Ferromagnetic resonance line width in insulating materials," *J. Phys. Chem. Solids*, vol. 1, no. 3, pp. 129–136; 1956.

[6] S. Geschwind and A. M. Clogston, "Narrowing effect of dipole forces on inhomogeneously broadened lines," *Phys. Rev.*, vol. 108, pp. 49–53; October, 1957.

[7] E. Schlömann, "Spin-wave analysis of ferromagnetic resonance in polycrystalline ferrites," *J. Phys. Chem. Solids*, vol. 6, no. 2/3, pp. 242–256; 1958.

[8] R. C. Le Craw, E. G. Spencer, and C. S. Porter, "Ferromagnetic resonance line width in yttrium iron garnet single crystals," *Phys. Rev.*, vol. 110, pp. 1311–1313; June 15, 1958.

of unity if ω is sufficiently smaller than ω_c and becomes very large as ω approaches ω_c. In (2) the RF field is assumed linearly polarized. If the experiment is performed on small samples of ellipsoidal shape, the linewidth should be inferred from the effective susceptibility (relating the RF magnetization to the RF magnetic field outside the sample) and h_{crit} represents the cavity field in the absence of the sample.

It is obvious from the preceding remarks that at high microwave frequencies (such as *X*-band) and for conventional ferrimagnetic materials, the saturation of the resonance usually requires the second order process. At low microwave frequencies (such as *L*-band), however, the first order process is usually predominant unless special precautions are taken to suppress it. Eq. (1) shows that, in order to achieve this aim, one must reduce the saturation magnetization and/or use thin samples magnetized perpendicular to their planes. If the signal frequency is approximately equal to the characteristic frequency given by (1), the critical field strength should be very sensitive to small changes in the signal frequency, the magnetization, and the sample shape.

Suhl has also calculated the stationary behavior at power levels beyond the critical field given by (2). His original calculations with respect to this problem apply only to the first order process. He has shown that under these conditions the susceptibility at resonance should vary inversely with the amplitude of the RF magnetic field, and this has been confirmed experimentally.[3,4]

One of the present authors[9] has recently extended Suhl's work to a calculation of the stationary response at high power levels for the case in which the second order process accounts for the saturation of the resonance. The principal innovation of the new theory consists in a more detailed consideration of line broadening mechanisms. In Suhl's theory the effect of dissipation is taken into account by means of phenomenological damping terms in the equations of motion. This damping is very important because it stabilizes the spin waves in the presence of the time-varying coupling produced by the excitation of the uniform mode. It can be shown that this phenomenological description is not sufficient if the linewidth is predominantly caused by inhomogeneity broadening. This situation is encountered in many of the ferrites where the availability of various sites in the spinel lattice gives rise to an inhomogeneously broadened line as discussed by Clogston *et al.*[5] It is also encountered in polycrystalline ferrites where crystalline anisotropy, in conjunction with the polycrystalline character of the sample, gives rise to similar effects.[6,7] In these cases, the dissipation must be taken into account in a more detailed fashion, because the results so obtained differ appreciably from those obtained with a phenomenological damping term.

This can be understood in a fairly simple way. In the absence of inhomogeneity interaction the motion of the spin-wave amplitudes is determined by the time-varying coupling produced by the large excitation of the uniform mode. The spin waves are not excited at low powers and become unstable at a well defined threshold.

Inhomogeneities give rise to a linear coupling between the uniform mode and the spin waves. Because of this coupling, those spin waves that have the right frequency are slightly excited by an applied microwave field even at very low powers. At higher powers the same spin waves are simultaneously subject to a time-varying coupling produced by the large amplitude of the uniform mode. The situation is then similar to that encountered in parametric amplifiers. The excitation of the important spin waves caused by the inhomogeneity interaction is greatly enhanced by the time-varying coupling. Even at powers below those required for instability some of the spin waves are excited to a comparatively high level. The excitation varies smoothly as the power is increased beyond the point at which instability would occur in the absence of inhomogeneity interaction.

The results of the revised theory can be stated as follows: at moderate power levels the susceptibility at resonance should vary linearly with the square of the amplitude of the RF magnetic field

$$\frac{\chi''}{\chi_0''} = 1 - C\left(\frac{h}{\Delta H}\right)^2. \tag{3}$$

Here χ_0'' is the susceptibility at low power levels. The constant C depends on the location of the uniform mode in the spin-wave band, the strength of the inhomogeneity interaction, and the correlation length characteristic of the dominant scattering process. A numerical calculation of this constant has not been possible because of mathematical difficulties and because the physical information necessary for such a calculation is not available at present. It is interesting to note that C is not necessarily positive. The experimentally observed values lie in the range between $+150$ and -30. At higher power levels, the susceptibility should vary inversely with the amplitude of the RF magnetic field

$$\frac{\chi''}{\chi_0''} = \frac{h_\infty}{h} \tag{4}$$

where

$$h_\infty = \Delta H \sqrt{\frac{\Delta H_k}{4\pi M_s}}. \tag{5}$$

In (3)—(5), χ'' is the effective susceptibility and h is the cavity field (assumed linearly polarized) in the absence of the small sample. The derivation of (4) is based on certain approximations which cease to be applicable if the power level is very high. It may, therefore, be expected that this equation breaks down at very high power levels. The experimental results that have so far been obtained, usually agree quite well with (4), even at the highest available power levels.

[9] E. Schlömann, "Ferromagnetic resonance at high signal powers," *Bull. Amer. Phys. Soc.*, vol. 4, p. 53; January, 1959.

Fig. 1 demonstrates the theoretical dependence of the resonance susceptibility on the power level. The broken line represents the results obtained without inhomogeneity broadening. As Suhl has shown, the susceptibility should be constant up to $h=h_{crit}$ (which equals h_∞), in this case. The curve shown for $h>h_\infty$ represents the $1/h$ dependence that one may expect in analogy to Suhl's results concerning the first order effect. The full line shows in a qualitative way the results obtained with the inclusion of inhomogeneity broadening. It is seen that the sharp break which previously characterized the onset of the nonlinear effects has been replaced by a gradual decline. The curve shown is valid for the special case in which $C(h_\infty/\Delta H)^2=\frac{1}{4}$. For different values of this parameter the curves will, of course, be different.

Suhl[10] has recently investigated the saturation of the resonance through the second order process taking into account inhomogeneity broadening in the manner suggested by Schlömann.[9] His results can be represented by a curve very similar to the one shown in Fig. 1. His curve also decreases as $1/h$ at very high powers. But the behavior at moderate powers is of the form $1-ch^4$.

II. Experimental Procedure

Fig. 2 shows a schematic diagram of the apparatus used for observing at 1300 mc the ferromagnetic resonance absorption under conditions of high peak power levels. The measurement is made on small specimens in a rectangular TE_{102} transmission cavity of high unloaded Q. By choosing an appropriate set of inductive irises, the loaded Q is adjusted to a value between 300 and 2000 according to the strength of the absorption being measured and the range of RF field values required. A pulsed magnetron provides $\frac{1}{2}$ megawatt pulses to a power divider which is adjusted to give constant amplitude cavity output as the dc magnetic field is varied. The incident power is measured at several points on the resonance curve by means of a directional coupler, a coaxial cutoff attenuator, and a crystal detector. The setting of the attenuator for constant scope deflection removes the dependence on the crystal detection law. A duty cycle of the order of $6\cdot10^{-5}$ is used to eliminate spurious effects due to heating of the specimen. The pulse length was 4 μsec.

III. Results

It was explained in Section I that a significant change in the critical field should be expected if the experimental conditions are changed in such a way that the first order nonlinear process is allowed in one case and forbidden in the other. Spencer *et al.*[11] and Le Craw *et al.*[12] have observed this effect by changing the frequency and the temperature, respectively. In the present

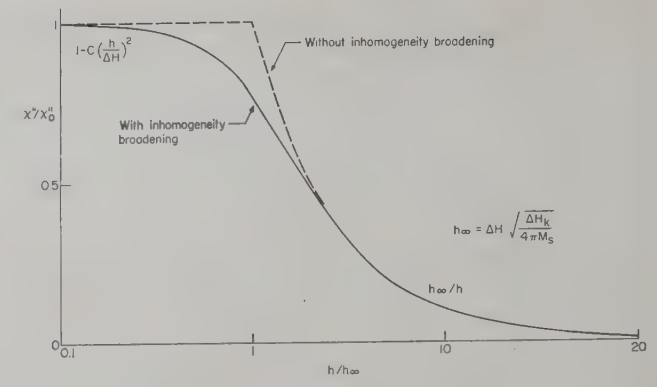

Fig. 1—Theoretical dependence of the susceptibility at resonance on the power level.

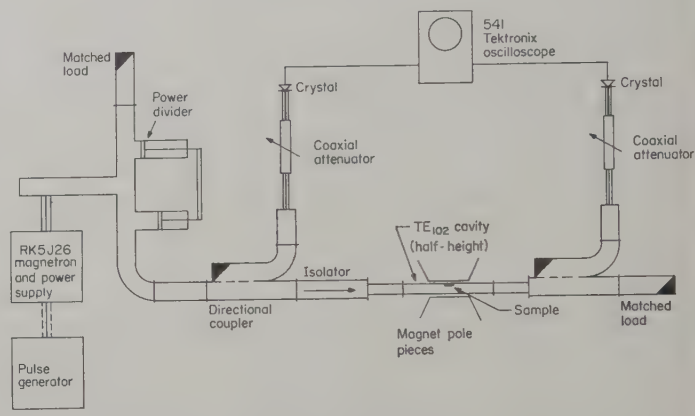

Fig. 2—Experimental equipment for high power measurements at L-band.

experiments the same effect has been observed by changing the composition (thus changing the saturation magnetization) and by changing the shape of the specimen. In Fig. 3 the susceptibility at resonance is plotted as a function of $1/h$ for a series of yttrium-gadolinium garnet disks of equal shape. In this representation the approximately linear dependence of χ'' on $1/h$ is most apparent, and the critical field h_∞ can be obtained by a simple extrapolation. It is seen that the critical field increases rapidly with increasing gadolinium content and is approximately twenty times higher for the sample with the largest gadolinium content than it is for pure yttrium garnet. The linewidth also increases in this series but only by a factor of less than three.

In these experiments a clear $1/h$ dependence of the susceptibility at very high power levels has not been observed. This is probably due to extraneous effects. The samples used for these experiments are disks and not ellipsoids as assumed in theory. In addition the internal dc magnetic field at resonance is rather small, so that the sample may not be completely magnetized. It is believed that these two facts account in large measure for the apparent residual susceptibility at very high power levels. In similar experiments at X-band[13] it has usually been found that the susceptibility varies as $1/h$ at high power levels.

[10] H. Suhl, to be published in *J. Appl. Phys.*

[11] E. G. Spencer, R. C. Le Craw, and C. S. Porter, "Ferromagnetic resonance in yttrium iron garnet at low frequencies," *J. Appl. Phys.*, vol. 29, pp. 429–430; March, 1958.

[12] R. C. Le Craw, E. G. Spencer, and C. S. Porter, "Ferromagnetic resonance and nonlinear effects in yttrium iron garnet," *J. Appl. Phys.*, vol. 29, pp. 326–327; March, 1958.

[13] J. J. Green and E. Schlömann, "High power ferromagnetic resonance at X-band in polycrystalline garnets and ferrites," this issue, pp. 100–103.

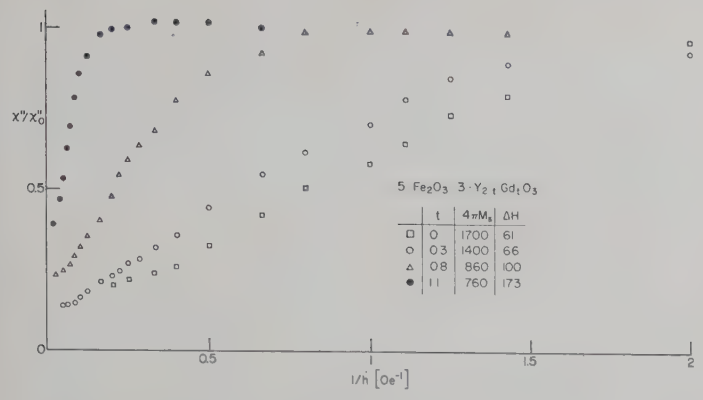

Fig. 3—Resonance absorption at high power levels for various yttrium-gadolinium garnets. Measurements at 1300 mc on disks ($\frac{25}{32}$-inch diameter by 0.050-inch thick).

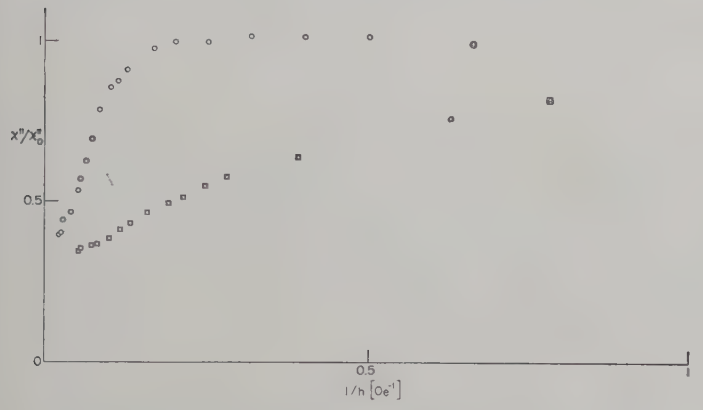

Fig. 4—Resonance absorption at high power levels for a disk (○) $\frac{25}{32}$-inch by 0.050-inch thick and a sphere (□) $\frac{5}{16}$-inch-diameter of a yttrium-gadolinium garnet (5 $Fe_2O_3 \cdot 3Y_{0.9}Gd_{1.1}O_3$). Measurements taken at 1300 mc, $4\pi M = 760$, $\Delta H = 173$ Oe.

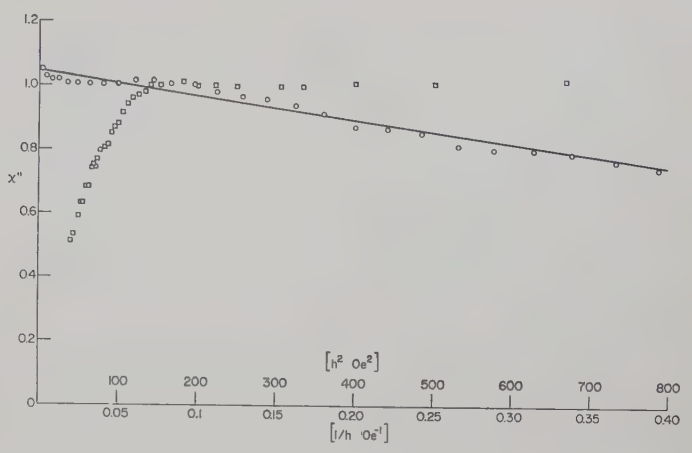

Fig. 5—Resonance absorption as a function of power level for a nickel ferrite-aluminate developed in this laboratory ($4\pi M_s$ 475 gauss, $\gamma = 2.1$ Mc/Oe, $\Delta H = 290$ Oe at X-band). Measurements taken at 1300 mc on a disk ($\frac{5}{8}$-inch diameter by $\frac{3}{16}$-inch thick). ○ refers to h^2 scale, □ to $1/h$ scale.

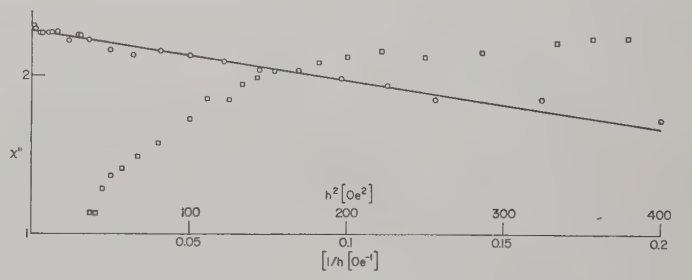

Fig. 6—Resonance absorption as a function of power level for a yttrium-gadolinium garnet (5 $Fe_2O_3 \cdot 3Y_{0.9}Gd_{1.1}O_3$: $4\pi M_s = 710$ gauss, $\Delta H = 200$ Oe). Measurements taken at 1300 mc on a disk ($\frac{25}{32}$-inch diameter by 0.050-inch thick). ○ refers to h^2 scale, □ refers to 1/h scale.

When the complete resonance line (χ'' vs dc magnetic field) was measured it was observed that with increasing power level the absorption maximum shifted toward lower fields. In the case of the yttrium garnet, the resonance line became very steep on the low field side at an RF field amplitude of approximately 6 Oe. This "fold-over effect" has been predicted theoretically by Anderson and Suhl[14] and has previously been observed by M. Weiss.[15] In all other samples except the yttrium garnet the effect was not noticeable. A theoretical analysis showed that for the values of saturation magnetization and linewidth (ΔH and ΔH_k) encountered in these experiments, the fold-over effect should not play an important role.

Fig. 4 shows the susceptibility as a function of $1/h$ for two samples of the same yttrium-gadolinium garnet: one, a thin disk; the other, a sphere. Again the large difference in the critical field strength associated with the transition from the first (sphere) to the second order nonlinear process (disk) is apparent.

If the susceptibility is plotted vs h^2 on a linear scale the linear dependence of the susceptibility on h^2 at moderate power levels becomes apparent. Figs. 5 and 6 show two examples. In both cases the second order nonlinear process accounts for the saturation of the resonance. It is seen that the linear law agrees quite well with the data over an appreciable range of power levels. In the present cases the initial third of the decline of the resonance susceptibility is governed by the linear law. The constants C of (3) for the two cases are 29 (for the nickel ferrite-aluminate) and 11 (for the yttrium-gadolinium garnet). A different yttrium-gadolinium garnet of the same nominal composition showed an initial slight increase of the susceptibility with power level (*i.e.*, $C < 0$).

IV. Conclusion

It may be seen from the last two figures that h_∞ for these materials is of the order of 25 Oe. This corresponds to approximately 1.7 megawatts in L-band waveguide of half the conventional height.[16] It should be remembered that a wave traveling in the forward direction of an isolator does not excite the resonance. Only the reflected power must be absorbed by the isolator.

[14] P. W. Anderson and H. Suhl, "Instability in the motion of ferromagnets at high microwave power levels," *Phys. Rev.*, vol. 100, pp. 1788–1789; December 15, 1955.

[15] M. T. Weiss, "Microwave and low-frequency oscillation due to resonance instabilities in ferrites," *Phys. Rev. Letters*, vol. 1, pp. 239–241; October, 1958.

[16] Half-height waveguide is generally used for isolators at this frequency.

With mismatches of the sort encountered in practical applications (typically less than two to one), an isolator using the materials discussed in this paper should function satisfactorily at peak power levels of several megawatts, if the necessary precautions are taken to suppress the first order nonlinear effect. Experiments using typical isolator configurations instead of the resonance cavity have shown that the onset of nonlinear effects in isolators can be predicted with fair accuracy from cavity measurement.

A further improvement of the power handling capacity of microwave ferrites appears quite feasible. In particular, it is not difficult at all to increase the linewidth and thus increase the critical field (h_{crit} or h_{∞}). This is not a promising line of attack, however, since the ratio of reverse to forward attenuation of resonance isolators decreases rapidly with increasing linewidth.[17] To improve the power-handling capacity one must, therefore, according to (5), decrease the saturation magnetization and/or increase the spin-wave linewidth ΔH_k. This can generally be achieved by suitable substitution of the magnetic ions in ferrites of the spinel and garnet type.

ACKNOWLEDGMENT

The authors would like to thank L. G. Rubin for his help in constructing the equipment used in this work. They are also indebted to Dr. S. L. Blum, D. A. Belforti and Miss S. Georgian for the preparation of the materials and for preliminary measurements.

[17] B. Lax, "Frequency and loss characteristics of microwave ferrite devices," PROC. IRE, vol. 44, pp. 1368–1386; October, 1956.

High Power Ferromagnetic Resonance at *X*-Band in Polycrystalline Garnets and Ferrites*

J. J. GREEN† AND E. SCHLÖMANN‡

Summary—**Resonance experiments have been performed at *X*-band on spherical samples of polycrystalline yttrium garnet, yttrium-gadolinium garnet, yttrium-holmium garnet and nickel-cobalt ferrite. The RF field strength extended up to 60 Oersted. In the case of yttrium garnet the samples differed considerably in density and hence in linewidth. At fairly low power levels the susceptibility at resonance varies linearly with the square of the RF magnetic field strength. At high power levels the susceptibility is inversely proportional to the amplitude of the microwave magnetic field. The "spin-wave linewidth" ΔH_k is inferred by extrapolation from the behavior at very high powers. It is found that ΔH_k is, to a large extent, independent of the linewidth ΔH observed by the usual low power experiments. In particular ΔH_k was found to be essentially the same (approximately 4 Oe) for all yttrium iron garnets (single crystals and polycrystals with linewidth varying between 1.8 Oe and 450 Oe). On the other hand, ΔH_k increases very rapidly if the yttrium is partially substituted by holmium ($\Delta H_k \sim 11$ Oe for 1 per cent substitution.)**

I. INTRODUCTION

IT was explained in the preceding paper[1] that at *X*-band frequencies and for conventional ferrimagnetic materials, the saturation of the resonance line involves the excitation of spin waves which have the same frequency as the signal (second-order nonlinear process). In addition, at these frequencies, one observes a subsidiary absorption peak below the main resonance which is attributed to the excitation of spin waves with frequencies equal to half the signal frequency (first-order nonlinear process). For spherical samples of the materials investigated in this paper the subsidiary peak lies considerably below the main resonance and (for this reason) becomes noticeable only at quite high power levels. This means that one never encounters a situation in which both nonlinear processes (first and second order are simultaneously important. Experiments at *X*-band are, therefore, better suited for a detailed investigation of the second-order nonlinear process than the *L*-band experiments reported in the preceding paper.[1]

The materials used in this investigation belong to four different families. One of these families comprises yttrium iron garnets of varying densities and hence varying linewidths (between 47 and 450 Oe). Two other families are derived from yttrium iron garnet by partial substitution of gadolinium or holmium for the yttrium. The fourth family is derived from nickel ferrite by partial substitution of cobalt for nickel.

II. EXPERIMENTAL PROCEDURE

Ferromagnetic resonance measurements were made at 9250 mc using a TE_{202} transmission cavity. The samples were mounted on a quartz rod and placed in the cavity at a point of maximum RF magnetic field. Sample absorption as a function of dc magnetic field was determined from the change in incident power necessary to maintain a constant transmitted power. The magnetic field strength at the sample was obtained from

* Manuscript received by the PGMTT, August 3, 1959. The portion of the work performed by J. J. Green was supported by the AF Cambridge Research Center, Contracts AF 19(604)-1084 and AF 19(604)-5487.

† Gordon McKay Lab., Harvard University, Cambridge, Mass.
‡ Research Div., Raytheon Co., Waltham, Mass.

[1] E. Schlömann, J. Saunders, and M. Sirvetz, "*L*-band ferromagnetic resonance experiments at high peak power levels," this issue, pp. 96–100.

a knowledge of incident power, cavity coupling, loaded Q and the cavity mode. This was done at one power level and all other power levels were compared to this reference level by means of a calibrated attenuator. The duty cycle was always less than 5×10^{-5}. At power levels where heating effects might occur, single pulses of one microsecond duration were used. A 2J51 tunable magnetron provided the microwave power which was sufficient to obtain cavity fields up to 60 Oe. Calibrated attenuators preceding each crystal made it possible to take readings with the crystals always at the same power level. All measurements were performed at room temperature on spherical samples. With increasing power level a slight shift of the resonance was observed in many cases. If this happened, the dc magnetic field was adjusted for resonance at each power level.

III. Results

Fig. 1 shows a set of typical saturation curves (susceptibility at resonance as a function of the amplitude of the microwave magnetic field on a logarithmic scale). The two curves which saturate at the lowest power levels (curves a and b) are obtained from measurements on single crystals of yttrium iron garnet. The two crystals differed in their surface treatment, since one (a) was polished (and had a linewidth of 3.9 Oe); and the other (b) had a rough surface (and a linewidth of 9.1 Oe).Curves (c) and (d) are typical saturation curves obtained with polycrystalline yttrium iron garnet and holmium-substituted yttrium iron garnet, respectively. In these cases the saturation occurs at higher power levels as might be expected in view of the larger linewidth. Curve (e) is a simplified theoretical curve. It was obtained from the results described in the previous paper by matching the two theoretical expressions (expected to be valid at moderate and high powers, respectively) in such a way that the resulting curve had a continuous slope.[2] It is seen that the theoretical curve can be fitted moderately well to any of the experimental curves by sliding it along the horizontal axis. A good fit, however, is not obtainable in this way. This is not surprising since the behavior of χ'' at moderate and at very high power levels is determined by different physical consideration. In order to obtain a good fit one needs at least two adjustable parameters, like C and h_∞ of the preceding paper.[1]

In order to demonstrate the validity of the theoretical formulas derived for moderate and very high power levels [(3) and (4) of the preceding paper[1]] the susceptibility should be plotted on a linear scale vs h^2 and vs $1/h$. The phenomenological parameters C and h_∞ can be obtained from such plots by simple extrapolation. In the present paper, we shall concentrate on the behavior at very high powers and hence use primarily the $1/h$ representation. Fig. 2 shows two typical sets of measurements obtained on polycrystalline yttrium

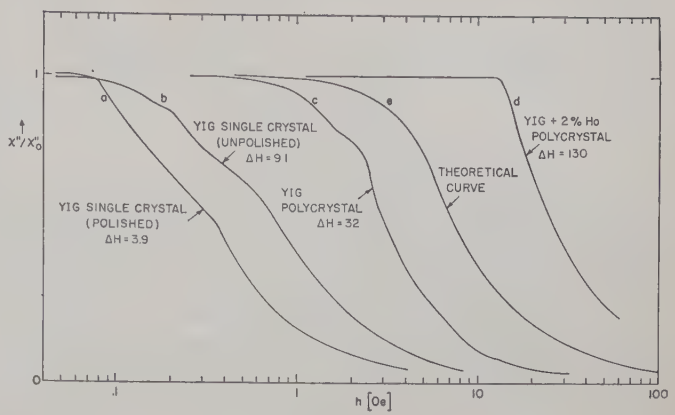

Fig. 1—Saturation curves for various yttrium garnets.

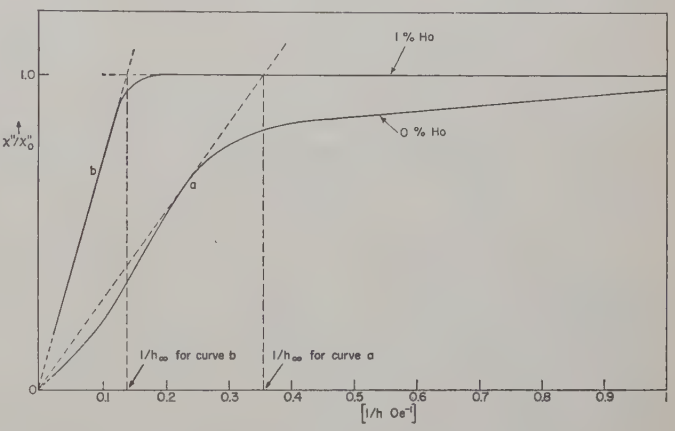

Fig. 2—Saturation curves for polycrystalline yttrium garnet and holmium-substituted yttrium garnet.

garnet (a) and yttrium-holmium garnet (b). It is seen that the latter obeys the $1/h$-law quite well almost over the complete nonlinear range. The former, however, shows appreciable deviations from the theoretical $1/h$-law. In cases such as these the phenomenological parameter h_∞ was obtained by drawing a tangent in the way indicated in the figure. It should be noticed that for any point on the curve (χ'' vs $1/h$) the slope of a line connecting it with the origin is proportional to the amplitude of the precessing magnetic moment. The angle between the precessing magnetic moment and the direction of the dc field is (in radians and using the notation of the previous paper[1])

$$u_0 = \frac{\chi''}{\chi_0''}\,\frac{h}{\Delta H}\,. \tag{1}$$

Here h is the amplitude of the RF magnetic field in the absence of the sample and the RF field is assumed linearly polarized. χ'' is the imaginary part of the effective susceptibility (which relates the magnetization of the sample to the magnetic field outside the sample). ΔH is the linewidth (total width). In case (a) of Fig. 2, the amplitude u_0 reaches a maximum with increasing power level and then decreases again. The maximum of u_0 is obviously given by

$$u_{0_{\max}} = \frac{h_\infty}{\Delta H}\,. \tag{2}$$

[2] This means that the two curves are joined at the point at which χ''/χ_0'' equals $\frac{2}{3}$, and that $C(h_\infty/\Delta H)^2=4/27$ in the notation of the preceding paper.

According to (5) of the preceding paper,[1] $u_{0_{max}}$ is related to the "linewidth" of the unstable spin waves by

$$u_{0_{max}}{}^2 = \frac{\Delta H_k}{4\pi M_s}. \tag{3}$$

The experimental results obtained with polycrystalline yttrium garnet are summarized in Fig. 3. The linewidth of these materials varied between 47 Oe and 450 Oe. It increases with decreasing density in an approximately linear fashion. This effect has been observed previously and is attributed to the presence of stray fields produced by nonmagnetic inclusions (such as pores).[3–6] Fig. 3 shows that for these materials the critical field h_∞ is very nearly proportional to the linewidth. Measurements of h_∞ on single crystals (with linewidths ranging between 1.8 Oe and 9.1 Oe) gave results which also agree quite well with the straight line drawn in the figure. We thus conclude that the maximum amplitude of the precessing magnetic moment is independent of the porosity. This implies that the spin wave linewidth ΔH_k is also independent of the porosity.[7]

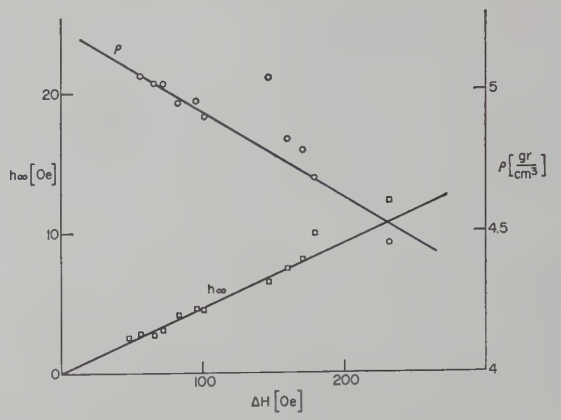

Fig. 3—High power effects in polycrystalline yttrium garnet. The critical field strength h_∞ is proportional to the linewidth ΔH, which increases with decreasing density ρ. The same dependence of h_∞ on ΔH was also observed in single crystals.

Fig. 4 summarizes the experimental results obtained with gadolinium-substituted and holmium-substituted yttrium garnet. Here the square of the maximum amplitude is plotted as a function of the gadolinium and holmium content (characterized by the composition parameter t). The cluster of points at $t=0$ represents the yttrium garnet data, which was also shown in Fig. 3. It is seen from Fig. 4 that $u_{0_{max}}{}^2$ increases with increasing gadolinium and holmium content. In the case of the gadolinium-substituted yttrium garnet most of the increase is attributable to the decrease in the magnetic moment. Pure gadolinium garnet has a very small saturation magnetization at room temperature, and, it is known that in the yttrium-gadolinium garnets the saturation magnetization decreases approximately linearly with the gadolinium content. At $t=1$ the saturation magnetization is, therefore, roughly half as large as it is at $t=0$. Fig. 4 shows that between $t=0$ and $t=1$ the square of the maximum amplitude increases by a factor somewhat larger than two. Thus ΔH_k has also increased but only by a rather small factor.

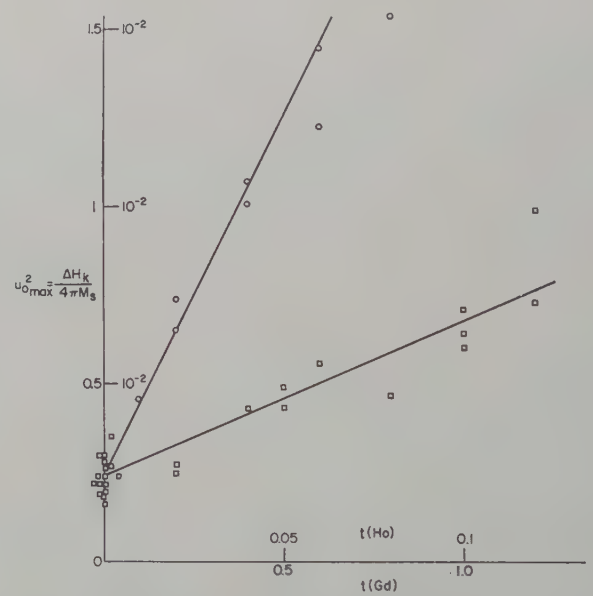

Fig. 4—Maximum amplitude of the uniform mode for polycrystalline samples of $5Fe_2O_3 \cdot 3Y_{2-t}Me_tO_3$ where Me=Gd (□) or Ho (○) as a function of the composition. Note the difference in the t-scales.

If holmium rather than gadolinium is substituted for the yttrium, a much more rapid increase of $u_{0_{max}}{}^2$ is observed. In this case the saturation magnetization is practically independent of the composition in the range of interest, so that the increase in $u_{0_{max}}{}^2$ must be attributed to an increase in the linewidth ΔH_k of the unstable spin waves. For yttrium garnet ΔH_k is approximately 4 Oe and it increases with holmium content at the rate of approximately 7 Oe per cent.

The last family of materials to be described in this paper consists of cobalt-substituted nickel ferrites. It is known that in these materials the linewidth first decreases with cobalt content, then reaches a minimum at approximately 3 per cent substitution, and finally increases again. This has been attributed to the fact that small cobalt substitutions tend to decrease the effects of crystalline anisotropy.[3,8,9] Since nickel ferrite has a

[3] E. Schlömann, "The microwave susceptibility of polycrystalline ferrites in strong dc fields and the influence of nonmagnetic inclusions on the microwave susceptibility," *Proc. Conf. on Magnetism and Magnetic Materials*, Boston, Mass., October, 1956.

[4] G. P. Rodrique, J. E. Pippin, W. P. Wolf, and C. L. Hogan, "Ferrimagnetic resonance in some polycrystalline rare earth garnets," IRE TRANS. ON MICROWAVE THEORY AND TECHNIQUES, vol. MTT-6, pp. 83–90; January, 1958.

[5] W. P. Wolf and G. P. Rodrique, "Preparation of polycrystaline ferrimagnetic garnet materials for microwave applications," *J. Appl. Phys.*, vol. 29, pp. 105–108; January, 1958.

[6] J. Snieder, "Ferromagnetic resonance in polycrystalline ferrites," *Appl. Sci. Res.*, vol. B7, pp. 185–232; 1958.

[7] The saturation magnetization varies only by a small amount in this series.

[8] M. H. Sirvetz and J. H. Saunders, "Resonance widths in polycrystalline nickel-cobalt ferrites," *Phys. Rev.*, vol. 102, pp. 366–337; April 15, 1956.

[9] J. E. Pippin and C. L. Hogan, "Resonance measurements on nickel-cobalt ferrites as a function of temperature and on nickel ferrite-aluminates," IRE TRANS. ON MICROWAVE THEORY AND TECHNIQUES, vol. MTT-6, pp. 77–82; January, 1958.

negative anisotropy constant K_1 and cobalt ferrite has a very large positive one, a compensation of the crystalline anisotropy is expected from a substitution in the range of a few per cent. Fig. 5 shows ΔH and $u_{0_{max}}{}^2$ as a function of the composition. The linewidth ΔH shows the extraordinary dependence on the cobalt content, which was described above. $u_{0_{max}}{}^2$ however, (and, therefore, ΔH_k since M_s is nearly constant) increases approximately linearly with the cobalt content.

IV. Discussion

The nonlinear effects discussed in this paper have important practical applications. The power-handling capacity of isolators and circulators is in large measure determined by the onset of nonlinearity. The optimum performance of ferrite parametric amplifiers depends on the high power properties of the materials used in such devices.[10] In most cases the nonlinear effects must be avoided but in some cases they can be used advantageously, as in parametric amplifiers and limiters. It is, therefore, very important to understand the factors that influence the onset of nonlinearities and to be able to control these factors.

The critical field h_∞, which characterizes the onset of nonliner effects can obviously be increased by increasing the linewidths ΔH and ΔH_k and by decreasing the saturation magnetization. In practically all applications a small linewidth ΔH is desirable. A useful improvement in the power-handling capacity can, therefore, be obtained only by increasing the spin-wave linewidth ΔH_k or by decreasing the saturation magnetization. The present experiments have shown that ΔH and ΔH_k very often differ by an order of magnitude and that, to a certain extent, they can be controlled independently.

The fact that ΔH_k is approximately independent of the porosity (and independent of the surface roughness of single crystal samples), suggests that this linewidth is characteristic of the intrinsic losses of the material. It has previously been observed by Le Craw and Spencer[11] that in single crystals of yttrium garnet ΔH_k is essentially independent of the surface roughness, whereas ΔH increases rapidly with the surface roughness.[12]

The fact that in the yttrium-holmium garnet ΔH_k increases rapidly with the holmium content can be understood in terms of a theory recently developed by de Gennes, et al.[13] According to this theory the magnetic moment of the rare earth ions (with the exception of gadolinium) relaxes extremely rapidly because of strong spin orbit interaction. For this reason small amounts of any rare earth metal (with the exception of gadolinium) in yttrium garnet should increase ΔH_k very rapidly. ΔH should be effected in essentially the same way, but for small substitution the increase in ΔH is not as readily and unambiguously observable because the linewidth is still predominantly caused by inhomogeneity broadening. Experiments on samarium substituted yttrium garnet have qualitatively confirmed the theoretical expectations.

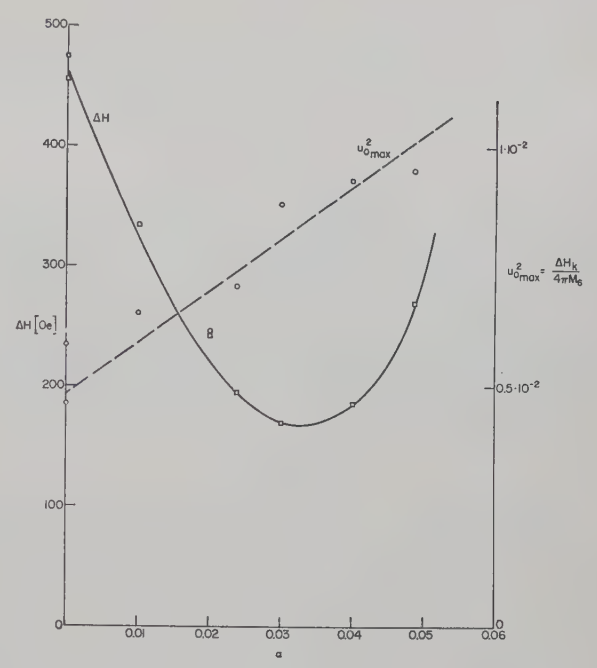

Fig. 5—Linewidth and maximum amplitude of the uniform mode for spherical samples of $Ni_{1-\alpha}Co_\alpha Mn_{0.02}Fe_{1.9}O_4$ as a function of the composition.

Similar arguments apply to the nickel-cobalt ferrite series. The magnetic moment of the cobalt ion is believed to relax appreciably faster than that of the nickel ion.[14] This can be inferred from the large linewidth observed in single crystal cobalt ferrite[15,16] and is also consistent with the large crystalline anisotropy of this material.

Acknowledgment

One of the authors (J. J. Green) is particularly indebted to Dr. L. C. Hogan for his suggestion to investigate the high power phenomena in ferrites and garnets. Both authors would like to acknowledge many stimulating discussions with Prof. R. V. Jones and Dr. M. H. Sirvetz. The technical assistance of Mrs. L. Lin, F. Molea, and C. Quadros is also gratefully acknowledged.

[10] R. W. Damon and J. R. Eshbach, "Theoretical limitations of ferrite parametric amplifier performance," presented at PGMTT meeting, Cambridge, Mass., June 1–3, 1959; G. E. Tech. Rept. 59-RL-2230E.

[11] R. C. Le Craw and E. G. Spencer, "Surface-independent spin-wave relaxation in ferromagnetic resonance of yttrium iron garnet," *J. Appl. Phys.*, vol. 30, pp. 185S–186S; April, 1959.

[12] In Le Craw and Spencer, *Ibid.*, ΔH_k is determined from the first onset of nonlinear effects, rather than by extrapolation from the high power behavior as in the present paper. The procedure followed in Le Craw and Spencer leads to much smaller values of ΔH_k, and it is believed to be in error, since it does not take into account the influence of inhomogeneities on the high power behavior. In the present context the difference between the two methods of obtaining ΔH_k is not very important, because the two values generally differ by a constant factor.

[13] P. G. deGennes, C. Kittel and A. M. Portis, to be published.

[14] R. L. White, "Ferromagnetic resonance line widths and g-factors in ferrites," *Phys. Rev. Letters*, vol. 2, pp. 465–466; June 1, 1959.

[15] J. O. Artman, "Microwave resonance relations in anisotropic single crystal ferrites," Proc. IRE, vol. 44, pp. 1284–1293; October, 1956.

[16] P. E. Tannenwald, "Multiple resonances in cobalt ferrites," *Phys. Rev.*, vol. 99, pp. 463–464; July 15, 1955.

Microwave Diode Cartridge Impedance*

R. V. GARVER† AND J. A. ROSADO†

Summary—**In any application of a semiconductor microwave diode, the impedance of the diode cartridge plays a very important role. Two commonly made assumptions, which are quite erroneous, are that 1) the impedance of the diode cartridge consists simply of a shunt capacitance and whisker inductance, and 2) the metal-to-semiconductor junction at microwave frequencies behaves approximately as it does at 10 mc. In this paper it is shown that the impedance of the diode cartridge at microwave frequencies can be measured accurately by substituting a carbon die for the semiconductor.**

Introduction

NEW uses of junction diodes at microwave frequencies as switches,[1] attenuators, phases modulators, frequency translators,[2] and amplifying elements,[3] make it more important than ever to understand the semiconductor junction at these microwave frequencies. To measure junction impedance at microwave frequencies, the junction must be in a cartridge and the cartridge impedance must be known. Early work of this type was done by M. C. Waltz.[4] In the present work some of the error found in the original technique has been reduced and a reactive anomaly[5] has been investigated.

Measurement Technique

Historically, two techniques have been utilized for measuring diode cartridge impedance at microwave frequencies. M. C. Waltz[4] replaced the semiconductor die in the diode by a carbon die and then placed the diode in a rectangular waveguide mixer mount. Observation of the microwave reflections with changing contacts on the carbon revealed the cartridge impedance. Penin and Skvortsova[6] fabricated diodes at the end of a 50-ohm coaxial line and used an open, short, and forward-biased diode to determine the cartridge impedance. Both groups of experimentalists also placed transformers before their diodes as an alternate technique which allowed them to measure diode junction impedances directly.

One point should be borne in mind here. Impedance measurements made in a waveguide are made with respect to the characteristic impedance of the waveguide. Measured impedances that differ from the waveguide impedance by a factor of ten or more are increasingly obscured by the waveguide impedance. Thus a rectangular waveguide is most useful for measuring impedances on the order of 500 ohms, while a coaxial waveguide is most suitable for measurements of impedances on the order of 50 ohms. For the most accurate impedance measurement, one would ideally vary the waveguide impedance to match that being measured. The greater bulk of point-contact diode impedances at microwave frequencies are in the 500-ohm region; thus it is most desirable to use a rectangular waveguide to make point-contact diode measurements.

Equivalent Circuits

The diode cartridge can be visualized as a linear, passive, lossless four-terminal network with two accessible terminals, the outside ends, and two inaccessible terminals, the terminals of the rectifying contact. The frequency-independent equivalent circuit for the cartridge may be impossibly complex, but for a given frequency it can be represented by three reactive elements in a π or T arrangement, or by any three independent lossless impedance transformations. For example, the equivalent circuit used by M. C. Waltz[4] consisted of 1) a length of transmission line, 2) a parallel susceptance, and 3) a transformer-turns ratio.

In order to evaluate the three elements of the equivalent circuit, it is necessary to substitute three known impedances for the rectifying contact. It should be noted that for all diodes that are supposed to have the same cartridge impedance, precautions must be taken to maintain the following constant: diode whisker length, straight and bent; whisker diameter; bend configuration; whisker tilt and centering of contact; and whisker orientation with respect to the waveguide. Of the three known impedances to be substituted for the rectifying contact one is an open, one a short, and the other, some form of resistor. The open consists of a diode of the type to be measured with the contact separated only enough to impede direct current. It is important that the image capacitance of the whisker to semiconductor be included in the equivalent circuit of the cartridge. This is insured by separating them only enough to prevent the flow of direct current.

The short is obtained by substituting solder for the

* Manuscript received by the PGMTT, June 3, 1959. Revised manuscript received September 11, 1959.

† Diamond Ordnance Fuze Labs., Washington, D. C.

[1] R. V. Garver, E. G. Spencer, and M. A. Harper, "Microwave semiconductor switching techniques," IRE TRANS. ON MICROWAVE THEORY AND TECHNIQUES, vol. MTT-6, pp. 378–383; October, 1958.

[2] E. M. Rutz and J. E. Dye, "Frequency translation by phase modulation," 1957 IRE WESCON CONVENTION RECORD, vol. 1, pt. 1, p. 201.

[3] A. Uhlir, Jr., "The potential of semiconductor diodes in high-frequency communications," PROC. IRE, vol. 46, pp. 1099–1115; June, 1958.

[4] M. C. Waltz, "A Microwave Resistor for Calibration Purposes," Bell Telephone Labs., Third Interim Rept. on Task 8 (Crystal Rectifiers), Signal Corps Contract DA-36-039-sc-5589; April, 1955.

[5] D. Leenov, "Small-Signal Admittance of a Gold Bonded Diode," Bell Telephone Labs., Tenth Interim Rept. on Task 8 (Crystal Rectifiers), Signal Corps Contract DA-36-039-sc-5589; January, 1957.

[6] N. A. Penin and N. E. Skvortsova, "The impedance of the rectifying contact in germanium and silicon detectors at microwave frequencies," *Radiotekh. Elektron.*, vol. 3, pp. 267–275; February, 1958. (Complete translation from International Physical Index, Inc., New York 35, N. Y., Electronics Express No. Ex 1A13.)

semiconductor and by soaking the pedestal in mercury. The mercury insures a low-impedance contact without excessive contact pressure which would distort the whisker and would change its impedance. Penin and Skvortsova[6] used a forward-biased diode junction for the resistor and Waltz[4] used resistive dice fabricated from pencil lead and resistors. The dice are substituted for the semiconductor dice and "resistive" contacts are made upon them. There is no assurance that a forward-biased diode junction is purely resistive, nor is there any assurance that carbon is purely resistive at high frequencies. Since the diode cartridge is being evaluated to study the semiconductor junction, no assumptions will be assigned to the semiconductor junction. Therefore the carbon mixtures are used in evaluating the cartridge impedance. In pencil lead and in resistors the carbon mixtures consist of high-conductivity carbon particles held together by low-conductivity bonding material. This inhomogeneity of conductivity in the material results in a distributed capacitance, the effect of which is observed for small area contacts. For contact areas sufficiently large the distributed capacitance effect is negligible. It is noted that the radius of contact is less than the skin depth of the carbon even for the lowest resistance-calibrating resistors used.

Techniques for canceling out the elements of the equivalent circuit allow the contact impedance to be measured more directly. 1) Placing a tuner before the diode or changing the position of the short after the diode, so that the difference in minima for the open and shorted contacts is $\lambda_g/4$ (where λ_g is the waveguide wavelength), 2) making all measurements with reference to the shorted contact minimum, and 3) taking the impedance of the configuration (which is computed from the known resistor) to include the transformer-turns ratio and the waveguide impedance, all allow the impedance of the diode contact to be directly observed from the Smith Chart. The above technique would appear to be the most elegant for making measurements, but for some contact impedances the diode is partially reflecting and cavity effects take place between the diode, short, and any tuning elements present. For example, with an open contact, as much as 90 per cent of the incident power can be absorbed by wall losses and the diode ceramic, and 3 per cent of the incident power can be forced out the coaxial choke. This reduces what should be an infinite VSWR to 1.7. This is an extreme example, but it demonstrates the cavity effect. Elimination of this effect requires a calculation which makes this technique as indirect and undesirable as a more passive observational technique.

To assure that cavity effects are not present, measurements are made with a matched load behind the diode. All measurements are made with reference to the exact center of the cartridge. The conductance of the matched load is easily and accurately subtracted from the measured impedances to give the diode impedance. Fig. 1 represents the impedances involved in the above

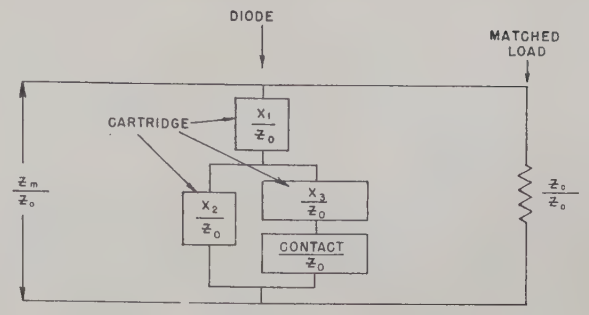

Fig. 1—Equivalent circuit of a microwave diode in a bilaterally matched waveguide section for a given frequency, using the T element arrangement for the diode cartridge impedance.

measurement technique. Z_m/Z_0 is the measured impedance taken with a slotted-line and Smith Chart Plot. X_1/Z_0, X_2/Z_0, and X_3/Z_0 are elements of a T equivalent circuit, for the cartridge. The T network is recommended for theoretical calculations of device behavior. For measurements of diode junctions and for less involved calculations of diode device behavior, simplicity is achieved by means of having the equivalent circuit consist of a length of transmission line, a series reactance, and a factor including the transformer-turns ratio and Z_0.

An Example—X Band

The 1N23 cartridge impedance has been extensively analyzed at 9300 mc. To mount the diode in the waveguide, a standard detector mount is modified by replacing the microwave-shorted end with a waveguide flange. The result is a transmission-type waveguide crystal mount. This crystal mount is connected directly to the SWR machine and a matched load is attached behind the crystal mount. The frequency remains constant and the reference plane of the diode center is constant; thus measurements can be facilitated by marking on the Smith Chart the minima that could be observed on the slotted line as shown in Fig. 2. Further simplification is attained by plotting the data across the center of the Smith Chart as admittance, subtracting $(Y_0/Y_0)=1+j0$, and crossing the center again to be rid of the matched load. By virtue of the matched load, all of the initial data in Fig. 2 falls within the small circle to the left of the chart center. If the resistors were all purely resistive, the data would lie on the dashed arc. Their deviation from the dashed arc was difficult to understand. Without knowledge of the mechanism causing the deviation, considerable uncertainty accompanies any evaluation of the equivalent circuit of the diode cartridge. Assuming the mechanism to be distributed capacitance from inhomogeneous conductivity in the resistive material, the dashed arc is drawn as the true curve from which to determine the equivalent circuit of the cartridge.

Fig. 3 is the initial data after computational removal of the matched load. Rotating the data points $0.233\lambda_g$ counterclockwise on the Smith Chart causes the $R=\infty$ data point to lie on $\infty+j\infty$. Subtraction of $+j$ 1.95

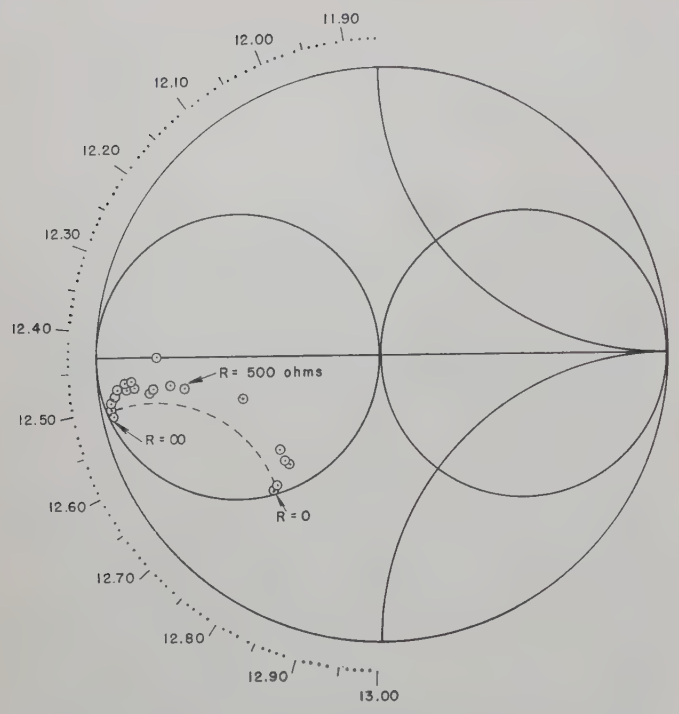

Fig. 2—Smith Chart plot of initial data from "resistive" contacts for evaluation of diode cartridge impedance. The data is measured with reference to the exact center of the diode. The matched load after the diode causes the data to fall within the circle to the left of the center of the chart.

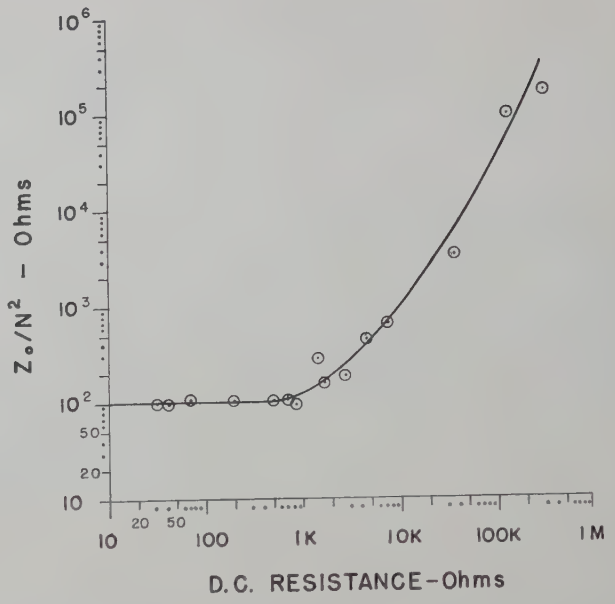

Fig. 4—Using an equivalent circuit for the diode cartridge consisting of a length of transmission line, a series reactance, and a transformer having turns ratio N, the factor Z_0/N^2 is plotted against the dc measured resistance to demonstrate the effect of the distributed capacitance of the carbonateous mixture upon which resistive contacts are made. The plot demonstrates that the effect is negligible for contacts whose dc resistance is less than 1000 ohms.

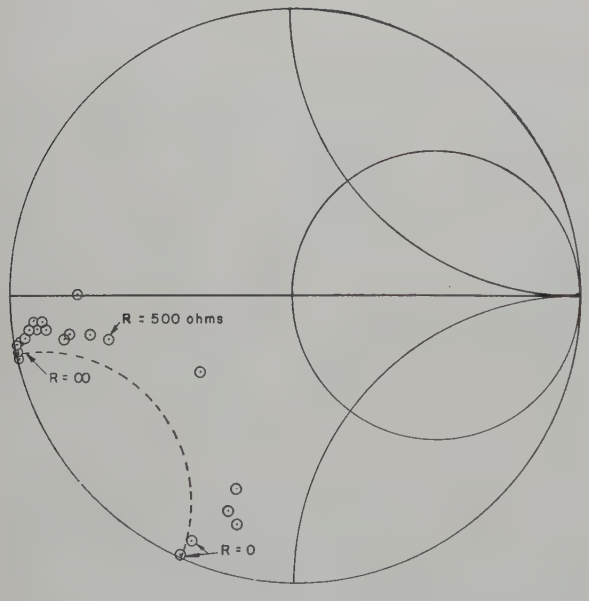

Fig. 3—Smith Chart plot of initial data after computational removal of the effect of the matched load.

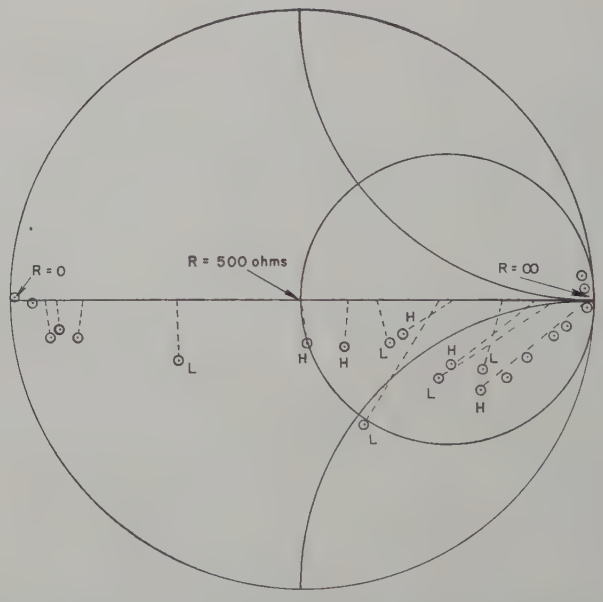

Fig. 5—Smith Chart plot of the "resistive" contact impedance with 500 ohms assumed as chart center. The L and H data points are from resistive contacts made respectively on pencil lead and on 10-ohm resistor material.

from the data points causes the $R=0$ data point to lie on $0+j0$. There remains the evaluation of the transformer-turns ratio factor. Dividing the Smith Chart resistive component of each data point into its dc measured resistance gives the factor Z_0/N^2 by which each data point must be multiplied in order to have it in units of ohms. In Fig. 4 this factor is plotted against the dc measured resistance. For high dc resistance (small area contact) it is seen that the factor is not a constant but increases with resistance. For low dc resistances it is a constant and this is assumed to be its correct value. With 500 ohms as the Smith Chart center and $Z_0/N^2=100$, the data of the resistors is plotted in Fig. 5. Dashed lines are drawn from the data points to the values they would have if they were purely resistive. Two points resulting from the distributed capacitance of the resistive material should be noted. One is that no high-frequency resistance can be greater than the dc

resistance. This fact forced the choice of the minimum Z_0/N^2. The other point is that one should be able to combine small area impedances with shunting resistances and capacitances as the area of contact is increased by reasonable approximations to attain a large area impedances. This can be done reasonably well with the data as plotted in Fig. 5. Deviations from conformity to this second requirement may be caused by the whisker point digging pits in the resistive material and touching loose particles or by the whisker point sliding along the surface of resistive material. The resistive material is mounted on a pedestal which is the end of a threaded screw that turns to change the contact pressure. For light-pressure contacts, slight nonecentering of the whisker point could result in the whisker point sliding along the surface of the resistive material. Such jumps in microwave impedance could not be described by additional parallel capacitors and resistors in the contact region.

To determine the impedances shown in Fig. 1, reference is made to Fig. 3. By placing this plot upon another Smith Chart so that the $R=\infty$ data point falls on the $\infty+j\infty$ point of the underlying Smith Chart, a curve of constant resistance can be traced from a high resistive data point R (which demonstrated negligible deviation of Z_0/N^2 in Fig. 4), to intersect the dashed arc. In Fig. 3 the reactance of the $R=\infty$ data point is termed Δ. The reactance of the $R=0$ data point is termed X_0. Then the following formulas apply:

$$\frac{X_1}{Z_0}=\Delta-\frac{X_2}{Z_0},$$

$$\frac{X_2}{Z_0}=\delta\left(1\pm\sqrt{1+2\frac{X_3/Z_0}{\delta}}\right),$$

and

$$\delta=\frac{\Delta-x_0}{2}.$$

X_3/Z_0 is found by trial and error by substituting R for the contact impedance of the equivalent circuit of Fig. 1 and computing the total diode impedance. Two values of X_3 can be found to satisfy the data, but the value which maintains all impedances nearest to unity is selected, since less error will be introduced into the calculations by it. The values found for the data shown are

$$\frac{X_1}{Z_0}=.474,\quad \frac{Z_0}{X_2}=1.745,\quad \text{and}\quad \frac{X_3}{Z_0}=1.15.$$

At first glance, it would appear that X_1 corresponds to the crystal holder choke, X_2 corresponds to the diode cartridge capacity, and X_3 corresponds to the whisker inductance. The whisker inductance would then be 10×10^{-9} henries, but physical measurements and lower-frequency measurements indicate its inductance to be 5×10^{-9} henries, ignoring whisker capacitance. X_2, the cartridge capacitance, measures 0.06 $\mu\mu$f here, but at lower frequencies it measures 0.02 $\mu\mu$f. The crystal holder choke is well designed and should exhibit no impedance. Consequently the impedances of the equivalent circuit of Fig. 1 cannot be attributed to individual effects but must be considered as a lumped equivalent circuit for the diode cartridge. The values of the equivalent circuit elements hold only at one frequency and in a full size X-band rectangular waveguide. At other frequencies or in a coaxial or a ridged waveguide or in other cartridges the parameters will have to be re-evaluated. The technique presented here should work under any circumstances.

Conclusion

It is concluded that: 1) at a given frequency, the diode cartridge can be represented by three independent lossless impedances or impedance transformations; 2) the best technique for measuring microwave diodes is to place the diode in a rectangular waveguide with a matched load thereafter; 3) the best technique for the evaluation of the cartridge impedance makes use of the substitution of resistive dice for the semiconductor; 4) the reactive anomaly observed with the contacts on the resistive dice is from distributed capacitance of the inhomogeneous resistive material; and 5) this effect is negligible for large area contacts.

Acknowledgment

The authors would like to express their gratitude to J. E. Tompkins and R. D. Hatcher for their continued interest and helpful discussions.

Theory of the Germanium Diode Microwave Switch*

R. V. GARVER†, J. A. ROSADO†, AND E. F. TURNER‡

Summary—The application of a generally neglected theory of microwave detection to the poorly understood problem of metal-to-semiconductor junction behavior at microwave frequencies is discussed. Experimental results are disclosed which support the theory and appear to be the first experimental verification of it. It is shown how the theory predicts that germanium microwave diodes should exercise direct switching action upon microwaves while silicon microwave diodes should not, as had been observed in the past but with no explanation.

Introduction

FOR several years it has been known that germanium microwave diodes exercise direct switching action upon microwaves while silicon microwave diodes do not.[1] The gross difference in switching action between germanium and silicon implies some fundamental difference between the germanium and silicon metal-to-semiconductor junctions at microwave frequencies. No satisfactory explanation of this difference has hitherto been published. Little is known of the microwave frequency behavior of metal-to-semiconductor junctions. The popular assumption is that at a given reverse bias the junction equivalent circuit elements (a parallel capacitor and resistor) are unchanged from 10 mc to 10,000 mc. If this were true, the rectifying efficiency of diodes would decrease much more rapidly with frequency than is actually observed. Lawson[2] has formulated a theory based on majority carrier trapping which purports to explain microwave detection; however, Lawson's theory has never been verified experimentally and consequently it is seldom used. Designers of microwave diode devices to date[3,4,5] use empirical techniques in the absence of a complete precise theory.

New uses of junction diodes at microwave frequencies as switches, attenuators,[6] phase modulators, frequency translators,[7] and amplifying elements,[8] make it more important than ever to know the behavior of junctions at microwave frequencies.

The impedance of a diode junction is determined by the flow of currents across the junction. The junction current is made up of minority carriers and/or majority carriers. At higher frequencies the junction impedance is determined by the trapping of these minority and/or majority carriers. Shockley[9] presented several solutions for the junction impedance assuming minority carrier current. Penin and Skvortsova[10] have made measurements on point-contact junctions for forward currents at microwave frequencies, showing some correlation between minority carrier theory and their data. Lawson[2] presented a solution for the junction impedance assuming majority carrier current. Presented here is experimental verification of his theory. M. Cutler,[11] studying dc characteristics of point-contact diodes, considered the case in which current consists of both minority and majority carriers and demonstrated their coexistence. For forward currents, Penin and Skvortsova[10] found fair agreement with minority carrier theory if they could assume very short minority carrier lifetimes on the surface of the semiconductor. This indicates that a large portion of the forward current is due to minority carrier flow in the semiconductor. The data for germanium presented here for a small reverse bias more closely fits Lawson's theory for majority carrier current than Shockley's theory for minority carrier current, while no good correlation can be made between the silicon data and majority carrier theory. Thus, it is concluded that the current, flowing for a small reverse bias on the germanium

* Manuscript received by the PGMTT, June 3, 1959; revised manuscript received, September 11, 1959.

† Diamond Ordnance Fuze Labs., Washington, D. C.

‡ Dept. of Physics, Washington and Lee University, Lexington, Va. Summers, Diamond Ordnance Fuze Labs., Washington, D. C.

[1] M. A. Armistead, E. G. Spencer, and R. D. Hatcher, "Microwave semiconductor switch," PROC. IRE, vol. 44, p. 1875; December, 1956.

[2] H. C. Torrey and C. A. Whitmer, "Crystal Rectifiers," M.I.T. Rad. Lab. Ser., McGraw-Hill Book Co., Inc., New York, N. Y., vol. 15, pp. 100–107; 1948. This work summarizes A. W. Lawson's "High-Frequency Rectification Efficiency of Crystals."

[3] G. C. Messenger and C. T. McCoy, "Theory and operation of crystal diodes as mixers," PROC. IRE, vol. 45, pp. 1269–1283; September, 1957.

[4] D. A. Jenny, "A gallium arsenide microwave diode," PROC. IRE, vol. 46, pp. 717–722; April, 1958.

[5] R. V. Garver, E. G. Spencer, and R. C. Le Craw, "High-speed microwave switching of semiconductors," *J. Appl. Phys.*, vol. 28, pp. 1336–1338; November, 1957.

[6] R. V. Garver, E. G. Spencer, and M. A. Harper, "Microwave semiconductor switching techniques," IRE TRANS. ON MICROWAVE THEORY AND TECHNIQUES, vol. MTT-6, pp. 378–383; October, 1958.

[7] E. M. Rutz and J. E. Dye, "Frequency translation by phase modulation," 1957 IRE WESCON CONVENTION RECORD, vol. 1, pt. 1, p. 201.

[8] A. Uhlir, Jr., "The potential of semiconductor diodes in high-frequency communications," PROC. IRE, vol. 46, pp. 1099–1115; June, 1958.

[9] W. Shockley, "The theory of p-n junctions in semiconductor and p-n junction transistors," *Bell Sys. Tech. J.*, vol. 28, pp. 435–489; July, 1949.

[10] N. A. Penin and N. E. Skvortsova, "The impedance of the rectifying contact in germanium and silicon detectors at microwave frequencies," *Radiotekh. Elektron.*, vol. 3, pp. 267–275; February, 1958. (Complete translation from International Physical Index, Inc., New York 35, N. Y., Electronic Express No. Ex 1A13.)

[11] M. Cutler, "Point contact rectifier theory," IRE TRANS. ON ELECTRON DEVICES, vol. ED-4, pp. 201–206; July, 1957.

point-contact diodes studied here, is largely majority carrier current.

It is shown that a difference exists between germanium and silicon and that the germanium should work well as a switch in the standard microwave diode cartridge while silicon should not. This confirms earlier observations.

Data on Diodes

At a fixed reverse bias voltage, the impedance of point contacts on N-type germanium and P-type silicon were measured from 1 mc to 10 kmc. Measurements from 1 mc to 200 mc were made on the Boonton parallel RC bridge. Measurements at C and X-band were made in waveguide by the techniques reported by Garver and Rosado.[12]

The equivalent circuit for the diode junction at reverse bias is assumed to be a parallel resistance and capacitance. Figs. 1 and 2 respectively show the resistance and capacitance for germanium and silicon as functions of frequency. Special weight is assigned to 9.3-kmc data because it is the frequency at which the measurement technique was refined. The bridge measurements are considered to be those of typical diodes, independent of donor density in the range of 10^{16}–10^{18} donors per cm^3 for Ge (*e.g.*, 1N263) and 10^{19} acceptors per cm^3 for Si (*e.g.*, 1N23).

Very little will be said concerning the silicon diode data. The equivalent circuit assumed for the plots of Figs. 1 and 2 is not valid above 2 kmc for silicon because of high spreading resistance. The forward and reverse data plotted in Fig. 5 is similar to the observations of Penin and Skvortsova[10] which come fairly close to minority carrier theory. The germanium diode data however, plotted as Resistance vs Reactance for changing current, gives more of a straight line which implies that the depletion layer capacitance (from majority carrier current) is predominant over the diffusion capacitance (from minority carrier current).

Lawson's Theory[2]

Lawson's theory evolves from considerations of the probability per unit time for the ionization of a bound impurity atom. Of N impurity atoms n_0 are ionized at room temperature leaving $N-n_0$ bound majority carriers. The relaxation time constant τ for this ionization process is found to be

$$\tau = \frac{n_0}{(2N - n_0)B},$$

in which B is the ionization probability in unit time.

[12] R. V. Garver and J. A. Rosado, "Microwave diode cartridge impedance," this issue, pp. 104–107.

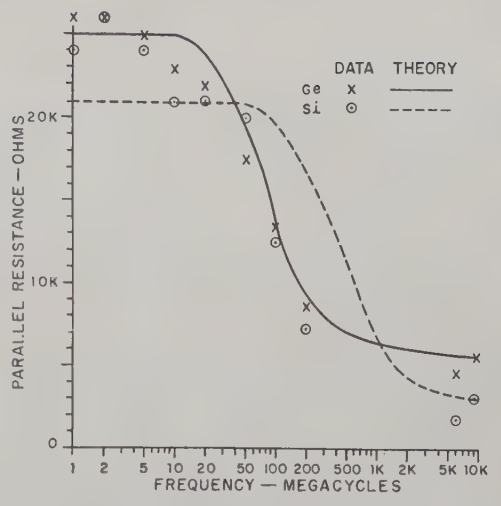

Fig. 1—Parallel resistance of a germanium and a silicon diode at a fixed reverse bias as a function of frequency.

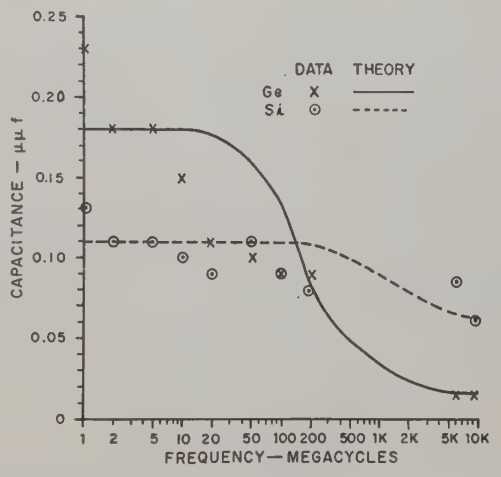

Fig. 2—Parallel capacitance of a germanium and a silicon diode at a fixed reverse bias as a function of frequency.

The portion of free-charge carriers with no field applied at room temperature is n_0/N, which should be about 1.00 for germanium. B may have any value from 10^6 seconds^{-1} to 10^{10} seconds^{-1}. Imperfections other than donors or acceptors in a material would change the value of an observed B because of the trapping of these additional impurities. The edge of a semicoductor, owing to the interruption of the lattice at an edge, contains impurities caused by irregularities in the lattice. The edge is also subject to absorption of gases which introduce impurities. And finally, the force exerted by a whisker and by heating in fabrication, can result in additional dislocation impurities and in possible diffused impurities that precede from the whisker into the semiconductor contact region or from the contact region further into the body of the semiconductor.

The parallel junction capacitances at zero frequency and infinite frequency are respectively C_0 and C_∞. The conductances are respectively G_0 and G_∞.

$$C_0 - C_\infty = \Delta_C \qquad G_\infty - G_0 = \Delta_G = G(\infty)$$

$$C(x) = C_0 - \Delta_C F_2$$

$$G(x) = G_0 + \Delta_G \frac{G(x)}{G(\infty)}$$

$$B = \frac{2}{3}\frac{\Delta_G}{\Delta_C} \qquad \frac{n_0}{N} = \frac{C_\infty}{C_0}$$

Fig. 3 shows F_2 and $G(x)/G(\infty)$ taken from Lawson[2]. It should be noted that the curves are incorrectly labeled in Torrey and Whitmer.[2]

According to minority carrier theory the conductance at infinite frequency becomes infinite. According to Lawson's theory the conductance at infinite frequency remains finite. For germanium the parallel resistance measured at lower frequencies (Fig. 1) would indicate essentially zero resistance at 10 kmc if minority carrier theory applied, but the data closely follow Lawson's majority carrier theory. In Fig. 2, the data for germanium deviate slightly from Lawson's theory. The discrepancy may be the result of B being multivalued or indiscrete. That is to say, more than one type of impurity may be dominant; for example, impurities frozen into the semiconductor lattice at different energy levels may give multiple discrete values of ionization energy or may even give a continuous range of ionization energies. Lawson's theory is based upon one discrete ionization energy.

To obtain the theoretical curves, it was assumed that

$$G_\infty = 1.82 \times 10^{-4} \text{ mhos}$$
$$G_0 = 0.4 \times 10^{-4} \text{ mhos}$$
$$C_0 = 0.18 \times 10^{-12} \text{ farad}$$
$$C_\infty = 0.012 \times 10^{-12} \text{ farad for germanium}$$

and

$$G_\infty = 3.76 \times 10^{-4} \text{ mhos}$$
$$G_0 = 0.476 \times 10^{-4} \text{ mhos}$$
$$C_0 = 0.11 \times 10^{-12} \text{ farad}$$
$$C_\infty = 0.057 \times 10^{-12} \text{ farad for silicon.}$$

This would indicate that 7 per cent of the carriers are free in germanium. This value for germanium is very low and would indicate that the energy level of the traps is much lower in the forbidden band than the donor impurity energy level. It might indicate that the depletion layer is receding only slightly into the neutral region, contributing only 7 per cent to the current, while the remainder of the current is coming from traps in the depletion region, ionized by the greater field caused by the ac test signal. The pulse reverse characteristic of germanium point-contact diodes is different from the dc reverse characteristic. This is also a result of trapping in the depletion region[13].

[13] G. Rupprecht, "Measurement of germanium surface states by pulsed channel effect," *Phys. Rev.*, vol. 111, pp. 75–81; July 1, 1958.

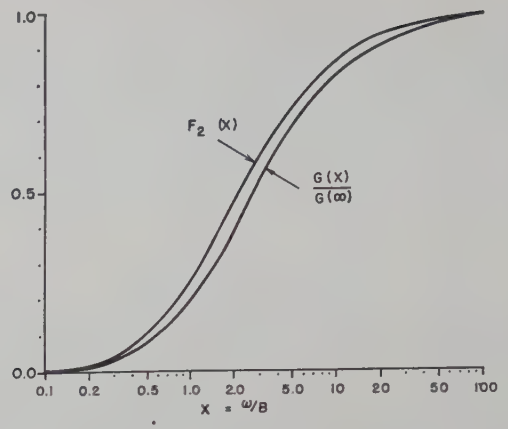

Fig. 3—Variable parameters of Lawson's Theory.[2] It is noted that the curves are incorrectly labeled there.

The values of B for germanium are 5.64×10^8 seconds^{-1}. These are of the anticipated order of magnitude. The lower melting point of germanium, and hence greater disturbance of its surface during fabrication, may account for the large amount of traps in the depletion region with energy gaps greater than those associated with the donor impurities.

To summarize, the current of point contacts on silicon and germanium at a fixed reverse bias may be either due to minority carriers, majority carriers, or both. The data reported here imply that the reverse current is mostly from majority carriers in germanium and from minority carriers in silicon.

Switching

If the diode is a reflecting discontinuity in a plane with a matched load behind it, then the attenuation of a diode switch is defined as the ratio in decibels of the microwave power getting past the diode, to the incident microwave power; and the impedance measured with reference to the exact plane of the diode, gives the attenuation according to $\text{db} = 10 \log (G/1-\Gamma^2)$, in which G is the combined conductance of the diode and matched load, and Γ^2 is the power reflection coefficient (Fig. 4). Eliminating the effects of the matched load and cartridge impedance,[12] attenuation as a function of diode junction impedance is obtained (Figs. 5 and 6). Projecting the reverse impedances of Figs. 1 and 2 into Figs. 5 and 6, shows that germanium gives 20 db or higher isolation while silicon gives less than 3 db. The forward bias data points are also shown in Fig. 5. It is seen that the higher spreading resistance of silicon gives greater than 3 db insertion loss, while the low spreading resistance of germanium allows 1 db or less insertion loss.

Conclusion

The experimental results indicate that germanium closely follows the majority carrier theory of Lawson. This appears to be the first experimental verification of

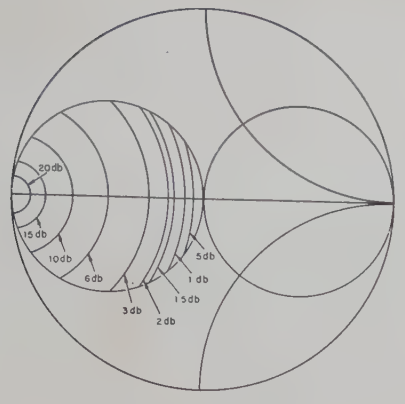

Fig. 4—Attenuation from a planar impedance in a transmission line.

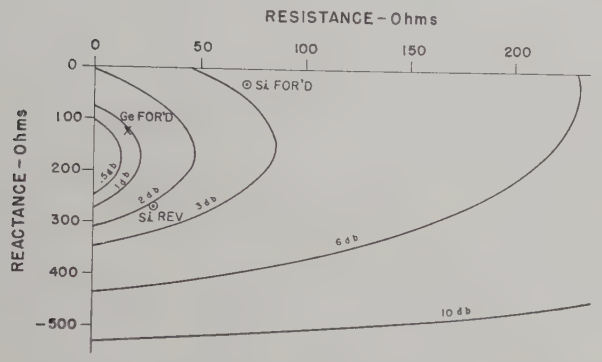

Fig. 5—Attenuation as a function of diode contact impedance for the 1N23 type cartridge at 9300 mc in full size standard *X*-band waveguide. The contact impedances of silicon and germanium are shown to demonstrate their switching behavior.

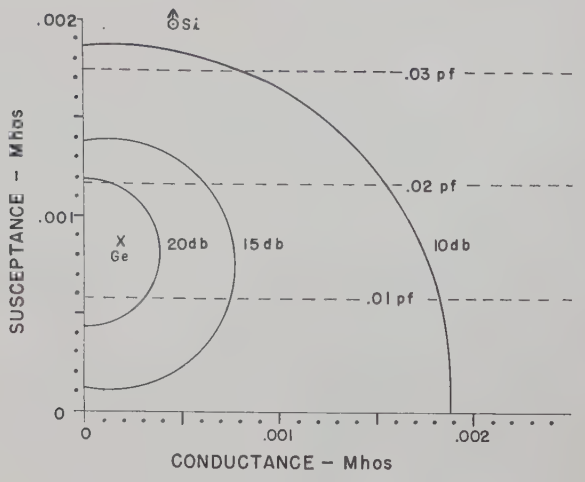

Fig. 6—Attenuation as a function of diode contact admittance for the 1N23 type cartridge at 9300 mc in full size standard *X*-band waveguide. The contact admittance of germanium at reverse bias is shown to demonstrate its good switching behavior.

Lawson's theory. Silicon, on the other hand, appears to follow the minority carrier theory of Shockley. Thus, the observed difference between the microwave switching capabilities of germanium and silicon is provided with a theoretical foundation.

Acknowledgment

The authors would like to express their gratitude to J. E. Tompkins and R. D. Hatcher for their continued interest and helpful discussions.

Improvement in the Square Law Operation of 1N23B Crystals From 2 to 11 kmc*

A. STANIFORTH† AND J. H. CRAVEN†

Summary—**Crystal rectifiers have been used for many years as video detectors in microwave measurements. In most of the applications the detection characteristic at low level is assumed to be square law. It is well known that, in general, this assumption is not justified, particularly if reasonable accuracy is desired. The conditions required to increase the dynamic range over which square law response may be achieved have been investigated experimentally. Results obtained in this laboratory have indicated that a forward bias current of 100 microamperes or more with a low video load resistance made the operation of the crystal closer to the ideal square law over a larger dynamic range.**

* Manuscript received by the PGMTT, June 4, 1959; revised manuscript received, September 16, 1959.

† Radio and Elec. Engrg. Div., National Research Council, Ottawa, Can.

Introduction

CRYSTAL diodes have been used for many years as low-level video detectors of radio-frequency energy both in microwave receivers and in laboratory measuring equipment. The superior low-level performance of the crystal as opposed to a bolometer, together with its small size and short-term stability, make it useful in such applications despite variations between crystals. The crystal rectifier is not limited to the measurement of average power or to low modulation frequencies as are bolometers and thermistors. In its square law region, the crystal is well suited to the comparative

measurements of peak power with either pulse or square-wave modulation.

It had previously been observed in this laboratory that the rectification characteristics of crystal diodes could be improved and the dynamic range of their response extended by the application of a forward bias current. Recently, a more complete investigation was carried out to determine the effect of such factors as dc load resistance, ac load resistance and bias currents on the law of video response of crystal rectifiers in several different types of crystal mounts.

The operation of a crystal diode in the microwave region is the result of a large number of interrelated factors which it is difficult to separate. The RF power applied to the crystal has a marked effect on its RF impedance[1] and also on its video impedance.[2] The values of the ac and dc load resistances into which the crystal feeds will also affect the operation. The application of a forward dc bias current has been found to affect the RF and video impedances and also the rectification efficiency[3,4,5] Some results obtained in this laboratory had also indicated that a forward bias current made the operation of crystal diodes closer to the ideal square law over a larger dynamic range and an investigation was set up to assess the effect of several variable factors on the law of crystal response.

Experimental Measurements

To carry out the required measurements of crystal law the equipment was set up as in Fig. 1. The output of the signal generator fed through a calibrated RF attenuator and a fixed pad to the crystal mount being used. The output of the crystal was connected through the bias unit and a calibrated video attenuator to the video amplifier and thence to the oscilloscope. Broadband untuned crystal mounts were used, most of the measurements being made on an NRC Mark V mount shown in Fig. 2. This mount has a bypass capacitance of approximately 30 $\mu\mu$f.

After adjustment of the variable being investigated (dc or ac load, biasing or change of crystal), the video attenuator was set to zero and the RF attenuator adjusted to give a certain convenient fixed deflection on the oscilloscope. The video attenuation was then increased in 5-db steps. At each step, the calibrated RF attenuator was adjusted to bring the output up to the original level and the setting recorded. For a perfect square law response, each step should require 2.5 db of RF attenuation to be removed for every 5 db of video attenuation inserted. By operating in this manner, the video amplifier signals remained at a constant level and the accuracy of the results depended mainly on the precision of the attenuators. The exponent of crystal law calculated from these readings is probably within the limits ± 0.02. The complete circuit of the crystal biasing unit is shown in Fig. 3. This provides dc loads of 1, 10 and 100 kilohms and ac loads of 50, 200 and 1050 ohms when a 50-ohm load is connected to each of the output terminals in turn.

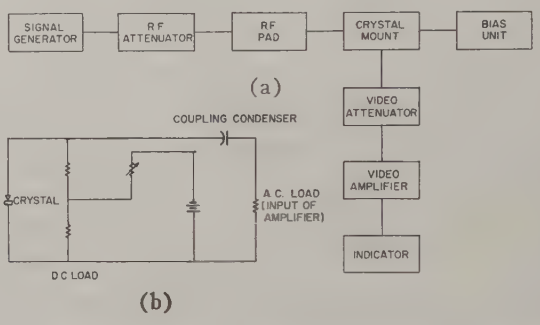

Fig. 1—(a) Block diagram of experimental setup. (b) Simplified crystal bias and coupling circuit.

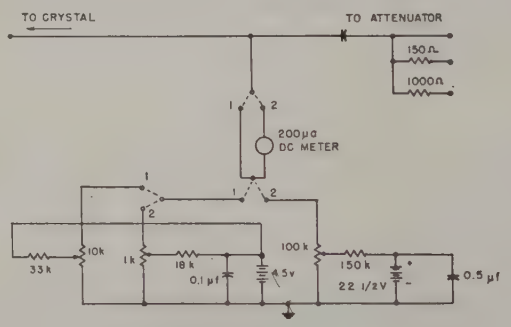

Fig. 2—Bias unit circuit.

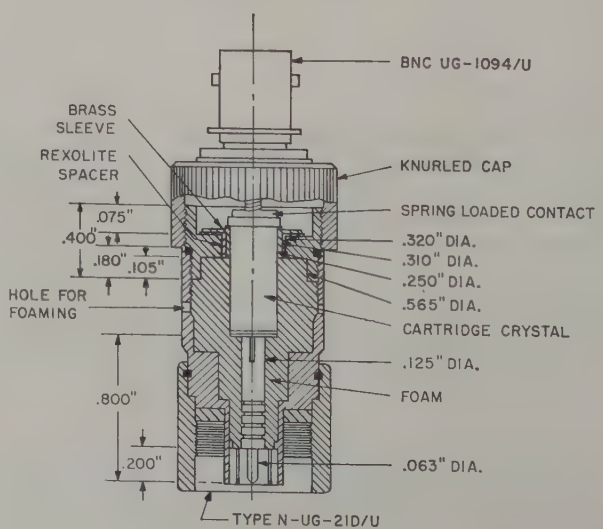

Fig. 3—Sectional view of NRC Mark crystal mount.

[1] H. N. Dawirs and E. K. Damon, "Measurements of crysta impedance at low levels," IRE Trans. on Microwave Theory and Techniques, vol. 4, pp. 94–97; April, 1956.

[2] E. R. Beringer, "Crystal Detectors and the Crystal Video Receiver," Rad. Labs., Mass. Inst. Tech., Cambridge, Mass., Rept. No. 638; November 16, 1944.

[3] W. E. Meyerhof, B. Serin, and R. H. Vought, "X-Band Crystal Performance with Bias," University of Pennsylvania, Philadelphia, Rept. No. NDRC 14-505; July 6, 1945.

[4] E. F. Gallaher and R. L. Crosby, "A transistorized crystal video receiver, *Proc. Natl. Elec. Conf.*, vol. 11, pp. 455–463; 1955.

[5] D. J. Grace, "Some applications of crystal rectifiers in broad-beam microwave circuits," *Microwave Crystal Rectifier Symp. Rec.*, Signal Corps Engrg. Labs., Ft. Monmouth, N. J.; February, 1956.

To facilitate the plotting of such a large number of response curves, the readings were plotted directly on graph paper with the aid of an X-Y plotter.

Effect of Bias and dc Load

After some preliminary measurements in which the characteristics of crystal rectifiers were investigated in rather general terms, experiments were set up to cover more specific conditions of operation. A series of measurements was made to determine the effect of various values of bias current and dc load resistance on the crystal characteristics with an ac load resistance of 50 ohms. The first measurements were made to determine the effect of bias on the crystal sensitivity. With equipment as in Fig. 1, the RF input required to produce a certain fixed video output was measured for different values of bias current and it was found that there was a broad maximum in the rectification efficiency with the peak at approximately 100 μa bias. For this set of measurements, the RF power level at the crystal input was about -25 dbm at 100 μa bias.

Further tests were then carried out to investigate the effects of both bias and dc load resistance. Typical results are shown in Figs. 4, 5 and 6. The curves have been normalized to the 0-db video attenuation level which occurred for 140-μa bias condition at about -35 dbm. The measurements of Fig. 4 were made with a pulse modulated input, an ac load of 50 ohms and a dc load of 100 kilohms. It can be seen that at zero bias the slope of the curve is approximately 2 at the lower end but approaches 3 at higher input levels. For small values of bias current, the slope of the curve becomes less than 2 with progressively lower slopes as the RF input is increased. For larger bias currents, the same general trend is seen but as the bias is increased the approach to the 2.00 slope becomes much closer. How-

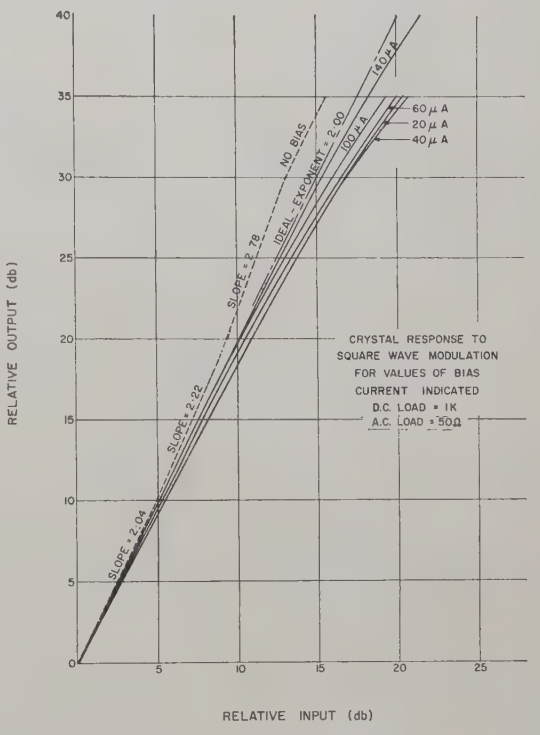

Fig. 5—Effect of bias on law of crystal response—square-wave modulation—1000 ohms dc load.

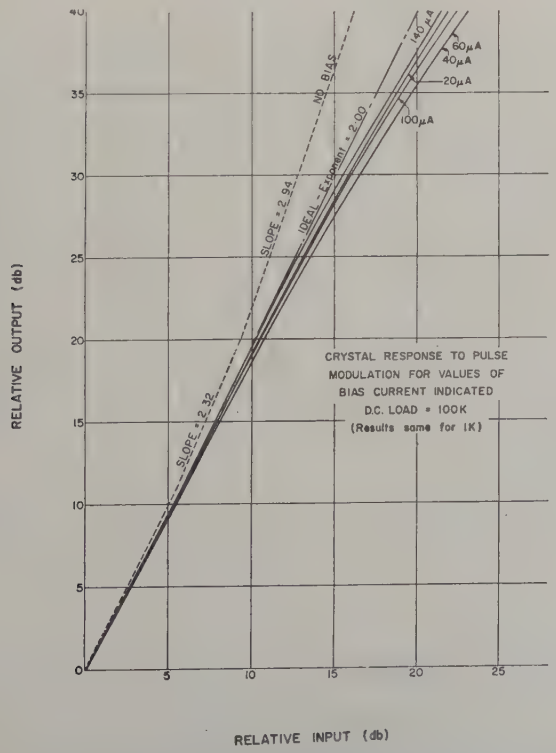

Fig. 4—Effect of bias on law of crystal response—pulse modulation—100 kilohms dc load (1000-ohm dc load similar).

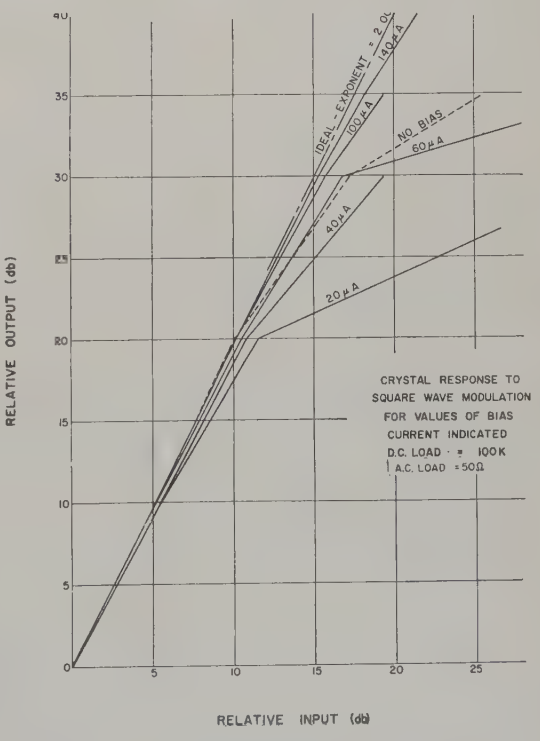

Fig. 6—Effect of bias on law of crystal response—square-wave modulation—100 kilohms dc load.

ever, above 140 μa the change of exponent is very small. Measurements made with a 1000-ohm dc load showed no significant difference.

Measurements on the same crystal with square-wave modulation and 1000-ohm dc load are shown in Fig. 5. The results are very nearly the same as those in Fig. 2. However, when the dc load was increased to 100 kilohms with square-wave modulation a very significant change occurred (see Fig. 6).

For zero bias, the slope of the curve was practically 2 for a good range of signals but at higher levels the slope approached 1, indicating linear rather than square law response. With the application of forward bias, the curve shows a more violent departure from square law for low values of bias but for values above 100 μa the slopes are essentially the same as those shown in Figs. 4 and 5.

It can be seen that for values of bias above 100 μa the exponent of the response law approaches the ideal value of 2.00 over the range measured, with the approach being nearer for larger bias currents. At large bias currents the response becomes practically independent of dc load conditions. The difference between the results for square-wave modulation with the 100-kilohm load and the results for other conditions arises from back biasing which is more pronounced for high-duty cycle and long-time constant conditions.

This back biasing is clearly indicated by the rapid increase of video resistance at higher power levels with square-wave modulation. A comparison of the video resistance for pulse and square-wave modulation with 140 μa forward bias for a typical crystal is shown in Fig. 7. This value of bias was chosen as being a reasonable compromise between the good square law obtained at higher bias and the maximum rectification efficiency obtained at lower bias.

From an examination of the zero bias curves of Figs. 4 and 5, it would appear that there is some value of dc load between 1000 and 100,000 ohms which would produce an exponent close to 2.00 for square-wave modulation. This is true, but the resistance value required to produce the desired result is rather critical and is sensitive to the particular crystal used and the PRF of the square-wave modulation. In particular cases, this method of obtaining good square law response might be justified but at the expense of being of very limited application. Some isolated crystals will give a good square law response with zero bias but will require a lot of measurement and selection to obtain.

With a bias current of 140 μa, the range over which the response of the crystal was nearly square law did not depend to an appreciable extent on the value of the dc load resistance. However, with a low value of dc resistance there was a gradual transition to linear response with increasing power levels, while with the higher values of dc load resistance the response changed abruptly from square law to a limited level due to back biasing (See Fig. 8).

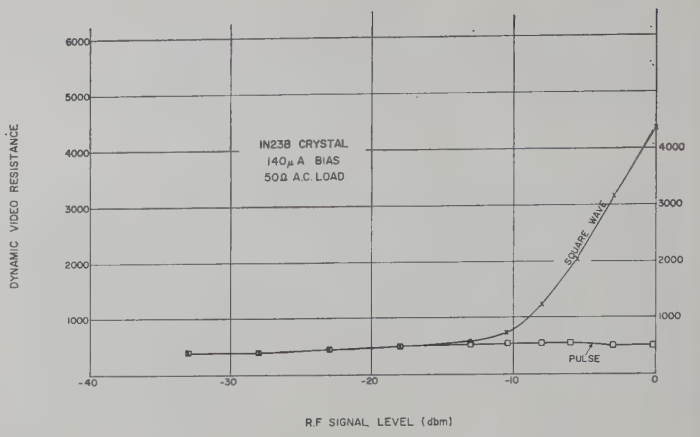

Fig. 7—Dynamic video resistance for pulse and square-wave modulation.

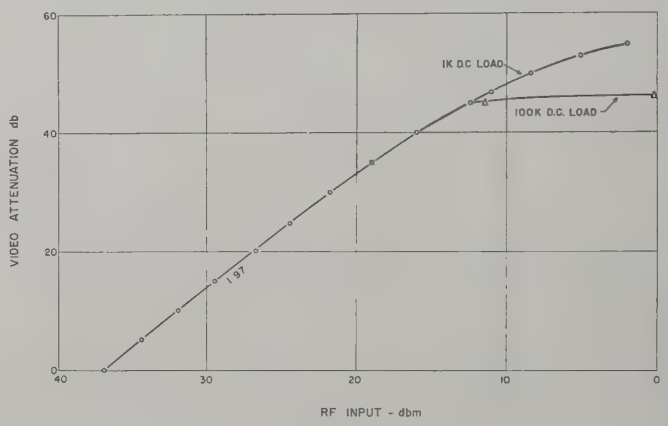

Fig. 8—Effect of dc load on crystal response.

Effect of ac Resistance

With a bias current of 140 μa, an assessment was made of the effect of the law of rectification with a change in the value of the ac load. Measurements were made on a group of crystals with ac loads of 50 and 1000 ohms with both pulse and square-wave modulation. The values of the exponents obtained for the four conditions are shown in Fig. 9. With square-wave modulation, there is decided difference between the two conditions. With the 50-ohm load, the exponents are more closely grouped and the average value is closer to the ideal 2.00. With pulse modulation, the effect is not quite so obvious but the 50-ohm load appears to give a slightly better exponent.

A much larger group of crystals (50) was measured at zero bias, 10-K ac load, and compared with measurements of the same crystals at 140 μa bias and 50-ohm ac load to obtain a quantitative comparison of the improvement obtained with combined bias and low ac load. For zero bias, the slope measured between input powers of −28 and −18 dbm, gave a value of 2.25 ± 0.20 for square wave and 2.30 ± 0.20 for pulse conditions. For 140 μa bias and 50-ohm ac load, the corresponding results were 1.98 ± 0.04 for square-wave and 1.98 ± 0.03 for pulse. A smaller number of crystals measured with

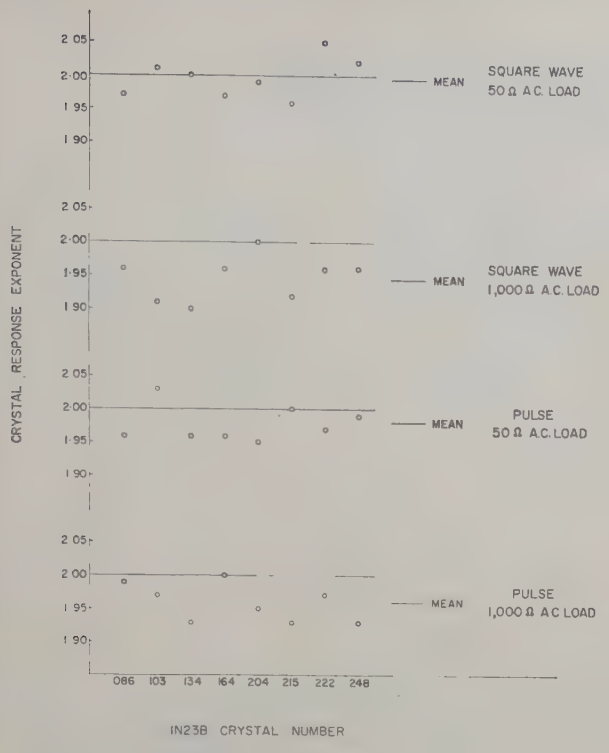

Fig. 9—Effect of ac load on crystal response.

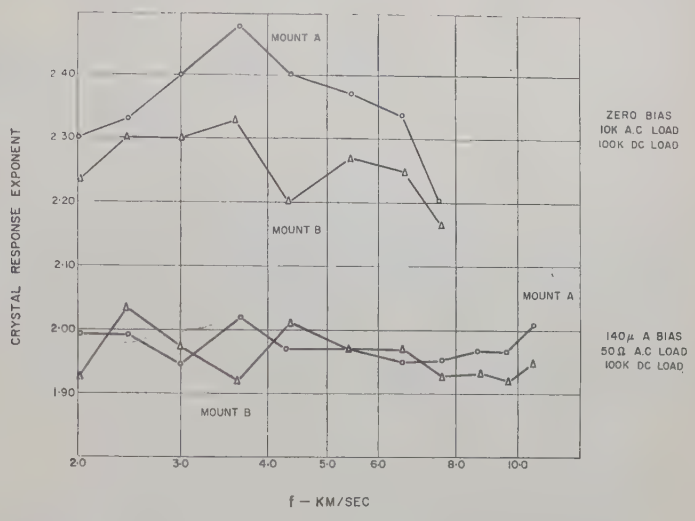

Fig. 10—Effect of bias with other crystal mounts (mounts A and B are commercially available broad-band crystal mounts).

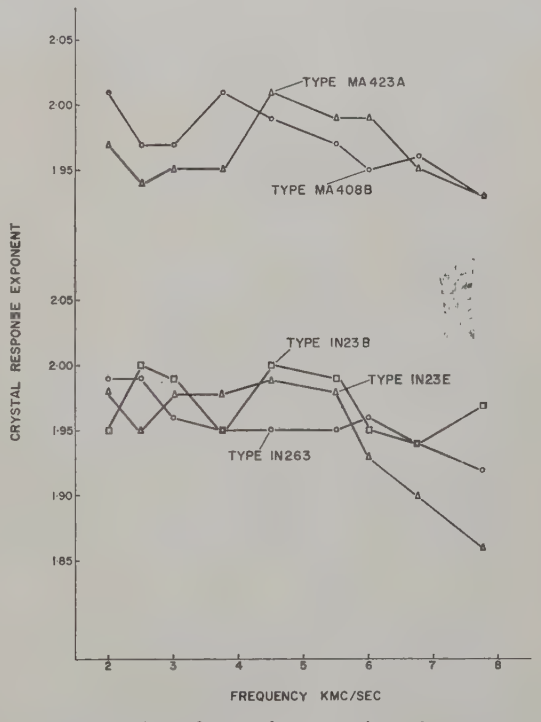

Fig. 11—Effect of crystal type on law of response (measured in NRC Mark V mount).

no bias, pulse modulation, and a 1-K ac load gave a value of 2.22 ± 0.21 indicating no appreciable improvement for a change of ac load under zero bias conditions.

Effect of Crystal Mount

The effect of the crystal mount on the law of the crystal was investigated by measuring the same crystal in several mounts under various conditions of bias and ac load. Typical results are shown in Fig. 10. With 140 μa bias and 50-ohm ac load, the crystal law was practically independent of the crystal mount used within the designed frequency range of the mount and remained close to the ideal 2.00 exponent. All mounts used were of the broad-band untuned type, with both coaxial and waveguide inputs.

Effect of Crystal Type

Although most of the measurements reported here were made on 1N23B type crystals, a number of runs were made with various other types to confim that the results were of general application. The measured exponents of several different crystals in an NRC Mark V mount are shown in Fig. 11. The exponents remain within the limits 1.98 ± 0.05 for the frequency range of the mount (2.0–5.5 kmc).

Conclusion

If it is desired to have a crystal rectifier of the 1N23B or similar type operate as near to the ideal square law as possible over a large dynamic range, it should be operated with a forward bias current of approximately 140 μa and the signal should be developed across a low resistance ac load (50 to 200 ohms). These conditions of operation will give satisfactory results with both square-wave and pulse modulation. These conditions appear to give a response with an exponent of 2.00 ± 0.05 with a wide variety of crystals, mounts and frequencies of operation provided the mounts are used within their design frequency limits.

Acknowledgment

Acknowledgment is made to other members of the National Research Council for their assistance in preparing this paper and to L. Erickson who carried out a large part of the measurement program.

An N-Way Hybrid Power Divider*

ERNEST J. WILKINSON†

Summary—**A circularly symmetric power divider is described which splits a signal into n equiphase equiamplitude parts where n can be odd or even. The power divider provides isolation between output terminals and approximately matched terminal impedances over about a 20 per cent band. A theory of operation is given which yields the necessary design parameters, and an experimental model is described which has a minimum isolation of −27 db between output terminals, an output VSWR of 1.6, and an input VSWR of 1.2.**

Introduction

THE problem of dividing up an input signal into a number of equiphase equiamplitude output signals is a familiar one to RF engineers, particularly those working in the field of phased arrays. It is often desired that the equiphase equiamplitude condition be obtained in a manner which is fundamentally independent of frequency, and, in addition, that a fairly high degree of isolation exist between output terminals over some specified frequency band. Two of the more commonly used power dividers are illustrated in Fig. 1. In Fig. 1(a), a corporate feed structure of T junctions provides the symmetry necessary to preserve the equiphase equiamplitude condition independent of frequency. In Fig. 1(b), circular symmetry is employed where all the output terminals are connected to the common center conductor of a coaxial line, and the combined load is matched by means of a quarter-wave transformer. To provide isolation between output terminals, the T junctions of Fig. 1(a) may be replaced by hybrid junctions. In addition to the cost and complexity of providing a number of separate, yet identical, hybrids, the corporate feed structure has the limitation of providing only a binary number of outputs. If nine outputs were required, for example, a 16-to-1 power divider would have to be used with $\frac{7}{16}$ of the power output being dissipated in matched loads. Fig. 1(b), on the other hand, because of the circular symmetry, provides any number of outputs. It has, however, the serious disadvantage of having no isolation between outputs, as the output terminals are badly mismatched because all loads appear in parallel across any given output terminal. This paper describes a device which possesses the circular symmetry of Fig. 1(b), so that it maintains phase and amplitude equality between any number of outputs independent of frequency, but, in addition, provides isolated and matched outputs.

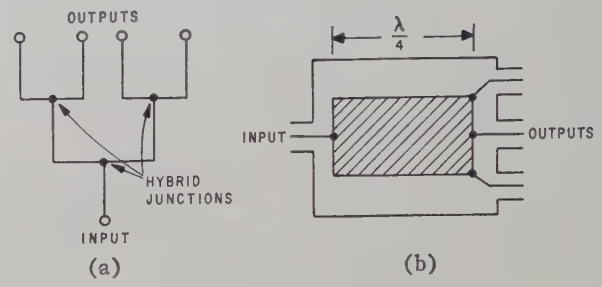

Fig. 1.

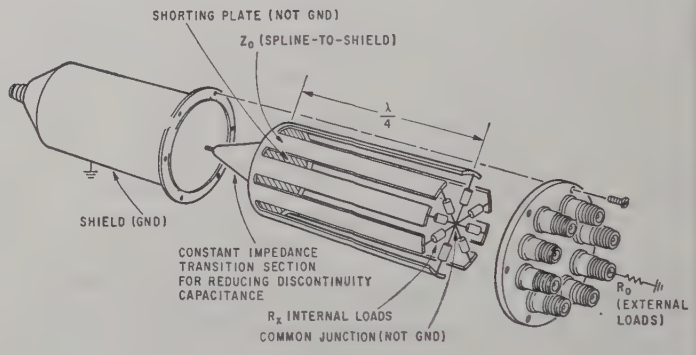

Fig. 2.

Theory of Operation

The power divider as sketched in Fig. 2 consists of a coaxial line in which the hollow inner conductor has been split into n splines of length $\lambda/4$. A shorting plate connects the splines at the input end,[1] and resistors are connected in a radial manner between each spline at the output end and a common junction. Output connectors are shown connected to the splines in an "in line" manner, although they may also be connected in radial fashion, *i.e.*, at right angles to the splines. When a signal is fed into the power divider, it divides by virtue of symmetry into n equiphase equiamplitude parts. No power is dissipated by the resistances when matched loads are connected to the outputs, since all splines will be at the same potential. However, if a reflection occurs at one of the output terminals, the reflected signal will split; part of it will travel directly to the remaining output terminals via the resistors, and the rest of it will travel back to the input, splitting again at the junction of the splines and then returning to the remaining output terminals. Thus, the reflected wave arrives at the remaining output terminals in two parts, and the path length difference between the two paths of travel will be 180° when the splines are $\lambda/4$ in length. It will be shown that when the value of the resistors and the characteristic impedance of the spline transmission lines are properly chosen, the two parts of the reflected wave are also equal in amplitude; hence, complete cancellation occurs.

* Manuscript received by the PGMTT, June 3, 1959; revised manuscript received, September 10, 1959.

† Sylvania Electronic Systems, Waltham, Mass.

[1] A tapered section is shown at the input end for reducing the discontinuity caused by the abrupt change in line sizes when a standard type N connector is used. A more convenient form of this device, which eliminates the need for a separate tapered section, can be realized by uniformly tapering the splined coaxial section itself.

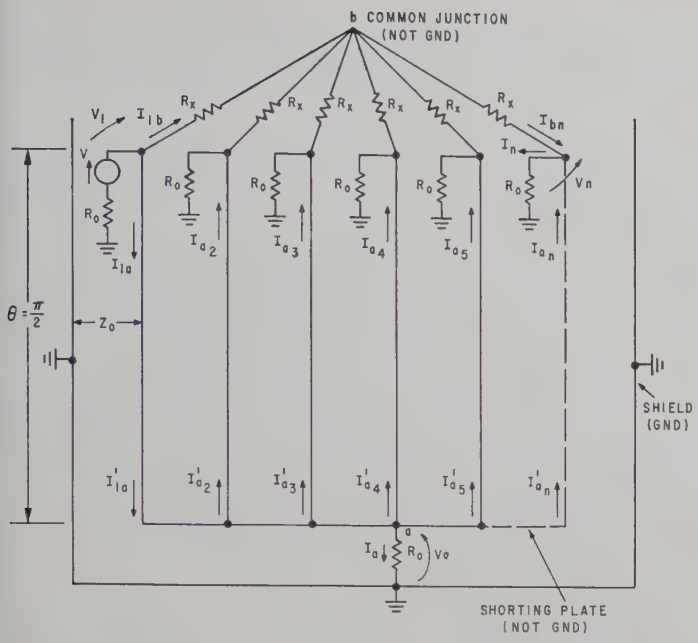

Fig. 3—R_0=external loads connected between splines and shield (GND); R_x=internal loads connected between splines and common junction point; Z_0=characteristic impedance of each spline-to-shield transmission line; V=voltage applied to a single output terminal; V_n=voltage appearing at nth output terminal; V_a =voltage appearing at input terminal.

Referring to Fig. 3, if a voltage V is applied to output terminal 1 by a generator of internal resistance R_0, then the voltages V_n appearing at the other output terminals must all be equal because of symmetry. Applying the transmission line equations when each spline transmission line is a quarter wavelength long ($\theta=\pi/2$), we have

$$\text{spline 1:}\quad V_1 = V_a\cos\theta + jI_{1a}'Z_0\sin\theta = jI_{1a}'Z_0$$

$$I_{1a} = I_{1a}'\cos\theta + j\frac{V_a}{Z_0}\sin\theta = j\frac{V_a}{Z_0}$$

$$\text{spline } n\text{:}\quad V_a = V_n\cos\theta + jI_{an}Z_0\sin\theta = jI_{an}Z_0 \tag{1}$$

$$I_{an}' = I_{an}\cos\theta + j\frac{V_n}{Z_0}\sin\theta = j\frac{V_n}{Z_0}.$$

It is also true that

$$I_{1a}' = \frac{V_a}{R_0} + (n-1)I_{an}'$$

$$I_{an} = \frac{V_n}{R_0} - \frac{I_{1b}}{n-1}$$

$$(I_{1b}+I_{1a})R_0 = V - V_1$$

$$\left(I_{1b}+\frac{I_{1b}}{n-1}\right)R_x = V_1 - V_n. \tag{2}$$

Combining (1) with (2) we obtain the following set of simultaneous equations for the unknown voltages V_1, V_a, V_n:

$$V_a + j(n-1)\frac{R_0}{Z_0}V_n + jV_1\frac{R_0}{Z_0} = 0$$

$$jV_a\frac{R_0}{Z_0} + \left(1+\frac{R_0}{nR_x}\right)V_n - V_1\frac{R_0}{nR_x} = 0$$

$$jV_a\frac{R_0}{Z_0} - \left(\frac{n-1}{n}\right)\frac{R_0}{R_x}V_n + V_1\left(1+\frac{R_0}{R_x}\left(\frac{n-1}{n}\right)\right) = V. \tag{3}$$

For perfect isolation $V_n=0$, (3) may be combined to yield

$$\frac{V_1}{V} = \frac{1}{1+\dfrac{R_0}{R_x}}$$

$$\left(\frac{R_0}{Z_0}\right)^2 = \frac{R_0}{nR_x}, \tag{4}$$

and for matched output admittances, we obtain

$$Y_1 = \frac{I_{1b}+I_{1a}}{V_1} = \frac{V-V_1}{R_0V_1} = \frac{1}{R_0}. \tag{5}$$

Combining (4) and (5) yields

$$R = R$$

$$Z_0 = \sqrt{n}\,R_0. \tag{6}$$

Thus, if the internal loads R and the characteristic impedance of the spline-to-shield transmission lines are adjusted according to (6), the outputs will be completely isolated and matched. The input impedance under these conditions will be the parallel combination of the n output loads R_0, after each has been transformed through a quarter wavelength of line Z_0. Hence,

$$Z_{\text{input}} = \frac{\dfrac{Z_0^2}{R_0}}{n} = R_0$$

or, in other words, the input of the power divider is also matched when the conditions for isolation between outputs are satisfied.

Experimental Results

In order to determine whether or not the isolation and matched output features could be realized in a power divider of practical design, a power divider of the type illustrated in Fig. 1(b), was modified according to the following procedure. Narrow slots were milled in the hollow center conductor of an 8-to-1 power divider of this type to create eight spline-to-shield transmission lines having a characteristic inpedance of approximately eight times that of the unslotted coaxial line whose characteristic impedance was $R_0/\sqrt{8}$. Hence, the spline-to-shield lines had

$$Z_0 = 8\frac{R_0}{\sqrt{8}} = \sqrt{8}R_0$$

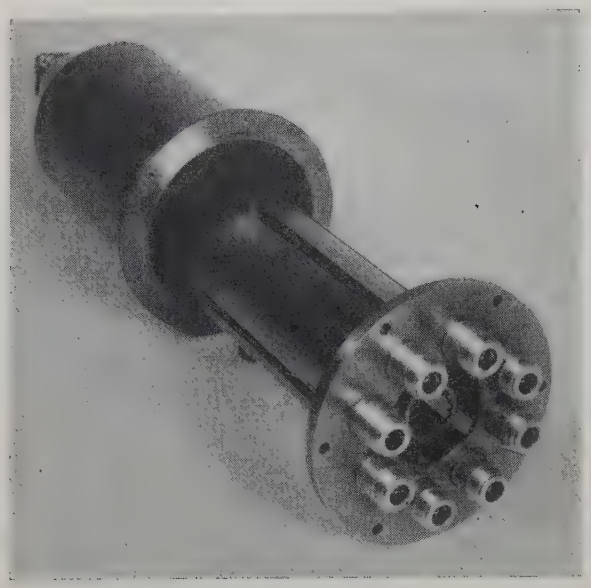

Fig. 4.

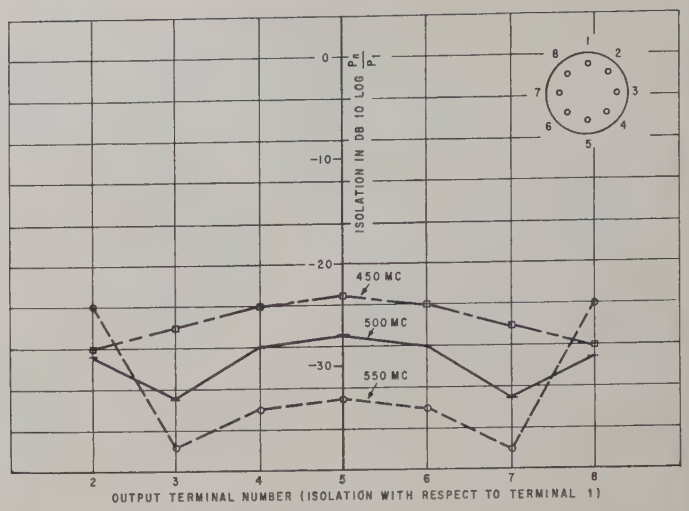

Fig. 5—Isolation between output terminals for N-way hybrid power divider.

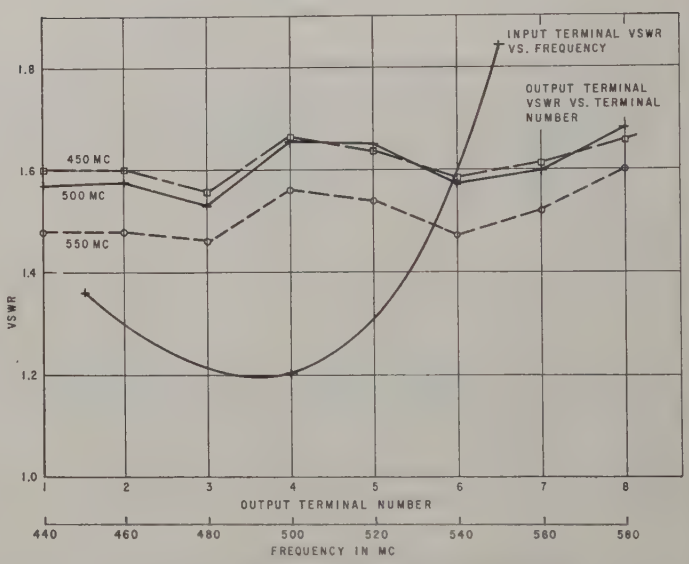

Fig. 6—VSWR characteristics for N-way hybrid power divider.

in accordance with (6). Eight resistors equal in value to R_0 (50 ohms) were then soldered to the ends of the splines, joining in a radial manner to a short circuiting ring (see Fig. 4). Isolation and output VSWR values were obtained using a parallel combination of three 150-ohm $\frac{1}{2}$-watt composition resistors for the 50-ohm internal loads. This combination was found to yield a very low reactance-to-resistance ratio at the operating frequencies. Standard General Radio 50-ohm loads were used to terminate the unused terminals when measuring VSWR and isolation characteristics. The measured isolation between outputs is plotted in Fig. 5 over the frequency range 450 to 550 mc. It will be noted, that at the center frequency of 500 mc the minimum isolation is 27 db, although it is not constant for all output terminals—a fact contrary to the theory based on the model of Fig. 3. The output VSWR is plotted in Fig. 6 and is about 1.6 at 500 mc, where the input VSWR is about 1.2. The output-to-input ratio was measured and found to be -9 db at all frequencies, indicating that the device was behaving as an 8-to-1 lossless power divider with negligible insertion loss.

The experimental model described above differs in several respects from the theoretical model. First, the theoretical model assumes a diameter which is negligible in wavelengths. In the experimental model it was 0.1λ. The principle effect of this appears to be that it shifts the center frequency for best performance to a lower value than the design frequency, and, perhaps, changes the effective resistance of the internal loads, since the current throughout the length of the resistors may no longer be uniform. Second, measurement of the phase between outputs showed several degrees of phase inequality, indicating that the perfect symmetry assumed in the theory had not been achieved in the splined structure and internal loads. Finally, the exact value of the characteristic impedance of the spline-to-shield transmission lines was probably not exactly $\sqrt{8}R_0$. Although the effects mentioned above can be overcome with further development work, the inequality of isolation between output terminals is believed to be due to a more fundamental reason. It will be noted that, shunting any pair of output terminals, there is a short circuited two-wire line formed by the pair of splines leading to these terminals. When the length of the splines is $\lambda/4$, an infinite impedance is shunted between output terminals; but at frequencies off the center frequency, a finite reactance appears between output terminals which is directly proportional to the characteristic impedance of the two-wire line formed by the splines. Because of the circular arrangement of output terminals, diametrically opposite splines (terminals 1–5 in Fig. 5), for example, would form a transmission line of higher characteristic impedance than adjacent splines (terminals 1–2 in Fig. 5). Since, the shunting effect is difference for each pair of output terminals, it is to be expected that the isolation will not be uniform for all terminals, except at the center frequency where there is no shunting effect for any terminal.

Correspondence

Higher Order Modes in Coupled Helices*

The problem of electromagnetic wave propagation in a system consisting of the two infinitely long concentric sheath helices in free space, shown in Fig. 1, may be approached as a boundary value problem. This has been done before for the case of the lowest mode,[1] but the determinantal equation which gives the propagation constants of the higher order modes has not been given before. This note describes the analysis which gives the propagation constants for all modes of propagation.

The expressions for the field components may be written in terms of the cylindrical wave functions.[2]

Region 1, $(r \leq r_1)$:

$$E_r^{(1)} = \left[\frac{i\beta}{\tau} I_n'(\tau r)a_n^{(1)} - \frac{\mu\omega n}{\tau^2 r} I_n(\tau r)b_n^{(1)}\right] F_n \quad (1a)$$

$$E_\theta^{(1)} = \left[\frac{-n\beta}{\tau^2 r} I_n(\tau r)a_n^{(1)} - \frac{i\mu\omega}{\tau} I_n'(\tau r)b_n^{(1)}\right] F_n \quad (1b)$$

$$E_z^{(1)} = [-I_n(\tau r)a_n^{(1)}]F_n \quad (1c)$$

$$H_r^{(1)} = \left[\frac{n\omega\epsilon}{\tau^2 r} I_n(\tau r)a_n^{(1)} + \frac{i\beta}{\tau} I_n'(\tau r)b_n^{(1)}\right] F_n \quad (1d)$$

$$H_\theta^{(1)} = \left[\frac{i\omega\epsilon}{\tau} I_n'(\tau r)a_n^{(1)} - \frac{n\beta}{\tau^2 r} I_n(\tau r)b_n^{(1)}\right] F_n \quad (1e)$$

$$H_z^{(1)} = [-I_n(\tau r)b_n^{(1)}]F_n. \quad (1f)$$

Region 2, $(r_1 \leq r \leq r_2)$:

$$E_r^{(2)} = \left[\frac{i\beta}{\tau} I_n'(\tau r)a_n^{(2)} - \frac{\mu\omega n}{\tau^2 r} I_n(\tau r)b_n^{(2)} + \frac{i\beta}{\tau} K_n'(\tau r)c_n^{(2)} - \frac{\mu\omega n}{\tau^2 r} K_n(\tau r)d_n^{(2)}\right] F_n \quad (2a)$$

$$E_\theta^{(2)} = \left[\frac{-n\beta}{\tau^2 r} I_n(\tau r)a_n^{(2)} - \frac{i\mu\omega}{\tau} I_n'(\tau r)b_n^{(2)} - \frac{n\beta}{\tau^2 r} K_n(\tau r)c_n^{(2)} - \frac{i\mu\omega}{\tau} K_n'(\tau r)d_n^{(2)}\right] F_n \quad (2b)$$

$$E_z^{(2)} = [-I_n(\tau r)a_n^{(2)} - K_n(\tau r)c_n^{(2)}]F_n \quad (2c)$$

$$H_r^{(2)} = \left[\frac{n\omega\epsilon}{\tau^2 r} I_n(\tau r)a_n^{(2)} + \frac{i\beta}{\tau} I_n'(\tau r)b_n^{(2)} + \frac{n\omega\epsilon}{\tau^2 r} K_n(\tau r)c_n^{(2)} + \frac{i\beta}{\tau} K_n'(\tau r)d_n^{(2)}\right] F_n \quad (2d)$$

$$H_\theta^{(2)} = \left[\frac{i\omega\epsilon}{\tau} I_n'(\tau r)a_n^{(2)} - \frac{n\beta}{\tau^2 r} I_n(\tau r)b_n^{(2)} + \frac{i\omega\epsilon}{\tau} K_n'(\tau r)c_n^{(2)} - \frac{n\beta}{\tau^2 r} K_n(\tau r)d_n^{(2)}\right] F_n \quad (2e)$$

$$H_z^{(2)} = [-I_n(\tau r)b_n^{(2)} - K_n(\tau r)d_n^{(2)}]F_n. \quad (2f)$$

Region 3, $(r \geq r_2)$:

$$E_r^{(3)} = \left[\frac{i\beta}{\tau} K_n'(\tau r)a_n^{(3)} - \frac{\mu\omega n}{\tau^2 r} K_n(\tau r)b_n^{(3)}\right] F_n \quad (3a)$$

$$E_\theta^{(3)} = \left[\frac{-n\beta}{\tau^2 r} K_n(\tau r)a_n^{(3)} - \frac{i\mu\omega}{\tau} K_n'(\tau r)b_n^{(3)}\right] F_n \quad (3b)$$

$$E_z^{(3)} = [-K_n(\tau r)a_n^{(3)}]F_n \quad (3c)$$

$$H_r^{(3)} = \left[\frac{n\omega\epsilon}{\tau^2 r} K_n(\tau r)a_n^{(3)} + \frac{i\beta}{\tau} K_n'(\tau r)b_n^{(3)}\right] F_n \quad (3d)$$

$$H_\theta^{(3)} = \left[\frac{i\omega\epsilon}{\tau} K_n'(\tau r)a_n^{(3)} - \frac{n\beta}{\tau^2 r} K_n(\tau r)b_n^{(3)}\right] F_n \quad (3e)$$

$$H_z^{(3)} = [-K_n(\tau r)b_n^{(3)}]F_n \quad (3f)$$

where

$$F_n = \exp[in\theta + i\beta z - i\omega t], \quad (4)$$

and

$$\tau = \sqrt{\beta^2 - k^2}.$$

Now in general we should sum over-all values of n and β in (1), (2) and (3); however, since the boundary conditions for sheath helices are the same for all θ and z, the orthogonality in θ and z allows the boundary conditions to be satisfied for each n and β.

We now apply the boundary conditions that $E_\parallel$ (the component of E parallel to the direction of conduction) be zero at all boundaries and that $E_\perp$ (the component of E perpendicular to the direction of conduction) and $H_\parallel$ be continuous across all boundaries. These conditions lead to the following results:

At $r = r_1$:

$$E_z^{(1)} + E_\theta^{(1)} \cot\psi_1 = 0 \quad (5a)$$

$$E_\theta^{(1)} - E_\theta^{(2)} = 0 \quad (5b)$$

$$E_z^{(1)} - E_z^{(2)} = 0 \quad (5c)$$

$$[H_z^{(1)} - H_z^{(2)}] + [H_\theta^{(1)} - H_\theta^{(2)}] \cot\psi_1 = 0, \quad (5d)$$

and likewise at $r = r_2$:

$$E_z^{(3)} + E_\theta^{(3)} \cot\psi_2 = 0 \quad (6a)$$

$$E_\theta^{(2)} - E_\theta^{(3)} = 0 \quad (6b)$$

$$E_z^{(2)} - E_z^{(3)} = 0 \quad (6c)$$

$$[H_z^{(2)} - H_z^{(3)}] + [H_\theta^{(2)} - H_\theta^{(3)}] \cot\psi_2 = 0. \quad (6d)$$

We may now substitute (1), (2), and (3) into (5) and (6) obtaining eight simultaneous equations. These equations may be written

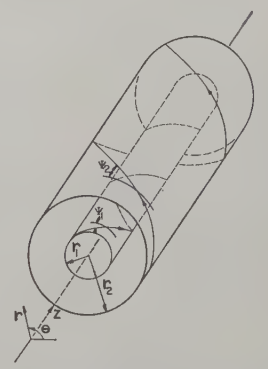

Fig. 1—Concentric sheath helices showing definitions of coordinates and dimensions. The arrows on the sheaths show the direction of conduction.

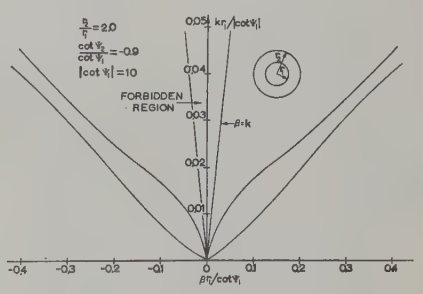

Fig. 2—Natural modes of propagation for $n = 0$.

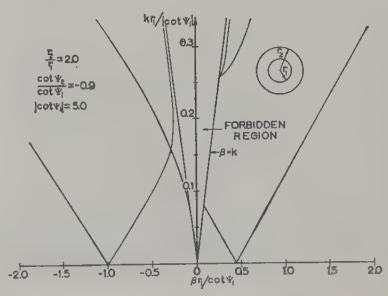

Fig. 3—Natural modes of propagation for $n = +1$. The curves for $n = -1$ are obtained by reversing the signs of the abscissa.

Received by the PGMTT, July 30, 1959.

[1] J. S. Cook, R. Kompfner, and C. F. Quate, "Coupled helices," *Bell Sys. Tech. J.*, vol. 35, pp. 127–178; January, 1956.

[2] J. A. Straton, "Electromagnetic Theory," McGraw-Hill Book Co., Inc., New York, N. Y., p. 360; 1941.

$$[(1+\xi)^2 P_{n1} + y^2/x^2 P_{n1}'] \cdot \left[\left(1+\frac{r_1}{r_2}\frac{\cot\psi_2}{\cot\psi_1}\xi\right)^2 P_{n2} + \left(\frac{\cot\psi_2}{\cot\psi_1}\right)^2 y^2/x^2 P_{n2}'\right]$$

$$-\left[\left(1+\frac{r_1}{r_2}\frac{\cot\psi_2}{\cot\psi_1}\xi\right)^2 R_n + \frac{\cot\psi_2}{\cot\psi_1} y^2/x^2 R_n'\right]$$

$$\cdot\left[(1+\xi)\left(1+\frac{r_1}{r_2}\frac{\cot\psi_2}{\cot\psi_1}\xi\right) R_n + y^2/x^2 \frac{\cot\psi_2}{\cot\psi_1} R_n'\right] = 0. \quad (8)$$

in a more compact form by defining the following notation:

$$A_1 = \frac{n\beta}{\tau^2 r_1} \quad A_2 = \frac{n\beta}{\tau^2 r_2} \quad B = \frac{i\omega\epsilon}{\tau}$$

$$c = \frac{i\mu\omega}{\tau} \quad I_{n1} = I_n(\tau r_1) \quad K_{n2} = K_n(\tau r_2), \text{ etc.}$$

Writing the equation with this notation and removing the common factor, F_n, we have:

$$I_{n1}(1 + A_1 \cot\psi_1)a_n^{(1)} + c\cot\psi_1 I_{n1}' b_n^{(1)} = 0 \quad (7a)$$

$$A_1 I_{n1} a_n^{(1)} + c I_{n1}' b_n^{(1)} - A_1 I_{n1} a_n^{(2)} - c I_{n1}' b_n^{(2)} - A_1 K_{n1} c_n^{(2)} - c K_{n1}' d_n^{(2)} = 0 \quad (7b)$$

$$I_{n1} a_n^{(1)} - I_{n1} a_n^{(2)} - K_{n1} c_n^{(2)} = 0 \quad (7c)$$

$$B\cot\psi_1 I_{n1}' a_n^{(1)} - I_{n1}(1 + A_1\cot\psi_1) b_n^{(1)} - B\cot\psi_1 I_{n1}' a_n^{(2)} + I_{n1}(1 + A_1\cot\psi_1) b_n^{(2)} - B\cot\psi_1 K_{n1}' c_n^{(2)} + K_{n1}(1 + A_1\cot\psi_1) d_n^{(2)} = 0 \quad (7d)$$

$$K_{n2}(1 + A_2\cot\psi_2) a_n^{(3)} + c\cot\psi_2 K_{n2}' b_n^{(3)} \quad (7e)$$

$$A_2 I_{n2} a_n^{(2)} + c I_{n2}' b_n^{(2)} + A_2 K_{n2} c_n^{(2)} + c K_{n2}' d_n^{(2)} - A_2 K_{n2} a_n^{(3)} - c K_{n2}' b_n^{(3)} = 0 \quad (7f)$$

$$I_{n2} a_n^{(2)} + K_{n2} c_n^{(2)} - K_{n2} a_n^{(3)} = 0 \quad (7g)$$

$$B\cot\psi_2 I_{n2}' a_n^{(2)} - I_{n2}(1 + A_2\cot\psi_2) b_n^{(2)} + B\cot\psi_2 K_{n2}' c_n^{(2)} - K_{n2}(1 + A_2\cot\psi_2) d_n^{(2)} - B\cot\psi_2 K_{n2}' a_n^{(3)} + K_{n2}(1 + A_2\cot\psi_2) b_n^{(3)} = 0. \quad (7h)$$

In order to find the permissible values of τ we must set the system determinant equal to zero. The expansion of the eighth order determinant is carried out elsewhere.[3] In order to write the determinantal equation in a compact form we define

$$P_{n1} = I_{n1}K_{n1}, \quad P_{n1}' = I_{n1}'K_{n1}',$$
$$R_n = I_{n1}K_{n2}, \quad R_n' = I_{n1}'K_{n2}',$$
$$P_{n2} = I_{n2}K_{n2}, \quad P_{n2}' = I_{n2}'K_{n2}',$$
$$x = \tau r_1, \quad y = k r_1 \cot\psi_1,$$

and

$$\xi = n\frac{\sqrt{\cot^2\psi_1 x^2 + y^2}}{x^2}\cdot\frac{\cot\psi_1}{|\cot\psi_1|}.$$

The general determinantal equation is then found to be

The values of τ which satisfy (8) give the propagation constants of the various modes of propagation. Setting $n=0$ in (8) we obtain the previously known expression for the lowest mode.[1] This mode is commonly used in the analysis of helical couplers for traveling-wave tubes. Letting r_2 approach infinity we obtain the equation for the modes on a single helix.[4] These special cases indicate the correctness of (8).

The solutions of (8) were found by an approximate method using a digital computer.[3] The modes of propagation for $n=0$, ± 1 are shown in Fig. 2 and Fig. 3. The curves for $n=0$ were calculated from published data,[1] while Fig. 3 is the result of the computer solution. Similar curves may be found for any value of n. The knowledge of these higher order modes should make it possible to obtain more accurate solutions to the coupled helix problem.

R. E. Hayes
Electronics Res. Lab.
University of Kansas
Lawrence, Kan.

[3] R. E. Hayes, "A Study of Coupled Helices," M.S. thesis, University of Kansas, Lawrence; May, 1959.

[4] S. Sensiper, "Electromagnetic Wave Propagation in Helical Conductors," Res. Lab. Electronics, Mass. Inst. Tech., Cambridge, Mass., Tech. Rep. No. 194, p. 7; May, 1951.

The Tetrahedral Junction as a Waveguide Switch*

A junction of two rectangular waveguides which are mutually cross-polarized becomes a magnetically controlled reactive switch when properly loaded by a ferrite rod magnetized longitudinally (see Fig. 1). It is a special case of a novel type of structure for which we propose the name *tetrahedral junction*. As a switch, it possesses:

1) very high insertion loss in the reflecting state, ~60 db;
2) loss in the transmitting state which is lower in principle than that attainable in any similar ferrite-waveguide device, <0.1 db;
3) high switching speed—1 μsec is attainable with conventional circuits and convenient currents;
4) large bandwidth, ~10 per cent;
5) little sensitivity to variations in applied field and saturation magnetization; and
6) small phase and small phase-variations with frequency and applied field in the transmitting state.

* Received by the PGMTT, August 2, 1959.

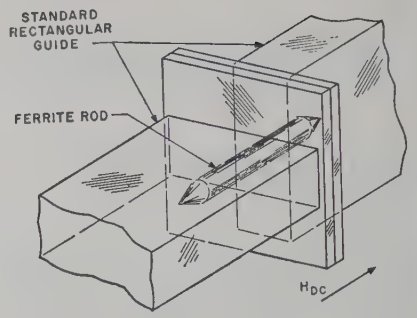

Fig. 1—The tetrahedral junction.

Our experimental and theoretical results indicate that there is room for further improvement in most of its significant properties.

In addition to its utility as a switch, the tetrahedral junction can also be used as a reversible gyrator. Further, its principle of operation is such that a dissipative element can be incorporated which converts the device into a matched modulator or reversible isolator.

The name tetrahedral derives from the fact that if the ends of the two crossed guides are separated and their parallel edges joined by planes, the resulting taper is in the form of a doubly-truncated tetrahedron. Some of our models are of this form, in particular, the one whose properties are reported above.

Our interest in this device is an outgrowth of our study of the Reggia-Spencer phase shifter;[1,2,3] it is one of the "novel effects" to which allusion is made by Weiss.[3] As in the case of the phase shifter, the behavior of the tetrahedral junction may be divided into two regimes: above a sharply defined frequency the device takes on the properties of a Faraday rotator; in a frequency range just below that of the Faraday effect regime, the junction exhibits its most interesting and useful characteristics. Here, however, it is inappropriate to speak of the phase shift regime, for the phase shift effects which are central to the Reggia-Spencer device are inessential, in fact undesirable, in this case. On the other hand, the modes of propagation[3] are of the same basic form in the two. In the presence of the magnetized ferrite, a wave entering the junction of Fig. 1 from the input end takes on a characteristic elliptic polarization. At the plane of the joint it is scattered into four significant components: a reflected and a transmitted propagating mode, and an evanescent mode in each guide which is also elliptically polarized. A model of this phenomenon, employing simplifying assumptions similar to those used by Weiss,[3] shows that under the proper conditions (involving the cross-sectional dimensions of the two guides, and the

[1] F. Reggia and E. G. Spencer, "A new technique in ferrite phase-shifting for beam scanning of microwave antennas," Proc. IRE, vol. 45, pp. 1510–1517; November, 1957.

[2] J. A. Weiss, "The Reggia-Spencer microwave phase shifter," *J. Appl. Phys.*, vol. 30, pp. 153s–154s; April, 1959. *Proc. AIEE Conf. on Magnetism and Magnetic Materials*, Philadelphia, Pa., November, 1958.

[3] J. A. Weiss, "A phenomenological theory of the Reggia-Spencer phase shifter," Proc. IRE, vol. 47, pp. 1130–1137; June, 1959.

diameter and magnetic parameters of the ferrite) the incident wave is fully matched into the transmitted wave. The only portion of the ferrite which contributes in an essential way to the effect is that located in the immediate vicinity of the joint; thus there is, so to speak, *no length* of active material involved in the principle. It is therefore possible to use only a small ferrite volume, with the advantage, among others, of minimizing the magnetic loss. When the ferrite is unmagnetized, the junction simply presents a transition to cutoff guide; the insertion loss available in this state is limited only by the precision of the mechanical structure.

The phase, insertion loss, and polarization in the transmitting state exhibit a number of well-defined features which agree qualitatively with the results of the simplified theoretical model. The latter, in turn, indicates how the effect may be exploited to fulfill the various specific application requirements. A full report on the theory and experimental data will be the subject of a forthcoming paper.

By way of acknowledgment, I wish to thank my colleagues for their interest and comments. I am particularly indebted to R. W. Judkins for his contributions to the various aspects of this work.

J. A. Weiss
Bell Telephone Labs., Inc.
Murray Hill, N. J.

Some Measurements of Traveling-Wave Tube Attenuators at 2000 MC*

Saturation in traveling-wave tube amplifiers, that is, the failure of the output to continue to rise as the input power is increased, can occur in several ways. The limit may arise through heating of the RF circuit, or if the circuit can be so made that this does not occur, the ultimate limit is provided by the amount of power that can be carried on the beam; large signal calculations of the behavior under these conditions have been made by several investigators.[1-4] It has also been observed, however, that the saturation limit is a function of the amount and distribution of loss in the attenuator, and recent calculations, for example by Rowe,[4] include the study of the limiting power output for various values of the loss parameter d. However, as pointed out by Caldwell,[5] the saturation limit in the attenuator may depend at least as much on any modification of the phase velocity in the attenuating region as on the amount of loss. This arises because in nearly all practical tubes the attenuator does not conform to either of the two ideal cases; *i.e.*, it is not completely distributed throughout the length of the circuit or concentrated at one point, but occupies an appreciable part of the total length. As a result of this, if the phase velocity of the circuit wave in the attenuating zone is modified, there is a reduced interaction between the circuit wave and the beam, since the beam velocity is arranged to give optimum interaction with the wave on the loss-free part of the circuit.

It is therefore of interest to know how the attenuation and phase velocity vary in practical attenuators, and the first object of the work described here is to relate these quantities to the surface resitivity of "Aquadag" colloidal graphite material coatings on the surface of ceramic rods, as has been done by Caldwell[5] for external sprayed attenuation.

Some measurements have therefore been made at 2000 mc using steatite rods which were sprayed with Aquadag mixture along the whole of the helix length. The coating surface resistivity was measured by the use of a four-terminal resistance bridge, from which current was passed through the coating between thin wire loops drawn around the outside, and the potential difference measured between two points 3 mm apart near their center. The resistivity was found to vary along the length of the coating by as much as 35 per cent, but since the total range investigated covered 8 decades the variations were not so great that a mean value could not be sensibly used (see Fig. 1).

The rods were then placed around a helix, which was mounted in a well-matched circuit, and the insertion loss was measured.

The phase velocity measurements were made by passing an external coupling loop along the length of the assembled helix, which for this purpose had a solid mandrel screwed into the end remote from the RF feed so that a large standing-wave was set up. The arrangement used is shown diagrammatically in Fig. 2. Because of the amount of attenuation present, and the need to avoid errors due to evanescent waves arising from the discontinuities at the ends, these measurements became progressively more difficult as higher surface conductivities were used. A better way of making the measurements would be to assemble the rods into sealed-off traveling-wave tubes, and to find the electron beam velocity for minimum attenuation at very low beam currents. This has not been possible because of the magnitude of the work involved.

Typical standing-wave patterns obtained are well shown in Figs. 3–6. Fig. 3 shows the pattern with no coating of "Aquadag" colloidal graphite material on the rods. It

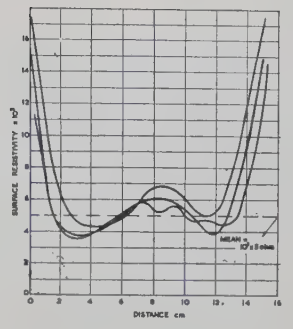

Fig. 1—Variation of surface resistivity with length.

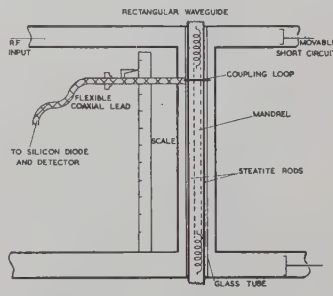

Fig. 2—Arrangement of pick-up loop.

may be seen that the pattern is distorted by the existence of evanescent fast-waves set up at the waveguide coupling, which could also account for the apparent increase of signal with distance shown in Figs. 5 and 6. The attenuation measurements were, of course, not made using this circuit, but instead a well-matched close-fitting circuit was used, in which only the slow mode was present. The surface resistivity in this case was taken as 10^8 ohms so that a representative point for the "no loss" case could be included in the curves. Fig. 4 shows the pattern for rods with a surface resitivity of 8×10^5 ohms. The wavelength measurements were taken over the four central minimas, since these were found to be uniformly spaced. In Fig. 5, the resistivity has been reduced to 5.9×10^3 ohms, and in Fig. 6 to 7.2×10^2. The lowest resistance coatings that it was possible to measure in this way had a surface resistivity of 3.4×10^2 ohms, which gave a total attenuation of 107 db, and a wavelength of 4 mm compared with the wavelength of 1.12 cm obtained for the uncoated rods. The results obtained from these measurements are shown graphically in Fig. 7. The measurements were carried out at 2000 mc, using a helix with a pitch of 1.5 mm, and for which $\gamma a_0 = 1.3$ when mounted between steatite rods and enclosed in a glass tube. The rod diameter was nearly 0.3 times the mean helix diameter.

The curves obtained by Caldwell for externally sprayed attenuators of "Dixonac" colloidal graphite material for use in the 500 mc region are shown for comparison in Fig. 8.

It is interesting to note that the general form of the curves is similar, although the values of attenuation are much lower for the 2000 mc curves, and the effect of resistive coatings on the phase velocity is apparently greater. This similarity is more surprising when it is borne in mind that in

* Received by the PGMTT, July 10, 1959; revised manuscript received, September 14, 1959.

[1] A. T. Nordsiek, "Theory of the large signal behaviour of traveling wave amplifiers," Proc. IRE, vol. 41, pp. 630–637; May, 1953.

[2] P. K. Tien, L. R. Walker and V. M. Wolontis, "Large signal theory of traveling-wave amplifiers," Proc. IRE, vol. 43, pp. 260–277; March, 1955.

[3] H. C. Poulter, "Large Signal Theory of Traveling Wave Tube," Stanford University, Stanford, Calif., Tech. Rept. 73; January, 1954.

[4] J. E. Rowe, "Design information on large signal traveling-wave amplifiers," Proc. IRE, vol. 44, pp. 200–210; February, 1956.

[5] J. J. Caldwell, "High power traveling-wave tube gain and saturation characteristics as a function of attenuation, configuration and resistivity," IRE Trans. on Electron Devices, vol. ED-4, pp. 28–33; December, 1953.

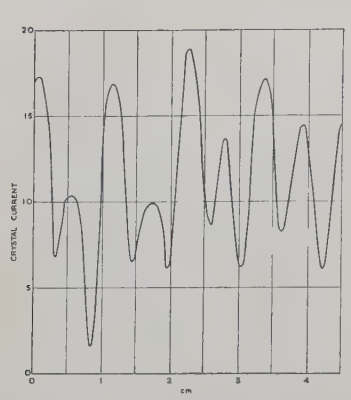

Fig. 3—Signal level along helix with no coating on rods.

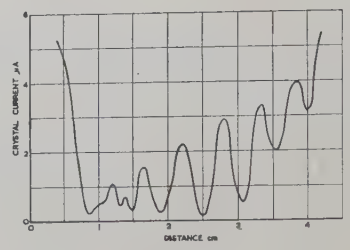

Fig. 5—Signal level along helix with surface resistivity 5.9×10^{8} ohms.

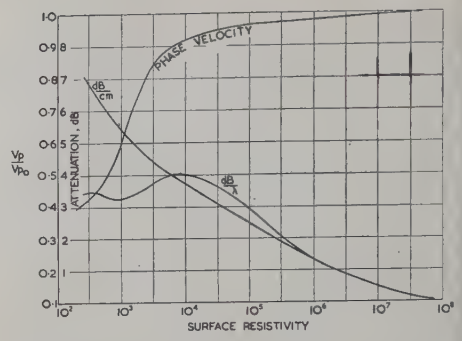

Fig. 7—Velocity and attenuation as a function of attenuation resistivity. Steatite rods at 2000 mc.

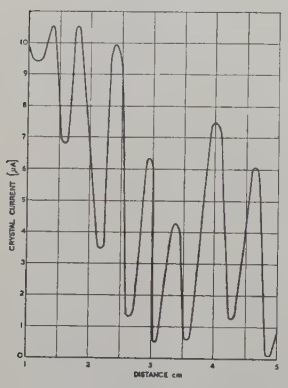

Fig. 4—Signal level along helix with surface resistivity 8×10^{5} ohms.

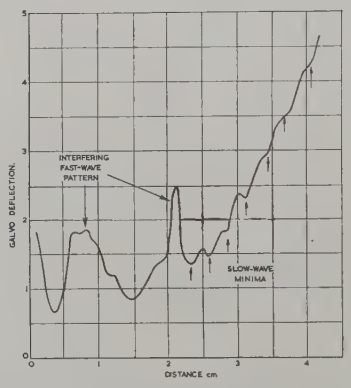

Fig. 6—Signal level along helix with surface resistivity 7.2×10^{2} ohms.

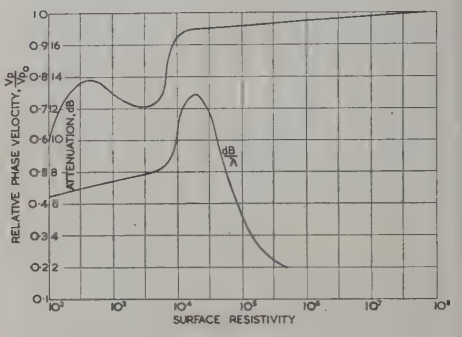

Fig. 8—Corresponding curves for attenuators, external, by J. J. Caldwell.

addition to the difference in frequency, attenuation obtained by resistive coatings actually in contact with the helix differs from that obtained from resistive coatings in the external field in that the attenuation obtained depends very critically upon the pressure of contact between the rods and helix. Indeed, it appears that with the configuration used very little attenuation can be obtained until there is actually a conducting path between the turns of the helix, for example, on rotating a single rod coated over only 180° of the surface, the attenuation changed abruptly from 2 db to 18 db when the helix came into contact with the coating.

A preliminary conclusion which might be drawn from these curves is that if it is desired to obtain the maximum gain from a travelling-wave tube of a given length, in which the attenuator occupies an appreciable part of the helix length, the resistivity of the coating should be considerably greater than that for which maximum attenuation /cm is obtained. In this way, the phase velocity of the wave can be maintained fairly near the value for the loss-free helix, and hence a larger degree of interaction in the attenuating region would be expected.

C. H. Dix
Research Labs.
The General Electric Co., Ltd.
Wembley, England

PGMTT News

1959 Annual PGMTT Meeting

During the spring of 1958, a joint decision was reached by the Boston Chapter of the Institute of Radio Engineers and the Administrative Committee of the Professional Group on Microwave Theory and Techniques to hold the 1959 annual meeting in the Boston area.

During the summer, a Symposium Committee under the chairmanship of W. L. Pritchard, a Technical Program Committee under the chairmanship of Dr. Henry Riblet and various subcommittees were formed. Dr. Karl Willenbrock, a member of the Symposium Committee, Assistant Director of the Gordon McKay Laboratory at Harvard and Vice Chairman of the Boston Section of the IRE, was instrumental in obtaining the cooperation of Harvard University.

The committee members were as follows:

Symposium Committee

Chairman, W. Pritchard, Raytheon Company
P. Crandall, National Company
C. Faflick, Sylvania Electric Prods., Inc.
Finance, W. From, Ewen Knight Corporation
I. Goldstein, Raytheon Company
R. Jones, Harvard University
J. Reed, Raytheon Company
Technical Program, H. Riblet, Microwave Development Labs., Inc.
Publicity, R. Rivers, Aircom, Inc.
P. Rizzi, Ewen Knight Corporation
Local Arrangements, T. Saad, Sage Laboratories, Inc.
Asst. Chairman, H. Scharfman, Raytheon Company
K. Willenbrock, Harvard University

Technical Program Committee

Chairman, H. J. Riblet, Microwave Development Labs., Inc.
C. Faflick, Sylvania Electric Prods., Inc.
I. Goldstein, Raytheon Company
R. Jones, Harvard University
J. Reed, Raytheon Company
P. Rizzi, Ewen Knight Corporation
K. Willenbrock, Harvard University

The symposium was held at Paine Hall through the courtesy of Harvard University's Music Department, on June 1–3, 1959.

There were 7 technical sessions, including one evening session at the Cambridge Electronic Accelerator, and a total of 43 papers were given. Ten of the papers were written by authors from educational institutions, 3 from research institutes, and 30 from commercial laboratories.

A banquet was held at Harkness Common on June 2, and featured addresses by Dean Harvey Brooks and Nobel Laureate, Professor Edward Purcell. Professor Purcell's address, "An Experiment in Communication," was concerned with the problem of communicating with an unknown, but hypothetically existing, race of intelligent beings in interstellar space.

The Microwave Prize for the best paper published in these Transactions during the previous year was awarded to Dr. L. Goldstein, and Honorable Mentions were given, for the first time, to Dr. S. B. Cohn and Dr. H. E. D. Scovil.

Of the 685 people who attended the annual meeting, 530 were members of the IRE, 130 were nonmembers and 25 were students.

Because of the large attendance and the extensive use of Harvard University facilities, a surplus of over one thousand dollars remained. This money is returned to the Treasury of the MTT Professional Group to support the Group publications and other activities.

Dean Harvey Brooks,
Harvard University

W. L. Pritchard,
Symposium Chairman

Prof. E. M. Purcell

T. Saad,
Chairman PGMTT

Seated at the banquet table from left to right: T. Saad, Mrs. Riblet, H. E. D. Scovil, Mrs. Brooks, E. M. Purcell, W. L. Pritchard, Dean H. Brooks, Mrs. Pritchard, S. B. Cohn, Mrs. Saad, and H. Riblet.

Among the attendees, above, left to right: A. Pomeroy, A. C. Beck, S. Rosenthal, W. W. Mumford, D. Fye, and E. Strumwasser

Left to right: I. Goldstein, J. Heller, N. Sakiotis, L. Swern, J. Cadheris, and N. Lippitz.

Intermission in front of Paine Hall.

Contributors

Aaron D. Bresler (S'43–A'46–M'55–SM'59) was born in New York, N. Y., on June 20, 1924. He received the B.E.E. degree from the City College of New York, N. Y., in 1944, and the M.E.E. and D.E.E. degrees, both from the Polytechnic Institute of Brooklyn, N.Y., in 1951 and 1959 respectively.

A. D. Bresler

From 1944 to 1947 he served with the U. S. Army Signal Corps. In 1947 he worked as a telephone engineer for the United States forces in Austria. From 1948 to 1951, and again from 1953 to 1955, he was an instructor in the electrical engineering department of the City College of New York. In 1951 he joined the staff of the Microwave Research Institute at the Polytechnic Institute of Brooklyn, where he was engaged in development work on microwave components for two years. In 1955 he rejoined its staff and engaged in analytical studies of propagation and diffraction phenomena in anisotropic waveguides; these studies formed the basis upon which the D.E.E. degree was awarded to him. Recently, he joined the staff of Jasik Laboratories, Inc., Westbury, N. Y., where he has specialized in the design and development of antennas and microwave components.

Dr. Bresler is a member of Tau Beta Pi, Eta Kappa Nu and Sigma Xi.

❖

John H. Craven (A'54) was born in Clacton, Essex, England on May 30, 1916. He received the B.S.E.E. degree from the University of British Columbia, Vancouver, in 1949 and the M.S. degree from the University of Toronto, Toronto, Ont., in 1950.

J. H. Craven

He served with the Royal Canadian Air Force from 1940 to 1945, having come to Canada in 1929. During 1950–1951 he worked at the Atomic Energy Project of the National Research Council at Chalk River, Ontario. Then he transferred to the Radio Division of the National Research Council in Ottawa, Ont., where he is presently employed. His work there has dealt with the development of a wide range of microwave devices.

Mr. Craven is an associate member of the British IRE.

❖

Richard W. Damon was born on May 14, 1923, in Concord, Mass. He received the B.S. degree in physics in 1944 and the M.A. and Ph.D. degrees in applied physics in 1947 and 1951, respectively, from Harvard University, Cambridge, Mass. From 1946 to 1948, and in 1950, he was a Teaching Fellow in Applied Physics at Harvard University.

R. W. Damon

During World War II, he was an electronics officer in the Naval Reserve, serving in underwater sound work at ship repair bases in Hawaii and the Philippine Islands. In 1948–49, he was employed as a magnetron development engineer at Raytheon Manufacturing Company, Waltham, Mass. He joined the General Electric Research Laboratory, Schenectady, N. Y., in 1951. His work there has been primarily in solid-state physics and has included photoconductivity, television camera tubes for the visible and X-ray regions, and the principles and applications of magnetic resonance phenomena.

Dr. Damon is a member of the American Physical Society, Sigma Xi, and the American Association for the Advancement of Science.

❖

Charles Cecil Eaglesfield was born on June 28, 1906 in Swansea, Wales. He attended Clifton College, Clifton and received the M.A. degree from Petershouse, Cambridge in 1928.

C. C. Eaglesfield

He joined Standard Telephones and Cables, London, in 1928 where he assisted in the early days of the Transatlantic radio telephone service and the first ship-shore radio telephones. He joined Mullard Radio Valve Company, London, Eng., in 1933, and there worked on television until the war, when he initiated a number of valves used in radar. In 1947, he rejoined Standard Telephones to work on valves for repeaters and similar projects, and in 1957 he transferred to Standard Telecommunication Laboratories, Harlow, Essex, Eng., where he is presently employed. At STL, he has been associated with a project for long-distance communication by waveguide.

Mr. Eaglesfield is an Associate Member of the Institution of Electrical Engineers.

❖

John R. Eshbach (S'47–A'51–M'57) was born on October 7, 1922, in Bethlehem, Pa. He received the B.S. degree in electrical engineering and M.S. degree in physics from Northwestern University, Evanston, Ill., in 1946 and 1947 respectively. From 1943 to 1946 he served in the U. S. Navy. In 1951 he received the Ph.D. degree from the Massachusetts Institute of Technology, Cambridge, where he had done research in the field of microwave spectroscopy.

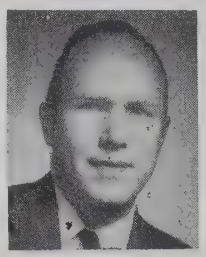

J. R. Eshbach

Since 1951 he has been with the General Electric Research Laboratory in Schenectady, N. Y., where he has done research on photoconductivity and has worked on television camera tube principles and the development of camera tubes. Recently he has become engaged in research on ferromagnetic resonance and the principles of ferrite devices.

Dr. Eshbach is a member of the American Physical Society, Eta Kappa Nu, Tau Beta Pi and Sigma Xi.

❖

Robert V. Garver (A'57) was born on June 2, 1932, in Minneapolis, Minn. He attended the University of Maryland, College Park, where he was awarded the Bachelor of Science degree in physics in 1956.

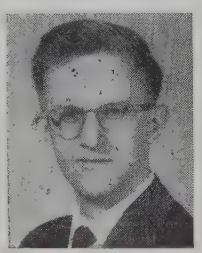

R. V. Garver

In 1956 he became affiliated with the Microwave Development Section of Diamond Ordnance Fuze Laboratories, Washington, D. C., where he has been working on microwave semiconductors.

Mr. Garver is a member of the American Physical Society.

❖

Jerome J. Green was born in Chicago, Ill., on October 10, 1932. He received the B.S. degree in physics from Northwestern University, Evanston, Ill., in 1954 and the M.A. and Ph.D. degrees from Harvard University, Cambridge, Mass., in 1955 and 1959, respectively.

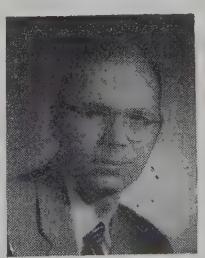

J. J. Green

Dr. Green is presently employed at the Research Division, Raytheon Manufacturing Company, Waltham, Mass., where he is engaged in experimental studies of ferromagnetic resonance.

Jôji Hamasaki, for a photograph and biography please see page 397 of the July, 1959 issue of these TRANSACTIONS.

❖

A. F. Harvey, for a photograph and biography please see page 482 of the October, 1959 issue of these TRANSACTIONS.

❖

Kaneyuki Kurokawa, for a photograph and biography please see page 397 of the July, 1959 issue of these TRANSACTIONS.

❖

Arthur A. Oliner (M'47–SM'52) was born in Shanghai, China, on March 5, 1921. He received the B.A. degree from Brooklyn College, N. Y., in 1941, and the Ph.D. degree in physics from Cornell University, Ithaca, N. Y., in 1946. While at Cornell, he held a graduate teaching assistantship in the physics department and also conducted research on an Office of Scientific Research and Development project.

A. A. OLINER

Since 1946, he has been with the Microwave Research Institute of the Polytechnic Institute of Brooklyn, N. Y., where he has been engaged in research in a variety of topics in the microwave field. He has also taught graduate courses in physics and electrical engineering, and is a research professor.

Dr. Oliner is Chairman of both the IRE Committee on Antennas and Waveguides and the IRE Professional Group on Microwave and Theory and Techniques. He is a member of Commissions 1 and 6.3 of URSI, the American Physical Society and Sigma Xi. He is also on the National Academy of Sciences Advisory Panel to the National Bureau of Standards.

❖

John A. Rosado was born on June 15, 1936, in Baton Rouge, Louisiana. In 1958 he received the degree of Bachelor of Arts in physics from Harvard University, Cambridge, Mass.

Upon graduation from Harvard, Mr. Rosado was employed by the Ordnance Corps, Diamond Ordnance Fuze Laboratories, Washington 25, D. C.

J. A. ROSADO

❖

Raman Lal Sarda was born on February 25, 1933 in Jaisalmer, India. He received the B.E. degree in telecommunications engineering from Government Engineering College, Jabalpur, India, in 1955.

After some short assignments, he joined the research staff of the newly started Central Electronics Engineering Research Institute, Pilani, in 1956.

R. L. SARDA

He worked there for some time on research projects, "Radar Detecting System" and "Linearity of Cavity Resonators." In 1958, he came to the United States for graduate studies on a scholarship from Mahindra Educational Trust, Bombay. He is currently finishing work for the M.S. degree in electrical engineering at Stanford University, Stanford, Calif.

❖

Joseph H. Saunders was born on January 18, 1919, in Freeport, Nova Scotia. He graduated from Wentworth Institute, Boston, Mass., in 1940, and did subsequent graduate study at Northeastern University in Boston.

J. H. SAUNDERS

From 1941 to 1947 he was employed by the Holtzer-Cabot Electric Company and the Faraday Electric Company as an engineer on protective signal systems. In 1947, he joined the Raytheon Company, Waltham, Mass. where his work has been mostly in the microwave field. At present he is engaged in the study of the microwave properties and applications of ferrites.

❖

Ernst Schlömann was born in Borgholzhausen, Germany on December 13, 1926. He received the M.S. degree in 1953 and the Ph.D. degree in 1954 in theoretical physics from the University of Göttingen, Göttingen, Germany. In 1954–1955 he did postdoctoral research at the Massachusetts Institute of Technology, Cambridge, Mass., in theoretical solid state physics.

E. SCHLÖMANN

He was employed at the Research Division, Raytheon Manufacturing Company, Waltham, Mass., from 1954–1955 on a part time basis. He joined Raytheon on a full time basis in August 1955, and is currently engaged in theoretical studies of ferromagnetism, particularly ferromagnetic resonance.

Dr. Schlömann is a member of the American Physical Society.

Jean-Claude Simon (SM'53) was born September 10, 1923, in Paris, France. He graduated from the École Polytechnique in 1944 and received the D.Sc. degree in mathematics and physics from the Sorbonne in 1952. In the summer of 1948 he was a member of the Foreign Summer Student Project at M.I.T., Cambridge, Mass.

J. C. SIMON

From 1947 to 1949 he was with the French Navy at the laboratory of ENS, Paris. In 1949 he became a physicist at the Compagnie Générale de Télégraphie sans Fil, Paris. In 1951 he was appointed head of the laboratory at CSF, and in 1957 he became technical director of the Applied Physics Department.

Dr. Simon has published 21 articles and papers, and he holds 30 French or foreign patents. He became a Laureat de l'Institut in 1952, the Ferrié Prize of the Society of Radioelectricians in 1953 and the Blondel Medal in 1959. He is a member of the French Society of Physics, the French Society of Radioelectricians, and the French Society of Statistics.

❖

Marshall H. Sirvetz was born in Lynn, Mass., in 1924. In 1950 he received the Ph.D. degree in chemical physics from Harvard University, Cambridge, Mass., where he did work in microwave spectroscopy.

M. H. SIRVETZ

After spending two years at Brookhaven National Laboratory, Long Island, N. Y., he joined the Research Division of Raytheon Manufacturing Company, Waltham, Mass., in March, 1953, where he is presently employed. His present work deals with the microwave properties and applications of ferrites and with solid-state microwave amplifiers.

❖

L. Solymar was born on January 24, 1930, in Budapest, Hungary. In 1952 he received the diploma of Electrical Engineer from the Technical University of Budapest, where he was assistant to the professor from 1952 to 1953.

L. SOLYMAR

From 1953 to 1956, he was a research engineer at the Research Institute of Telecommunication, Budapest, and was engaged in antenna theory

and design. In 1956 he became a research engineer at the Standard Telecommunication Laboratories Ltd., Harlow, Essex, Eng., where he is presently employed and where he has been concerned with various topics in microwave transmission.

❖

Allan Staniforth (A'45–M'55–SM'58) was born in Alberta, Can., on October 9, 1915. He received the B.A.Sc. degree at the University of British Columbia, Vancouver, in 1938.

A. Staniforth

He worked for the Canadian Broadcasting Corporation for three and one-half years as transmitter supervisor. Since that time, he has been with the Radio and Electrical Engineering Division of the National Research Council, Ottawa, Canada.

❖

Edward F. Turner, Jr. was born on April 21, 1920, in Newport News, Va. He received the B.S. degree in physics and the B.A. degree in mathematics from Washington and Lee University, Lexington, Va., in 1950. Upon completion of the M.S. degree from the Massachusetts Institute of Technology, Cambridge, Mass., in 1952 and the Ph.D. from the University of Virginia, Charlottesville, Va., in 1954, he taught for three years at George Washington University, Washington, D. C. He has spent his summers doing research at the Naval Research Laboratory and the Diamond Ordnance Fuze Laboratory in Washington, D. C., principally in the the fields of High Resistance Measurements and Semiconductor Switching of Microwaves. At present he is Professor of Physics at Washington and Lee University.

E. F. Turner

Dr. Turner is a member of Phi Beta Kappa, Sigma Xi, and Sigma Pi Sigma.

❖

B. H. Wadia (S'50–A'53) was born on October 1, 1927, in Surat, India. He received the B.E. degree in electrical and mechanical engineering, in 1948, from the University of Bombay, Bombay, India. He received the M.S. degree in 1950 and the Ph.D. degree in 1954, both in electrical engineering from Stanford University, Stanford, Calif. While at Stanford, he was a research assistant, and subsequently a research associate in the Electronics Research Laboratories.

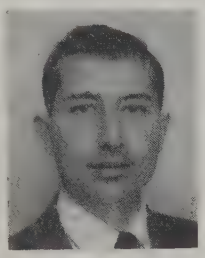

B. H. Wadia

After his academic work, he joined the engineering staff of Machlett Laboratories, Inc., Springdale, Conn., and was given the position of Product Engineer (UHF Tubes). At the end of 1956, he returned to India and was made assistant director in charge of the Central Electronics Engineering Research Institute, Pilani, Rajsthan, India. He was instrumental in setting up one of the first organizations devoted exclusively to electronic engineering, research and development work in that country. At present he holds a teaching position in the Department of Electrical Engineering at the newly organized Indian Institute of Higher Technology, Bombay, India.

Dr. Wadia is a member of Tau Beta Pi and Sigma Xi.

❖

Ernest J. Wilkinson (S'52–A'53) was born in Fall River, Mass. on May 23, 1927. He received the B.S. degree in electrical engineering from Northeastern University, Boston, Mass., in 1952 and the M.S. degree in electrical engineering from Stanford University, Stanford, Calif. in 1956.

E. J. Wilkinson

From 1952 to 1953 he was employed by Sandia Corporation, Albuquerque, N. M., and from 1953 to 1954 he worked for Sylvania Electric Products, Inc., then located in Boston, Mass. He returned to Sylvania in 1956 and is presently working in the Electronics Department of the Missile Systems Laboratory located in Waltham, Mass.

Mr. Wilkinson is a member of Tau Beta Pi and Eta Kappa Nu.

EXPANSION

to keep pace with the growing challenge of

ELECTRONICS

at GRUMMAN AIRCRAFT

Grumman Aircraft Engineering Corporation's long and continuing responsibilities for the design of Avionics Systems for ASW, AEW, Reconnaissance, and all-weather attack aircraft has necessitated vast facilities expansion. A new five million dollar Avionics Center will provide 62,000 square feet of floor space devoted exclusively to activities involving test, evaluation and integration of Avionics Systems.

Concurrent expansion of our staff of electronics engineers and scientists has created positions for men anxious to participate in varied and intellectually stimulating programs utilizing the most modern of facilities.

★ **Communications Engineer.** EE or Physicist with knowledge of communication theory including advantages of various modes of modulation and effects of propagation within and out of the atmosphere. To keep advised of the state of the art of communications systems for data, voice and video links for air-to-ground, air-to-air, space-to-ground transmissions and reception; to recommend radio frequencies and modulation techniques for various missile and space craft communication applications; to conduct preliminary design of communication systems in order to estimate weight and power requirements; to propose and conduct research on advanced communication systems.

★ **Radio Interference Control Engineers.** Engineers to analyze the source of conducted and radiated interference caused by the interaction of complex electronic equipments and systems, and develop methods and techniques to suppress the interference in the advanced design state of aircraft and missiles.

★ **Radome or Antenna Design Engineer.** BSEE or Physics degree with a minimum of 3 years' experience in radome design. Background in classical Electromagnetic theory and advanced math essential. Work consists of analysis and synthesis of radomes or antennas on current and advanced designs including the use of the IBM computer facilities to develop design techniques.

★ **Communications Equipment Engineer.** BSEE with a minimum of 5 years' experience with thorough knowledge of single sideband theory and its application. Should possess a complete understanding of AM, FM, PM and single sideband modulation processes and their application as well as techniques. Must have experience in analyzing and testing communications receivers and transmitters, and should be thoroughly familiar with HF and UHF antennas and associated propagation problems. A background in digital equipment, encoders, decoders and magnetic storage devices is an important consideration.

★ **Radar Systems Engineer.** BSEE with a minimum of 5 years' experience in design development and analysis of advanced radar systems. Capable of integrating the Radar into complex airborne Avionics Systems including the following specific skills; Analysis of System, Compatibility with Weapons System, Preparation of Specifications, Vendor Liaison and Direction, Test and Evaluation, Flight Development.

You are invited to investigate these opportunities by sending your resume to Mr. A. Wilder, Engineering Personnel Director, Dept. GR-70, who will arrange an interview at your convenience. (U.S. Citizenship required).

GRUMMAN AIRCRAFT ENGINEERING CORPORATION

Bethpage • Long Island • New York

PHYSICISTS and RESEARCH ENGINEERS

THE RADIATION LABORATORY OF THE JOHNS HOPKINS UNIVERSITY

HAS POSITIONS FOR PHYSICISTS OR RESEARCH ENGINEERS IN THE FIELD OF:

MICROWAVE PARAMETRIC PHENOMENA

AND FOR RESEARCH ENGINEERS IN THE FIELDS OF ELECTROMAGNETIC ENVIRONMENT STUDIES AND RADAR

THIS UNIVERSITY LABORATORY OFFERS A VARIETY OF INTERESTING PROBLEMS IN FUNDAMENTAL RESEARCH FOR QUALIFIED PERSONS WITH ADVANCED DEGREES CAPABLE OF INDEPENDENT AND CREATIVE EFFORT.

- Favorable Arrangements for Doctoral and Post Doctoral Study in the University Graduate School
- Faculty Privileges for Senior Staff
- Excellent Laboratory Facilities Located Near the University Campus
- Broad Opportunities for Personal Development

ADDRESS INQUIRIES TO:

RADIATION LABORATORY
THE JOHNS HOPKINS UNIVERSITY
Homewood Campus, Baltimore 18, Md.

THERE'S MORE TO A D-B BROADBAND WAVEMETER THAN JUST THE DIAL!

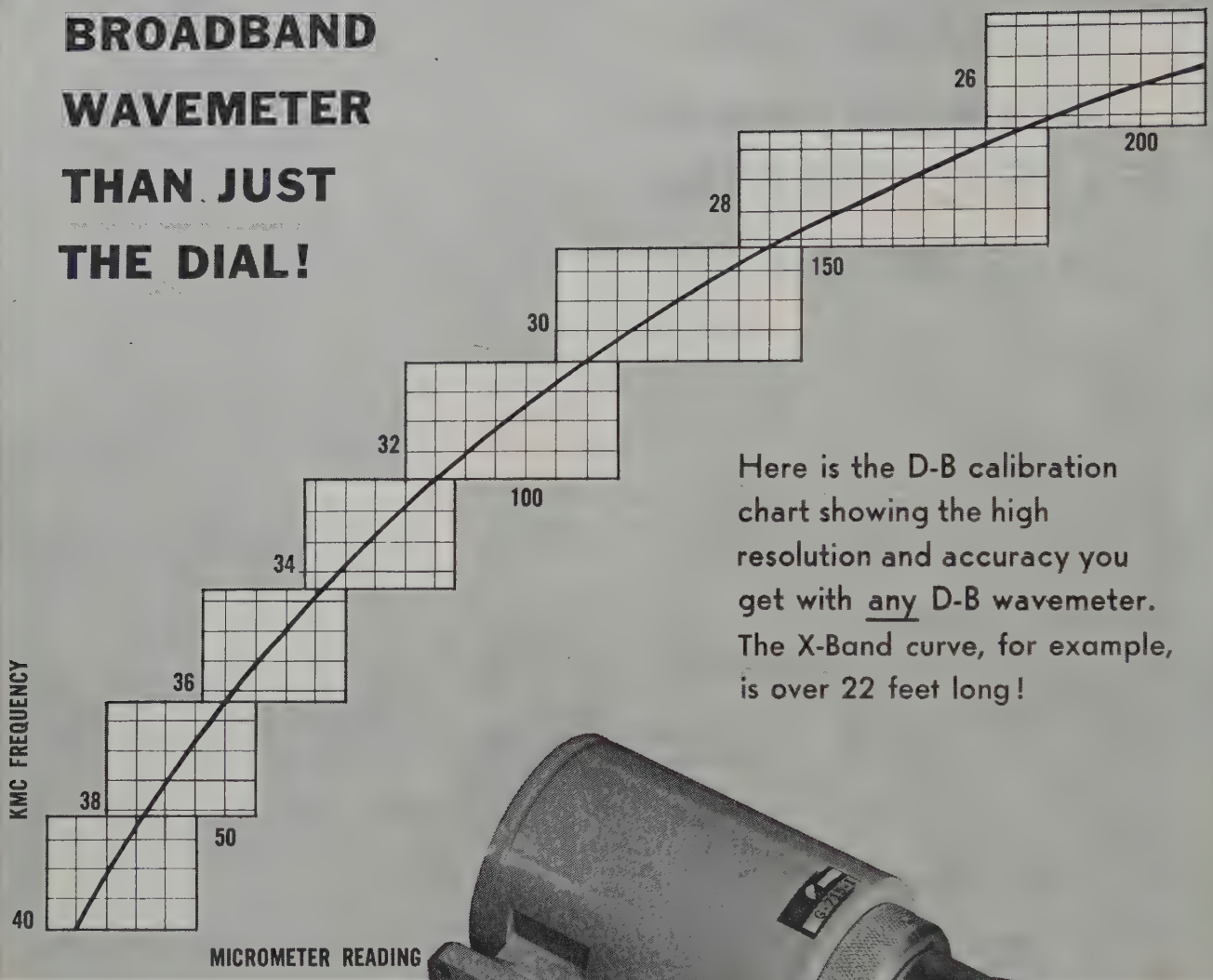

Here is the D-B calibration chart showing the high resolution and accuracy you get with any D-B wavemeter. The X-Band curve, for example, is over 22 feet long!

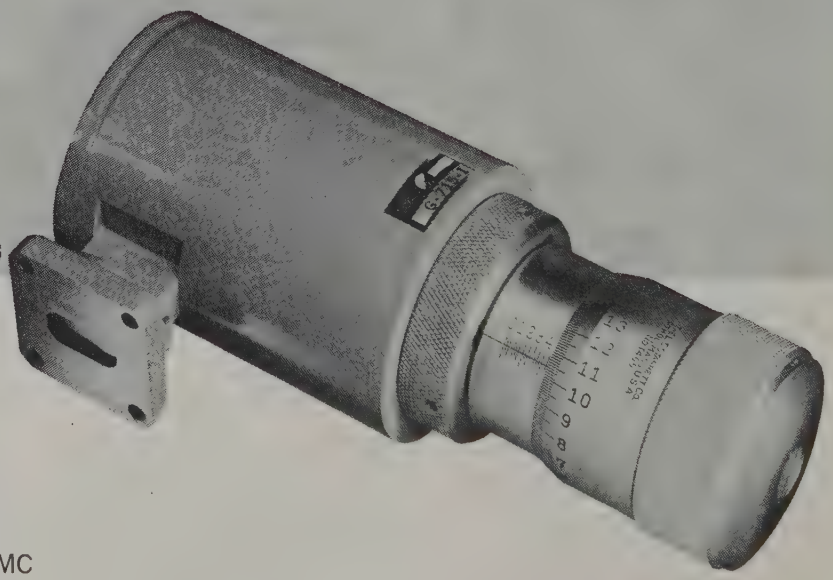

Fail-Safe Design— loss of gas pressure makes unit immediately inoperative.

Twelve models cover from 2.6 KMC to 140 KMC. Write for complete data in Bulletin D-B 715.

DE MORNAY-BONARDI

DE MORNAY-BONARDI

780 SOUTH ARROYO PARKWAY • PASADENA, CALIF.

INSTITUTIONAL LISTINGS

The IRE Professional Group on Microwave Theory and Techniques is grateful for the assistance given by the firms listed below, and invites application for Institutional Listing from other firms interested in the Microwave field.

AIRTRON, INC., A Division of Litton Industries, 200 East Hanover Ave., Morris Plains, N.J.
Designers and Producers of Complete Line of Microwave Electronic and Aircraft Components

COLLINS RADIO CO., Texas Division, Dallas, Tex.
Complete Microwave and Transhorizon Communication Systems

ITT LABORATORIES, 500 Washington Ave., Nutley 10, N.J.
Line-of-Sight and Over-the-Horizon Microwave Systems; Test Equipment and Components

LITTON INDUSTRIES, Electron Tube Div., 960 Industrial Rd., San Carlos, Calif.
Magnetron, Klystrons, Carcinotrons, TWT's, Backward Wave Oscillators, Gas Discharge Tubes, Noise Sources

MICROWAVE CHEMICALS LABORATORY, INC., 282 Seventh Ave., New York 1, N.Y.
Single Crystals and Polycrystalline Y.I.G. and Related Ferrites Designed for Your Devices

MICROWAVE DEVELOPMENT LABS., INC., 92 Broad St., Babson Park 57, Mass.
Designers, Developers and Producers of Microwave Components and Assemblies, 400 mc to 70 kmc

WHEELER LABORATORIES, INC., Great Neck, N.Y.; Antenna Lab., Smithtown, N.Y.
Consulting Services, Research & Development, Microwave Antennas & Waveguide Components

The charge for an Institutional Listing is $50.00 per issue or $140.00 for four consecutive issues. Applications for Institutional Listings and checks (made out to the Institute of Radio Engineers) should be sent to Tore N. Anderson, PGMTT Advertising Editor, 1539 Deer Path, Mountainside, N.J.

GAMMA-RAY — 10^{20} CPS
10^{19} CPS
X-RAY — 10^{18} CPS
10^{17} CPS
ULTRA-VIOLET — 10^{16} CPS
10^{15} CPS
VISIBLE LIGHT
10^{14} CPS
INFRA-RED — 10^{13} CPS
1,000 KMC
100 KMC
MICRO-WAVES — 10,000 MC
1000 MC
TV — 100 MC
COMM. AM-FM — 10 MC
1000 KC
ULTRA-SONIC — 100 KC
10 KC
AUDIO — 1 KC
100 CPS
10 CPS
0
FREQUENCY

"...working in the 90-220 kmc frequency ranges?"

- *Crystal, Bolometer, and Thermistor Mounts.*
- *Harmonic Generators.*
- *Series, Shunt and Hybrid Tees.*
- *Slotted Sections.*
- *Precision Variable Attenuators.*
- *Standard Gain Horns.*
- *E/H Tuners.*

Other components shown below.

Slotted section, shown here, actual size.

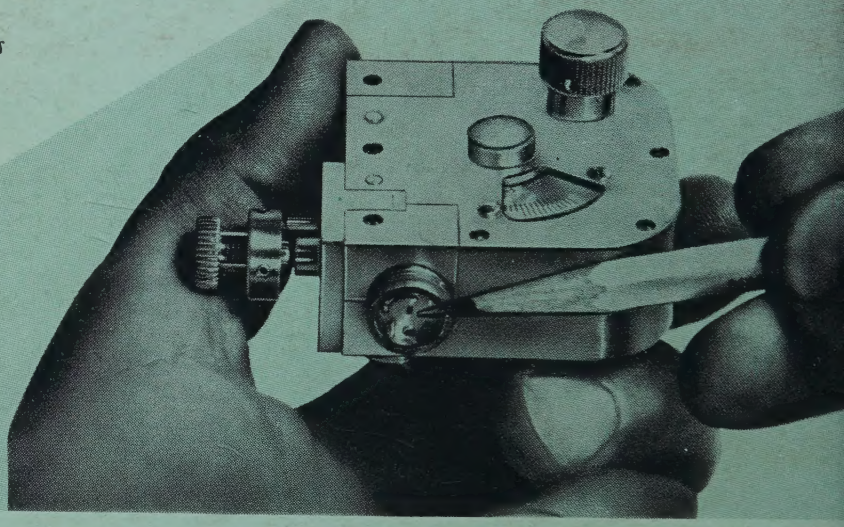

FXR's Newly Developed and Proven 2-3 MM Components are Marvels *of Precision and Reliability*

These miniature F-Band and G-Band components are not scaled down versions of their lower frequency counterparts. Rather, they are instruments of individuality and precision — products of advanced microwave engineering and new manufacturing techniques.

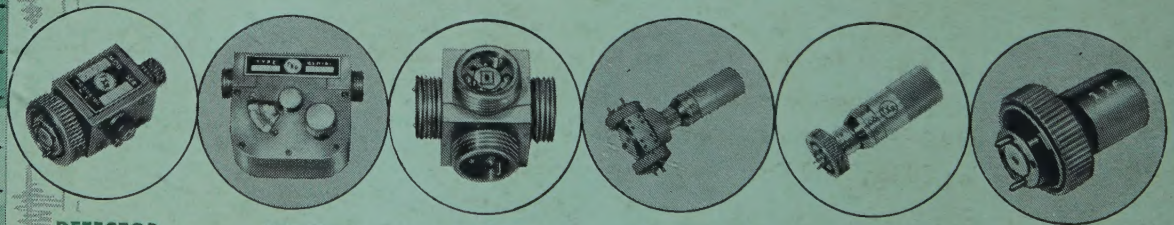

DETECTOR MOUNT · PHASE SHIFTER · E/H TEE · FREQUENCY METER · ADJUSTABLE SHORT · TERMINATION

Brochure, including price list, available on request!

FXR, Inc.

Design · Manufacture · Development

Woodside 77, N. Y.

Precision Microwave Equipment · High-Power Modulators · Radar Components · Electronic Test Equipment